NUCLEAR INSTRUMENTS & METHODS

A JOURNAL ON ACCELERATORS, INSTRUMENTATION
AND TECHNIQUES IN NUCLEAR PHYSICS

EDITOR: K. SIEGBAHN - UPPSALA

VOLUME 7

APRIL 1960 — JUNE 1960

NORTH-HOLLAND PUBLISHING COMPANY — AMSTERDAM

PRINTED IN THE NETHERLANDS
DRUKKERIJ MEIJER N.V. WORMERVEER AND AMSTERDAM

NUCLEAR INSTRUMENTS AND METHODS

This issue of Nuclear Instruments and Methods is devoted to late professor

H. W. D. SKINNER, *Liverpool.*

A distinguished scientist and an appreciated member of our editorial board has left us.

THE EDITOR

EDITORIAL BOARD:

J. B. ADAMS (CERN)
F. A. ALSINA (Buenos Aires)
E. AMALDI (Rome)
H. L. ANDERSON (Chicago)
K. T. BAINBRIDGE (Cambridge, Mass.)
P. R. BELL (Oak Ridge)
R. E. BELL (Montreal)
A. BERTHELOT (Saclay)
H. BRINKMAN (Groningen)
E. H. COOKE–YARBOROUGH (Harwell)
S. DE BENEDETTI (Pittsburgh)
M. DE HEMPTINNE (Louvain)
A. DE-SHALIT (Rehovoth)
M. DEUTSCH (Cambridge, Mass.)
S. DU TOIT (Pretoria)
B. S. DŽELEPOV (Leningrad)
W. GENTNER (Heidelberg)
P. C. GUGELOT (Amsterdam)
H. HALBAN (Paris)
O. HAXEL (Heidelberg)
P. HUBER (Basel)
S. KIKUCHI (Tokyo)
J. KOCH (Copenhagen)
M. S. KOZODAEV (Moscow)
S. LIVINGSTON (Cambridge, Mass.)
E. M. MCMILLAN (Berkeley)
M. G. MEŠČERJAKOV (Moscow)
P. B. MOON (Birmingham)
M. L. OLIPHANT (Canberra)
W. PAUL (Bonn)
A. S. RAO (Bombay)
G. SALVINI (Rome)
P. SAVIĆ (Belgrade)
P. SCHERRER (Zürich)
CH. SCHMELZER (CERN)
R. TANGEN (Oslo)
D. TAYLOR (Northampton)
V. I. VEKSLER (Moscow)
G. VON DARDEL (CERN)
O. WERNHOLM (Stockholm)
R. R. WILSON (Cornell)
S. D. WINTER (Saclay)

APRIL 1960 VOLUME 7 (1960) No. 1

GREGG M. SINCLAIR LIBRARY
UNIVERSITY OF HAWAII
8-7-63

NUCLEAR INSTRUMENTS & METHODS

A JOURNAL ON ACCELERATORS, INSTRUMENTATION AND TECHNIQUES IN NUCLEAR PHYSICS

EDITOR: K. SIEGBAHN - UPPSALA

CONTENTS

CARL E. ANDERSON, ARTHUR R. QUINTON, WILLIAM J. KNOX and ROBERT LONG, Apparatus for the investigation of heavy ion induced reactions 1
MILORAD MLADJENOVIĆ, Recent developments of beta spectrometers 11
W. PARKER, M. DE CROËS and K. SEVIER, Jr., Some methods in the preparation of radio-active materials for use in beta-spectroscopy 22
YU. K. AKIMOV, V. I. KOMAROV, O. V. SAVCHENKO and L. M. SOROKO, The separating of particles according to their ionization value in several scintillation counters 37
G. B. B. CHAPLIN and A. J. COLE, A linear gate of 10 to 100 mμsec duration 45
S. GORODETZKY, R. RICHERT, R. MANQUENOUILLE et A. KNIPPER, Convertisseur temps-amplitude à pouvoir de résolution élevé 50
WILLIAM H. ELLETT and GORDON L. BROWNELL, A total absorption gamma ray spectrometer combining sodium iodide and plastic scintillators 56
NICOLAI MITROFANOV and J. J. VAN LOEF, Detection of neutron and photon induced fission by ZnS(Ag) mixed with uranium and thorium compounds 63
H. W. NEWSON and R. M. WILLIAMSON, High resolution neutron spectroscopy 67
G. ANDERSSON, G. RUDSTAM and T. STENSTRÖM, Recoil technique in cyclotron bombardments using powder targets 73
BO SJÖGREN, Combination of magnetic analyzers in nuclear reaction experiments 76
G. HENNEBERKE, An electron accelerator in pressurized tank for 3 mA at 1.5 MV direct voltage 89
BOOK REVIEWS 99

NORTH-HOLLAND PUBLISHING COMPANY - AMSTERDAM

NUCLEAR INSTRUMENTS AND METHODS

A journal on accelerators, instrumentation and techniques in nuclear physics

EDITOR: K. SIEGBAHN, UPPSALA

EDITORIAL BOARD:

J. B. ADAMS (CERN)
F. A. ALSINA (Buenos Aires)
E. AMALDI (Rome)
H. L. ANDERSON (Chicago)
K. T. BAINBRIDGE (Cambridge, Mass.)
C. J. BAKKER (CERN)
P. R. BELL (Oak Ridge)
R. E. BELL (Montreal)
A. BERTHELOT (Saclay)
H. BRINKMAN (Groningen)
E. H. COOKE-YARBOROUGH (Harwell)
S. DE BENEDETTI (Pittsburgh)
M. DE HEMPTINNE (Louvain)
A. DE-SHALIT (Rehovoth)
M. DEUTSCH (Cambridge, Mass.)
S. DU TOIT (Pretoria)
B. S. DŽELEPOV (Leningrad)
W. GENTNER (Heidelberg)
P. C. GUGELOT (Amsterdam)
H. HALBAN (Paris)
O. HAXEL (Heidelberg)
P. HUBER (Basel)
D. J. HUGHES (Brookhaven)
S. KIKUCHI (Tokyo)
J. KOCH (Copenhagen)
M. S. KOZODAEV (Moscow)
S. LIVINGSTON (Cambridge, Mass.)
E. M. MCMILLAN (Berkeley)
M. G. MEŠČERJAKOV (Moscow)
P. B. MOON (Birmingham)
M. L. OLIPHANT (Canberra)
W. PAUL (Bonn)
A. S. RAO (Bombay)
G. SALVANI (Rome)
P. SAVIĆ (Belgrade)
P. SCHERRER (Zürich)
CH. SCHMELZER (CERN)
H. W. B. SKINNER (Liverpool)
R. TANGEN (Oslo)
D. TAYLOR (Northampton)
V. I. VEKSLER (Moscow)
G. VON DARDEL (CERN)
O. WERNHOLM (Stockholm)
R. R. WILSON (Cornell)
S. D. WINTER (Saclay)

INSTRUCTIONS FOR CONTRIBUTORS

Contributions may be sent to the Editor, Professor K. Siegbahn, Institute of Physics, University of Uppsala, Sweden, either directly or through the intermediation of one of the members of the Editorial Board. Contributions may be written in English, French or German but should always, except for very short papers, be supplied with a brief abstract in English. Figures should be in inked original drawings or glossy prints and they should be sufficiently large. Contributors should make sure that important details in drawings and photographs will show up clearly in the diminished copy used by the publisher.

Books for review should be sent to Professor Siegbahn.

Objective and descriptive material on endeavours and product developments from the industry for the section "Spotlight on Industry" should be sent directly to the publishers, North-Holland Publishing Company, P.O. Box 103, Amsterdam.

Nuclear Instruments and Methods is published monthly. The subscription price of a volume of 360 pages is $ 17.00 (130 s), postage free.

Subscriptions should be sent to the publishers, North-Holland Publishing Company, P.O. Box 103, Amsterdam or to any subscription-agent.

No part of this issue may be reproduced in any form, by print, photoprint, microfilm or any other means without written permission from the publisher.

110" synchro-cyclotron for the acceleration of protons to 150 MeV and of deuterons to 80 MeV. (Photo by courtesy of "Laboratoire de Physique Nucléaire de la Faculté des Sciences de Paris")

PHILIPS

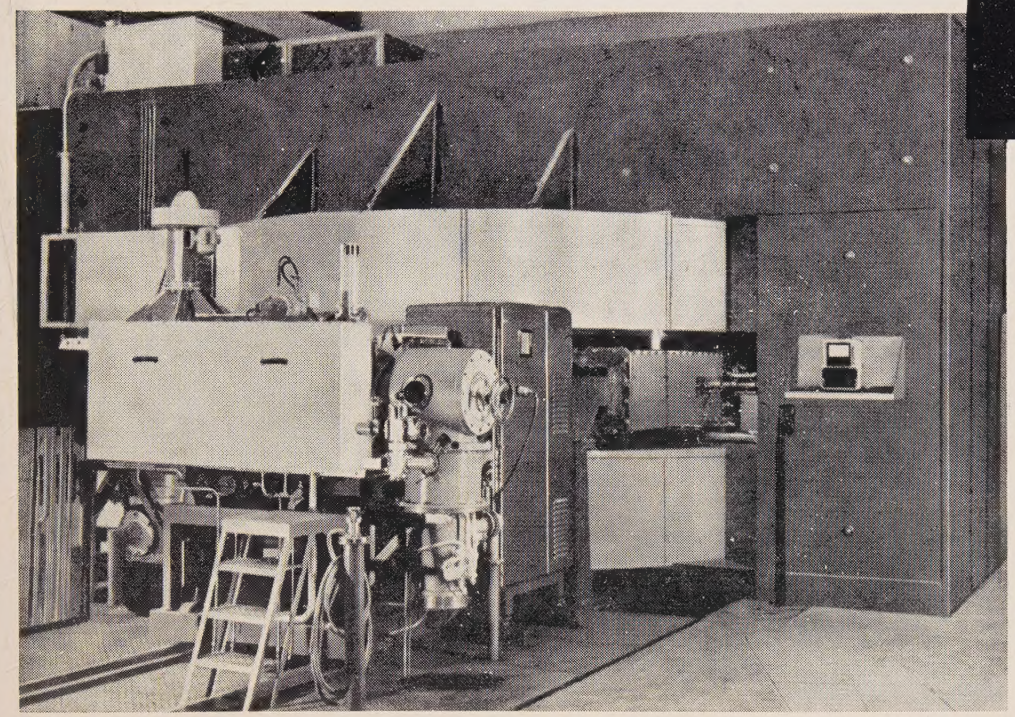

PHILIPS *equipment for*
Nuclear Physics and Atomic Energy

This synchro-cyclotron has been put into operation recently. During the testing period it operated at 160 MeV and produced a proton current of over 5 μA. Philips engineers are now installing a beam extracting mechanism, together with focussing and deflecting magnets for the external beam. Similar machines can be supplied for various energy ranges.

- Synchro-cyclotrons for various final energies.
- Cockcroft-Walton accelerators.
- Generators for very high d.c. voltages.
- Linear electron accelerators.
- Reactor control instrumentation.
- Radiation measuring and detection equipment.
- Civil defence instruments.
- Area monitoring instrumentation.
- Geiger counter tubes.
- Photomultipliers.
- Radio-active isotopes.
- Air & gas liquefiers.

PHILIPS
Nuclear Equipment

For further information please apply to one of the following addresses:

N.V. PHILIPS' GLOEILAMPENFABRIEKEN, Scientific Equipment Department, Eindhoven-Holland
RESEARCH & CONTROL INSTRUMENTS LTD., Instrument House, 207/215, King's Cross Road, London WC 1
PHILIPS ELECTRONICS INC., Instruments Division, 750, South Fulton Avenue, Mount Vernon, N.Y. U.S.A.

Pulse Height Analysis

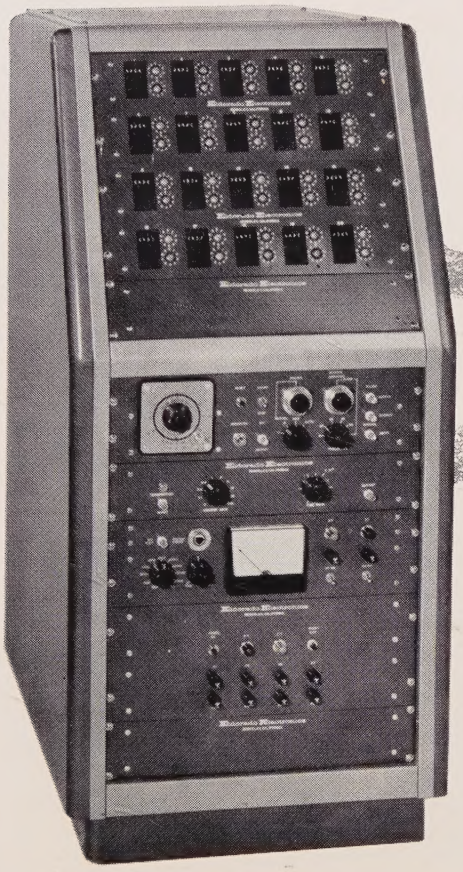

Hours faster with the

Eldorado 4100

The Eldorado 4100 is the fastest multi-channel pulse height analyzer commercially available to the nuclear physicist. Its high resolution and exceptional stability dramatically shorten many experiments. For example, an experiment requiring from 7 to 42 hours with a time conversion type analyzer can be done in 8 to 25 minutes with the 4100. Such performance considerably reduces research costs.

APPLICATIONS *The 4100 is particularly well-suited for experiments requiring accurate analysis of (1) isomeric states, (2) isotopes with extremely short half-lives, (3) isotope mixtures having complex photo-peak structures.*

SPECIAL ADVANTAGES

Stability. The 4100's double pulse resolution—better than 1.0 microsecond—is achieved without sacrifice of stability. The system's stability figures (see specifications) compare favorably to the best for slower computer-type analyzers. Since lower ordered channels are free from non-linearity, each data point in the spectrum is equally useful and valid.

Low Dead Time. Users of the 4100 can often neglect count-loss correction factors because dead time is less than 0.2 microsecond. At an input counting rate of 300,000 counts per minute, dead time is less than 2% of the total experiment time.

KEY SPECIFICATIONS **Number of Channels,** 20. **Channel Width,** 1 volt, nominal. **Channel Width Stability,** Typically, better than 1% of a channel per week. **Zero Level Stability,** Better than 0.1% per week. **Window Width,** 20 volts, nominal. **Window Position Range,** 5 to 105 volts in 5 preset steps or continuous. **Channel Count Capacity,** 1,000,000. **Double Pulse Resolution Complete Analyzer,** 1.0 microsecond at window amplifier input. **Channel Scalers,** 10.0 microseconds.

For more details, write for Eldorado Bulletin D-4100.
Please address Dept. 79

Eldorado Electronics

2821 TENTH STREET • BERKELEY 10, CALIFORNIA

256 THE TMC 256-CHANNEL PULSE ANALYSIS SYSTEM

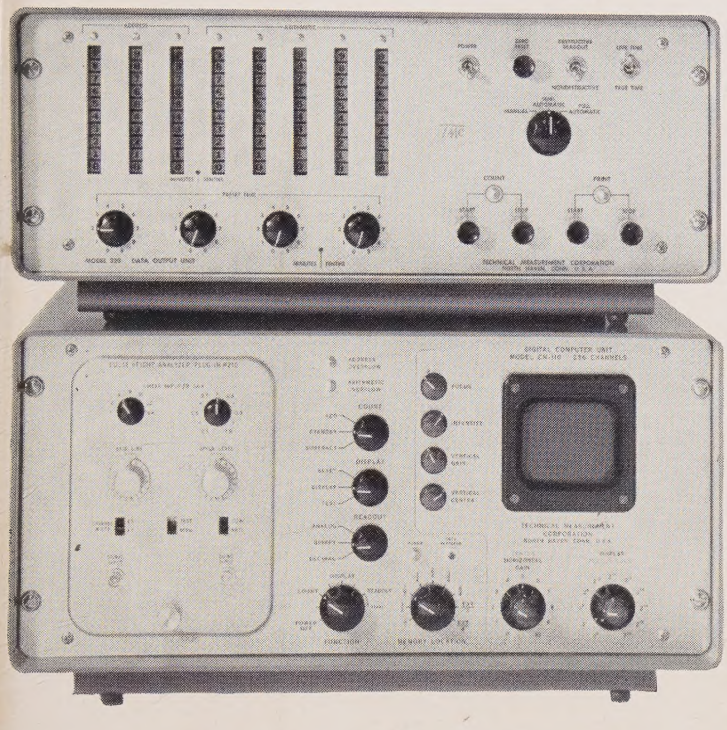

#220 DATA HANDLING UNIT usable as an active timer, event counter and readout device ... effective or actual counting times may be selected from 0.1 to 999.9 minutes in 0.1 min. steps ... manual, semi- or fully automatic operation, destructive and non-destructive readout.

TIME-OF-FLIGHT MEASUREMENT #211 plug-in ... built-in delay of 0, 1, 2, 3 times address cycle ... choice of 9 channel lengths from 0.25 to 64 μs. ... automatic channel advance

PULSE HEIGHT ANALYSIS — #210 plug-in ... built-in linear amplifier, pulse generator ... 10-74 μs. dead time ... ±0.5% linearity

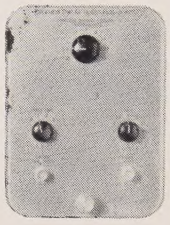

The Model CN-110 digital computer assembly ... only 8¾" high ... weighs 30 lbs. with plug-in ... operates on 25 watts

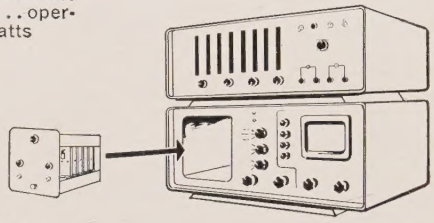

ONE BENCH-TOP INSTRUMENT...

Becomes a different pulse analyzer every time you change the logic

PULSED NEUTRON MEASUREMENT — #212 plug-in ... analysis channel lengths from 10 to 2560 μs. ... 10 μs. storage time ... (a high speed arithmetic scaler is supplied with the CN-110 at no extra charge when the 212 unit is purchased with it)

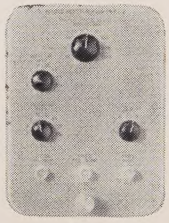

With just one CN-110 in your laboratory you have 256 channels of the pulse analysis you need — whether it's pulse height, time-of-flight, pulsed neutron or a special program. When you plug in the logic network, the instrument becomes a ready-to-use analysis system for that program. And you can change them in the time it takes to loosen a thumbscrew. Total weight is only 30 lbs., all circuits are transistorized — making this today's most versatile, compact pulse analyzer for research, field work or regular laboratory use. *They are now in production and deliveries are being made.*

THE BASIC UNIT IS A COMPLETE DIGITAL COMPUTER with all the circuitry for a 256-channel magnetic core memory and has the advantages of completely enclosed, plug-in memory ... choice of memory sub-groups ... pushbutton data transfer ... instantly selected analog, binary or digital readout.

FOR DATA HANDLING, a readout instrument has been designed specifically for use with the CN-110. The compact #220 data handling unit can be used as a live-timer during data gathering and as a readout system afterward. The #220 can be used with various types of paper tape printing and punching instruments.

Other readout devices that you can use with the CN-110 include strip chart and X-Y recorders, magnetic computer tape, punched paper cards.

Write for the new 6-page bulletin which contains complete details of the CN-110 and all accessories.

TECHNICAL MEASUREMENT CORPORATION TMC 441 WASHINGTON AVE., NORTH HAVEN, CONN.

Hunting for neutrons?

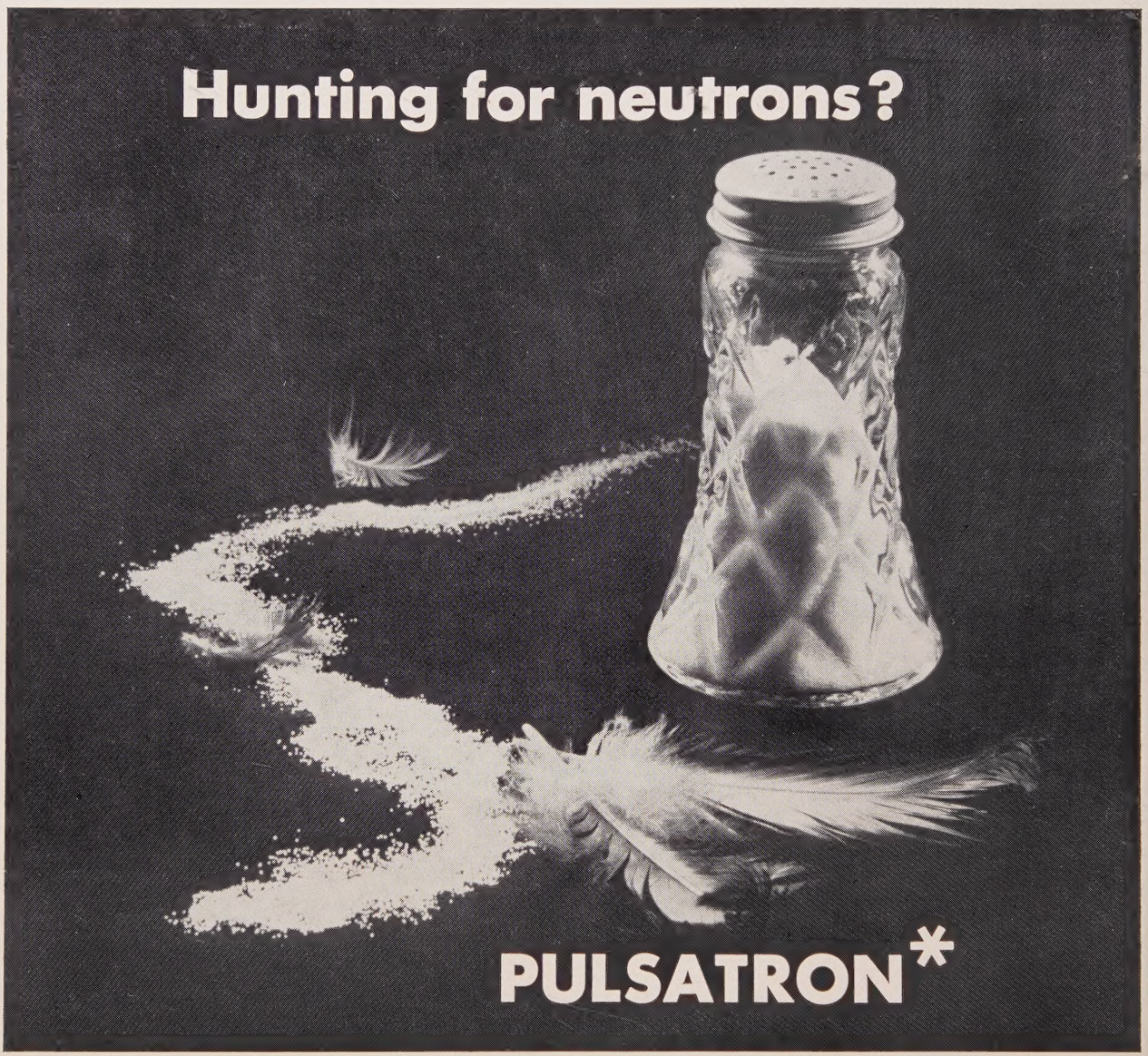

PULSATRON*

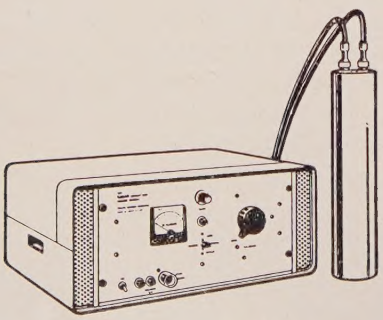

* the Kaman neutron source

small - lightweight - portable

10^7 neutron/pulse - nominal.
5 microseconds — pulse length.
Adjustable - 1-10 pulses/sec.
H^3 (d, n) He^4 reaction.
Accelerator Unit — 4" OD x 18" long.
Control Unit — 21¾" x 15¼" x 10½".

The NT-60-8 Pulsed Neutron Generator Assembly . . . *an Exclusive Development by*

KAMAN NUCLEAR
COLORADO SPRINGS, COLORADO
A Division of the Kaman Aircraft Corporation

Research and Development in Nuclear Weaponry and Instrumentation.

NEW EH 130 PULSE GENERATOR

DOES ALMOST EVERY PULSER JOB BETTER!

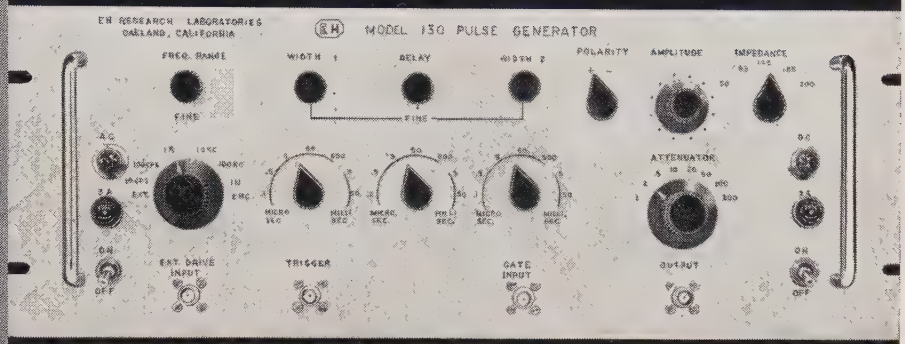

EH Model 130, f.o.b. Oakland, California, $1175

SPECIFICATIONS

REPETITION RATE
10 cps to 1 Mc

RISE AND FALL TIME
Less than 10 millimicroseconds

RELATIVE PULSE DELAY
200 millimicroseconds to 50 milliseconds

JITTER (Pulse widths, relative delay, rep rate)
0.1 percent

TRIGGER OUTPUT
Positive 25 volt pulse

EXTERNAL DRIVE
3 volts rms required (0.1 volt or 2 mμsec equivalent jitter referenced to Pulse Output)

ELECTRONIC GATE
10 volts required

OUTPUTS
Two Pulses at one output connector, independently variable in width and relative delay

PULSE WIDTHS
100 millimicroseconds to 50 milliseconds

PULSE AMPLITUDE
0 to 50 volts maximum
0 to 500 ma maximum

POLARITY
Positive or Negative Pulses available

DUTY FACTOR
50 percent

OUTPUT IMPEDANCE
50, 93, 125, 185 or 200 ohms available (selected by front panel switch)

OUTPUT ATTENUATOR
1:1 to 200:1 coarse selector, 3 to 1 vernier control

Here at last is a pulse generator which can shoulder a broad range of applications . . . a flexible, reliable pulser whose fast rise and low jitter features make it the most advanced instrument of its kind. With its provisions for external drive and electronic gating, its enormous range in pulse widths and delays, and the arbitrary cable impedance feature, you'll find the E-H 130 indispensable for almost any pulser job. Call, write or wire E-H for more information today.

E-H RESEARCH LABORATORIES, INC.
163 ADELINE STREET • TEMPLEBAR 4-3030 • OAKLAND 20, CALIFORNIA

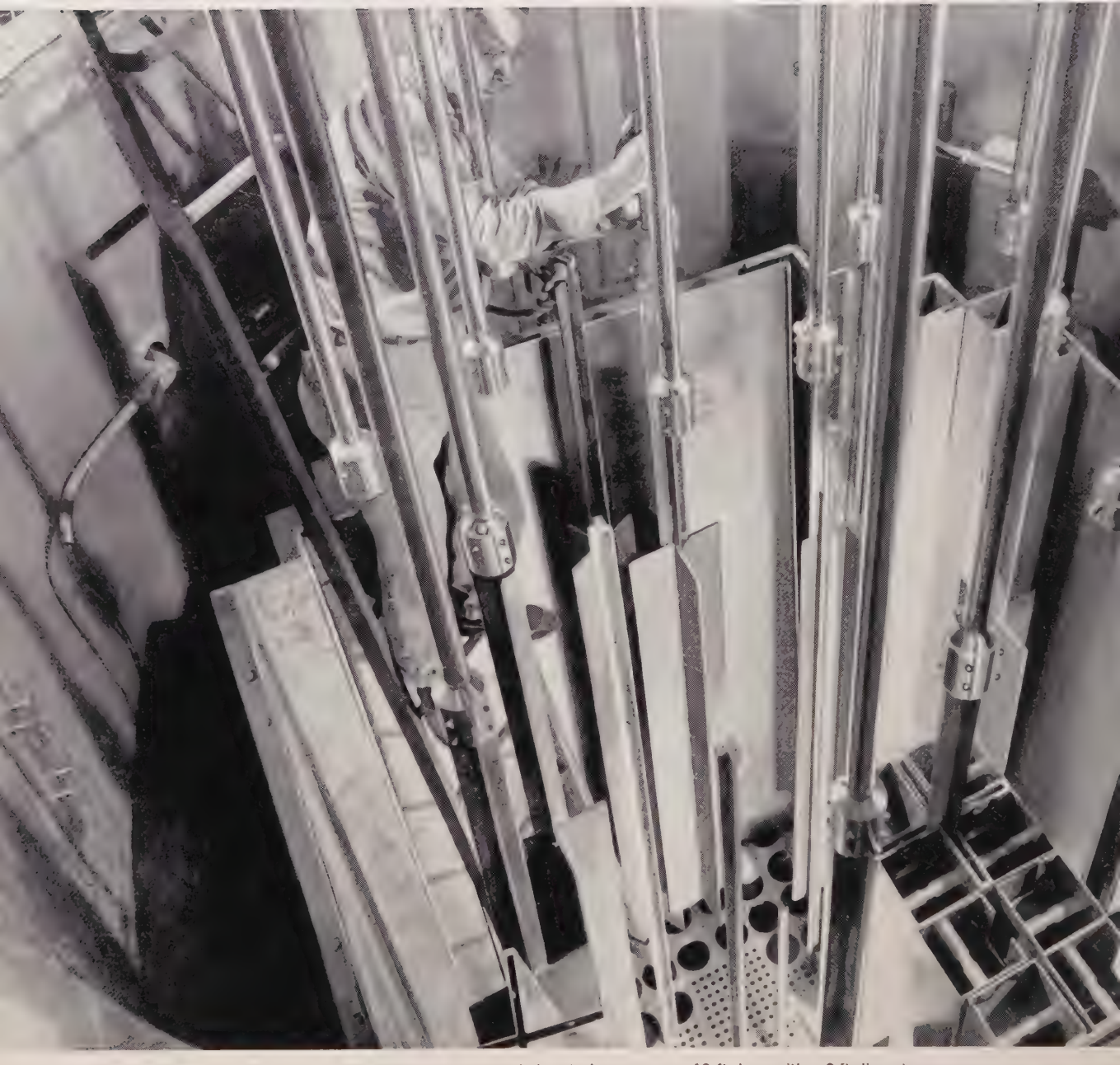

CRITICAL FACILITY TANK at Greendale Laboratories measures 12 ft deep with a 9-ft diameter.

Allis-Chalmers offers unmatched reactor versatility

ALLIS-CHALMERS GREENDALE RESEARCH and development center for nuclear power includes the critical facility containing a full-scale mock-up of the Pathfinder reactor.

Trailblazer for Pathfinder

Full-scale critical facility speeds nuclear superheat calculations at Allis-Chalmers Greendale Laboratories

When this reactor at Allis-Chalmers nuclear test facility "went critical" *on schedule* late in 1959, a big step was taken toward successful completion of the world's first power reactor with integral nuclear superheat. The initial use of this valuable research tool will be for studies of the reactor core for Pathfinder. This controlled recirculation boiling water reactor is owned and will be operated by Northern States Power Co., Minneapolis, Minnesota.

This is just one of the major test facilities at Greendale Laboratories. Others include a steam separator test loop, complete facility for developing underwater handling techniques, a battery of corrosion loops, heat-transfer loops, water purification filter tests, and other experimental facilities.

These modern development facilities round out the comprehensive service Allis-Chalmers offers the nuclear power field. In addition to broad engineering and production capacity—plus more than a half-century's association with electrical power generation, transmission and distribution — Allis-Chalmers has a staff of specialists experienced in reactor design, construction, and operation. Here is a source of complete responsibility from investigation to start-up.

Ask for new facilities book 43B9541 — This 28-page brochure covers different reactor designs, laboratory and production capabilities. *See your Allis-Chalmers representative, or write Atomic Energy Division,* ***Allis-Chalmers,*** *Milwaukee 1, Wis.*

ALLIS-CHALMERS

A-1246-R

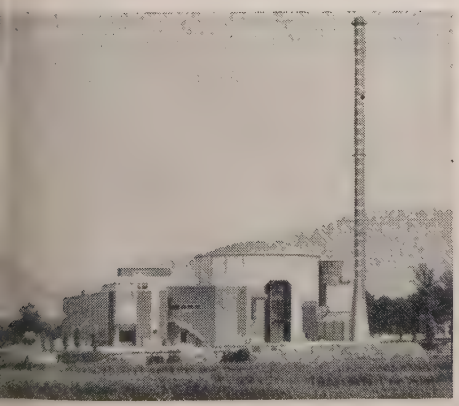

CNRN (Italian National Committee for Nuclear Research, Milan, Italy). 5,000-kw heavy-water research reactor.

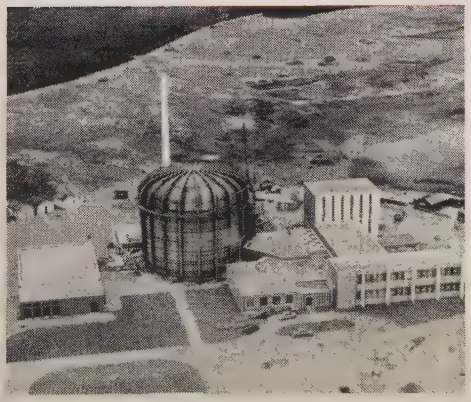

RCN (Reactor Centrum Nederland, Amsterdam). High-flux materials testing and research reactor. Reactor vessel is immersed in a pool.

R-2 (Atomic Energy Co. of Stockholm). High-flux research reactor for fuel development and nuclear research.

NEW FROM TEXAS NUCLEAR CORP.

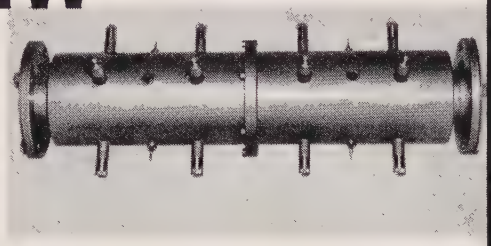

- For focusing an ion beam at large distances from the accelerator
- Cancels astigmatism produced by analyzing magnet
- Increases useful ion beam intensity

TEXAS NUCLEAR CORPORATION
P. O. Box 9267 Austin 17, Texas
WRITE DEPT. E

FOR SCINTILLATION & PROPORTIONAL COUNTING
Non-overloading Linear Amplifiers
MODELS 108 and 108 p

* GAIN–40,000, continuously variable
* RISE TIME–0.2 microsecond
* ACCEPTS + AND — PULSES

Tremendous Dynamic Range
EXCEEDS 1,000,000 (0.1 mV to 100 V)

Excellent linearity for small pulses in the presence of tremendous overloads that paralyze other amplifiers.
Model 108 P includes precision trigger type Pulse-Height Selector.

Model 413 Mercury relay precision sliding Pulser

The one pulser that fills every need of the Nuclear Physics Laboratory
0 to 100 Volts

10 full scale ranges from 1 mV to 100 volts
Fast rise and exponential decay of 1, 3, 10. 30, and 100 microsec simulate pulses from scintillation, proportional and Geiger counters.
Incorporates both manual control and precision motor drive.
The ideal instrument for precise calibration and test of pulse-height analyzers and other nuclear instrumentation.

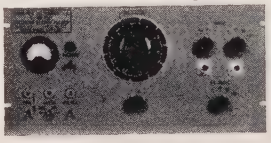

Window widths are determined AUTOMATICALLY, 10 × more ACCURATELY, 40 × FASTER than with conventional pulsers.

Model 108 Amplifier . . . . . $ 545.00
Model 108 P Amplifier (includes pulse-height selector) $ 595.00
Model 413 Precision Sliding Pulser . . . . . $ 630.00
Prices f.o.b. Silver Spring. Md.

RADIATION INSTRUMENT CO.
P.O. BOX 733 SILVERSPRING, MARYLAND, U.S.A.

Scintillation Counters

A new fluorescent glass developed by the British Scientific Instrument Research Association for scintillation counters is available in experimental quantities from:

LEVY WEST LABORATORIES. LTD.
WEMBLEY HILL ESTATE – WEMBLEY
MIDDLESEX — ENGLAND

NORTH-HOLLAND BOOKS

Paul Ehrenfest

COLLECTED SCIENTIFIC PAPERS

XII + 632 pages

Guilders 45,00 (90s.)

This volume makes widely scattered publications readily available. All Dutch articles appear here in English; the German publications are in the original language.

Sole Agency for U.S.A.:
Interscience Publishers Inc. — New York
NORTH-HOLLAND PUBLISHING COMPANY - AMSTERDAM

Carbotrimètre®

for the dosing of low-energy β-emitters in liquid scintillators (^{3}H, ^{14}C, ^{35}S ^{45}Ca, etc...)

* ***Minimum detectable energy level:***
10 KeV

* ***Detection efficiency:***
(a) 5% for tritium-treated water
(b) 10% for non-polar tritium-treated molecules
(c) 50% for carbon-14

* ***Sensitivity:***
(a) detection limit for tritium: 2.10^{-10} curies in 15 min.
(b) detection limit for carbon-14: $1.5.10^{-11}$ curies in 15 min.

* ***Random coincidence*** (with scintillator)
< 50 i.p.m. (within 3–60 v range)

* Measuring time presettable from 10 seconds to 16 hours

* Provision for analysis in two ranges sharing common threshold

Electronic circuit comprising:
—2 preamplifiers and 2 amplifiers (overall gain: 1,500—rise time: 0·06 microsecond)
—1 coincidence selector (resolution time: 0·2 microsecond)
—1 2-band pulse-height selector (variable 3 to 100 v).

LE Belin

licence C.E.A.

LABORATOIRE INDUSTRIEL D'ELECTRONIQUE BELIN
296, Avenue Napoléon-Bonaparte - RUEIL-MALMAISON (S & O) FRANCE
Téléphone : 967-15-54 - Câbles : BELINUSINE-RUEIL

® Registered Trade Mark

a Complete Scintillation Service

phosphors and counters

PLASTIC, LIQUID AND CRYSTAL PHOSPHORS

* PLASTIC PHOSPHOR NE 102, light output 65% anthracene, available in all sizes and shapes up to one ton, in thin sheet form, in fine tubes for the construction of scintillation flow counters, or as filaments for the construction of scintillation nuclear track chambers.
* BORON POLYESTER PLASTIC PHOSPHOR NE 400 and NE 401 (88% B^{10}) for neutron detection. Standard sizes from 0.5 to 5.0 inches diameter.
* SCINTILLATION CHEMICALS of highest purity P.B.D., POPOP, T.P.B., p-terphenyl, PPO, D.P.H., alpha-N.P.O., D.M.C., B.B.O., B.P.O., D.P.A., D.P.S., vinyltoluene, styrene, xylene, toluene, methyl borate, phenylcyclohexane, monoisopropylbiphenyl.
* SCINTILLATION CRYSTALS by Harshaw. Exclusive concessionaire in Great Britain for NaI(Tl), CsI(Tl), LiI(Eu), and Li^6I(Eu). NaI(Tl) available in sizes up to 9″ diameter x 9″thick, and down to 0.015″ thick with 0.005″ Be windows for X-ray counting and spectrometry. Resolution with standard sizes 7–8% on Cs^{137} line. CsI(Tl) down to 0.005″ thick for alpha and proton studies. Li^6I(Eu) in special low temperature mounts for fast neutron spectrometry.
* NEW! Photomultiplier-NaI(Tl) combinations with direct coupling of crystal to photomultiplier and giving improved resolution.
* LIGHT PIPES * SCINTILLATING GELS
* SPIRAL FLOW CELL NE801 * LOADED LIQUID SCINTILLATORS

Write now for Bulletins and Price List

Nuclear Enterprises (G.B.) Ltd.

BANKHEAD MEDWAY, SIGHTHILL, EDINBURGH 11, SCOTLAND. (TEL. CRA 5262)

Associate Company: Nuclear Enterprises Ltd., 1750 Pembina Highway, Winnipeg, Canada.

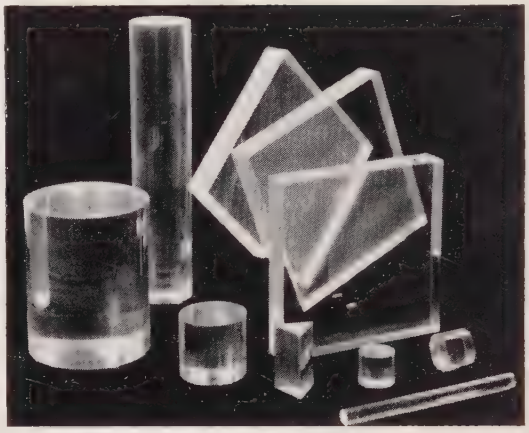

PRECISION NUCLEAR INSTRUMENTS

* Non-overloading Linear Pulse Amplifier NE 5202 of the Fairstein type.
* Pre-Amplifier and Cathode Follower NE 5202A.
* Single Channel Pulse Height Selectors NE 5102 and NE 5103.
* Shielded Scintillation Head Units NE 5501-3.
* Highly Stabilised EHT Supplies NE 5302 (1.5 kV) and NE 5303 (5kV).
* Complete assembly for C14 and tritium counting NE 8301.
* Complete Human Body Monitors and low level counting facilities.
* Ratemeter NE 5401 with six ranges and five time constants.
* Scanning scintillation spectrometer NE 8601.
* C.D.C. 100 Channel Transistorised Kicksorter

ndh 1408X

NORTH-HOLLAND BOOKS

TURNING POINTS IN PHYSICS

A
Series of Lectures
given at
Oxford University
in
Trinity Term 1958

1959 5 × 7½″
viii + 192 pages
Guilders 10.50
20s.

by
R. J. BLIN-STOYLE
D. TER HAAR
K. MENDELSSOHN
G. TEMPLE
F. WAISMANN
D. H. WILKINSON

with an introduction
by
A. C. CROMBIE

Sole Agency for U.S.A.: Interscience Publishers Inc. – New York

NORTH-HOLLAND PUBLISHING COMPANY — AMSTERDAM

★ DIGITRON

TYPE DISPLAY

NOW MINIATURISED

FOR INSTANTANEOUS CLOSE-RANGE READOUT

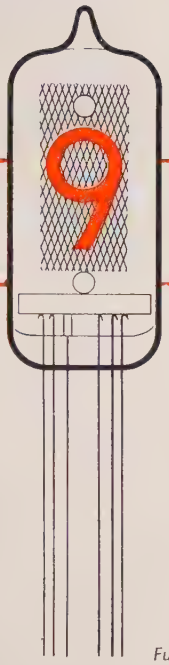

Full Size

THE GR. 10. W

In many digital applications it is often wasteful of valuable equipment space to employ the larger types of numerical indicators. The equipment design may call for a much more personalized type of display such as that required for control consoles, desk equipments, and similar layouts.

It is with these applications in mind that we introduce a newcomer to the DIGITRON range.

Whilst retaining the basic construction of the standard GR.10.G numerical indicator tube, the GR.10.W, being wire ended, can be soldered directly into the circuit and enables the designer to make full use of the display area by mounting these miniatures immediately adjacent to each other. This represents a considerable improvement in the readout facility at close range.

Like previous DIGITRONS, the numerical design of the GR.10.W is "human engineered" to eliminate readout error and again numbers are visible over wide viewing angles.

The miniature side-viewing GR.10.W with its robust construction, vivid presentation and its "no base" facility represents a big step forward in miniature display techniques.

OTHER SIDE-VIEWING DIGITRONS INCLUDE:

DIGITRON GR.2.G

Designed to display "plus" or "minus", this tube will find many applications in digital equipments requiring unambiguous sign display.

DIGITRON GR.10.G

The original DIGITRON—providing a clear numerical readout up to 50 feet over wide viewing angles. Ideal for audience readout.

DIGITRON GR.4.G

A recent introduction to the DIGITRON range, the GR.4.G displays $\frac{1}{4}$, $\frac{1}{2}$, $\frac{3}{4}$, or 1 in vivid numbers styled for easy readout. Suitable for applications concerned with monetary display.

May we send you full information on the DIGITRON range of display tubes. Write to: TECHNICAL SERVICE DEPT.

Full Size

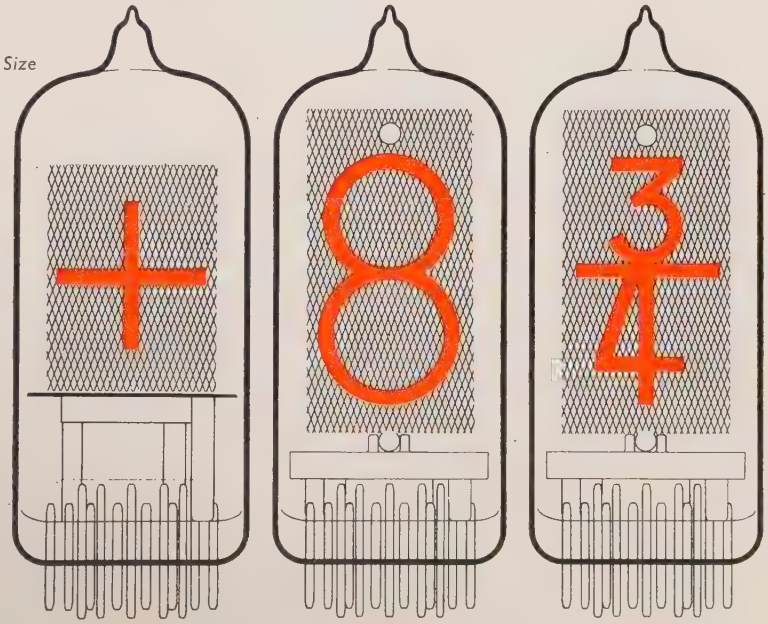

GR.2.G GR.10.G GR.4.G

ETELCO

TUBE DIVISION

BEESTON, NOTTINGHAM

T E L ENGLAND

★ *Digitron is an Ericsson trade mark*

ETELCO LIMITED · HEAD OFFICE · 22 LINCOLN'S INN FIELDS LONDON W.C.2

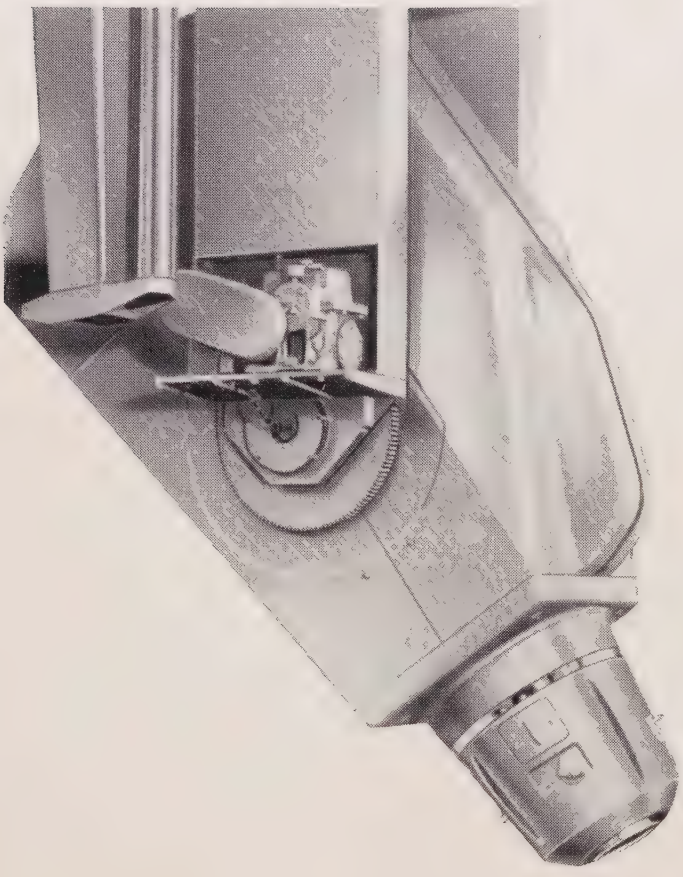

electron linear accelerators for research, industry and medicine

by Mullard Equipment Limited

Electron Linear Accelerators manufactured by Mullard Equipment Ltd. are the logical result of wide and detailed experience in this field. Machines for all types of applications are available, from the standard 4.3 MeV model to equipments specially built to meet individual requirements with electron beam energies up to 50 MeV.
The units are designed for continuous operation, ease of control and high reliability.

STANDARD MACHINE OPERATING AT 4.3 MeV

Mean power output at 500 pulses per second	850 W (electrons)
Maximum pulse repetition frequency.....	500 p.p.s.
Electron pulse length.....	1.65 microseconds
When used as an X-Ray source maximum X-Ray output is approximately.....	600 röntgens per minute at 1 metre

MULLARD EQUIPMENT LIMITED

Mullard House · Torrington Place
London W.C.1 · Tel: LANgham 6633

RESEARCH Now regarded as indispensable in many research laboratories Linear Accelerators can be fitted with supplementary heads to provide X-Rays or neutrons. Present day applications include investigation of properties of irradiated materials; preservation of food; basic studies on structure of organic molecules; modification of the properties of plastics.

INDUSTRIAL RADIOGRAPHY The compact accelerator design with wide range of movements and precision positioning enables radiographs of complicated heavy metal sections to be taken with minimum setting-up times. The high X-Ray output gives short exposure time and the extremely small (2mm) focal spot gives the highest possible definition. Penetration is sufficient to radiograph steel sections up to 12 inches thick.

MEDICAL THERAPY The use of Linear Accelerators for X-Ray and Electron Medical Therapy is well established. These machines give rapid treatment times with precisely defined fields and negligible 'penumbra' effects. Skin and exit dosages are minimised.

ME 664

STANDARD FUNCTIONNAL UNITS . . .

FRENCH ATOMIC ENERGY COMMISSION SYSTEM

. . . master-key to nuclear instrumentation

Standard functional units are assembled in cabinets in order to be used as complete assemblies : scales for counting, amplitude selectors, ratemeters, etc...

REGISTER UNIT TYPE TND.1
Function :
counting (registering)
Dekatron divider

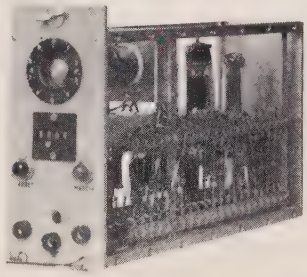

TIMER UNIT (SLOW RESPONSE)
TYPE TAL.2

Intended for automatic pre-set counting

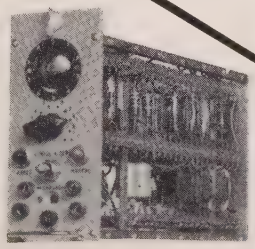

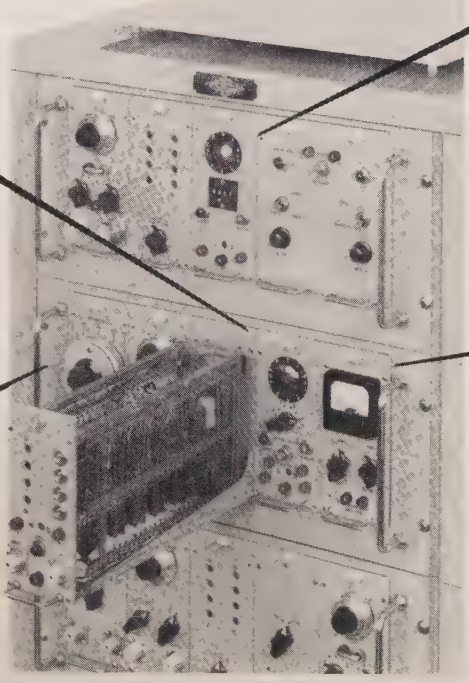

VERY HIGH TENSION UNIT

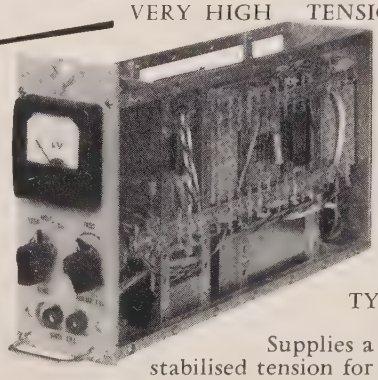

RATEMETER TYPE TIS.1
supplies a tension or a current proportionnal to the number of counts received

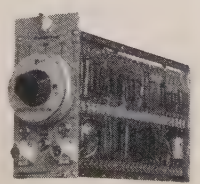

TYPE THT.4

Supplies a very high stabilised tension for detectors, pre-amplifiers

L'ÉLECTRONIQUE APPLIQUÉE

96/100, rue Maurice Arnoux • MONTROUGE • ALE 45-20, 83-20
25, rue du Docteur Finlay • PARIS 15e • TÉL. SÉGUR 14-75

The place of the Particle Accelerator in Basic Research...

Radiation Effects on Microorganisms — X

The inactivation or "killing" of microorganisms, by use of penetrating ionizing radiation from particle accelerators, has many commercial applications in food preservation and sterilization of drugs and medical supplies. One such application, the sterilization of sutures, is now being successfully carried out with a HIGH VOLTAGE microwave linear accelerator by Ethicon, Inc. Allied programs are under study by Massachusetts Institute of Technology, Army Quartermaster Corps, and other organizations using Van de Graaff accelerators. Much research, however, remains to be done on specific effects, radiation controls, and dosimetry.

Microbiological Factors

In terms of specific energy inputs, microorganisms are much more sensitive to ionizing radiation than to heat. With radiation, then, the energy requirements are lower than are the corresponding *thermal* needs for the same lethal effect. A sterilizing dose raises the temperature of the sample only a few degrees, even when that dose is administered in a fraction of a second without heat removal.

Various types of organisms respond differently to radiation. In fact, considerable differences may occur among the members of any one group of microorganisms. The survival curve of a strain is usually an exponential function of the dose. Therefore, the number of survivors at any dose is directly related to the original population of organisms. Also, complete kill can never be achieved, regardless of dose, in a large sample. These facts are not peculiar to the action of ionizing radiation. They seem to follow a law of nature. Thus, sterilization by any method is an arbitrary choice of a safety factor, which depends upon the degree of reduction, or "kill", desired, and on the original contamination.

Form ●	Maximum Energy Units for Lethal Dose (Rads)
Man and animals	1,000
Sprouting tissues	10,000
Insect eggs	100,000
Adult insects and parasites	200,000
Non-spore-forming bacteria	500,000
Yeasts and molds	1,000,000
Spore-forming bacteria	2,000,000

Relative Radiation Sensitivity of Organisms for Inactivation

The variation in lethal dose for different organisms is shown in tabular form on this page. The more complex forms of cell organization are included to emphasize their higher sensitivity to radiation. The total range of response from "least sensitive" to "most sensitive" is more than 2000-fold.

The environment of microorganisms also influences survival. A food medium is protective against destruction, in comparison with a simple nutrient broth containing an organism. Removal of oxygen also increases resistance, as does freezing prior to irradiation. On the other hand, the rate of administering radiation dose, which can vary more than a thousand-fold among various radiation sources, does not seem to affect bacterial resistance.

Chemical Changes

Irradiation produces other effects, because chemical bonds are broken and reformed. For instance, while total chemical changes in irradiation-sterilized food are calculated to be well below 1% under the most unfavorable conditions, flavor and odor changes are often noticeable. They are progressive with dose, and thresholds are apparent.

Little is known quantitatively about these effects. Like microorganisms, the various chemical components differ in their sensitivity to radiation. An indirect effect can take place with energy transfer from one molecule to another. In this way, minor components are affected, and new compounds can be formed.

Van de Graaff Accelerators

Among other interesting research being conducted with Van de Graaff® electron accelerators is that to determine whether individual cell survival in a microbial population subjected to a lethal radiation dose resulted from spontaneously occurring mutants.* The results indicate that radiation resistance is not built up in the bacterial strains studied.

The Van de Graaff accelerator is particularly suited to research in the effects of radiation on microorganisms. Since both the particle energy and the beam current are easily varied and accurately controlled over a wide range, precise and reproducible doses can be obtained with these machines. *Brochures describing available accelerators and their capabilities, as well as technical reports and reprints on the biological effects of radiation, are available upon request.*

*Koh, Morehouse, and Chandler; (1956) *Applied Microbiology*, 4, 153

HIGH VOLTAGE ENGINEERING CORPORATION

BURLINGTON MASSACHUSETTS

High Voltage Servicing Company, Ltd.
London, England

High Voltage Engineering (Europa) N.V.
Amersfoort, The Netherlands

NUCLEAR INSTRUMENTS AND METHODS 7 (1960) 1–10; NORTH-HOLLAND PUBLISHING CO.

APPARATUS FOR THE INVESTIGATION OF HEAVY ION INDUCED REACTIONS†

CARL E. ANDERSON, ARTHUR R. QUINTON, WILLIAM J. KNOX and ROBERT LONG

Yale University, New Haven, Conn.

Received 20 November 1959

An integrated system for studying nuclear reaction mechanisms is described, including detection and identification of particles, and analysis and storage of data. Reaction products ranging from protons to fission fragments are identified and their energies are measured. Observations are made with 1° angular resolution at any angle from $8\frac{1}{2}°$ to $171\frac{1}{2}°$. Without loss of vacuum the detectors may be moved or calibrated and the target may be changed. By a combination of photographic recording and multichannel analysis, products with cross-sections ranging down to fractions of a millibarn can be measured in the presence of products having large cross-sections. Examples are shown of spectra of protons, alpha particles, fission fragments and fragments ranging from lithium to magnesium produced by heavy ion bombardment.

1. Introduction

When heavy ions with energies as high as 10 MeV per nucleon are used as projectiles for nuclear reaction studies, one is presented with a bewildering assortment of products. Even if the neutrons, photons and beta rays can be ignored, it is necessary to consider the emission from the target of particles ranging in mass from fission fragments to protons. Deuterons and tritons[1]) may be produced in significant quantities. It is known that alpha particles[2]) are emitted and He^3 may be a completing evaporation product[3]). There will be elastically scattered heavy ions and a great variety of similar particles produced in direct interactions. Radiochemical studies have already shown that reactions described as stripping[4]), pick-up[5]), transfer[6]) and spallation[7]) will be of interest.

A particle detector for reaction studies under these circumstances must be capable of identifying the particle as well as measuring its energy. At the same time it must be capable of measuring a wide range of energies, for the protons emitted in evaporation processes range in energy from 2 MeV to 40 MeV depending on the target and angle of observation.

For energy measurements we have used a thallium activated cesium iodide crystal. The pulse height from such a system determines the energy of the particle only if the particle has been identified also. In this connection the response of CsI(Tl) to a variety of energetic particles has been measured and reported elsewhere[8]).

Particle identification can be achieved by simultaneously measuring another property besides energy. Momentum or range could be measured, but taking data in this way would be laborious. Instead, the energy loss per unit path (dE/dx) has been used and for this purpose the sensitivity and versatility of the proportional counter have been exploited. This choice means, in addition, that one has available a counter of fair resolution for energy measurements of short range particles. We have examined heavy ion induced fission with this counter. Again the

† This work was supported by the U. S. Atomic Energy Commission.

[1]) A. Zucker, Nuclear Physics 6 (1958) 420.

[2]) D. M. Parfanovich, N. V. Rabin and A. M. Semchinova, Soviet Physics JETP 4 (1957) 99.

[3]) I. Dostrovsky, P. Rabinowitz and R. Bivins, Phys. Rev. 111 (1958) 1659.

[4]) T. Sikkeland, S. G. Thompson and A. Ghiorso, Phys. Rev. 112 (1958) 543.

[5]) R. Kaufman and R. Wolfgang (private communication).

[6]) M. L. Halbert and Z. Zucker, Phys. Rev. 108 (1957) 336.

[7]) S. A. Barabushkin, A. S. Karamian and G. N. Flerov, Soviet Physics JETP 5 (1957) 1055.

[8]) A. R. Quinton, C. E. Anderson and W. J. Knox, Phys. Rev. (in press).

range of the measurements over which the system must be able to work is very great, since the energy loss per unit path of 40 MeV protons and 80 MeV fission fragments differ by more than two orders of magnitude.

The cross-sections for the processes to be studied are likely to vary from fractions of a millibarn to barns, so one must carefully consider the handling and display of the data from the counters measuring E and dE/dx. It has been found that a combination of photographic and multi-channel analysis techniques permit measurement of cross-section over a wide range of values.

To understand the nuclear reactions that have been mentioned, it is also necessary to determine the angular distribution of the reaction products. For this purpose we have constructed a versatile reaction chamber which allows detection of particles from $8\frac{1}{2}°$ to $171\frac{1}{2}°$, with approximately 1° angular resolution.

This combination of reaction chamber, particle detectors and methods of recording data should be of general interest in studies of nuclear reaction mechanisms.

2. The Reaction Chamber

A sketch of the reaction chamber is shown in fig. 1. It is constructed from 1″ thick aluminum plate. The cylindrical section was rolled to an inside diameter of 24″ and seam welded using heliarc techniques. This section was then machined to obtain parallel ends and circular cross-section. The bottom vacuum seal is of the static ○-Ring type but the top seal allows rotation while vacuum is held to 10^{-5} mm of Hg. This was achieved by the use of Teflon strips as bearing material, making use of its property of lower coefficient of friction under load. The Teflon strips were manufactured by wrapping an 8 foot length of $\frac{1}{16}$″ thick sheet around a 4″ diameter mandrel and then parting off strips of the proper dimension. The strips were then inserted into the grooves as shown in the sketch and the ends shaped to make a 30° lap joint. The large ○-Ring was fabricated from 3 commercially available rings butt-jointed with Pliobond Cement and cured while held in a simple jig. Under vacuum the ○-Ring is compressed by approximately 0.010″. However, it may be of interest to note that a fairly good vacuum ($\approx$ 50 microns) can be obtained with the Teflon bearing alone acting as vacuum seal.

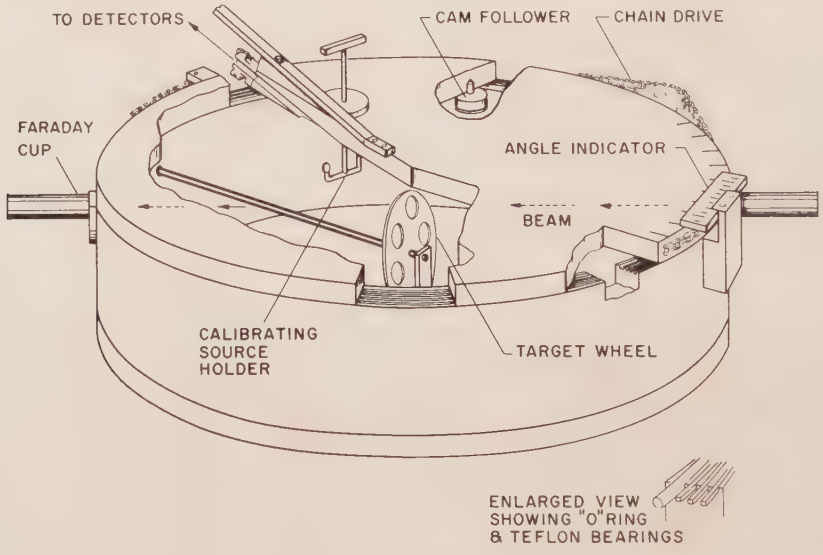

Fig. 1. Scattering chamber.

Rotation of the upper lid is achieved by means of the chain drive, using six needle bearings (cam followers) equally spaced on a 23″ diameter circle to define the axis of rotation. A ten to one

reduction worm and gear are used to facilitate turning by a hand crank. Indeed, surprisingly little torque is required to rotate the lid.

A six-hole target wheel is mounted inside the chamber and can be rotated from the outside by means of a $\frac{1}{4}''$ diameter shaft and ○-Ring seal, to allow change of target without loss of vacuum.

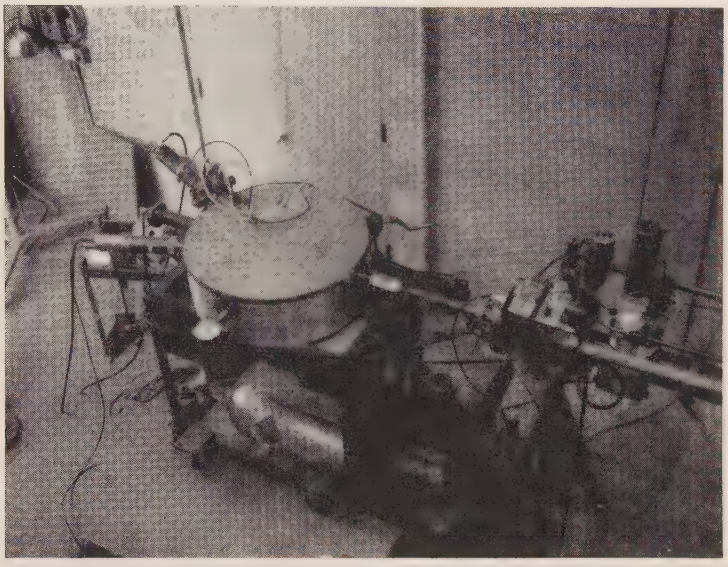

Fig. 2. Photograph of chamber and associated equipment connected to the Heavy Ion Accelerator.

The wheel is set at 45° to the beam axis and is placed so that the thin target is on the intersection of the beam axis, the center of the chamber and the line of sight of the particle detectors. The reaction-particle path to the detectors is defined by a $\frac{1}{2}''$ diameter hole bored through the edge of the top lid at an angle of $8\frac{1}{2}°$ to the lid surface. The entire path to the detector is free of windows to allow measurement of very short range particles.

Angular divisions are marked on the top plate every five degrees and by use of the lucite plate marked in degrees, the observation angle can be set to within $\frac{1}{5}$ of a degree. As the detector describes a cone about the target, the true laboratory angle is obtained from the relation $\cos\theta = \cos 8.5° \cos\phi$, where ϕ is the angle indicated on the plate.

Targets are mounted on the six-hole rotatable wheel with one hole left blank as a check on background problems. Frequent calibrations of the detectors are made by raising a source of alpha particles (ThC, ThC′) into the particle path in the top plate. As an additional refinement to enable detection of protons and alpha particles at small angles, an aluminum foil can be interposed between the target and the detectors to stop the overwhelming number of elastically scattered beam particles.

The entire apparatus including reaction chamber, counter gas system, power supplies, detectors, and monitoring counters is mounted as shown in fig. 2 (Photograph). We have found that only about an hour is required to connect to the linear accelerator.

3. The Proportional Counter

A simplified drawing of the proportional counter is shown in fig. 3. It is made of brass, with hard-soldered feed-through high-voltage terminals, and is assembled with standard neoprene ○-Ring vacuum seals. The outer shell is at ground potential while the anode, a 5 mil phosphor bronze wire, can be maintained at voltages at least as high as 2 kV. This anode is mounted centrally on the long axis of the counter which is essentially a $2'' \times 1'' \times 1''$ box.

Particles can enter the counter through a thin window held between two gridded plates with ○-Ring seals. At times aluminized $\frac{1}{4}$ mil mylar has been used, but the most useful material

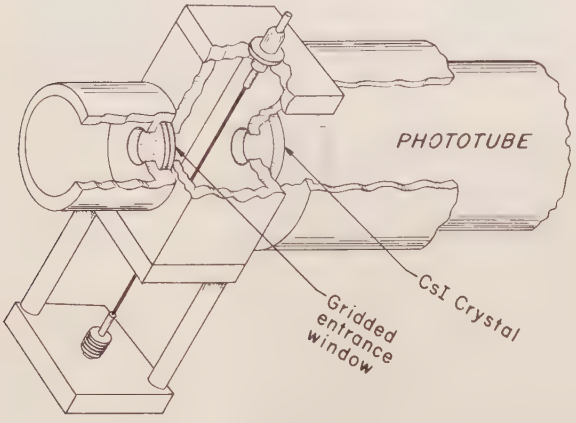

Fig. 3. Proportional counter and CsI scintillator mounting.

found to date has been nickel of nominal surface density 500 μg/cm^2. Such a window can be used when detecting fission fragments and because of its low absorption is helpful at all times in minimizing the low energy cutoff of the system. The gridding has about 75% transmission and consists of closely packed No. 55 drill holes. With two gridded plates it is found that the pressure difference across the window can be positive or negative without ruptures developing.

the anode wire. This simplifies construction, means that signals can be taken out of the counter conveniently and further ensures that to a good approximation all particles pass through the same electric field. With the high voltage off, calibrating pulses can be coupled to the system via the normally unused feed thru insulator. On the wall opposite to the gridding structure is a $\frac{1}{2}$" hole behind which a cesium iodide crystal is mounted, with appropriate ○-Ring seals. This hole is small enough to minimize field distortion, but large enough so that any particle entering the proportional counter from the target can strike the scintillator if it has sufficient range. To obtain stable counter operation, we used a continuous gas flow system with manostat pressure regulation. Typical results using commercially available counter gas (90% argon, 10% methane) are shown in fig. 4. This technique avoids the usual gain changes associated with a sealed counter due to small leaks and outgassing of the counter walls.

Depending on the experiment, pressures between 15 cm and 60 cm of mercury are used. Measurements with low energy alpha particles show that the counter gas and air are closely similar in absorption properties, and this means that the gas path is equivalent to 1 mg/cm^2 of aluminum when the counter pressure is 15 cms

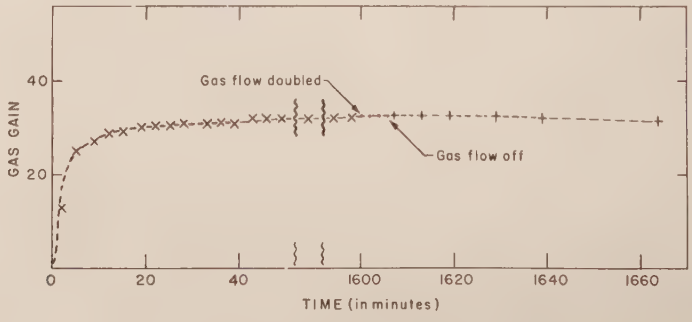

Fig. 4. Gas gain of proportional counter vs time.

Because of the square cross-section of the counter, the length of the path of all particles passing through is constant except for a negligible effect due to the finite acceptance angle. The particles move perpendicularly to

of Hg. Fig. 5 shows gas gain versus counter voltage for three useful pressures.

A source of ThC, ThC′ alpha particles is used for routine checks and calibrations of both the gas counter and the scintillator. It is well

known that the resolution in a dE/dx counter cannot be calculated on the basis of the random fluctuations in the number of ion pairs created

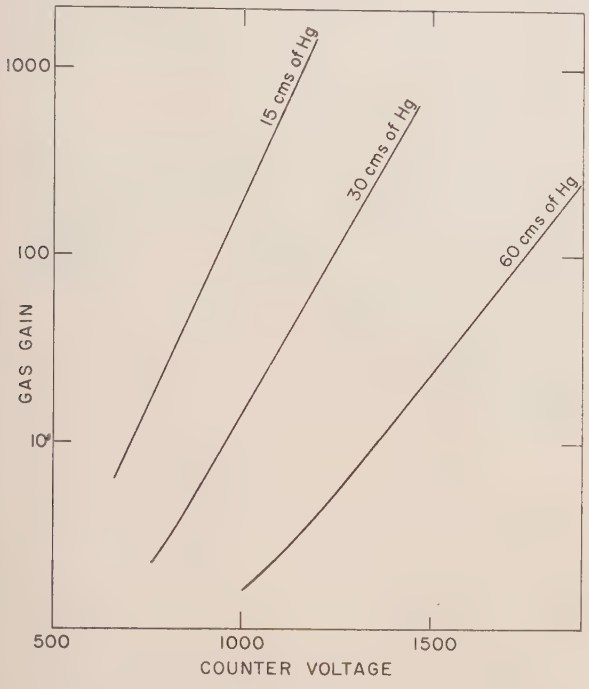

Fig. 5
Gas gain of the proportional counter vs counter voltage

by the passage of the particle. This is because a few delta ray events occur, in which comparatively large amounts of energy are lost, and the fluctuations about the average of this small number are the dominating factor as far as resolution is concerned. Hence for a thickness of matter Δx, one expects an energy loss $\Delta E \pm \Omega$ where the mean square deviation is given approximately by $\Omega^2 = 4\pi Z_i^2 e^4 NZ\Delta X$.

In this equation[9]), derived by Bohr, NZ is the number of electrons per unit volume of the stopping material, $Z_i e$ the charge on the incident ion and Δx is the path length. We find that we approach the theoretical resolution, calculated by using the above straggling equation, within 50%, for incident particles ranging from protons to oxygen ions. It is of interest to note that Ω does not depend upon the energy of the particle. Experimentally, this prediction is verified as shown by the constant width of the oxygen curve, for example, in fig. 11. Further, using natural alpha particles, we have observed that the resolution $2.8\,\Omega/E$ is inversely porportional to the square root of the gas pressure in the proportional counter, again in agreement with the theory. Fig. 6 shows the resolution of the proportional counter when operated at 61 cm Hg, 1150 volts, to the α particles from ThC, ThC'. The energy loss is 2.3 MeV for the 6.1 MeV α and 1.6 MeV for the 8.8 MeV α.

One serious limitation of the proportional counter for use with a pulsed accelerator is its inherent long recovery time. This property causes a lowering of the gas gain of the counter when a high counting rate or a high background of low energy events cause sufficient space charge in the counter to lower the wire potential. This effect is most easily observed by changing the intensity of the accelerator beam while measuring the dE/dx of elastically scattered

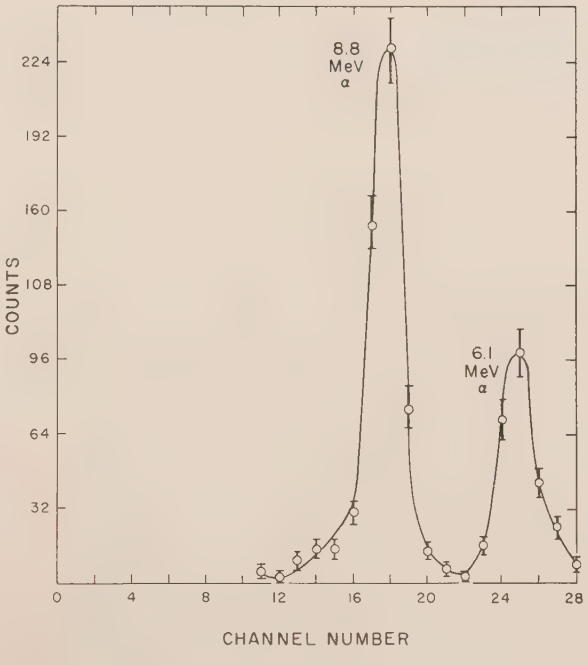

Fig. 6
Pulse height response of proportional counter used as a dE/dx detector for the alpha particles from ThC and ThC'.

particles. For the particular case of an oxygen beam bombarding a gold target with a gas gain of more than twenty, we find that more than a

[9]) Experimental Nuclear Physics, E. Segrè, Editor, Vol. I (John Wiley and Sons, Inc., New York, 1953) p. 242.

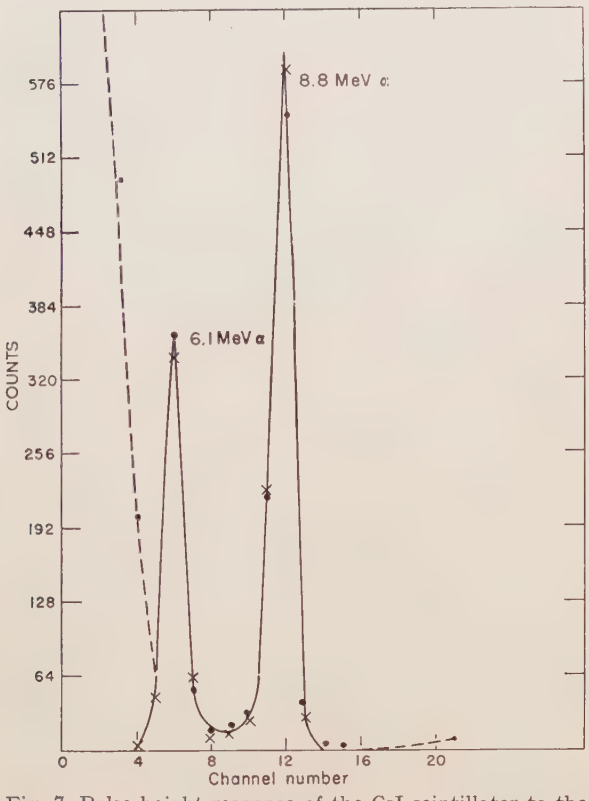

Fig. 7. Pulse height response of the CsI scintillator to the ThC and ThC′ alpha particles.

few counts during a two millisecond beam burst lead to loss of counter resolution which is ascribable to changes in gas gain. To minimize this effect, the gas gain is set as low as possible and the particle counting rate is maintained below that at which resolution changes are noticed.

4. The Scintillation Counter

A cesium iodide (thallium activated) crystal was used solely for its lack of hygroscopic properties and the resultant ease of handling. The pulse height was found to be insensitive to cleaning procedures. We used toluene to remove silicone oil and vacuum grease, and then polished the crystal with a soft tissue. As a moisture seal was unnecessary, the bare crystal formed the end wall of the proportional counter. The crystal thickness was $\frac{1}{16}''$ in order that the most energetic protons, expected to be emitted in evaporation processes, could be stopped. The crystal was light coupled to a RCA 6342A phototube by a $\frac{1}{2}''$ lucite light pipe. Fig. 7 shows the resolution of the crystal for the α particles from ThC, ThC′ which is used as a calibrating source.

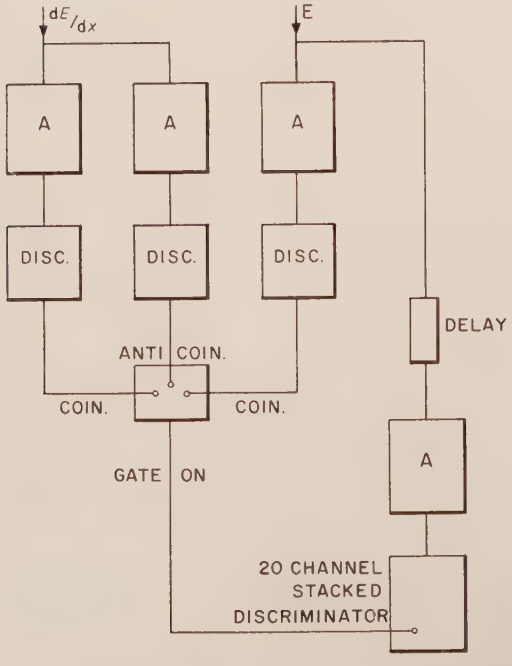

Fig. 8a

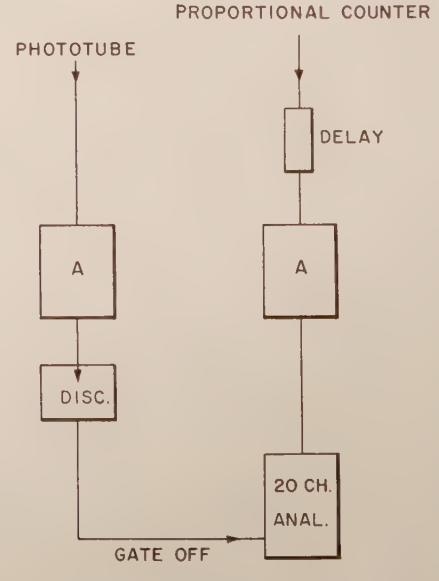

Fig. 8b

Fig. 8. Block diagrams of Multichannel Analyzer system in (a) as used for observation of evaporation spectra and in (b) as used for study of fission fragment spectra.

5. Data Recording

Two data handling systems are presently in use. One is a fast stacked-discriminator multichannel analyzer, the other a plotting X-Y oscilloscope.

The first method is particularly adapted to the study of the energy spectra of low mass particles, but is also useful for the measurement of fission fragment energy spectra. It consists of a Baird Atomic 20 Channel Pulse-Height Analyzer and three Franklin Amplifiers (double delay line clipped), each with internal single channel pulse height analyzers. The block diagram of the circuits is shown in fig. 8a. The anticoincidence amplifier is used to extend the ten volt maximum window of the Franklin analyzers. With the addition of this amplifier, the extremely large range of dE/dx pulse heights can be accommodated. By varying the dE/dx pulse height accepted to gate the 20 channel analyzer which measures the particle energy, the energy spectra of protons from 2 to 60 MeV and alpha particles from 4 to 60 MeV have been measured. Some confusion can occur in that deuterons, tritons, He^3 and He^6 may appear in one of the dE/dx windows. However, by simultaneously monitoring with the plotting oscilloscope, we can determine the relative number of these events.

For the measurement of the energy spectra of fission fragments which stop in the proportional counter, the system is rewired as in the block

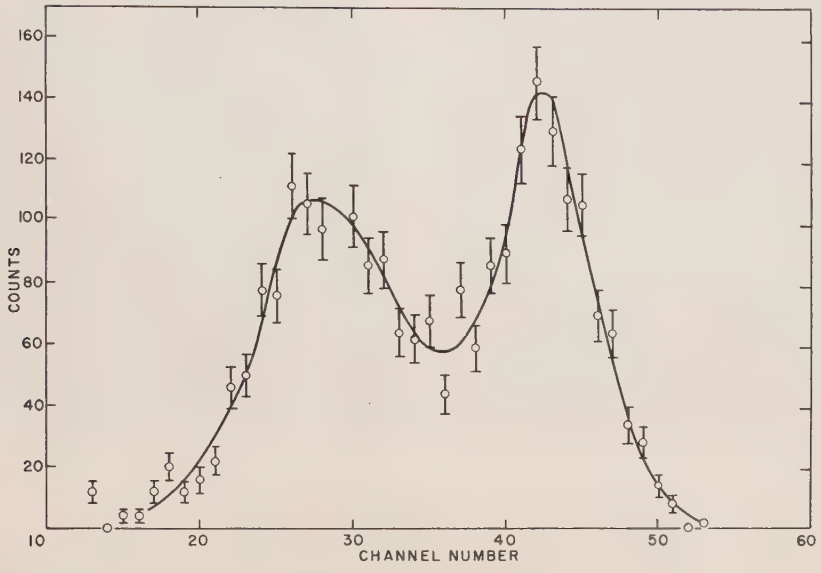

Fig. 9. Single fragment energy spectrum of Cf^{252}.

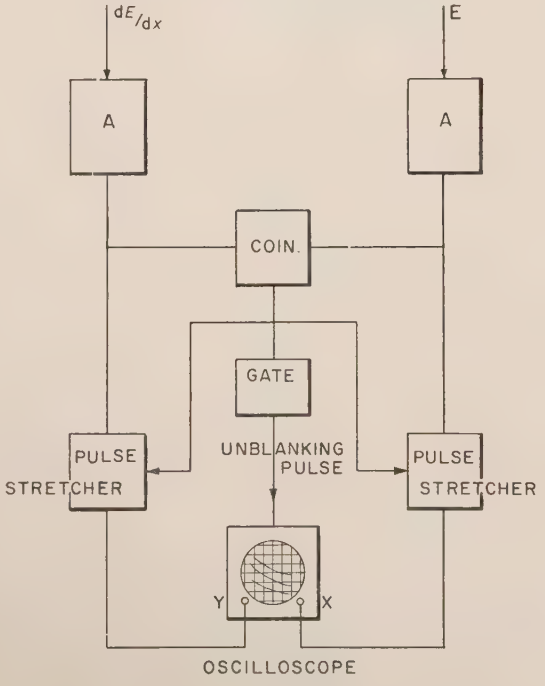

Fig. 10. Block diagram of plotting oscilloscope.

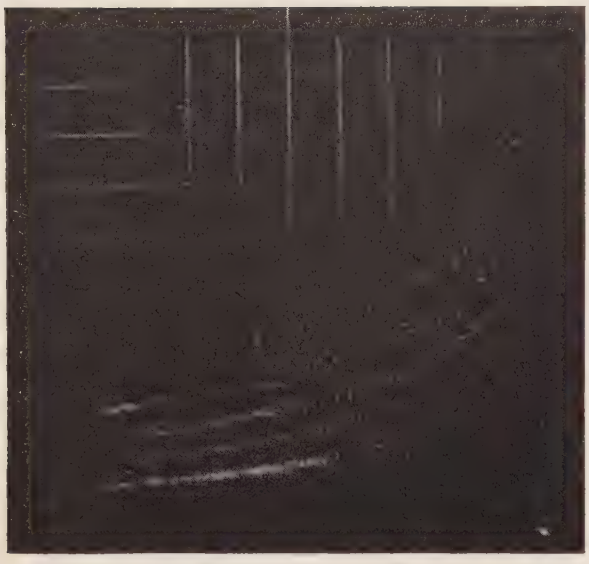

Fig. 11a

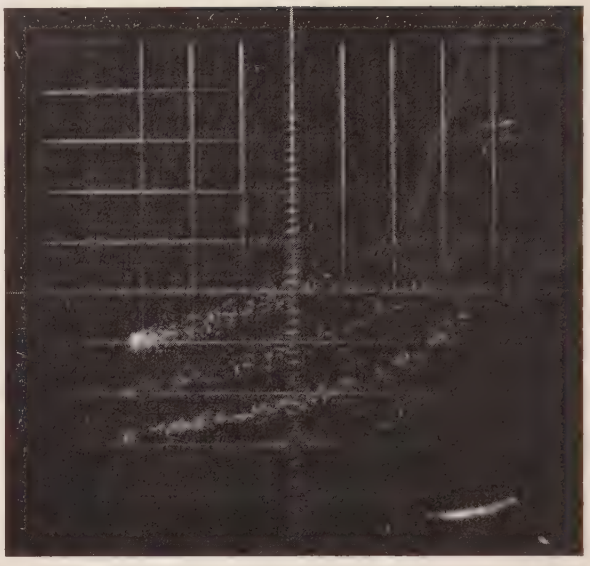

Fig. 11b

Fig. 11. Photographs of direct interaction products. The abscissa is energy increasing to the left. The ordinate is the rate of energy loss increasing toward the top.

(a) Products observed from the 160 MeV oxygen ion bombardment of aluminum at 13° 6′. The dense region on the left is the elastically scattered oxygen ions. The other curves, in order of decreasing dE/dx, are nitrogen, carbon, boron, beryllium, lithium, and only part of the helium curve shows on the lower right.

(b) Products observed from the 190 MeV fluorine ion bombardment of polyethylene at 8°30′. The dense lower curve is carbon; the others proceeding to greater dA/dx are nitrogen, oxygen, fluorine, neon, sodium and magnesium.

diagram shown in fig. 8b. Any particle reaching the CsI crystal is rejected. These particles are the products of direct interactions as well as do not reach the crystal give such small pulses, i.e. less than 5 MeV, that they do not confuse the fission spectra. Fig. 9 shows the spectra

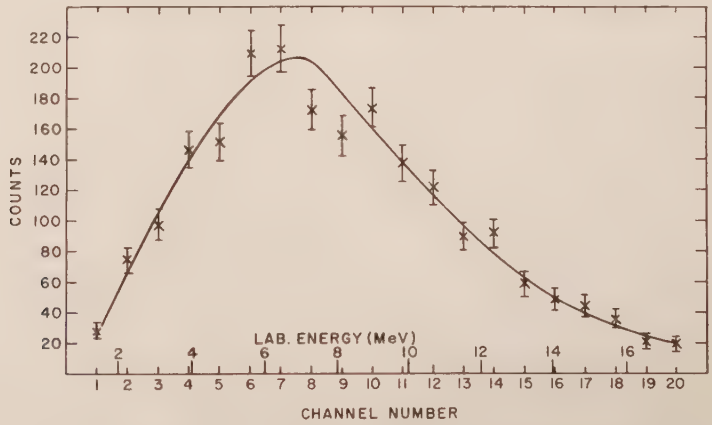

Fig. 12. Proton energy spectrum at 60° in the laboratory from the 160 MeV oxygen ion bombardment of nickel.

elastically and inelastically scattered beam particles. Low mass particles of low energy that obtained of the fission of Cf^{252}, which agrees with the data of Milton and Frazer† [10]).

† The Cf^{252} source was kindly lent to us by Arnold Friedman of the Argonne National Laboratory.

[10]) J. C. D. Milton and J. S. Frazer, Phys. Rev. **111** (1958) 877.

6. The Plotting Oscilloscope

The block diagram of the plotting oscilloscope is shown in fig. 10. The oscilloscope is a Tektronix 536 with a P-11 phosphor cathode ray tube to match the spectral sensitivity of photographic film. The camera is a Beattie Coleman approximately 1:1 camera with a Polaroid film holder. Both Polaroid Type 44 and 46L film are used. Typical photographs are shown in fig. 11. Each spot represents a detected particle. Its location on the photograph is determined by its energy and its rate of energy loss. Each curved line represents particles of the same Z, since dE/dx is approximately proportional to MZ^2/E. This simple relationship is modified by the dependence of the pulse height response of CsI

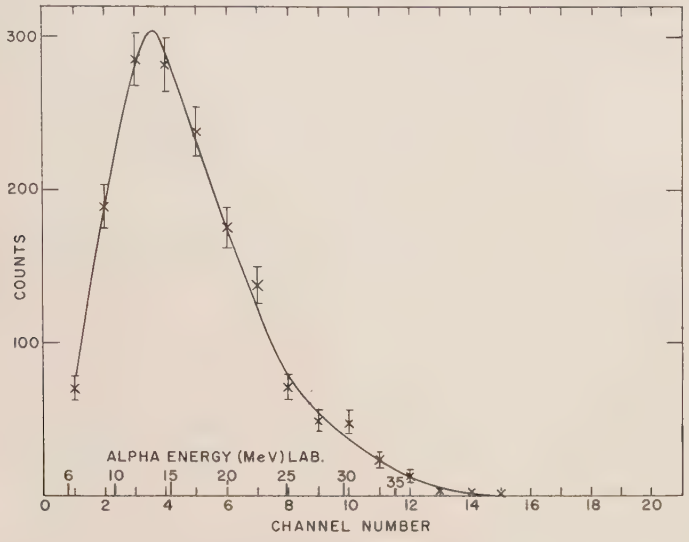

Fig. 13. Alpha energy spectrum at 60° in the laboratory from the oxygen ion bombardment of nickel.

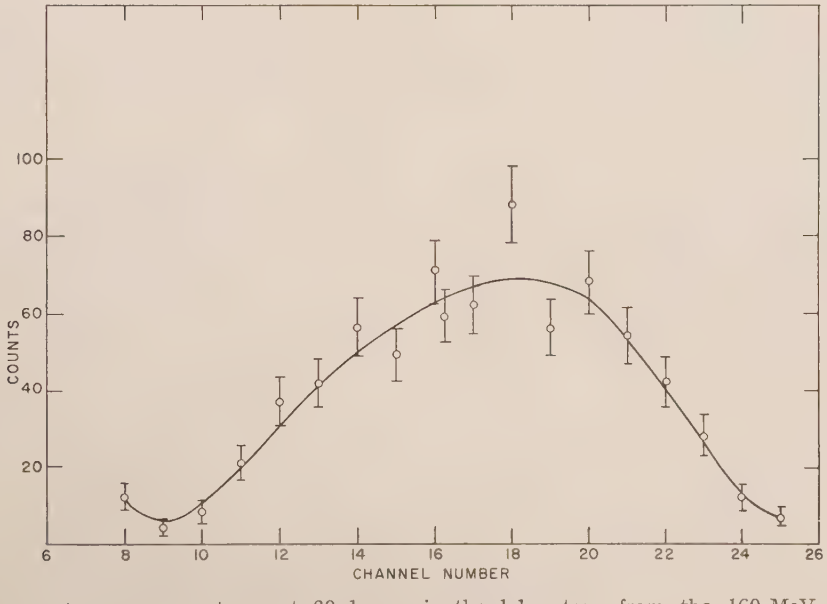

Fig. 14. Single fragment energy spectrum at 30 degrees in the laboratory from the 160 MeV oxygen ion bombardment of gold.

on the type of particle as well as nonlinearity of response, and further by the dependence of the effective charge of the particle with energy. Obviously, each curve should be further separated into particles of different mass. That this seems not to be achieved in these photographs can be due to lack of the necessary resolution, but also to the ratio of the cross-section for the production of different mass particles. This equipment is presently being used to measure the angular distribution of several different kinds of reactions. These include the evaporation spectra of protons and alpha particles from the 160 MeV oxygen ion bombardment of nickel, the fission product spectra from the gold bombarded by 160 MeV oxygen, and the spectra of particles emitted in direct interactions resulting from the gain and loss of nucleons by the bombarding particle. Examples of the data are given in figs. 11 to 15.

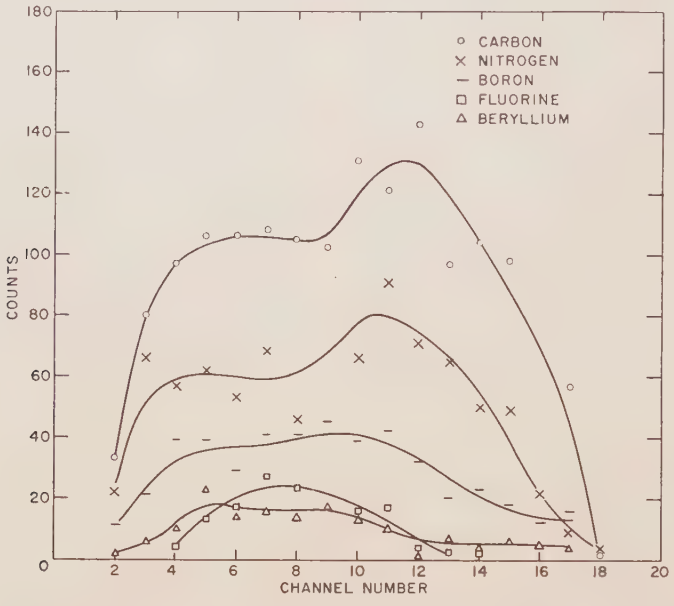

Fig. 15. Laboratory energy spectra at 17.2° of fluorine, nitrogen, carbon, boron, and beryllium ions produced by the 160 MeV oxygen ion bombardment of aluminum. Data taken from photographs limited to several hundred events each. The curve for oxygen is omitted for clarity. It closely follows the nitrogen curve.

NUCLEAR INSTRUMENTS AND METHODS 7 (1960) 11–21; NORTH-HOLLAND PUBLISHING CO.

RECENT DEVELOPMENTS OF BETA SPECTROMETERS

MILORAD MLADJENOVIĆ

"B. Kidrich" Institute of Nuclear Sciences, Belgrade

Received 13 November 1959

A review is given of recent experimental and theoretical developments in beta spectrometry. The most critical points for further development of beta spectrometers are briefly discussed. Some new proposals are also mentioned.

Although an enormous amount of data has been accumulated in nuclear spectroscopy, hundreds of decay schemes are still incompletely known. Many of the problems left can be succesfully solved only with apparatus considerably better than those now used in most laboratories. The present review was undertaken with the aim of discussing briefly the actual critical points in the development of beta spectrometers, taking into consideration the latest achievements. It is assumed that the reader is aquainted with some of the several excellent review articles on beta spectrometers[1–7]). References shall be given only for later articles, which are not covered by the review articles of K. Siegbahn[6]) and T. R. Gerholm[7]).

1. High Dispersion Spectrometers

1.1. DOUBLE FOCUSING SPECTROMETERS

The magnetic field in the median plane of the double focusing spectrometers is given by

$$H(r) = H(r_0)\left(\frac{r_0}{r}\right)^n \qquad 0 < n < 1$$

where r_0 is the radius of the equilibrium orbit. For such rotationally symmetric fields the charged particles are focalised in axial and radial directions, after the angles

$$\phi_r = \frac{\pi}{\sqrt{1-n}}\ , \quad \text{radially}$$

$$\phi_z = \frac{\pi}{\sqrt{n}}\ , \quad \text{axially}\ .$$

If we define dispersion D as

$$D = p\left(\frac{\mathrm{d}s}{\mathrm{d}p}\right)$$

we get

$$D = \frac{2r}{1-n}\ .$$

In the case of homogenous field ($n = 0$), dispersion D_h is

$$D_\mathrm{h} = 2r\ .$$

We get, therefore,

$$D = \frac{D_\mathrm{h}}{1-n}\ .$$

Since $n < 1$, this kind of field gives higher dispersions than the homogeneous field. It would be of interest to get the value of n as close to 1 as possible. The value of n depends on the choice of angles ϕ_z and ϕ_r, which must satisfy the double focusing condition. The choice is by no means unique, although the simplest one is obvious, and the only one thoroughly explored up to now. It is the type first developed by K. Siegbahn and N. Svartholm,

[1]) E. Persico and C. Geoffrion, Rev. Sci. Instr. **21** (1950) 945.
[2]) P. E. Cavanagh, Progress in Nuclear Physics **1** (1950) 140.
[3]) P. Grivet, J. Phys. Radium **11** (1950) 582; **12** (1951) **12**.
[4]) N. F. Verster, Progress in Nuclear Physics **2** (1952) 1.
[5]) R. W. Hayward, Advances in Electronics **5** (1953) 97.
[6]) K. Siegbahn, Beta- and Gamma-Spectroscopy (1955), Chap. III.
[7]) T. R. Gerholm, Handbuch der Physik **33** (1956) 609.

which is obtained when one simply puts

$$\phi_z = \phi_r$$

giving

$$n = \tfrac{1}{2}\,, \qquad D = 2D_{\mathrm{h}}\,,$$

$$\phi_z = \phi_r = \pi\sqrt{2} = 255°.56\,.$$

We shall first consider this type of spectrometer and then discuss the other possibilities.

1.1.1. *Double focusing spectrometers with* $n = \frac{1}{2}$.
The field in the median plane can be developed in a series.

$$H(r) = H_0 \sum_{s=0}^{\infty} a_s \left(\frac{r - r_0}{r_0}\right)^s .$$

The first two coefficients are fixed ($a_0 = 1$, $a_1 = -\frac{1}{2}$), while the remaining can be chosen more freely, according to adopted beam geometry and the resolution—transmission characteristics. There are three best values of coefficient a_2: $\frac{1}{8}$, $\frac{2}{8}$ and $\frac{3}{8}$. The value of $\frac{3}{8}$ makes the resolving power less sensitive to axial opening, while $\frac{1}{8}$ is less sensitive to the radial opening. The value of $\frac{1}{4}$ has also been used, but seems to be less satisfactory[8]).

From the point of view of resolution—transmission characteristics the values of $\frac{3}{8}$ and $\frac{1}{8}$ give nearly the same performances. Still $a_2 = \frac{3}{8}$ has some minor advantages[8]). Some higher order focusing terms are smaller, and it can be used as a spectrograph, focalising a part of the spectrum on the photographic plate.

From the economical point of view it appears that for iron-free $a_2 = \frac{3}{8}$ is more convenient, while the electromagnets should have relatively smaller gap for $a_2 = \frac{1}{8}$.

We should add also that in the case of wide radial aperture ($a_2 = \frac{1}{8}$), there is a possibility for larger number of lower energy electrons to arrive by trochoidal paths into the detector, and distort the spectrum.

The higher order coefficients have been calculated by several authors and are given in the table below.

There is some disagreement between the various authors in regard to the theoretical coefficients. The precise experimental evidence for the characteristics of various possibilities is still lacking, since it is difficult to construct the magnets giving the field with such a high precision.

The desired field form can be obtained either by using the iron pole-pieces or with iron-free coils.

Spectrometers with iron. The spectrometer magnets can be designed either with complete cylindrical symmetry or as sectors. The former type has been exclusively used in beta spectroscopy, while sectors are for economy reasons prefered in heavy particles work.

The most critical problems in the design of a high performance iron spectrometer are:

1. Design of the pole-piece shape to give the desired field distribution with high precision.

2. The absolute constancy of the field distribution, especially at very low fields.

[8]) G. E. Lee-Whiting and E. A. Taylor, AECL No. 381 (1956).

[9]) N. F. Verster, Physica **16** (1950) 815.

[10]) P. P. Pavinski, Izv. Akad. Nauk SSSR, Ser. Phys. **18** (1954) 227.

[11]) A. V. Zolotavin, A. M. Petrunkin and H. H. Halkiopova, Pribori i Tehnika experimenta No. 6 (1957) 27.

[12]) P. H. Stoker, Ong Ping Hok, E. F. de Haan and G. J. Sizoo, Physica **20** (1954) 337.

	a_0	a_1	a_2	a_3	a_4	a_5	a_6
Verster[9])	1	$-\frac{1}{2}$	$+\frac{1}{8}$	+ 0.0625	— 0.121		
Pavinskii-Zolotavin *et al.*[10–11])	1	$-\frac{1}{2}$	$+\frac{3}{8}$	— 0.1875	+ 0.0586		
Stoker *et al.*[12])	1	$-\frac{1}{2}$	$+\frac{5}{8}$	— 0.2083	+ 0.193		
Wild and Huber[13])	1	$-\frac{1}{2}$	$+\frac{3}{8}$	— 0.2986			
Lee-Whiting and Taylor[8])	1	$-\frac{1}{2}$	$+\frac{3}{8}$	— 0.2986	+ 0.240	— 0.2017	+ 0.1768

All the iron D.F. spectrometers published so far have more or less achieved the fit to the a_2 coefficient and not higher. Wild and Huber[13]) have proposed a design with which they aim to fit the theoretical distribution up to the a_3 coefficient.

Because of the field strength dependance of the iron permeability and because of the remanence, one could expect that the field shape should vary, especially at low fields. This problem has been studied recently by Bergkvist[14]).

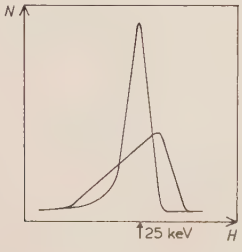

Fig. 1. The line width dependence on the remanence, as found by Bergkvist. The lower line was obtained with a nondemagnetized field.

Fig. 1 shows how seriously a line can be distorted by a remanent field. The upper line was taken with a demagnetized spectrometer, while lower

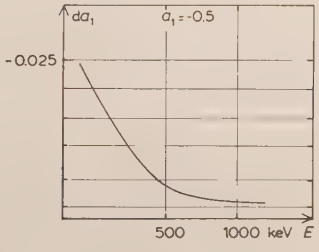

Fig. 2. The dependence of a_1 coefficient on the remanence (Bergkvist).

was obtained by first increasing the field to the strength necessary for the focalisation of 4 MeV electrons, and then measuring the 24 keV line. Measuring the continuous spectrum at the same energy Bergkvist finds that the counting rate is changed between 1.7–7% for premagnetized field, the change being dependent on the position of the shutter (7% for shutter at 157°). Bergkvist also finds that the a_1 coefficient decreases at low energies as shown in fig. 2. All these variations are perhaps not too important when working with the resolutions of the order of 1%, but when one wants to have line widths, of 0.1% and less, they may become serious and represent a definite disadvantage of iron D.F. spectrometers.

Iron-free D.F. Spectrometers. In principle, one should be able to achieve a higher degree of accuracy, and design the coils to fit the field coefficients perhaps up to a_4. There are infinitely many solutions of the coil geometry. Up to now only three different designs were used.

1. Siegbahn-Edvarson geometry which was also used by Mladjenović[15]) and the Vries[16]).

2. Moussa-Bellicard geometry, also used by Baird, Nall and Haines[17]) and, somewhat modified, by Baranov[18]).

3. Lee-Whiting, Graham[19]) geometry.

The coil geometries are given in fig. 3, while the dimensions and ampereturn parameters are summarized in table 1.

The first two types were designed to fit the coefficients up to a_2. Siegbahn-Edvardson and Moussa-Bellicard have $a_2 = \frac{3}{8}$, while Baranov is using Pavinskii field which is close to $a_2 = \frac{1}{8}$. The spectrometer constructed by Graham *et al.*[19]) was designed to fit the theoretical field up to a_4.

The critical adjustment of the field shape is much easier with iron-free spectrometers. One can look for a precise fit to the theoretical field by varying coil heights and current ratios. Thus Baranov[18]) finds that by varying the distance between the coils, he obtains the fields with $a_2 = \frac{3}{8}$, $\frac{1}{8}$ or $\frac{1}{4}$. The Siegbahn-Edvarson type is

[13]) H. Wield and O. Huber, Helv. Phys. Acta **29** (1957) 224.

[14]) K. E. Bergkvist, Arkiv för Fysik **12** (1957) 381.

[15]) M. Mladjenović, Proceedings of the Rehovoth Conference on Nuclear structure (1958); Full report shall be published in "Bulletin" of Inst. "B. Kidrich".

[16]) De Vries, Private Communication; Article on the spectrometer to be published.

[17]) Q. Baird, J. C. Nall and S. K. Haines, Bull. Amer. Phys. Soc. **3**, No. 4 (1958) 316.

[18]) V. F. Baranov, Pribori i Tehnika Experimenta No. 3 (1958) 15.

[19]) R. L. Graham, G. T. Ewan and J. S. Geiger, Bull. Amer. Phys. Soc. **4**, No. 1 (1959) 64; and private communication by R. L. Graham.

easily adjusted by shunting one of the coils with a variable resistance and measuring the line widths. Once the right turns ratio is found one has to add or substract the necessary number of turns in order to eliminate the shunt. In this way Mladjenović obtained six times narrower lines by changing from the initially designed

$$\frac{n_2}{n_1} = 4.5 \qquad \text{to} \qquad \frac{n_2}{n_1} = 5\,.$$

Due to the possibility of producing better fits to the theoretical field shapes, the iron-free double focusing spectrometers have given very high resolutions. The highest resolutions were

Graham	0.013%
Mladjenović	0.018%
Siegbahn, Edvarson	0.019%.

On the other hand the transmission of iron-free D.F. spectrometers is generally lower than with iron spectrometers, due to the difficulty of creating the right field shape in a great volume, and an uneconomical increase of coil dimensions. The maximum transmission of iron-free spectrometers is about 1%, while D.F. spectrometers with iron can go up to 3%. Iron-free spectrometers are less economical, and maximum energy which they can focalise is generally smaller than it is in the case with iron spectrometers.

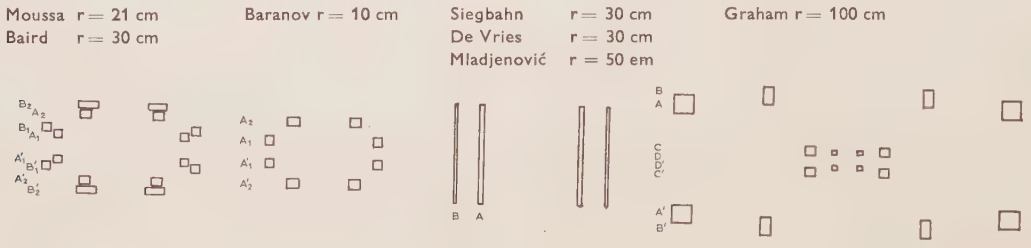

Fig. 3. Iron-free spectrometers coil geometries.

Case $n \neq \frac{1}{2}$. The dispersion can be in principle increased enormously by increasing n to a value very close to 1. The general condition for double-focusing in the field $H = H_0(r_0/r)^n$ is given by the relation

$$M\phi_r = N\phi_z$$

where M, N are whole numbers.

TABLE I

	Moussa Baird *et al.*	Baranov	Siegbahn, de Vries, Mladjenović	Graham *et al.*
Coil radii	$A_1 = 1.75\ r_0$ $A_2 = \quad r_0$ $B_1 = 2.06\ r$ $B_2 = 0.555\, r$	$A_1 = 0.953\, r_0$ $A_2 = 1.666\, r_0$	$A = 0.8\, r_0$ $B = 1.2\, r_0$	$A = 1.9756\, r_0$ $B = 0.9667\, r_0$ $C = 0.4506\, r_0$ $D = 0.1547\, r_0$
Coils distance from median plane	$A_1 = 0.35\ r_0$ $A_2 = 0.9\ r_0$ $B_1 = 0.515\, r_0$ $B_2 = 1.145\, r_0$	$A_1 = 0.366\, r_0$ $A_2 = 0.902\, r_0$	height $= 1.64\, r_0$	$A = 0.6684\, r_0$ $B = 0.7977\, r_0$ $C = 0.1279\, r_0$ $D = 0.0888\, r_0$
Turns ratio	$A_1 = 1$ $A_2 = 1.83$ $B_1 = 1.309$ $B_2 = 2.705$	$n_A/n_B = 1.827$	$n_A/n_B = 5$	$n = 1$ $n = 0.421$ $c = 0.226$ $n = 0.0429$

We obtain then from

$$M \frac{\pi}{\sqrt{1-n}} = N \frac{\pi}{\sqrt{n}}$$

$$n = \frac{N^2}{M^2 + N^2} .$$

Since dispersion is proportional to $1/(1-n)$ we get

$$D \approx \left(1 + \frac{N^2}{M^2}\right) .$$

We see that we should take $M = 1$ and increase N if we want to increase the dispersion.

Siegbahn-Swartholm field corresponds to $N = 1$. Taking $N = 2$ we get

$$\phi_r = 2.24\pi , \qquad \phi_2 = 1.12\pi .$$

Radial focusing angle is greater than 2π. The beam meets the source before the focalisation. If N is still higher the beam crosses the source and detector several times. This has the disadvantage that some beam is lost and the background is increased, especially in the presence of continuous spectrum. Lee-Whiting[20]) has treated this case theoretically and shown that no second order aberrations increase appreciably with the increase of N. He also discusses the question of continuous background.

Although the spectrometer with the beam having more than one revolution seems at first sight unconvenient, the advantages of very high dispersion are tempting. There are also possibilities to avoid the beam crossing. In mass spectroscopy where high dispersion is more important than high transmission, one can only use the radial focusing properties of fields with $n \neq \frac{1}{2}$. Then the focalisation can be achieved with a sector. The case $N = 2$ was mentioned at the Symposium on Mass Spectroscopy, held at NBS, 1951, while the first mass spectrometers of this type were built by Alekseevskii *et al.*[21]). They have built two spectrometers of 180° sectors with $n = 0.87$ and 0.89, and obtained the expected dispersion.

† A new and ameliorated version of the magnet on which prof. Kelman has been working lately, has not yet been published.

The possibility of using double focusing with $N > 1$ with the beam making less than 2π, was proposed by the author[22]). The idea is to use, more than one n value so combined to a total angle smaller than 2π. Perhaps the easiest combination is the homogenous field and a field with high N. The dispersion is then not so high as if the whole field was with N large, but it can be still much higher than for $n = \frac{1}{2}$.

If one takes for instance $n = 0.95$, it can be shown that the total angle of revolution is 237°, while the angle of the sector with $n = 0.95$ is 73°. No account was taken of the edge effects, at limits between the sector and homogenous field. It is impossible to make the pole-pieces giving exactly the theoretical field, and the next step is to see what is the effect of field distorsions at the sector boundaries.

1.2. PRISM SPECTROMETER

The only existing type of high dispersion spectrometer, which is comparable to and, in some respects perhaps, better than the Siegbahn-Swartholm type of double focusing spectrometer is the prism developed by Kelman and collaborators[23–25]). The difference between this type and most of the others is that here by analogy with optics, the dispersing and focalising field are separated. The apparatus is similar to the one of the earliest beta spectrometers, built by Klemperer, and consists of two lenses and one prism between them. The source and the counter are placed in the foci of the two lenses. The beam which comes out from the first lens is parallel and after passing through the prism gets parallel again (fig. 4).

The most critical part of the apparatus is the deflecting magnet. In order to conserve the parallelism of the beam the field has to be symmetric in the direction parallel to the edges of the pole pieces. The achievement of good symmetry has presented some problem. Kelman uses three different kinds of coils, and parallel rectangular shaped pole-pieces†.

[20]) G. E. Lee-Whiting, Can. J. of Phys. **35** (1957) 570.

[21]) N. E. Alekseejevskii, G. P. Prudkovskii, G. I. Kosourov and S. I. Filmonov, Dokl. Akad. Nauk SSSR **100** (1955) 229.

In the deflecting magnet the radial projection of the beams remains parallel, while there is a focalisation in the axial direction. This focalisation is produced by the fringing field, which is acting as a cylindrical lens. The focal length of the cylindrical lens depends on the angle α which the beam makes with the normal to the pole-edges. If one wants to have the beam symmetrical on both sides of the prism, the median plane should contain the coinciding foci of the cylindrical lenses at the entry and exit side of the prism. Kelman finds that the angle α should then be equal to 58°. The source has rectangular shape. In order to compensate for the rotation of the image in the lens, the source and counter slit are placed at an angle to the vertical axes. (The whole apparatus is in horizontal position.)

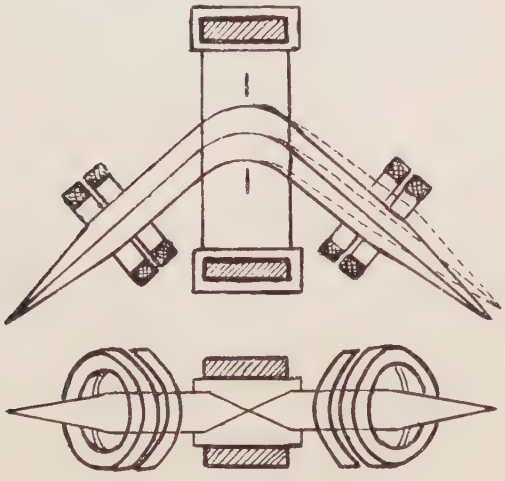

Fig. 4a

The dispersion of the prism is given in this case by the relation

$$D = 2f \tan \alpha$$
$$= 3.2f$$

where f is the focal length of the exit lens. The dispersion can be increased by increasing the

[22]) M. Mladjenović, Meeting on Nuclear Spectroscopy, Sept. 1959, Beograd, to be published.

[23]) V. M. Kelman and D. L. Kaminskii, ŽETF **21** (1951) 555.

[24]) V. M. Kelman, D. L. Kaminskii and V. A. Romanov, Izvestia Akad. Nauk SSSR, Ser. Phys. **18** (1954) 148.

[25]) V. M. Kelman, Vestnik Akad. Nauk SSSR, No. 7 (1958) 75.

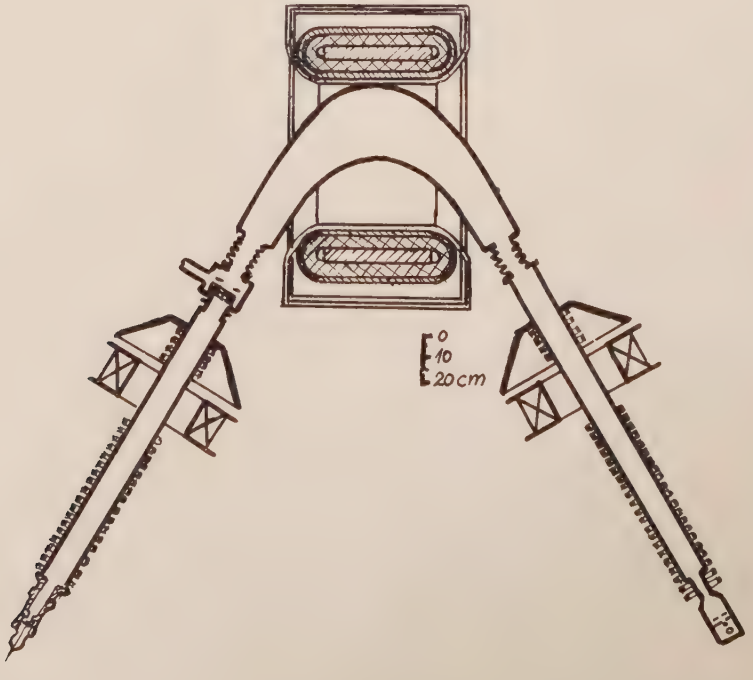

Fig. 4b

Fig. 4. Kelmans prism spectrometer: a. Geometry, b. Cross-section of spectrometer in a horizontal plane.

distance between the counter, source and the corresponding lenses. This is probably the most important advantage of this type of spectrometer.

When the focal length is increased the transmission should not decrease only if the dimension of the magnet and coils allow an increase of the entry slit.

The resolving power can be defined as

$$R = \frac{\text{Source width} + \text{slit width} + \text{aberrations}}{\text{linear dispersion}}$$

$$= \frac{S + Q + 2d_{\text{sph}} + \Delta_\varphi + \Delta_H}{\Delta}.$$

We have taken into account three contributions to the aberrations: d_{sph}, Δ_H and Δ_φ.

First, we have the spherical aberrations of the two lenses d_{sph}. They are proportional to the cube of the aperture angle θ. The aperture angles have been very small so far, so that the contribution of the spherical aberrations is almost negligible.

Next is the contribution of the prism to the line width Δ_φ, which is approximately l^2/f, where l is the height of the source. It is of the order of 0.01.

Finally, we have to take into account the possibility that the required actual proportionality between the fields in the prism and the lenses may deviate from the theoretical value, due to remanence, saturation, or other causes. Suppose that the field in one lens is smaller by an amount ΔI from the required value I. The corresponding contribution to the line-width is roughly

$$\Delta_H = 2d\,\frac{\Delta I}{I}$$

$$\simeq 10\,\frac{\Delta I}{I}$$

since d is the width of the parallel beam before entering the prism, and is of the order of 4–5 cm.

The transmission can be varied by changing the focal lengths. This is not as convenient as in the case of the double focusing spectrometer where one only has to change the slits.

The existing apparatus has been adapted and used for very high resolution, low transmission work. It is rather large V-shaped device, having arms nearly three meters long. The typical results are

source size:	10×1 mm^2	10×0.5 mm^2
transmission	0.02%	0.01%
resolution	0.04%	0.02%

1.3. PERMANENT MAGNET SPECTROGRAPHS

The technique of permanent magnet spectrography was developed mainly by Ellis and collaborators, and recently improved by Slätis[26–28]). Being valuable, especially for the measurement of short-lived sources, these spectrographs have three limitations: 1. One direction focusing; 2. Only first order focusing; 3. Difficult intensity measurement.

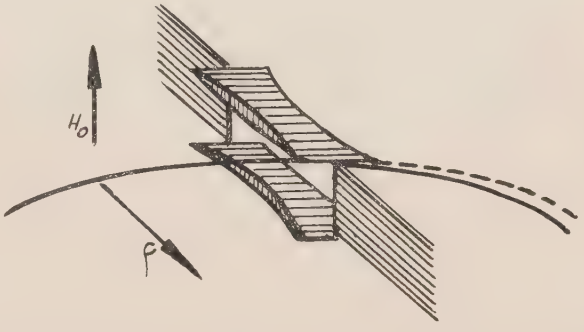

Fig. 5. Additional lenses placed at the entrance slit of a permanent magnet spectrometer, proposed by Walen.

1. One direction focusing. This limitation is not very serious. A prolongued exposure in a stable field, makes up for the loss of transmission, and allows the measurement of weak lines.

2. The radial focusing of homogenous field is limited to the first order. Walen has proposed[29]) the use of small correcting lenses, placed at the entrance slit, which should give second order focusing. The correcting lenses are shown in fig. 5. The usual source-slit-plate geometry has to be altered to a form given in fig. 6.

[26]) H. Slätis, Arkiv för Fysik **6**, No. 41 (1953).
[27]) H. Slätis, Arkiv för Fysik **8**, No. 43 (1954).
[28]) H. Slätis, Nuclear Instruments **2** (1958) 332.
[29]) R. J. Walen, Nuclear Instruments **1** (1957) 242.

When flat sources are used, the line width can be reduced by properly inclining the source[30–31]).

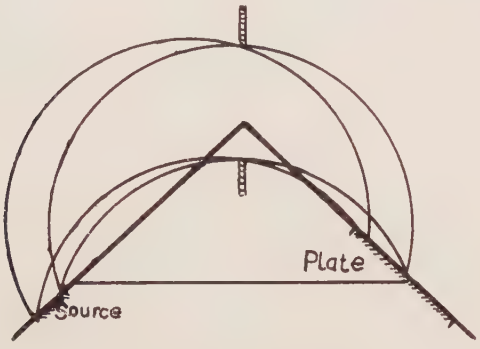

Fig. 6. Geometry of permanent magnet spectrometer proposed by Walen.

3. Three corrections have to be applied for the intensity measurements: (a) Radial dependance of the transmission, (b) Blackening-intensity curve, and (c) Blackening-energy curve. The problem of corrections, which was discussed by several authors, can be more easily solved if the spectrometer is so designed that a G.M. counter can be employed alternatively with the plate[32]). First correction can then be accurately determined for a given source and geometry. It can be conveniently done with a technique, borrowed from mass spectroscopy, of measuring a line with the detector slit several times wider than the line-width[33]). A trapezoidal line is obtained, the height of which gives the absolute number of electrons in the line. The height of such a wide line (fig. 7) can be measured with a greater accuracy than the area of narrow lines. By measuring the same line at different radii a precise correction curve can be made. On the other hand, by measuring in the same way some of the strongest lines, the other two corrections can be checked.

The use of electron sensitive nuclear emulsions may extend the usefullness of permanent magnet spectrographs to very weak sources and low energies. Several authors applied[34–36]) the electron sensitive nuclear emulsions for the

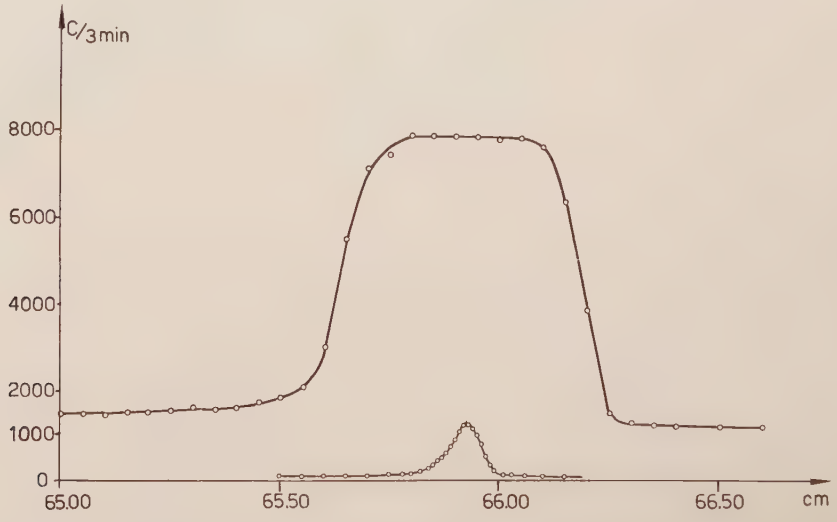

Fig. 7. The line intensity measurements with a wide slit. The counter slit widths are: 0.2 mm for the small line and 5 mm for the large line. The source width is 0.2 mm, and the distance of the line from the source is $2\varrho = 67$ cm.

[30]) W. A. Wooster, Proc. Royal Soc. **114** (1927) 729.

[31]) R. Stepić and M. Mladjenović, Meeting on Nuclear Spectroscopy, Sept. 1959, Beograd, to be published.

[32]) M. Mladjenović, Bulletin of "B. Kidrich" Institute, No. 6 (1956) 53.

[33]) M. Marinkov, R. Stepić and M. Mladjenović, to be published.

[34]) I. A. Antonova, Izvestia Akad. nauk SSSR **20** (1956) 896.

[35]) P. Kleinheins: Zeit. Naturforsch. **11** (1956) 252.

[36]) H. R. Reitman, H. Schneider and I. J. van Heerdin, Phys. Rev. **110** (1958) 1093.

[37]) Z. Sujkowski and H. Slätis, Arkiv för Fysik **14** (1958) 101.

detection of weak conversion lines. The sensitivity is increased by two orders of magnitude in comparison with the usual total blackening measurements. The difficulties are caused by the background tracks. It is preferable to use the freshly prepared plates from emulsion in gel form.

Slätis[28,37]) has applied this technique to the measurement of Auger electrons of low energy, which cannot be observed on the usually employed films.

Rapid increase of background and more elaborate procedure are probably the reasons why this technique has not yet come into wider use.

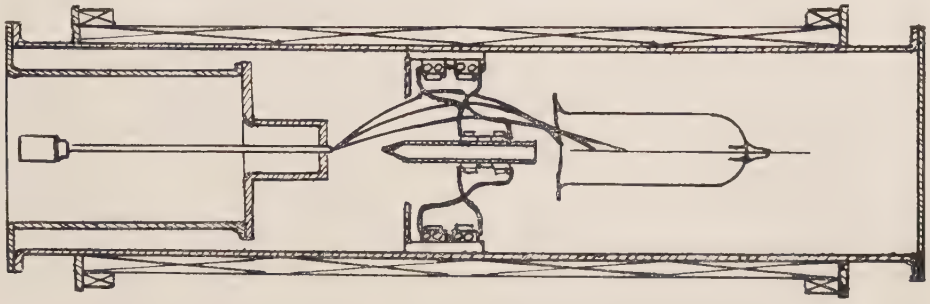

Fig. 8. Homogenous field lens with correcting thoroidal coils (Kelman, Dolmatova).

2. High Transmission Spectrometers

High transmission is in great demand, not only for the measurement of weak sources, but also for coincidence work. A high transmission spectrometer is of much greater value if it can be easily adapted for β—β and β—γ coincidence measurement. This is easier to do when the source and detector are outside of the magnetic field.

There are two main types of high transmission spectrometers: lens and orange. The first is easy to make, the second performs better.

2.1. LENS SPECTROMETERS

The requirement that the source and the detector should be in zero field favors the iron-clad lenses. Simple types of such spectrometers, convenient for coincidence work have been described[38,39]), the latter one giving 4% transmission, at 2% resolution. Although many different types of lenses were made, it is probable that one could make still better iron clad lenses, approaching the transmission of 10%. The main difficulty is that one can not make exact theoretical computations as in the case of homogeneous field, and has more to rely on the general arguments and the experience.

The resolution of many existing lenses, as well as future ones, can be ameliorated with a technique recently developed by Dželepov and Kelman groups in Leningrad. The idea is to correct the spherical aberration by adding a torus coaxially with the lens.

The problem is simpler in the case of solenoids with homogenous field, since then it can be solved analytically. Dolmatova and Kelman[40]) have computed the form of the torus giving the ring focus without spherical aberrations (fig. 8). The resolution improved by a factor of three, while the transmission was somewhat reduced. They give the following data

	Solid angle	Transmission	Resolution
without	8.7%	7.7%	5.7%
with correcting torus	8.7%	6.5%	1.9%

[38]) H. Slätis and C. J. Herrlander, Rev. Sci. Instr. **26** (1955) 613.

[39]) Mladjenović, Proceedings of Rehovoth Conference, 1958; to be published in "Bulletin "B. Kidrich".

[40]) K. A. Dolmatova and V. M. Kelman, Dokl. Akad. Nauk SSSR **113** (1957) 1244.

The same problem was taken up for short lenses by Dželepov and collaborators[41,42]). The form, position and the field strength of the torus were looked for empirically. A triangular shaped torus of eight slices (fig. 9) placed near the detector improved the point focusing by a factor 2.5. At a solid angle of 2% the point focus resolution was improved from 7.8% to 2.6%.

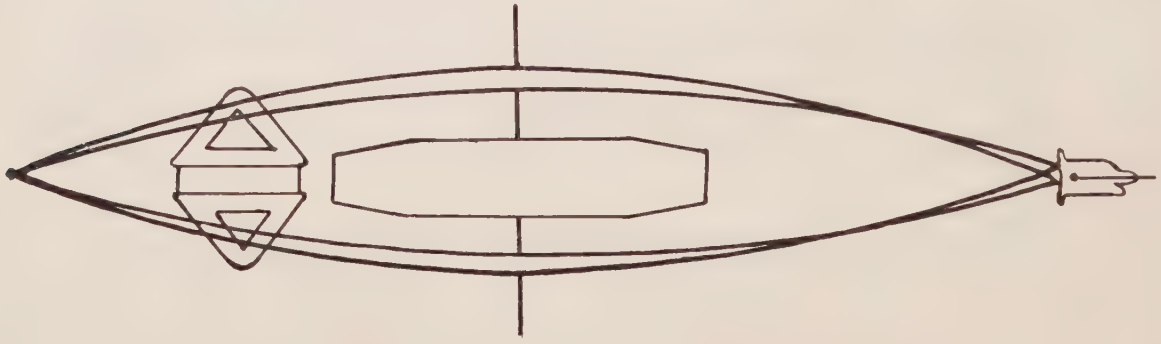

Fig. 9. Point focusing short lens with correcting thoroidal coils (Dželepov *et al.*).

2.2. THE TOROIDAL SPECTROMETER (ORANGE)

The idea of constructing a toroidal spectrometer has probably occured independently to various physicists. Harris[43]) proposed in 1947 the construction of a toroidal spectrometer for cosmic rays. At the same time Szalay initiated the construction of such a spectrometer. The theoretical calculations were done by Horvath[44]) and the construction finished by Berényi[45]). O. B. Nielsen, Kofoed-Hansen and Linhard first published the theoretical treatment[46]), and then constructed a small orange[47]). Recently O. B. Nielsen has finished a larger apparatus of the same type[48]). The work on toroidal spectrometers is also going on in Buenos Aires by Mallmann and collaborators[49–52]). Prokofiev[53]) also constructed an orange spectrometer.

The iron-free torus was first built by Vladimirskii and collaborators[54]), and later modified by Tretjakov, Goldin and Grišuk[55]). Another orange spectrometer was recently finished in the same laboratory by Burgov[56]).

The main advantages of the torus are: very high transmission, comparatively good resolution, source and detector in zero field, and the possibility to treat the problem analyticaly.

Iron orange. The most critical problem in the design is the profile of the iron sector. The theoretical treatment is not difficult if one disregards the fringing field and assumes that the field between the pole pieces is exactly proportional to $1/r$. Then for a given entrance profile, the exit profile can be analytically computed. The deviations from the ideal field are due to two causes:

1. The fringing flux. For most of the beam it has the effect of cylindrical lens, whose focal length depends on the angle α of the ray with the

41) B. S. Dželepov, Ho Sen Čan and P. A. Tiškin, Izvestia Akad. Nauk SSSR **20** (1956) 947.

42) V. A. Sergejenko, PTE, No. 4 (1957) 13.

43) W. T. Harris, Phys. Rev. **71** (1947) 310.

44) J. Horvath, Experientia **5** (1949) 112.

45) A. Szalay and D. Berényi, Acta physica A.S. Hugarieae **10**, No. 1 (1959) 1.

46) O. Kofoed-Hansen, J. Linhard, O. B. Nielsen, Mat. Fys. Medd. Dan. Vid. Selsk. **25**, No. 16 (1950).

47) O. B. Nielsen and O. Kofoed-Hansen, Mat. Fys. Medd. Dan. Vid. Selsk. **29**, No. 6 (1955).

48) O. B. Nielsen, Private Communication; also Nuclear Physics **12** (1959) 389.

49) C. A. Mallmann, Physica **18** (1952) 1139.

50) C. A. Mallmann, Publ. CNEA (Argentina) **1**, No. 1 (1953).

51) L. Lagatta, C. A. Mallmann, C. Molina, Vedia, J. Peyre and J. Suarez Etchepare, Second UN International Conference on peaceful uses of Atomic Energy, Report 1973.

52) J. Suarez Etchepare, Second UN International Conference on peacefull uses of Atomic Energy, Report 1974.

53) Prokofiev, Latv. P. S. R. Zinat. Akad. Vestis, No. 1 (1957) 137.

54) V. V. Vladimirskii, E. K. Tarasov and Yu. V. Trebuhovskii, PTE, No. 1 (1956) 13.

55) E. F. Tretjakov, L. L. Goldin and G. I. Grišuk, PTE, No. 6 (1957) 22.

56) N. A. Burgov, Private Communication.

normal to the edge. It is necessary to keep this angle constant, as much as possible. One convenient choice is $\alpha = 0$ which gives the circular profile with the center in the source.

2. The field is stronger at the surface of the iron than in the central plane of the gap.

The final profile is usually semi-empirical. The theoretically designed profile is tested with a narrow beam and corrected to improve the focusing[47]).

The presence of several iron sectors introduce the possibility of defocusing due to non inhomogeneities, remanence and misalignment. As a matter of fact all the iron orange spectrometers which are in operation now, have the resolution of one sector at least 100% higher than the resolution of all sectors together.

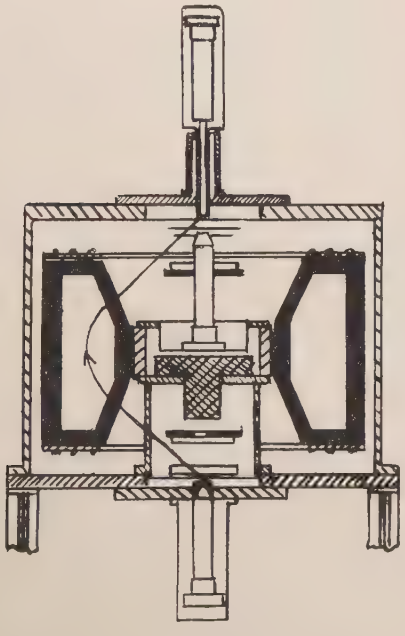

Fig. 10. Iron free orange (Tretjakov *et al.*).

Iron-free orange spectrometer (fig. 10). The design of profile can be made in the same way as for a spectrometer orange iron, since the field varies as $1/r$. The number of sectors is much larger (30–50), so that relative sector width is reduced. The field approximates then more closely to the ideal form, and the theoretical profile can be used.

The latest of Moscow iron free orange spectrometers designed by Burgov[56]) is expected to have the resolution given by the relation

$$\frac{\Delta H\rho}{H\rho} = 1.2\,\frac{R_{\mathrm{det}}}{f}$$

where the crystal detector has the radius R_{det} equal half of the height. Since $f = 50$ cm, the resolution is of the order of 1% for a transmission of 8%.

The main problem with the coil construction is to obtain a large number of ampere turns. The first instrument had 36 turns, and a current of 1500 amps was used to focalize 1.2 MeV electrons. Burgov's apparatus has 750 turns, stacked into 50 groups. With the current of 100 amps, 3.5 MeV electrons are focalised.

It is of interest, to compare the performances of iron and iron-free oranges. The data for two latest apparatus of about equal size are given below

	Source	Transmission	Resolution
Iron free (Burgov) (theoretical)	diam. 10 mm	8%	1%
Larger iron orange (Nielsen)	3 × 6 mm	9%	1.3%

The actual performances of both types are about the same. It should be stressed that although orange spectrometers are much better than the existing lens spectrometers, they are still in the initial stage of development. Further work in profile line should bring about an improvement of resolution. Due to well known inherent limitations of iron instruments it could be expected that the iron free orange spectrometer should lend itself more readily to further improvements.

Acknowledgements

The author is greatly indebted to Drs. N. A. Burgov, De Vries, R. L. Graham, C. A. Mallmann and O. B. Nielsen for kindly giving the additional unpublished information on their spectrometers.

NUCLEAR INSTRUMENTS AND METHODS 7 (1960) 22–36; NORTH-HOLLAND PUBLISHING CO.

SOME METHODS IN THE PREPARATION OF RADIO-ACTIVE MATERIALS FOR USE IN BETA-SPECTROSCOPY†

W. PARKER, M. DE CROËS†† and K. SEVIER, Jr.

Institute of Physics, University of Uppsala, Sweden

Received 11 November 1959

The initial results of an investigation dealing with the most appropriate methods for the preparation of radioactive materials for use in beta-spectroscopy are reported. A short review of the methods and techniques developed for this type of preparation is presented, and, where possible, improvements are suggested. The investigation has been carried out in four main parts, namely, thin film preparation and thickness determination, electro- and vacuum deposition, and miscellaneous techniques, and is reported in the same order. In conclusion, tables designating the deposition efficiencies obtained from the preparation of 45 different radio-active materials by employement of the various methods are given.

Authors' Note: The authors believe that there is a considerable amount of information relative to radio-active source preparation not in published form. It would be very much appreciated if any reader of this article would send to the authors any such information in order that the proposed continuation of this investigation may be made as complete as possible.

1. Introduction

When measuring low energy regions of beta-spectra, preparation of the active source is an important factor in so much as excessive mass may distort the true spectral distribution[1,2]).

Self-absorption and scattering due to large mass present in the active deposit[3]) and also backscattering caused by unsuitable source support material all contribute to such distortions of the spectrum. The specifications usually necessary for sources used in beta-spectroscopy may be expressed in a few words.

1. Thin uniformly distributed active deposit.

2. Thin, electrically conducting support material of low atomic number. The first of these requirements can only be satisfied where either high specific activity is available or where large deposition area, relative to mass, can be tolerated. The second requirement is even less easily satisfied. Metals such as aluminium, having low atomic number and although being most desirable as a source support material, are frequently unsuitable from the preparation point of view, since at the thicknesses usually required, these foils are fragile and soluble in the weakest acid and alkaline solutions. Thin organic films, less than 40 $\mu g/cm^2$, may be prepared without difficulty and would appear at first sight to solve the problem. Insoluble in acidic and alkaline solutions and having negligeable backscattering effect, films of this description have one serious drawback, i.e., they are not electrically conducting. As a consequence of this, if the preparation chosen is chemical, involving the use of acidic and alkaline solutions, a metal substrate inert to these solutions must be employed. Thus much of the initial advantage in using an organic film is lost. On the other hand, where vacuum deposition is decided upon, aluminium

† This paper forms part of the thesis to be presented in connection with beta-spectroscopy studies by M. De Croës for the degree of docteur en Sciences Physiques.

†† On leave from the Université de Louvain, Belgique.

[1]) C. S. Wu and L. Feldman, Phys. Rev. **76** (1946) 697.

[2]) J. H. Hamilton, Thesis, University of Indiana, U.S.A. Private communication.

[3]) W. E. Nervik and P. C. Stevenson, Nucleonics **10**, No. 3 (1952) 18.

or like metals may form the substrate. Unless, however, one is prepared to evaporate large quantities of the desired active material, the thin film in question must be positioned rather near to the vapour source. Without elaborate precautions, this last will surely endanger the safety of the film by the possibility of its burning. Another disadvantage is the inability of a thin organic film to support any slight excess in mass which may result in the fracture of the film during the measurement and the consequent risk of contamination to the measuring apparatus. Where the high-energy region of the beta-spectrum is measured, the source requirements are not always so critical as those dealt with above. Comparatively thick backing materials as well as large mass can be tolerated. One can therefore assume that where a technique or method is suitable for preparing a source requiring high specifications, the same preparation for the latter type of measurement will present less difficulty.

Having established the requirements to be fullfilled by the source, the question now arises concerning the most suitable type of deposition. The method and techniques developed over a period of time are as varied as they are numerous. If one is to approach the method of preparation from the quality of the source produced, electromagnetic mass separation can probably be considered as the most suitable[4, 5]). Here atoms of the separated material penetrate the surface of the collecting foil which can be mounted directly for measurement; also, chemical separation is not always necessary. Unfortunately, the poor efficiency and, in some cases, the difficulty of changing from one element to another make this method impracticable except in certain cases. In a previous publication by one of us[6]) an apparatus is described for the *vacuum deposition* of active material, and, although this method of deposition affords the means of obtaining thin homogeneous deposits with a reasonable yield efficiency, the technique of *electro-deposition* is probably less prone to failure. The main advantage of electro-deposition is that in the event of the preparation failing, the activity can easily be saved and an alternative solution or method employed; failure in a vacuum system will frequently result in the complete loss of the activity. Apart from the methods mentioned above, there are still the various odd methods to be considered which often find application in dealing with a particular material where other more elaborate arrangements fail. Some idea about the methods and techniques developed for the type of preparation dealt with in the present investigation can be gained from the following: electro-phoretic[7]), ion-ejection[8]), cathodic sputtering[9]), painting technique[10]), lacquer suspension[11]), slurry technique[12]), and, finally, the drop method. If one is to judge by current literature, little or no development has been carried out in connection with the above mentioned. The main object of the present investigation is to try to bring together the rather widely scattered information relative to work of this description. In addition, as much of the previously reported work as feasible has been and will continue to be repeated and, if possible, improved.

2. Preparation of Source Support Material

2.1. INTRODUCTION

The undesirable backscattering of the beta-rays giving rise to distortion of the experimentally observed spectra, is the effect of both the Z- (atomic number) dependent scattering relationship, and also the thickness of the film chosen as backing for the activity. By consideration of this, backscattering can be reduced by the selection of a film of appropriate thickness

[4]) I. Bergström *et al.*, Arkiv för Fysik **1**, No. 11 (1949) 281.

[5]) G. Andersson, Arkiv för Fysik **12**, No. 14 (1957) 331.

[6]) W. C. Parker, Nucl. Instr. **5** (1959) 143.

[7]) F. P. Cranston *et al.*, Rev. Sci. Instr. **27**, No. 11 (1956) 973.

[8]) D. J. Craswell and J. Milsted, J. Nucl. Energy **4** (1957) 51.

[9]) F. R. Lipsett, Brit. J. Appl. Phys. **6** (1955) 442.

[10]) R. B. Belser and W. H. Hicklin, Rev. Sci. Instr. **27**, No. 5 (1956) 293.

[11]) K. M. Glover and P. Borrel, J. Nucl. Energy **1** (1955) 214.

[12]) H. Slätis, Beta and Gamma Ray Spectroscopy, Ed. K. Siegbahn (1955) 259.

and Z-value. The former of these can be realized by the use of films of an organic composition, where the constituents are of low Z-value, or films of elements of low Z-value or their compounds. The latter circumstances are dependent upon the method of the preparation of the film. Since the thickness of the film may not be obvious upon initial inspection, there have been certain techniques developed where determination of film thickness and thickness distribution can be comparatively facilitated. These techniques will be treated briefly later in this section.

The main necessary property of a backing is that it should be conducting so as to prevent charging of the source. This may be realized in two ways. The backing itself can be an electrical conductor, thus calling for the use of metals; a drawback here is that the metal can have only a certain minimum thickness, and, consequently, the initial advantage of a thin film is lost. The alternative is to use a non-conducting backing material and to deposit a very thin layer of metal substrate on this film. This can be done most suitably by vacuum deposition. Also, the deposition of the metal substrate upon a non-conducting film alows the technique of electro-deposition to be employed.

2.2. MYLAR

Mylar, being a polyester compound, has found extensive use in source preparation application as windows for G-M counters, and, more recently, as a backing for uranium converters[13]). It can be obtained in a number of various thicknesses, the thinnest being approximately 0.9 mg/cm^2. Mylar is stable at temperatures up to 150° C, above which it apparently decomposes. During the heating process, the thickness distribution may change quite noticably, e.g., if the mounting is a metal ring during heating, the film sometimes becomes thinner at the center and thicker at the edges. It is inert to the acids usually employed in preparation work, easy to handle, and strong. Mylar is ideal for certain applications where a thick backing is of no consequence.

2.3. FORMVAR

Ethylen dichloride, or formvar, as it is more commonly known, is soluble in trichlorethylene. Films of this material are made by removing a clean glass plate from a submerged position in this solution and allowing the plate to dry. The film is cut through at the edges of the glass plate and floated off on the surface of distilled water. The film is then removed from the water surface by use of a wire loop and subsequently mounted.

A method for obtaining reproducibly uniform films of this material has been described by Revell and Agar[14]), and, briefly, is as follows. A glass funnel of appropriate dimensions and fitted with a tap is filled with a solution of formvar in chloroform and a glass plate is suspended in the solution from the top. Since the thickness is dependent upon the rate at which the glass plate is removed from the solution, well controlled film thickness can be obtained by draining off the solution via the tap at a given rate. These films can be made having a thickness on the order of 3 μg/cm^2 and the film thickness distribution has been found by the above authors to be within 3%.

Organic films, of course, can not always be used in the technique of electro-deposition if the medium is of a similar complex. In this event, use is made of metallic or oxide films.

2.4. ZAPONLACQUER

Thin films of zapon may be prepared by allowing a drop of lacquer to spread by surface tension on the surface of distilled water. The conventional method of removing the film from the water's surface by means of a wire loop can often lead to the film breaking. It has been found that a more convenient method is to press an inverted glass down upon the film covering the water and submerge the two. The film will stick to the rim and outer wall of the glass which may then be removed from the water and the adhering film allowed to dry. Using an adhesive, there is little difficulty in mounting the films

[13]) P. Erman and W. C. Parker, Nucl. Instr. **4** (1959) 257.
[14]) R. S. M. Revell and A. W. Agar, Brit. J. Appl. Phys. **6** (1955) 23.

onto suitable source rings. A method described by Hamilton[2]) for obtaining an approximation of the film thickness is as follows. One drop of zapon is dried upon a previously weighed piece of aluminium foil and the combination is reweighed. Assuming that an amount of laquer equal to that which was weighed can be dropped and spread on a water surface and mounted over a known area, the thickness of the film can approximately be calculated in $\mu g/cm^2$. Another method of thickness determination is based on the use of interference colors of the film.

Zapon films are inert to acids, have a low effective Z-value, are strong, and are stable at temperatures up to 60° C. Furthermore, zapon films are easier to prepare than formvar films. Also zapon is much less prone to mechanical failure than formvar; the thicker films, above 200 $\mu g/cm^2$, can be handled without fear of breakage.

2.5. METAL FOILS

The necessity of materials having low atomic number, so as to minimize backscattering, rather restricts the application of metal foils. The most frequently used are aluminium, silver, gold, and platinum. The last three are employed because of their comparitive inertness to certain acids. The use of aluminium foils 180 $\mu g/cm^2$ has been successfully employed for a number of preparations[16]), but special care is necessary when handling such foils which are seldom free from holes. Any form of shock, e.g., violent evacuation of the vacuum chamber, may cause the foil to fracture. For this reason the film is usually sandwiched between zapon films after deposition of the active material. In general, the above remarks relative to aluminium apply to most thin metal foils, and for this reason, greater attention has been paid to the alternative materials available.

2.6. CARBON FILMS

A method for production of carbon films, self-supporting and with a thickness down to 4 $\mu g/cm^2$, has recently been published[17]). The authors have constructed an apparatus for carbon film preparation using the above method which is as follows: A nickel foil 4.5 mg/cm^2 thick is heated in a chamber containing methyl iodide at a pressure of between 0.254 and 2.54 mm Hg. In this way, the methyl iodide is decomposed upon contact with the heated nickel to form a thin carbon deposit. Since the deposit

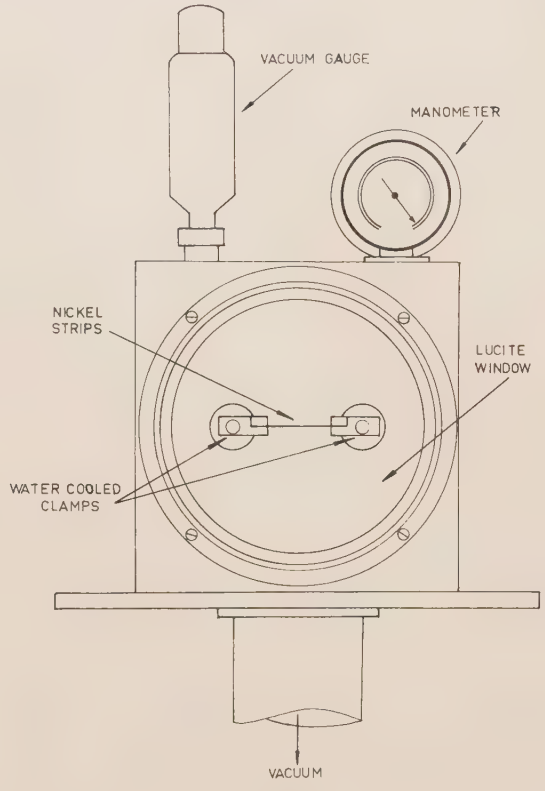

Fig. 1. Carbon foil apparatus.

is formed on both sides of the nickel, two strips may be used back to back, thereby obtaining two films at one operation. After being removed and mounted on a suitable frame, the nickel is removed by dissolving it in a solution composed of one part H_2SO_4, two parts water, and two parts HNO_3. The apparatus used by the authors[18]) is shown in fig. 1.

The advantages of carbon films make them ideal source support material. Because of their

[15]) K. M. Greenland, Vacuum **11**, No. 3 (1952) 216.
[16]) D. E. Bradley, Brit. J. Appl. Phys. **5** (1954) 65.
[17]) E. Kashy *et al.*, Nucl. Instr. **4** (1959) 167.
[18]) W. C. Parker and K. Sevier, to be published.

low Z-value, such films have great potential value for use in beta-spectroscopy. Their ability to withstand a temperature of 3500° C makes them very suitable for use in vacuum deposition. They are conducting and thus require no form of metal substrate to prevent charging of the source. Since carbon is insoluble in acidic, alkaline, and organic solutions, only one difficulty arises if required for electro-deposition. Namely, carbon films lose their mechanical strength when wet. However, if the films are dried in a supported position, no difficulty should be encountered.

2.7. ALUMINIUM OXIDE FILMS

The preparation of aluminium oxide films is worthy of considerable attention. There have been several methods of preparation mentioned in literature[19, 20]), and the difference between them has usually been the physical appearance of the piece of aluminium to be coated by the oxide. Seemingly, the easiest method to use is that described by Harris[21]) and is briefly presented here. A strip of commercial aluminium foil is anodized in a solution (3% by weight) of ammonium citrate. Upon the completion of the process and the attainment of the desired thickness of oxide film, the foil is removed from the solution and one side is painted with strong NaOH solution to dissolve the film on that side. The subsequently free metal surface is then treated with HCl and the clear anodized film of the other side of the foil is left. Caution must be taken to wash the foil in distilled water to remove the NaOH at the appropriate time so that all of the film is removed on that side. It was found that the thickness of the film increases nearly linearly with the anodizing voltage applied. Hauser and Kerler[22]) have noted that with their electrolyte of ammonium citrate and citric acid in the ratio of 1 : 1, the purity must be extremely high. The intersection of the electrolyte surface and the metal and also any submerged electrical junctions are very suseptible to sparking caused by the presents of impurities. The range of thickness of these films was between 25 and 250 $\mu g/cm^2$. The current used was between 10 and 100 mA/cm^2. The procedure has been simplified and an improved apparatus developed by the authors†.

Aluminium oxide films are very useful as backing for active sources because of the low Z-value. There is 90% electron transmission at ≈ 6 keV with 25 $\mu g/cm^2$ and also at ≈ 25 keV with 250 $\mu g/cm^2$. Aluminium oxide films are resistant to heat to the temperature of 2000° C, and thus vacuum deposition can be used to deposit the activity. Also, since these films are negligibly soluble in weak acidic or organic solutions, electrodeposition with the use of a metal substrate can be used to deposit the activity. Aluminium oxide is quite soluble in alkaline solutions. The films are gas tight, fragile, and electrically non-conducting.

2.8. DETERMINATION OF THICKNESS DISTRIBUTION

In beta-spectroscopy measurements it is often important to know the thickness and thickness distribution of both the active deposit and the material supporting the deposit. Methods available for the determination of foil and film thickness are as varied as they are numerous[15]). Mechanical, optical, electrical, as well as radioactive methods have a vast literature and are far beyond the scope of the present investigation. The last method, however, is particularly suited for the often necessary and quick determinations required in connection with source preparation. There exists comprehensive information describing suitable apparatus to investigate the penetration of alpha- and beta-particles through thin materials[23–33]). Hence, in the present investigation, this form of measuring has been employed, and, for the purpose of completeness, a brief description of the instrument will be given††.

† To be published.

†† To be published in Nuclear Instruments and Methods.

[19]) L. Holland, Vacuum Deposition of Thin Films (Chapman and Hall, London, 1956).

[20]) G. Hass, Vacuum **11**, No. 4 (1952) 331.

[21]) L. Harris, J. Opt. Soc. Amer. **45**, No. 1 (1955) 27.

[22]) U. Hauser and W. Kerler, Rev. Sci. Instr. **29**, No. 5 (1958) 380.

2.9. ALPHA ABSORPTION

Having an alpha-energy of 5.258 MeV, Po^{210} is frequently used for the thickness determination of thin films and foils. Davison[27]) described a technique of particular interest. A G-M tube, and a Po^{210} source are fixed at a known distance from each other. The pressure variation of dry air between the two avoids the inverse square effect on the beam intensity and gives a sharper slope at the end of the range. The foil or film in question is placed between the source and the counter, and the corrected counting rate is measured at different pressures—this may be expressed as a ratio to the maximum counting rate. If the relative counting rate is plotted against the pressure, we obtain a curve as shown in fig. 2. In this curve no film has been introduced and the well defined range of the alpha particles is shown. The introduction of a film, if uniform, between the counter and the source will give the dotted curve parallel to that already obtained, but displaced by Δp, which can be termed the "air equivalent" of the film. A film that is not uniform will give a curve that is not parallel to the first one and the difference in slopes of these curves will be a measurement of the inhomogeneity of the thickness.

An alternative arrangement, such as that described by Enge *et al.*[26]), where the distance between the counter and the source is variable, is also suitable for the measurements in question. Here the source position is changed by use of a micrometer screw and is set at a given distance from the activity. After observing the counting rate, the film is interposed. The decrease in the counting rate is compensated for by reducing the source-to-counter distance. The "air equivalent" is read from the micrometer scale. Of the two methods described, the one of Davison was

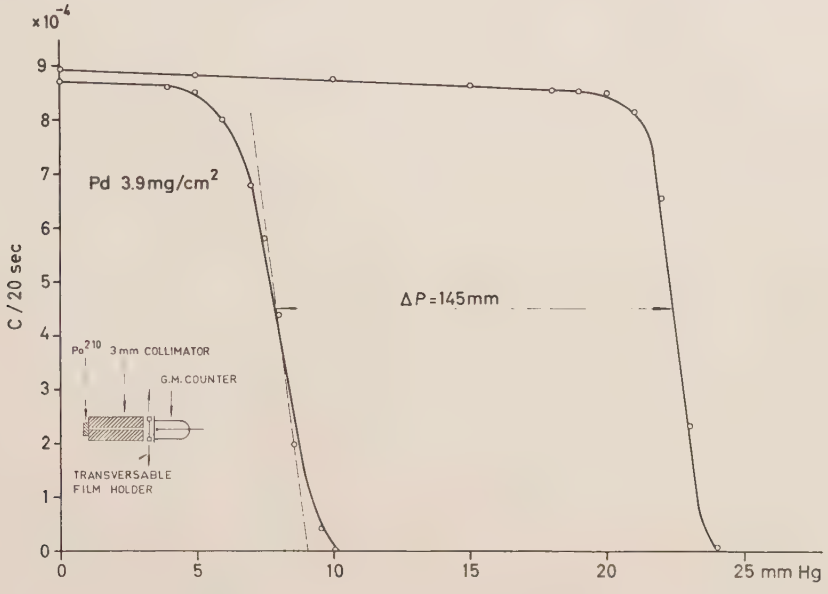

Fig. 2. Thickness determination by alpha absorption, Po^{210}.

[23]) H. A. Bethe, Rev. Mod. Phys. **22**, No. 2 (1950) 213.
[24]) W. C. Barber, Rev. Sci. Instr. **24** (1953) 469.
[25]) E. N. Shaw, Radioisotope Conference **2** (1954) 140.
[26]) H. A. Enge *et al.*, Rev. Sci. Instr. **28**, No. 2 (1957) 145.
[27]) W. H. T. Davison, J. Sci. Instr. **34** (1957) 418.
[28]) K. Ramavateram and D. J. Porat, Nucl. Instr. **4** (1959) 238.
[29]) K. Siegbahn, Thesis. Nobel Institute for Physics, Stockholm, Sweden (1944).
[30]) K. Siegbahn and H. Slätis, Arkiv för Math., Astr. and fysik. **134**A, No. 6.
[31]) J. H. Peterson and J. R. Downing, J. Opt. Soc. Amer. **41** (1951) 862.
[32]) L. Mandel, Brit. J. Appl. Phys. **5** (1954) 287.
[33]) O. Te-tchao, J. Phys. Rad. **17**, No. 12 (1956) 1019.

thought to be most suitable, and the authors' apparatus is constructed accordingly (schematic in fig. 2). There are, however, two main differences. The first of these is that the source is situated behind a 1 mm diameter aluminium collimator, and, secondly, the film is fitted to a horizontally traversible carriage controlled by a micrometer screw. The determination is made in the same manner as that of Davison with the added advantage that, because one obtains a number of selected absorption points over the films' area, an accurate determination is possible. A mean thickness distribution obtained by the authors for Pd is shown in fig. 2.

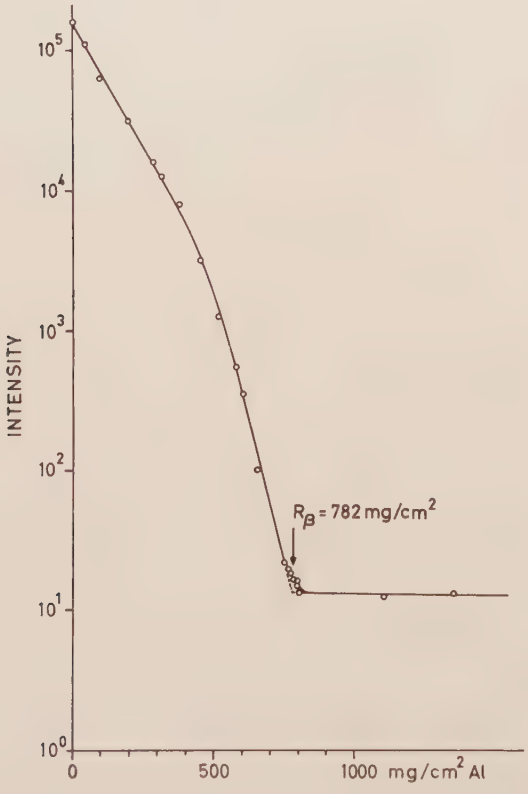

Fig. 3. Beta absorption by Al sources P^{32}.

2.10. BETA ABSORPTION

The apparatus used for these measurements follows the conventional lines of construction[31, 32, 33]). For this investigation the source of beta-rays is Ni^{63} which has the convenient half-life of 85 years. The method of measurement employs the use of absorbers of known thickness from which a calibration curve can be derived for different materials. Fig. 3 gives the results for a thick film of aluminium obtained using P^{32}.

3. Electro-Deposition

3.1. INTRODUCTION

The technique of electro-deposition is one of the best known methods in the preparation of radio-active sources, providing that consideration is given to the purity of the chemicals and reagents employed, and also that apparatus used in the preparation is kept scrupulously clean. Most of the information relative to electro-deposition is, of course, derived from industrial applications[34, 35]), but industrial procedures may not work for tracer amounts, and procedures not applicable to industrial platting may serve well with tracer activities. The main disadvantage of the formulas given is that they are intended for use with large capacity plating baths.

Apparatus developed for the preparation of thin films of active materials have been reported[36, 37, 38]), and, although usually developed for a particular purpose, such apparatus is suitable for a wide range of applications. That described by Dodson *et al.* has the following construction. A base block of suitable dimensions and fitted with small hooks, supports the desired backing material (metal foil or organic film plus metal substrate) on top of which is placed a rubbergasket and a glass tube in that order. The glass tube is fitted with glass hooks at corresponding positions to those on the base block. In this way the assembly is held rigid and made water tight when either springs or rubber bands are fitted between the two sets of

[34]) J. Wiley, Modern Electroplating, Ed. A. G. Gray, (New-York, 1953).

[35]) H. J. S. Sand, Electrochemistry and electrochemical analysis. 1–3 (Blackie and Son ltd., London, 1946).

[36]) R. W. Dodson *et al.*, Miscellaneous Phys. and Chem. Techniques of Los Alamos Project (Ed. Graves and Froman, London, 1952).

[37]) C. J. Maletskos and J. W. Irvine, Nucleonics **14**, No. 4 (1956) 84.

[38]) G. N. Yakovlev *et al.*, J. Nucl. Energy **5**, No. 1 (1957) 159.

hooks. The diameter of both the gasket and tube is dependent on the area required to be coated with activity.

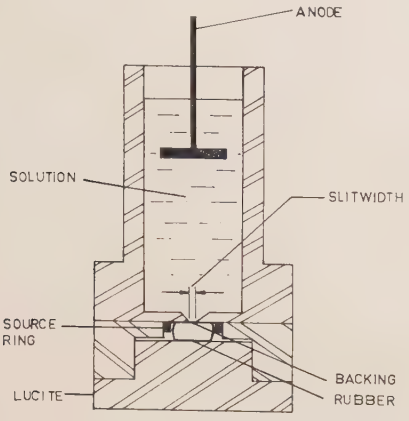

Fig. 4. Electro-deposition cell. (Due to C. de Vries.)

An apparatus recently constructed[39]) can be seen in fig. 4. This particular deposition cell has been used extensively for the preparation of sources as used in an iron free double focusing spectrometer. Constructed almost entirely from lucite, the main advantage of this deposition cell is the variable aperture employed for defining the active area. The usual dimension of active area required is 1×10 mm, and some good results have been obtained making use of organic films with a metal substrate. The deposition cell employed by the authors of the present investigation is similar to that described above, the only difference being that instead of a variable aperture, a series of masks of suitable dimensions may be used, the smallest of which has the dimensions 0.05×10 mm and has found application in the preparation of sources suitable for a semi-circular photographic spectrometer[40]). It should be pointed out that an advantage of using lucite as a construction material for deposition cells is that the activity does not have the tendency of depositing on the walls of the container as is sometimes the case when glass is used. Examples of this are the isotopes of gold and silver. Also such a cell can be constructed as a self-contained unit and consequently presents little difficulty when considering radiation shielding.

3.2. EXPERIMENTAL INVESTIGATION

For the purpose of the reported phase of the investigation, the following conditions have been observed while considering electro-deposition.

1. All deposition media have been kept as simple as possible, i.e., no additive agents were contributed to the solution unless absolutely necessary.

2. In all experiments the electrodes were of a standard dimension, 5 mm diameter. However, it was observed that the use of a cylindrical graphite anode considerably improved the homogeneity of the activity deposit[35]). This last should find particular application where the cathode is in the form of a wire. Since approximately every fifth preparation was required for actual measurement, the cathode varied in both dimension and material depending on the type of measurement. Usually the material required for these measurements was of an organic nature with a metal substrate. However, all the results presented are based on the dimensions given above.

3. The time of deposition in each case was maintained for a period of one hour at a current of 40 mA. According to Castos[41]), providing that all other factors remain constant, the rate of deposition increases almost linearly with the current.

4. Because the source support material usually employed for preparation work is organic with an evaporated metal substrate, all acidic and alkaline solutions were maintained at a concentration of 0.1 N so as to reduce the danger to the backings.

5. It has been pointed out that when the electrolyte is either stirred, heated, or both, the rate and quality of deposition will improve[35]). In the present investigation, such refinements have been excluded so that the results can be considered as minimum yields.

[39]) C. de Vries, Institute for Nuclear Physics, Amsterdam (private communication).

[40]) W. C. Parker and E. Karlsson, Nucl. Instr. to be published.

[41]) C. Casto, Analytical Chemistry of the Manhattan Project, Ed. Rodden (New York, 1950).

3.3. EFFICIENCY OF DEPOSITION

The determination of the deposition efficiency was carried out by means of a gamma-ray detector. Since some activities were of short, half-life and, in consequence, decayed rapidly, the efficiency of the deposition was measured after completion of the preparation. Both the solution and cathode were measured alternately and in order to avoid the difference in geometry of the above, the distance chosen for the measurement was 30 cm from a NaI crystal 2×1 inch. In order to obtain as accurate determination as possible, a given number of points were taken over the spectrum and the difference in peaks deducted. The results obtained using the technique of electro-deposition are summarized in tables 1 thru 4. As previously stated, all depositions were carried out under the following conditions:

Time of deposition — 1 hour
Acid and alkaline solution — 0.1 *N*
Deposition current — 2.0 mA/mm^2
Dimension of electrodes — 5 mm diameter.

4. Vacuum Deposition

4.1. INTRODUCTION

The problems encountered in the vacuum deposition of radio-active materials have been pointed out previously[6]), and it is sufficient to mention them only briefly at the present time. However, before considering this method as a means of preparation, there are certain very definite facts that should be considered.

1. Some form of receptical should be employed as the vapour source, and its removal from the apparatus facilitated for the purpose of loading the activity. Such vapour sources can be designed so as to provide collimation of the vapour stream, consequently reducing the solid angle, and in turn, the contamination of the apparatus.

2. Sometimes the activity is difficult to obtain, or obtainable only in limited quantities; therefore a reasonable deposition efficiency is essential and one must consider whether or not the measurement in question demands the possible, but not certain, quality of deposit obtainable by this method.

TABLE 1

Deposition medium 0.1 *N* HCl

Isotope	Half-life	Yield (%)	Isotope	Half-life	Yield (%)
Sb^{122}	2.8 d	25	Ni^{57}	36 h	40
Au^{194}	39 h	20	Os^{191}	15 d	25
Cr^{51}	27.8 d	20	Pt^{197}	18 h	30
Cd^{115}	43 d	17	Pd^{109}	13.6 h	80
Cu^{64}	12.8 h	30	Re^{186}	3.7 d	16
† Co^{56}	77 d	3.5	Ag^{110}	270 d	10
Hg^{203}	47 d	50	Sn^{121}	27 h	22
Ir^{194}	19 h	45	† Zn^{69}	51 min	2

TABLE 2

Deposition medium 0.1 *N* NH_4OH

Isotope	Half-life	Yield (%)	Isotope	Half-life	Yield (%)
Ge^{71}	11.4 d	2	Mn^{56}	2.6 h	1
Ga^{72}	14.1 h	13	Pb^{200}	21 h	50
† Co^{56}	77 d	20	Tl^{200}	26 h	80
In^{116}	54 min	8			

Table 3
Other deposition media

Isotope	Half-life	Media	Yield (%)
As^{76}	26.5 h	$NH_4OH + HCl$	20
† Bi^{210}	5 d	$HNO_3 + NH_4OH$	40
Ca^{45}	164 d	Pyridine	5
Mn^{56}	2.6 h	H_2SO_4	1
Sr^{87}	2.9 h	Pyridine	4
Tl^{200}	26 h	Acetamide	40

† References for electro-deposition: Zn–Co [37]), Bi [60]), Eu [61]), Gd [62]), Dy, Ho, Tm, Yb, Lu, Tb [63]).

The following references tefer to the text books employed during the electro-deposition phase of the investigation: [34, 35, 56, 57, 58, 59]).

Table 4
Rare earth elements

Isotope	Half-life	Solution	Yield (%)
La^{140}	40.2 h	Pyridine	30
Ce^{143}	33 h	Pyridine	63
Pr^{142}	19 h	Pyridine	40
Nd^{149}	1.8 h	Pyridine	20
† Eu^{152}	9.2 h	Ethyl al.	5
† Gd^{159}	18.0 h	$(NH_3)_2SO_4$	10
† Dy^{165}	2.32 h	Pyridine	2
† Ho^{166}	27.3 h	Pyridine	20
† Tm^{170}	127 d	Pyridine	26
† Yb^{175}	4.2 d	Pyridine	14
† Lu^{177}	6.8 d	Pyridine	3
† Tb^{160}	75 d	Pyridine	10

3. Unless particularly designed for handling active material, the spread of contamination outside the apparatus can be extemely rapid. In order to prevent this, it is necessary that suitable vapour traps are placed in the pumping system, and so designed that replacement can be achieved with a minimum of difficulty. Although sometimes impracticable, the apparatus should be completely demountable.

Probably the greatest disadvantage with the usual arrangements for the vacuum deposition of active material is the fact that large amounts of activity are required in order to achieve small effect[6]). Also, some elements are difficult to evaporate because of high temperatures required, or due to their compounds decomposing during vacuum processing; in both these instances, collimated vapour sources are more efficient than the more conventional type.

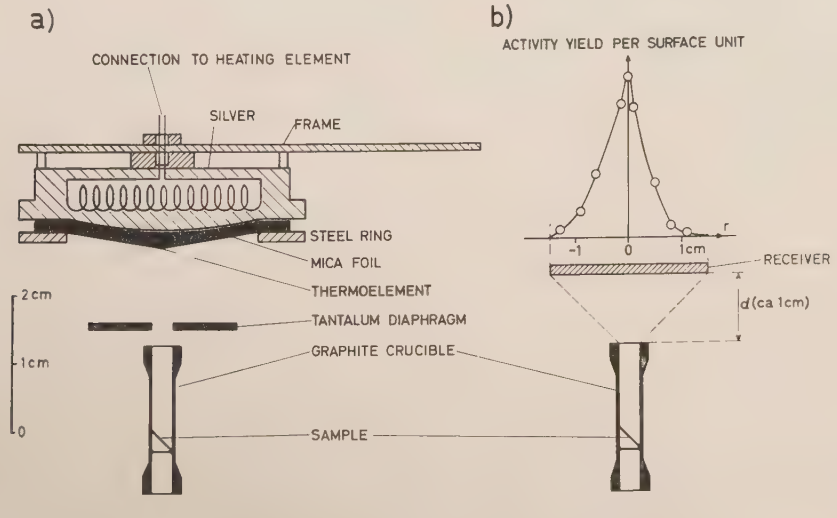

Fig. 5. Vacuum deposition arrangement. (Due to H. Frauenfelder.)

[56]) J. Wiley, Applied Inorganic Analysis, Ed. Hillebrand (New York, 1955). [57]) Analytical Chemistry of the Manhattan Project, Ed. Rodden (New York, 1950). [58]) Miscellaneous Phys. and Chem. Techniques of the Los Alamos Project, Ed. Graves and Froman (London, 1952). [59]) Robinson and Stokes, Electrolyte Solutions (London, 1959). [60]) I. Lindgren, and C. M. Johansson, Arkiv för Fysik **15**, No. 33 (1959) 445. [61]) V. M. Kellman, Nucl. Phys. **2** (1957) 395. [62]) V. S. Shirley, Nucl. Phys. **4** (1957) 395. [63]) J. W. Mihelich *et al.*, Phys. Rev. **108** (1957) 989.

4.2. APPARATUS

Apparatus used for the deposition of active material has been frequently described. These can be divided into two catogaries: (a) where no collimation is afforded the vapour stream, but shields of plastic or other suitable material employed to facilitate decontamination, (b) the use of collimated vapour sources which restricts contamination from the solid angle point of view, with the additional advantage that less active material is required for the deposition. Frauenfelder[42]) made use of collimated vapour sources which were made from graphite and directly heated. This apparatus was not originally intended for use in preparation work, but it does serve as a guide to what the design of such apparatus should be based upon. Since we assume that the vapour source, or crucible, forms the all important part of such apparatus, only these as used in the above apparatus are shown in fig. 5. For more extensive information, reference to Frauenfelder's thesis is recommended. Biram[43]) described a rather novel form of strip vapour source the construction of which may be seen in fig. 6. Biram points out that this type of heater is easy to construct and capable of reaching the required temperature rapidly. The radiation shield is made in one piece and supports a tungsten rod around which is wound a thin wire of the same material so as to prevent the molten evaporant collecting on different parts of the heater. The greatest advantage of this type of heater, as applied to active work, is that it can be replaced at relatively small expense, and, for certain applications, it may prove ideal, i.e., the preparation of strip sources as used in spectrometers of the double focusing type.

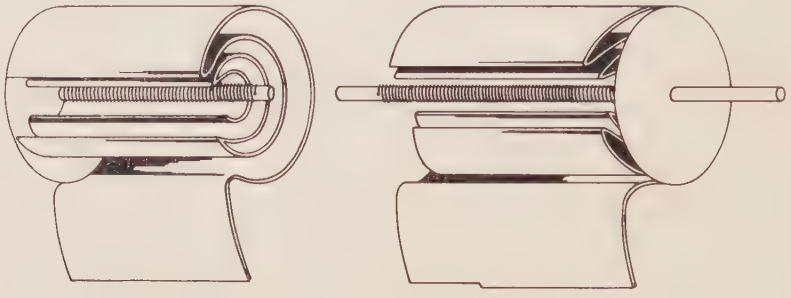

Fig. 6. Vapour Source. (Due to Biram.)

Some crucibles described by Stockendal and Bergkvist[44]) have been used extensively for

[42]) H. Frauenfelder, Acta Phys. Helv. **23** (1950) 347.
[43]) J. Biram, Vacuum **11**, No. 2 (1952) 154.
[44]) R. Stockendal and K. E. Bergkvist, Nucl. Instr. **1** (1957) 53.

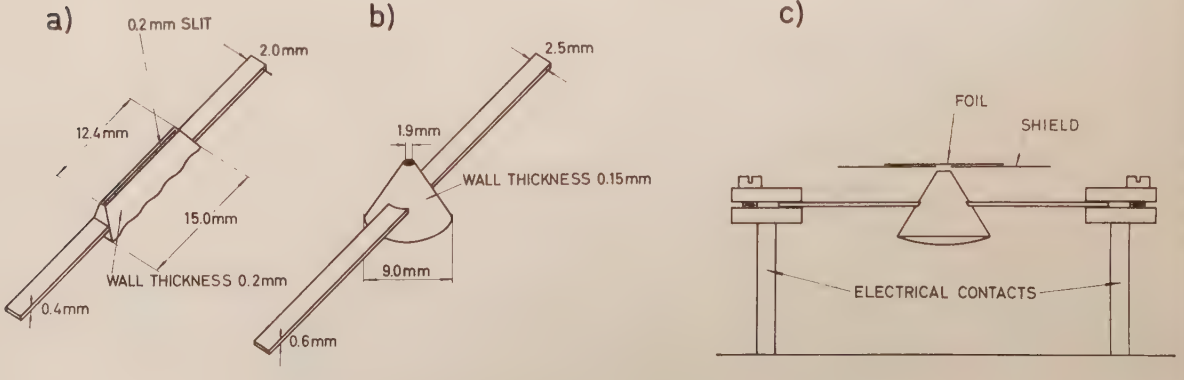

Fig. 7. Deposition crucibles. (Due to Stockendal and Bergkvist.)

active preparations in connection with various spectrometers. The main objection to these crucibles would appear to be in the loading of

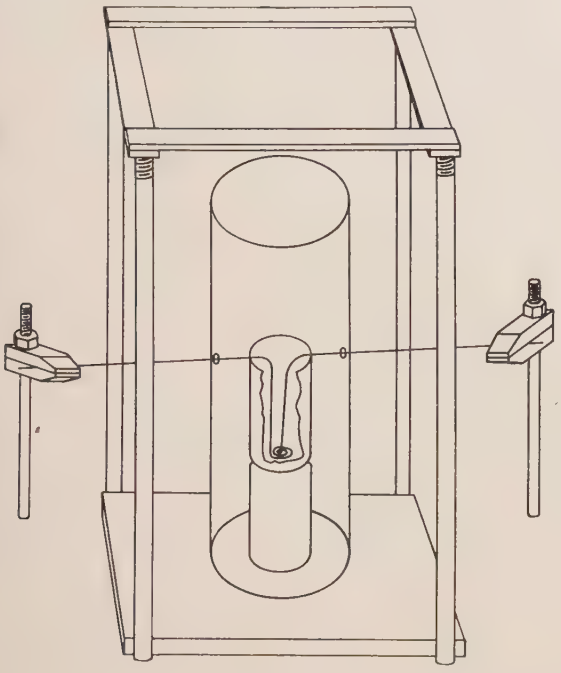

Fig. 8. Active evaporation device due to Barr and Blackburn.

active material; also, because of their construction, fig. 7, the work must be undertaken by a goldsmith who can work with the material used. However, as previously reported[44]), these crucibles have found extensive application giving yields in the region of 90% with excellent uniformity. An apparatus reported by Innman and Quigley[45]) for the evaporation of radio-active and toxic materials relies on the removal of protective covers in order to allow quick decontamination caused by a vapour source of open description. An effective device for use with existing vacuum apparatus is that employed by Barr and Blackburn[46]). The arrangement is shown in fig. 8. However, for the type of work dealt with here, rather large quantities of active material are still necessary. Bühring and Heintze[47]) have recently described an apparatus for the deposition of active material. Heated by electron bombardment, it makes use of collimated crucibles. Other apparatus adaptable for this type of work have been described by O'Bryan[48]), Hill[49]), Kelly[50]), and Flinta[51]). The apparatus used by the authors is that described by Parker[6]). For a theoretical treatment dealing with the focusing properties of vapour sources, the reader is refered to the following: Heavens[52]), Preuss[53]), Rossmann and Yarwood[54]), and Chomet and Yarwood[55]).

4.3. EXPERIMENTAL

As with that part of the investigation dealing with electro-deposition, certain rules were established for this type of deposition and are as follows:

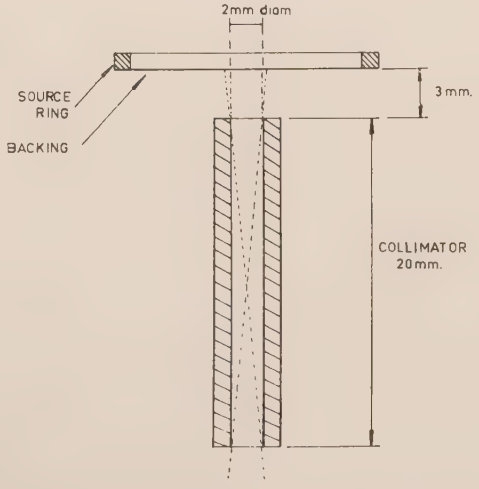

Fig. 9. Vacuum deposition; experimental arrangement.

1. The material, where possible, was taken up in ether in a compound form and loaded into the crucible cup. The ether was then evaporated by means of a heat lamp. The crucible employed, that which was previously reported[6]), had a

[45]) M. C. Innman and D. Quigley, J. Sci. Instr. **35** (1958) 226.
[46]) L. W. Barr and D. A. Blackburn, J. Sci. Instr. **36** (1959) 197.
[47]) W. Bühring and J. Heintze, Nucl. Instr. **6** (1959) 286.
[48]) H. M. O'Bryan, Rev. Sci. Instr. **5** (1934) 125.
[49]) H. A. Hill, Rev. Sci. Instr. **27**, No. 2 (1956) 1086.
[50]) J. C. Kelly, J. Sci. Instr. **36** (1959) 89.
[51]) J. Flinta, Vacuum **11**, No. 3 (1952) 259.
[52]) O. S. Heavens, Proc. Phys. Soc. London B **65** (1952) 788.
[53]) L. E. Preuss, J. Appl. Phys. **24**, No. 11 (1953) 1401.
[54]) M. G. Rossmann and J. Yarwood, Brit. J. Appl. Phys. **5** (1954) 7.
[55]) S. Chomet and J. Yarwood, Brit. J. Appl. Phys. **6** (1955) 343.

collimator 2 mm diameter and 20 mm long.

2. The dried activity was measured in the same manner as that employed for electrodeposition, i.e., at a distance of 30 cm from a 2 × 1 inch crystal. As before, a given number of points were taken over the spectrum thus allowing a more accurate yield determination to be obtained.

3. On completion of the deposition, the crucible cup was measured a second time followed by the source support material. Again the spectrum was measured and the peaks deducted. Where necessary, the decay was taken into consideration. The schematic diagram, fig. 9, shows the arrangement employed for all the depositions carried out.

For the sake of convenience, the half-lives of the active materials have been given in the vacuum deposition table. Unless otherwise stated, all depositions were made onto aluminium 2 mg/cm^2.

5. Miscellaneous Techniques

In dealing with source and window technique, Slätis[12]) describes the various methods and techniques concerning the preparation of radioactive sources. Apart from those already dealt with there are the following:

5.1. EVAPORATION OF DROPLETS

Although suitable in certain cases, the drop method, where the activity in solution is dropped onto the required backing, mostly results in poor homogeneity. When measuring high energies, this last is not always important. However, for the fewer regions it is probable that large deviations from the true spectra will be observed[1, 2]). Slätis points out that variations in intensity of radiation from different parts of the source, can be as much as 100:1 which is probably due to the growth of crystals and the precipitation of active material[2]). The uniformity of such sources can be somewhat improved by the use of insulin, thus enabling the active solution to spread more uniformly over the required area. Finally, the deposit can be dried by slow evacuation in a vacuum system.

TABLE 5

Vacuum deposition

Isotope	Half-life	Yield (%)	Isotope	Half-life	Yield (%)
Sb^{122}	2.8 d	60	Au^{194}	39 h	90
Cr^{51}	27.8 d	100	Cd^{115}	43 d	25
Cu^{64}	12.8 h	90	Co^{60}	5.2 y	90
Ni^{57}	36 h	90	Pt^{197}	18 h	90
Pd^{109}	13.6 h	70	Ag^{110}	270 d	90
Sn^{121}	27 h	22	Zn^{69}	51 min	30
Ge^{71}	11.4 d	50	Ga^{72}	14.1 h	85
In^{116}	54 min	50	Mn^{56}	2.6 h	70
Pb^{200}	21 h	90	Tl^{200}	26 h	90
As^{76}	26.5 h	100	Bi^{210}	5 d	80
S^{35}	87 d	90	Ca^{45}	164 d	90
Sr^{87}	2.9 h	70	Rb^{86}	19 d	15–50
P^{32}	14 d	15–50	Se^{75}	180 d	90
La^{140}	40.2 d	40–70	Ce^{143}	33 h	90
Pr^{142}	19 h	40–70	Nd^{149}	1.8 h	40–70
Eu^{152}	9.2 h	40–70	Gd^{159}	18.0 h	65
Dy^{165}	2.32 h	—	Ho^{166}	27.3 h	40–70
Er^{171}	7.5 h	—	Tm^{170}	127 d	—
Yb^{175}	4.2 d	80	Lu^{177}	6.8 d	60
Sm^{153}	1.96 d	40–70	Tb^{160}	73 d	75

5.2. SLURRY TECHNIQUE

With the slurry technique, a glass tube of appropriate diameter is pressed against the backing material in question and the activity, in the form of a fine powder in solution, is allowed to settle. The solution is then removed and the deposit dried. With sources produced in this manner, the active deposit should be covered with a thin film so as to avoid loss of activity during measurement, and the consequent spread of contamination.

5.3. ZAPON SPREADING TECHNIQUE

An alcoholic solution of the nitrate of the substance to be deposited is mixed with a dilute solution of zapon lacquer in alcohol, acetone, or zapon thinner. The resulting solution is spread over the foil backing, dried, and ignited to remove the organic substances and convert the nitrate to oxide[40]). Zapon films been coated on aluminium, platinum, brass, copper, iron, steel, molybdenum, and nickel.

5.4. ELECTRO-PHORETIC

A fine powder of the material required for preparation is mixed in alcohol so as to form a stable suspension. This suspension is transfered to a metal cylinder, approximately 10 mm in diameter, and the backing material placed along its axis. A potential of between 300 and 800 volts is applied between the backing material and the cylinder. A diagram of the two types of apparatus (one for deposition on wires and the other for deposition on strips) used by the authors is shown in fig. 10. It has been pointed out that it is sometimes necessary to change the polarity depending on the material in question. Also, the charging of the particles can be enhanced by the addition of a minute quantity of a solution of HCl and alcohol (pH about 1) or, alternatively, approximately 0.1 mg of tannic acid. The described method has found particular application to the preparation of sources as used in a permanent magnet spectrograph[7]). Apparently, the only objection to the extended use of this technique is that the active material must be capable of forming a suspension in a non-conducting medium, and also that rather large amounts of active material are necessary to obtain a satisfactory suspension. However, it is possible to obtain thin

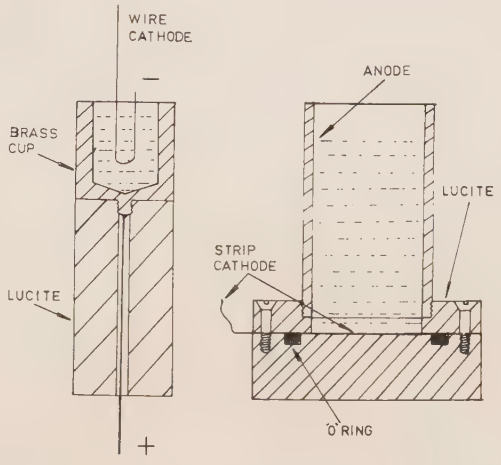

Fig. 10. Electro-phoretic cells for wire and strip sources.

deposits having reasonable uniformity. In table 6 can be seen the efficiencies obtained for some of the rare earth elements. Usual time of deposition was 10 to 60 seconds.

TABLE 6

Electro-phoretic deposition
Alcoholic amylic, iso.

Isotope	Half-life	Yield (%)
La^{140}	40.2 h	80
Pr^{142}	19 h	65
Nd^{149}	1.8 h	40
Eu^{152}	9.2 h	85
Dy^{165}	2.32 h	85
Tm^{170}	127 d	65
Yb^{175}	4.2 d	80
Lu^{177}	6.8 d	55

5.5. ION EJECTION

A method for the preparation of thin films of radio-active material developed by Carswell and Milsted[8]) would appear to offer extensive possibilities for the type of preparation necessary in beta-spectroscopy. As with the electrophoretic technique, the material is in a non-conducting solution. Briefly, the procedure is

as follows: A capillary tube is drawn down to form a fine jet of such dimension that under normal conditions no liquid can escape. A wire of suitable dimension is inserted to within a few millimeters of the tip of the jet and the free end connected to the positive side of a high voltage supply capable of providing 3 to 10 kV.

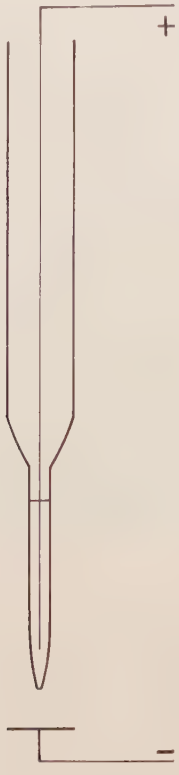

Fig. 11. Principle of ion ejection.

The receiving backing is placed at a distance of about one centimeter below the jet and connected to the negative side of the h. v. unit. When the voltage is applied, the liquid is ejected along with any ejected charged particles as a fine mist which evaporates. Consequently, the particles of active material are collected by the backing. The principle of the method can be seen in fig. 11. Carswell and Milsted have used this method for the preparation of thin alpha sources and claim that the method compares favourably with vacuum deposition; they point out that the use of auxillary electrodes to shape the electric field and afford focusing of the charged particles offers many possibilities.

5.6. DUST COLLECTION TECHNIQUE

Activity in solution is placed in a container maintained at a positive gas pressure. An escape aperture passes into a second chamber maintained at a negative gas pressure. As a consequence of this arrangement, the solution is drawn from one chamber to the other at an extremely high velocity. Situated immediately after the aperture is a heater kept at the boiling temperature of the solution in question. The required backing material is placed in line with the axis of the aperture and collects the dried dust.

5.7. CATHODIC SPUTTERING

What is probably the oldest deposition technique, that of cathodic sputtering, appears to have been rather neglected as far as source preparation is concerned. The possibilities of pre-preparation of material for irradiation are extensive. Metals such as Os, Ir, Pt, Rh, and Ru, which are difficult to deposit by normal vacuum deposition methods, present little difficulty where cathodic sputtering is employed. The ability to build up thick uniform deposits with good adhesion is a further advantage.

Acknowledgements

The authors would like to express their thanks to Professor Kai Siegbahn for his interest in this work and also to Dr. T. R. Gerholm and the beta-spectroscopy group for the many helpful discussions and suggestions. Further, our thanks are due to the Stockholm reactor group R. 1. for their co-operation in providing the many irradiations necessary for this investigation. One of us, M. De Croës, wishes to express her graditude to Professor Siegbahn and his staff for their kind hospitality during her stay at the Institute of Physics, Uppsala, which was made possible by a research grant from the I. I. S. N., Belgium.

NUCLEAR INSTRUMENTS AND METHODS 7 (1960) 37–44; NORTH-HOLLAND PUBLISHING CO.

THE SEPARATING OF PARTICLES ACCORDING TO THEIR IONIZATION VALUE IN SEVERAL SCINTILLATION COUNTERS

Yu. K. AKIMOV, V. I. KOMAROV, O. V. SAVCHENKO and L. M. SOROKO

Joint Institute for Nuclear Research Laboratory of Nuclear Problems, Dubna, U.S.S.R.

Received 8 October 1959

A telescope of scintillation counters is described by means of which it is possible to register rare processes of particle emission with high ionization and small range against a background of outside radiation with smaller ionization.

Both normal plastical scintillators 6 mm thick and filmlike scintillators 0.5 mm thick on a polistirole base with the addition of 1% of tetraphenylbutadien were used in the counters.

The counting responses of the telescope are given for the separation of deuterons from protons with the impulse $p = 900$ MeV/c, nuclei He^3 from deutrons with the impulse $p = 730$ MeV/c, and also for α-particles with the energy 800 MeV.

The apparatus here described has been used in experiments, investigating the processes:

$$p + d \rightarrow \pi^+ + H^3, \quad d + d \rightarrow He^3 + n, \quad d + d \rightarrow \pi^0 + He^4.$$

1. Introduction

In many experiments there arrises the problem of separating particles according to the value of their ionization losses in counters and simultaneously measuring an other of the three kinematical characteristics of the particle: the average range, energy and impulse. However, because of the partial overlap of the ionization spectra (fig. 1) it is impossible to completely eliminate registrations of particles with smaller ionization (group 1), without lowering the effectiveness of the registration of the emitted particles (group 2) with higher energies. The limit given by the far spreading "tail" in the ionization spectrum can be restricted by analysing the value of the ionization losses simultaneously in several counters.

One of the separating methods using several counters—separating according to the smallest amplitude—was proposed by L. D. Landau[1]), first applied by S. J. Nikitin[2]) and later by A. G. Meshkowski and L. G. Sokoloff[3]). The point of this method is that the smallest of all the amplitudes in several counters is chosen to be analysed.

[1]) L. D. Landau, Journ. of Phys. **8** (1944) 201.
[2]) S. J. Nikitin, JETP **8** (1948) 577.
[3]) A. G. Meshkovski, L. C. Sokoloff, JETP **30** (1956) 840.

In the problem of dividing two groups of particles with the help of amplitude discrimination an other approach is possible. The point of it is that one selects only such events with the help of a registrating device, when the amplitude of the pulses is higher then the discrimination threshold U_D in all the counters simultaneously.

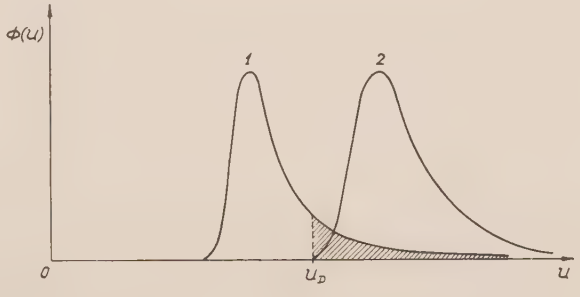

Fig. 1

Amplitude selecting in several counters at the same time and not only in one makes it possible to diminish random amplitude distortions, which imitate slow particles. Such distortions originate when impulses overlap in time and under the influence of "stars" called forth by fast particles, passing through the counters.

2. Registrating Apparatus

The telescope meant for separating particles in the above described way is composed of six scintillation counters. Five of these counters connected for coincidences, are spectrometric (FEU-29) and the sixth counter (FEU-19) is connected for anticoincidences with the first five.

made of aluminum foil and were arranged on plexiglass light pipes. The inhomogeneity of light collecting by such a reflector, which was found experimentally by irradiating different parts of the scintillator with a collimated beam of γ-quants Co^{60} did not exceed 10%.

When registering particles with a large range protons and deuterons—normal plastical

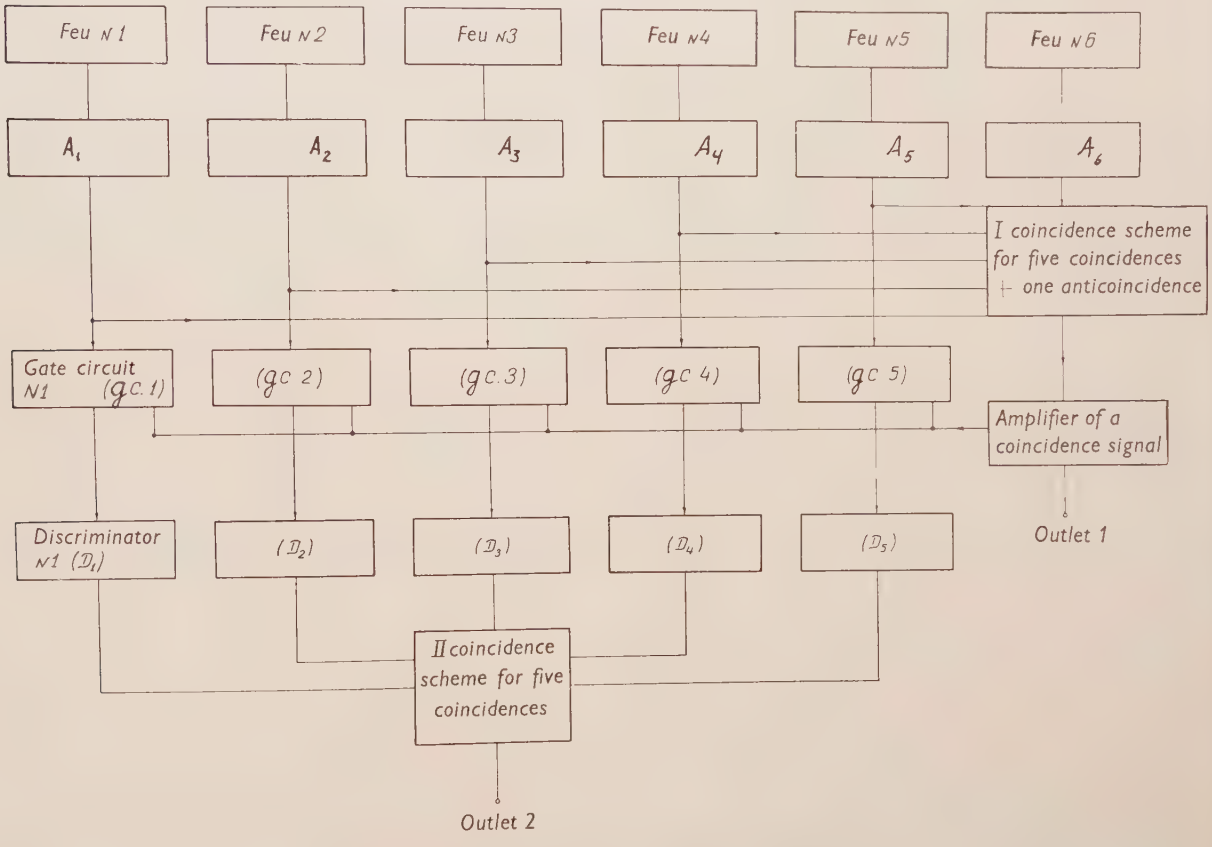

Fig. 2. Block-scheme of the radiotechnical apparatus.

When registering heavy charged particles with small range, for instance nuclei He^3 and He^4, film-like scintillators 0.5 mm thick were used. The film was prepared by pouring a heated solution of ready-made polimerisate-polistirole with added 1% of tetraphenyl-butadien in toluene on a strictly horizontal surface of mirror glass and by subsequent drying at room temperature[4]).

Film scintillators sized between 20×35 mm and 42×60 mm were placed in a reflector

scintillators 6 mm thick were used, made of polistirole with added 2% of p-terphenyl and 0.2% of αNPO.

The block-scheme of the radiotechnical apparatus is given on fig. 2. Pulses from each of the spectrometric photomultipliers (1–5) are amplified in a linear amplifier (A_i) and pass through a linear gate circuit (G.C.) to the discriminator (D). The gate circuit ($1 \div 5$) is controlled by output

[4]) M. N. Medvedjev, E. N. Matvejeva, L. Jiltsova (priv. comm.).

pulses from the first coincidence circuit, to which pulses come from the outlet of the linear amplifiers in each channel (1–5). After discrimination the pulses are registered by the second coincidence circuit. The apparatus so connected selects only such events, when pulses originate simultaneously in all the counters except the anticoincidence counter and the amplitudes of the pulses at the outlets of the amplifiers exceed the discrimination threshold U_D.

Thanks to the introduction of the gate circuits and the first coincidence circuit one has the following advantages:

(a) The dead time effect is reduced since the background pulses do not pass through the discriminator.

(b) There arrises the possibility of measuring ionization spectra in any number of channels and moreover the counting at the outlet of the first coincidence circuit is monitory.

(c) The resolving time of the whole system is reduced, since pulses come to the coincidence circuit before the discriminator, not after it.

A principle scheme of the apparatus is given on figs. 3 and 4. The photomultipliers are loaded by the input resistance of the phase invertors (L_{01}–L_{06}). The anode lead of the phase invertor for alternating current is the wave impedance of the cable RK-50, along which the pulses are passed to the basic radiotechnical scheme. Pulses are amplified by two linear amplifiers with negative feedback (L_5, L_6, L_7, L_8A). From the anode of L_8A pulses are transmitted along the cable RKZ-400 to the inlet of the lamp L_{23} in the gate circuit (L_{21}–L_{23})[5]). From the cathode of the same lamp L_8A pulses pass to the amplifier (L_8B, L_9) working in the saturation regime. The amplitude of the pulses at the outlet of the amplifier is 5 volts and has negative polarity. If these impulses appear simultaneously on all channels a coincidence is registered. The resolving time of the coincidence circuit is about equal the pulse duration, that is about 10^{-7} sec. The number of channels of the coincidence circuit (L_{10}–L_{15})[6]) can be

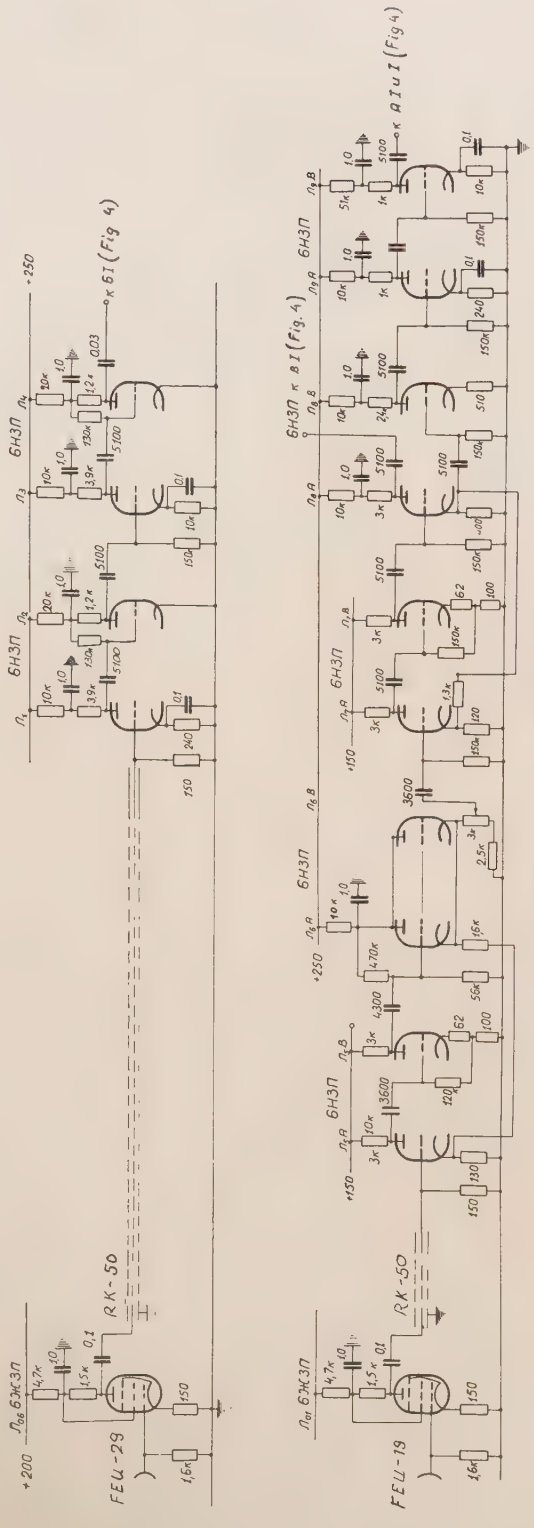

Fig. 3. Principle scheme of the amplifier channels.

[5]) Yu. K. Akimov, PTE **2** (1957) 216.
[6]) Yu. K. Akimov, PTE **1** (1957) 95.

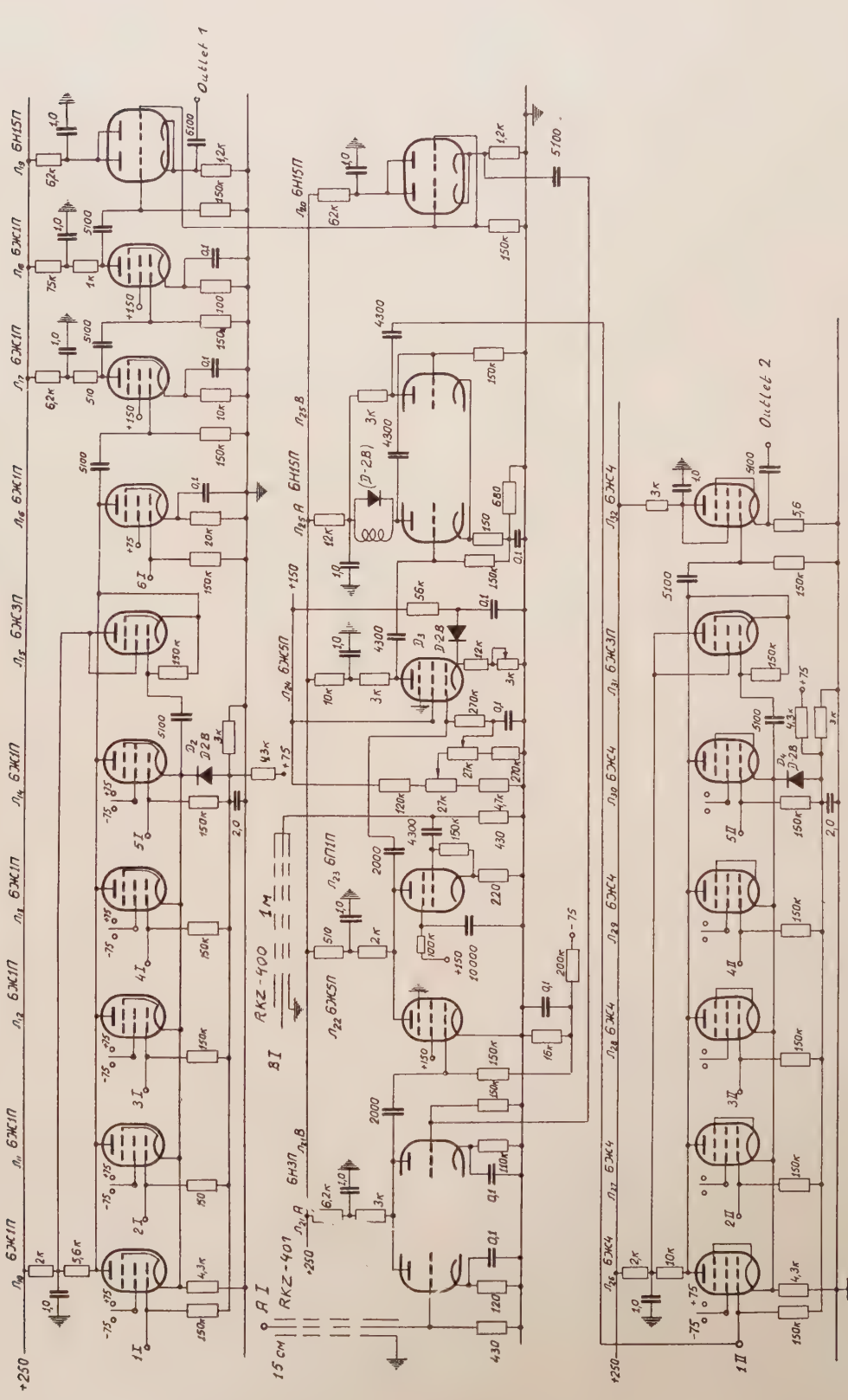

Fig. 4. Principle scheme of the apparatus.

changed by switching the screen grid with the potential + 75 volts to — 75 volts.

The pulses from the anticoincidence counter are amplified to the amplitude 6 volts and positive polarity in the four-cascade amplifier (L_1–L_4) working in the saturation regime. To limit overshoots of positive polarity one normally lets a small current pass through the grid circuits of the lamps L_2 and L_4 by connecting the grid resistance (130 k) to the anode by-pass. The anticoincidence pulses open the lamp L_{16} which is usually closed, the anode of which is connected with the anodes of the lamps L_{10}–L_{14} and suppress the coincidence pulses.

If there is no anticoincidence pulse, the pulses from the coincidence circuit are amplified (L_{17}, L_{18}) to the amplitude 9 volts positive polarity and pass through the cathode follower L_{19} to a scaling block and through the cathode follower L_{20} to the closed right half of the double triode $L_{21}B$. To the left half of the lamp $L_{21}A$ pulses in negative polarity, which have passed through the cable section RKZ-401, are passed from the lamp L_9B. The result of this is that pulses of negative polarity originate at the anode of lamp L_{21} and pass to lamp L_{22}. Since this lamp is normally closed, pulses from the linear amplifier pass through lamp L_{23} to the inlet of the discriminator (L_{24}, L_{25}) without amplitude distortions. In those cases when there is no coincidence, pulses do not pass to the right half of the triode $L_{21}B$. The result of this is that pulses coming from the left half of $L_{21}A$ open the lamp L_{22}. The anodes of the lamps L_{22} and L_{23} are connected with each other. Pulses with negative polarity in the anode of the lamp L_{22} suppress pulses with positive polarity, which arise on the anode of lamp L_{23}. The above mentioned cable lengths RKZ-400 (10^{-7} sec) and RKZ-401 (7×10^{-8} sec) have been introduced so as to time-coordinate the instants when the pulses come to the gate circuit.

The overall amplification factor of each channel from the outlet of the photomultiplier to the inlet of the discriminator, can be varied from 30 to 70 by regulating a variable resistance (3 k) at the outlet of the first linear amplifier. When the amplitude of the pulses at the inlet of the discriminator vary from 0 to 30 volts the amplification factor does not change for more than 20%.

The discriminator consists of the closed lamp L_{24} and a sensitive kipp oscillator L_{25}[7]). The lamp L_{24} is closed by the cathode circuit. A divider, common for all fine discriminators, gives the potential to the control grids of the lamps and can vary the potential from 0 to 29 volts. The potential of each cathode, which balances the action threshold of the discriminators, is arranged independently between the limits + 28 volts and + 32 volts, by adjusting the variable resistance (3 k) in the cathode circuit. Amplitude limiting is achieved with the help of the diode D_3, since deep negative feedback through the cathode resistance begins to function for large pulses, which close the diode.

After the kipp oscillator the pulse length is about 1.5×10^{-6} sec. These pulses pass to the second coincidence circuit which is analogical to the first one. Pulses from the outlet of the coincidence circuit pass through a cathode follower (L_{30}) to the scaling block.

3. Counting Response

Measurements of the counting response of the telescope were made under conditions analogous to those which have been previously described[8]). An extracted beam of protons with the energy 670 MeV created secondary particles in a target. A system of collimators and a deflecting magnet made it possible to separate particles emitted by a hydrogene-holding target the angle 5°. When the deflecting magnet created a certain field the telescope registered deutrons from the reaction $p + p = d + \pi^+$ with the impulse 900 MeV/c and also protons from the reaction $p + p \rightarrow \pi^0 + p + p$ and $p + p \rightarrow \pi^+ + n + p$ with the same impulse.

The first stage of the tuning was the balancing of the channel characteristics with each other

[7]) Yu. D. Bajukov, M. S. Kozodajev, A. A. Markov, A. I. Sinajev and A. A. Tjapkin, PTE 6 (1958) 34.

[8]) Yu. K. Akimov, O. V. Savchenko and L. M. Soroko, JETP 37 (1959) 46.

by changing the amplification factors in the channels and the voltage on the photomultipliers.

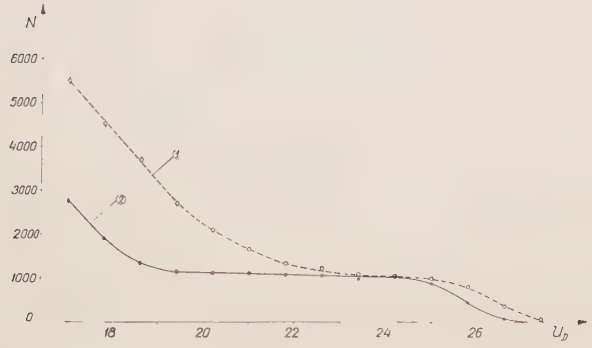

Fig. 5. The separating of deuterons from protons in 6 mm thick scintillators. Curve 1 for single-channel selecting, curve 2 for four-channel selecting.

On fig. 5 the integral counting curve is shown for one counter 6 mm thick, measured at the voltage 875 volts on the photomultipliers and the same curve for the case of four-channel selection. The counting response for four-channel selection has a broad plateau from 19 to 25 volts, which corresponds to the counting of deuterons. In the case of single-channel selection the width of the plateau was three times smaller—from 23 to 25 volts. This comparison shows that the separation of protons and deuterons by singlechannel amplitude selection is practically impossible when one passes into the region of higher values of the particles momentum, under the condition that the ratio of the number of protons and deuterons stays the same as before. This transition is connected with the increase of the straggling in the ionization spectrum.

When the width of the scintillators is decreased the straggling will also increase. The effect of engaging many selection channels for scintillators 0.5 mm thick is shown on fig. 6. The experiment was made under analogous conditions ($\theta_d = 5°$). The curve "1" applies to the integral spectrum of the pulse amplitudes in the first counter, the curve "2" when the amplitude selection is done in the second and fourth counter, the curve "3" is for the first, third and fourth counter, and last, the curve "4" is for selection in all five counters. One can see from fig. 6 how the counting response of the system improve as the number of channels for amplitude selection increases. For instance the extreme left point on the plateau length on the five-channel selection curve corresponds to an admixture of protons worth 60% of the number of deuterons in the case of single-channel selection.

Absolute measurements show that the efficiency of deuteron registering when five-channel selecting with thin scintillators, stays the same as with scintillators 6 mm thick in the limits of 5%.

An investigation of the spectrometric characteristics of a telescope with thin scintillators was made on α-particles with the energy 800 MeV which were elastically scattered on carbon

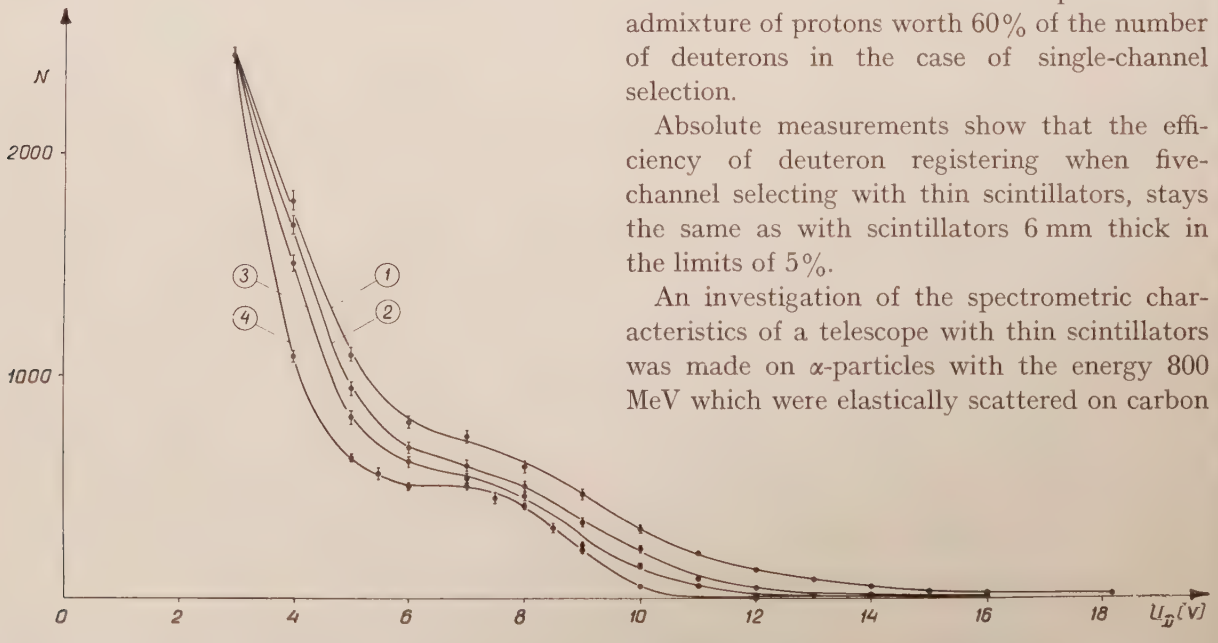

Fig. 6. The separating of deuterons from protons in 0.5 mm thick scintillators. Curve 1 selection in the first counter, curve 2 selection in the first and fourth counter, 3 in the first, third and fourth counter, 4 selection in all five counters.

nuclei under the angle 5°. The results of the measurements are shown on fig. 7. The curve 1 applies to the five-channel selection, the curve 2 to the single-channel one. The halfwidth of

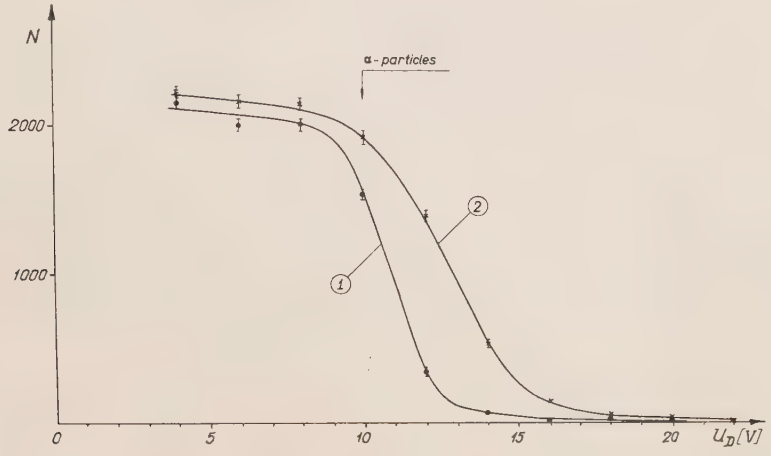

Fig. 7. Counting response of the system for α-particles with the energy 800 MeV. Curve 1 five-channel selecting, curve 2 single-channel selecting.

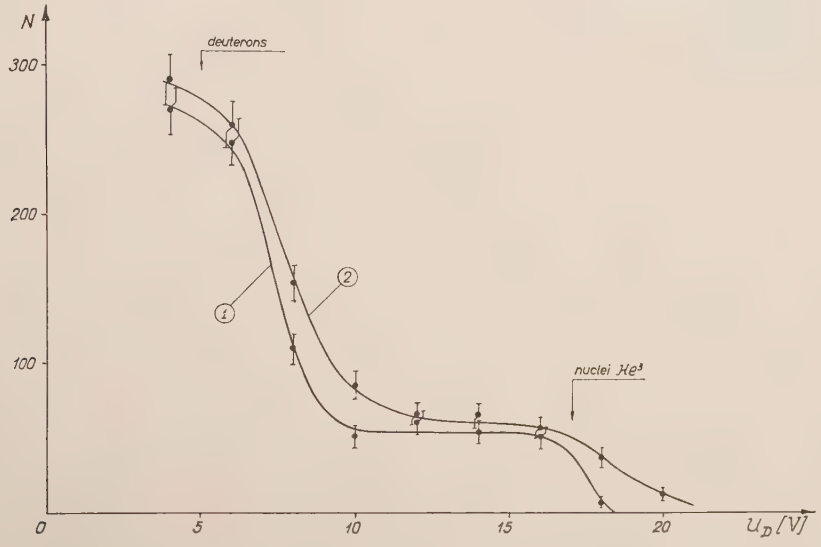

Fig. 8. Separating nuclei He^3 from deuterons with connected anticoincidence counter. Curve 1 five-channel selection, curve 2 single-channel selection.

the differential curve, applying to the integral curve on fig. 7 is 38% for single-channel selection and 26% for five-channel selection. The efficiency of the registration of α-particles practically does not change when the number of selection channel increases.

Another example separating particles, which was observed on a beam of deuterons with energy 400 MeV is the experiment in which nuclei He^3 ($E_{He^3} = 360$ MeV) were separated from deuterons ($E_d = 137$ MeV) with effective impulse 730 MeV/c. In this experiment an anticoincidence counter was used, which made it possible to select particles by range also. According to calculations deuterons and He^3 nuclei had ranges 12.4 and 13.0 g/cm^2 Cu correspondingly and were simultaneously captured by a master filter in the telescope. Results

of the measurement are shown on fig. 8. The curve 2 applies to the single-channel selection, curve 1 to the five-channel selection.

4. Conclusion

1. To register charged particles with high ionization and short range on the background of outside radiation with smaller ionization a method is proposed of separating particles in several scintillation counters by selecting those cases, when the ionization value exceeds a certain value U_D in all counters simultaneously.

2. This method makes it possible to appreciably decrease the contribution of particles with small ionization, which is conditioned by the tail in the ionization spectrum, and to lower the background, which is called forth by the formation of "stars" and by the overlap of pulses. The efficiency of registering the basic radiation is not effected.

3. The established apparatus is meant for registering rare processes of heavy charged particle emission, for instance the reactions $p + d \to He^3 + \pi^+$ or $d + d \to He^3 + n$, and chiefly to investigate the process of π^0 meson formation in the reaction $d + d \to \pi^0 + He^4$.

4. Besides the nuclei H^3, He^3 and He^4 this apparatus makes it possible to register nuclei Li^6 and Be^8. Their registrations thresholds are $E_{Li^6} = 110$ MeV and $E_{Be^8} = 170$ MeV.

NUCLEAR INSTRUMENTS AND METHODS 7 (1960) 45–49; NORTH-HOLLAND PUBLISHING CO.

A LINEAR GATE OF 10 TO 100 mμsec DURATION

G. B. B. CHAPLIN and A. J. COLE

Atomic Energy Research Establishment, Harwell, Didcot, Berks.†

Received 15 October 1959

A simple and reliable linear gate, which uses 2 diodes and a transformer is described as part of a system which includes a pulse stretching amplifier and fast gate-pulse generator. The gate has a switching time of 5 mμsec and accepts input signals with amplitudes ranging from 150 mV to 5 V. The amplifier produces output pulses of 5 μsec duration with 1% linearity in the range 2 mA to 70 mA.

A constant error of 1 mA at the output is introduced by the gate whilst the signal breakthrough is less than 1% over a wide range of temperatures.

The appendix includes details of a high-level amplifier which is suitable for use with present day pulse analysers.

1. Introduction

The function of the linear gate is to be interposed between a source of pulses, which may be random in amplitude, and an output circuit so that when the gate is closed the pulses are inhibited, and when opened the pulses are passed to the output circuit. In some applications (e.g. nuclear particle counting systems) the time for which the gate is open may be quite short, and the transient voltages produced when the gate opens or closes may be comparable in size to some signal pulses and hence be indistinguishable from them.

Attempts have been made to reduce the transient voltages by injecting artificial transients of opposite polarity, but the procedure can be complicated and the results may vary with time or temperature.

In the system described below the transients are integrated over a period which is long compared with the gate width (i.e. time open) so that the "reactive" transients produce zero output.

As an example of the system a gate is described which accepts input pulses up to 5 volts in amplitude and of 40 mμsec duration from low impedance cable (e.g. 100 Ω) and produces output pulses up to 70 mA in amplitude and stretched to 4 μsec to operate a multichannel pulse amplitude analyser. A gate width of 50 mμsec is adequate for such an input pulse although in the present system the width can be varied from 10 to 100 mμsec if necessary.

2. Circuit Operation

Referring to fig. 1: the signal pulse is applied to a transformer primary winding and the output

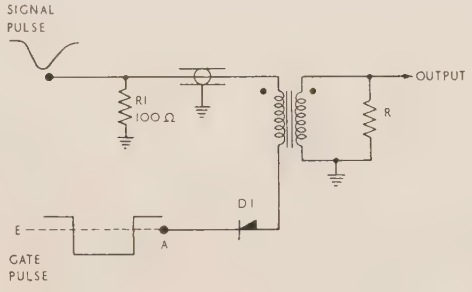

Fig. 1

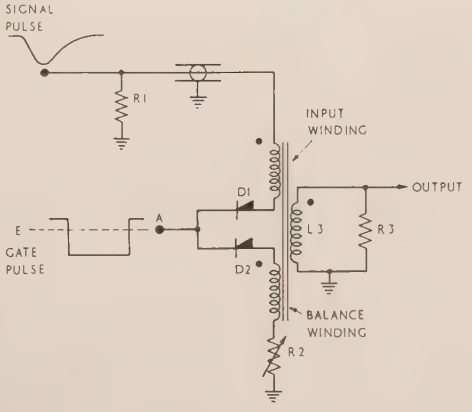

Fig. 2. Gate transformer.
D1, D2: GEX 39. Transformer: FX 1011 pot core.

pulse taken from a secondary winding. In the absence of a gate pulse the diode D_1 is biassed in the reverse direction so that a signal pulse is

† Present address: The Plessey Company, Ltd., Roke Manor, Near Romsey, Hamshire, England.

not able to cause current to flow in the transformer primary and there is therefore no output pulse. If, however, a gate pulse is present the diode D_1 will conduct and so present a low impedance to the lower end of the transformer primary. A signal pulse can therefore cause current to flow in the primary and hence produce an output pulse on the secondary winding.

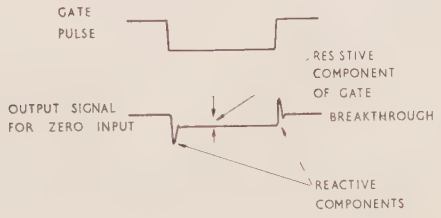

Fig. 3

The application of the gate pulse itself causes a voltage to be induced in the secondary winding which is indistinguishable from that due to the input signal. To overcome this defect a third winding is added to the transformer as in fig. 2. This balancing winding is connected to the gate pulse by another diode D_2 and a variable resistance R_2, and is in antiphase to the input winding. The value of R_2 is approximately equal to the impedance of the input cable (100 Ω) and is adjusted until the resistive component of the gate break-through is zero (fig. 3).

However, owing mainly to stray capacity on the transformer and diodes, there remain reactive components of breakthrough which occur at the instants of opening and closing the gate. Although these are of considerable voltage amplitude the nett charge transferred is zero, and so their effect can be greatly reduced by passing them through an integrator having a time constant long compared with the gate width. The integrator can be a simple resistance-capacitance

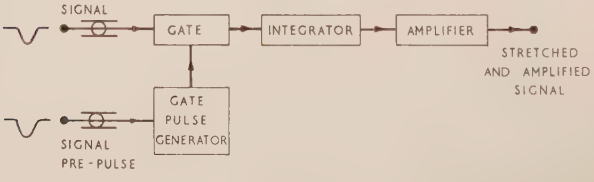

Fig. 4.

network or may be incorporated in the amplifier which follows the gate. It is important that the time constant of the transformer output winding L_3/R_3, (fig. 2), should be at least of the same order as the integration time constant, otherwise the signal will acquire reactive characteristics and will itself be attenuated by the integrator.

A block diagram of the gate is given in fig. 4. The purpose of the amplifier is to increase the maximum amplitude of the pulses to 70 mA so they can be processed by a multichannel pulse amplitude analyser.

3. Circuit Design

3.1. INTEGRATION TIME CONSTANT

The time constant of the integrator shown in fig. 4 must be made large compared with the gate width in order to reduce the effect of the switching transients. It should not, however, be too long compared with the transformer recovery time constant, L_3/R_3, otherwise the signal itself will suffer attenuation.

In the present system, the integration is included in the amplifier in the form of negative feedback and is split into two halves each with a time constant of 2μsec.

3.2. TRANSFORMER

The primary inductance of the matched gating transformer (fig. 2) is determined by the chosen value of the recovery time constant, which is in turn influenced by the integration period. A value of 4 μsec for the transformer recovery time constant is sufficient in the present case to prevent loss of gain, so that the primary inductance becomes 4 μsec $\times$ 200 Ω = 800 μH for a signal source impedance of 100 Ω.

However, the actual construction of the primary winding is influenced by the need to minimise gate pulse and signal breakthrough and the need to keep the gate switching time as short as possible. Signal breakthrough is caused mainly by currents induced in the input half of primary winding through stray capacity to earth and by direct capacitive coupling to the secondary. Hence, the input winding should be well isolated from the rest of the transformer. On the other hand, gate breakthrough and

switching time considerations require very close coupling and so the transformer design is a compromise between these conflicting requirements.

The properties of the transformer used in the present system, together with details of the method of construction, are given in Appendix 1.

The current gain of the first pair of transistors (J_1 and J_2) is approximately defined by the ratio of R_6 to R_7, whilst the integration time constant is determined by the condenser in parallel with R_7.

Similar considerations apply to the second pair of transistors (J_3 and J_4) which produce an output pulse of 70 mA peak amplitude on a 100 Ω load, suitable for application to a multichannel amplitude analyser via the High Level Linear Amplifier described in Appendix 2.

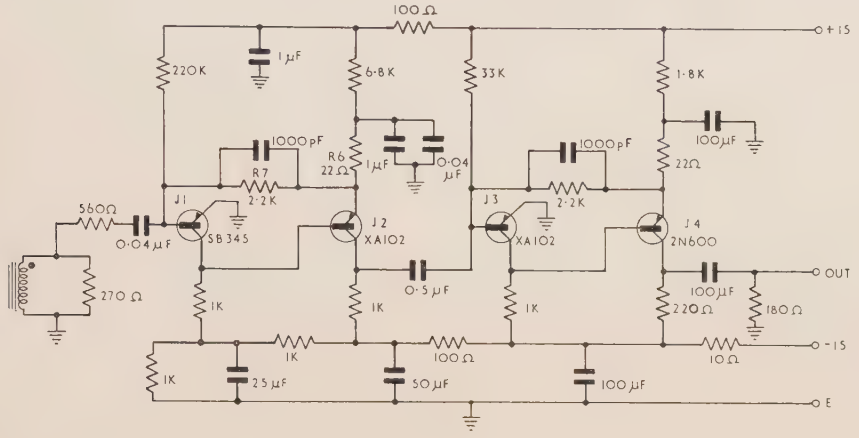

Fig. 5. Amplifier.

3.3. DIODES

The maximum switching speed of the gate is determined by the choice of the diodes D_1 and D_2 as well as by the coupling transformer.

A suitable diode should have low hole storage and forward resistance together with a high reverse impedance and turnover voltage. Such a diode is the type GEX 39, which combines the ability to switch in less than 5 mμsec with a reverse impedance of 1 pF and 200 kΩ at a bias of — 10 V.

The forward conducting potentials of the diode D_1 and D_2 are matched to within 50 mV at a current of 10 mA to preserve the symmetry between the two halves of the primary circuit when the gating pulse is applied.

3.4. AMPLIFIER

The amplifier shown in fig. 5 accepts pulses from the gate transformer having a maximum amplitude of about 2.5 mA and produces output pulses of 4 μsec duration and 70 mA maximum amplitude. The amplifier uses normal feedback techniques to define the gain and bandwidth (as described in reference[1])).

The maximum pulse repetition frequency is limited by the permissible dissipation of J_4, to just over 10 kc/s and at this rate there is adequate time for the amplifier to recover between pulses.

3.5. GATE PULSE GENERATOR

The gate pulse generator (fig. 6) consists of two transistors, both operating in the avalanche mode[2]).

Normally the transistors are cut off and are biassed into the avalanche region by a current of one milliamp drawn from their collectors. Under these conditions a transistor acts as a regenerative switch which, when triggered, bottoms in a time which can be less than 10 mμsec.

[1]) G. B. B. Chaplin, C. J. N. Candy and A. J. Cole, Transistor stages for wide band amplifiers, Proc. I.E.E. Paper No. 2892 Vol. **106**, Part B. Supplement No. 16.

[2]) G. B. B. Chaplin and A. R. Owens, A method of designing avalanche transistor trigger circuits, Proc. I.E.E. Paper No. 2944, Vol. **106**, Part B. Supplement No. 16.

When the transistor A_1 is triggered, a negative pulse of approximately 30 V amplitude is produced at the emitter, switching off diode D_3 and supplying 50 mA to the gate transformer at point A. At the same time D_5 is cut off and the potential of A_2 base falls until the transistor is triggered after a time delay determined by C_2, R_4 and R_5. The collector potential of A_2

Input pulse amplitude	up to 5 V
Input pulse duration	40 mμsec
Gate width	50 mμsec
Gate switching time	5 mμsec
Output pulse amplitude	up to 70 mA
Output pulse width	4 μsec
Gate breakthrough at output	1.0 mA †
Signal breakthrough at output	less than 1% †

† In the temperature range 20–50° C

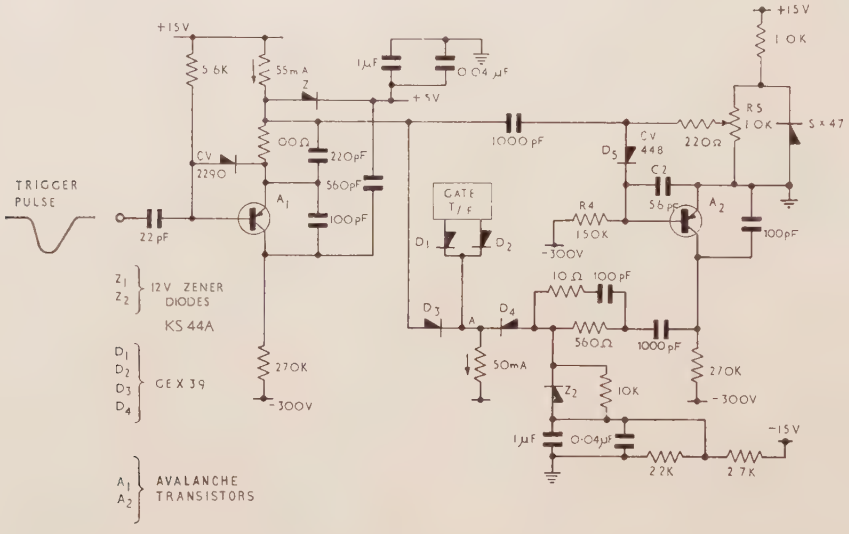

Fig. 6. Gate pulse generator.

thus rises from about — 50 V to earth potential and removes the bias current from the gate transformer by taking point A positive via D_4.

The zener diodes Z_1 and Z_2 limit the height of the pulses applied to D_3 and D_4 to a value which can be withstood by the diodes.

The system described above produces a pulse at point A with rise and fall times of about 2 mμsec and of a width variable by R_5 from 10 mμsec up to a maximum value of 100 mμsec. The triggering delay is less than 5 mμsec for a 2 V signal pre-pulse, whilst the jitter is less than 0.5 mμsec.

4. Performance

The performance of the system outlined in fig. 4, and composed of the elements shown in figs. 2, 5 and 6, is as follows:

A plot of input pulse height against output pulse height deviates less than 1% from a straight line over the range of output signals 2 mA to 70 mA.

Acknowledgements

The authors would like to express their gratitude to Mr. E. H. Cooke-Yarborough, Dr. C. J. N. Candy and Dr. T. J. Gooding for many helpful comments.

Appendix

1. PROPERTIES AND CONSTRUCTION OF THE GATE TRANSFORMER

The windings were wound in the following order on a ferroxcube pot core type FX 1011.

1. 16 turns of 38 swg wire.
2. 8 turns of 38 swg wire.
3. 1 layer of paper, 0.02 inches thick.

4. 16 turns of 38 swg wire.
5. 1 layer of paper; 0.02 inches thick.
6. 8 turns of 38 swg wire.
7. 16 turns of 38 swg wire.

Windings Nos. 1 and 7 were connected in series to form the secondary.

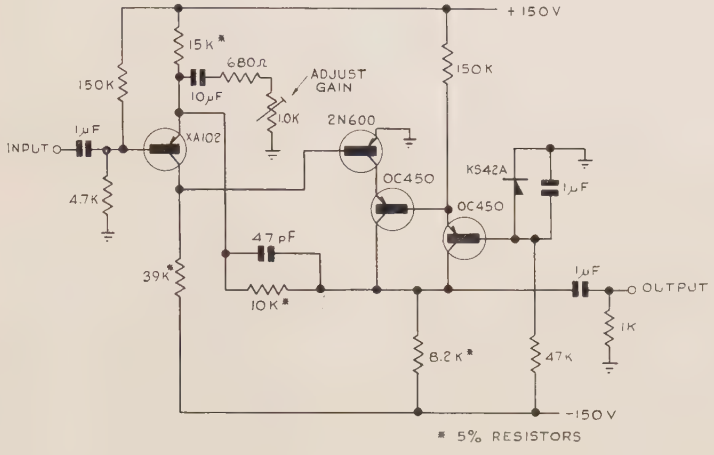

Fig. 7.

Windings Nos. 2 and 6 were connected in series to form the balance winding.

Winding No. 4 is the input winding.

Primary inductance = 910 μH (16 + 8 + 8 turns).

Secondary inductance = 910 μH (16 + 16 turns).

Leakage inductance of input winding with both halves of balance winding S/C = 0.9 μH.

Leakage inductance of the secondary winding with primary S/C = 1.75 μH.

Capacity between input and balance windings = 11.0 pF.

Capacity between input and secondary windings = 12.0 pF.

2. HIGH LEVEL LINEAR AMPLIFIER

Many multichannel pulse amplitude analyzers in operation at the present time use valves and require input pulse heights up to a maximum of 50 V.

The amplifier shown in fig. 7 was therefore developed for use as a pre-amplifier for a multichannel pulse analyzer which required an input pulse of 50 V maximum amplitude with a duration of 4 μsec.

The performance of the amplifier when tested with pulses of 4 μsec duration is as follows:

Gain: variable from 5 to 15

Linearity: better than 0.2% in the range of outputs 0–50 V

Stability: better than 1% over 48 hours

Maximum continuous pulse repetition frequency: 10 kc/s

Input impedance: greater than 1 kΩ

Output impedance: 1 kΩ.

The amplifier was supplied from a source impedance of 100 Ω and fed a load of 15 kΩ in parallel with 300 pF.

NUCLEAR INSTRUMENTS AND METHODS 7 (1960) 50–55; NORTH-HOLLAND PUBLISHING CO.

CONVERTISSEUR TEMPS–AMPLITUDE A POUVOIR DE RESOLUTION ELEVE

S. GORODETZKY, R. RICHERT, R. MANQUENOUILLE et A. KNIPPER

Institut de Recherches Nucléaires, Université de Strasbourg

Reçu le 8 décembre 1959

A fast time-to-amplitude converter is described which secures reliable operation. Its intrinsic resolution is of the order of 10^{-10} sec. The resolution curve for Co^{60} gamma rays exhibits a full width at half maximum of about 4×10^{-10} s. Further improvements of the apparatus are indicated.

1. Introduction

L'utilisation de circuits analyseurs de temps pour les mesures de coïncidences différées conduit à un gain sensible en précision et en durée de mesure; de nombreux circuits ont été réalisés[1–8]). Leur mise en œuvre présente parfois quelques difficultés. Le circuit que nous décrivons est un dérivé du montage de R. E. Green et R. E. Bell[8]). Il présente une grande sécurité de fonctionnement et une excellente stabilité à long terme (aucune dérive sur les durées de plusieurs jours). Son temps de résolution intrinsèque de 1.3×10^{-10} s est comparable à celui des meilleurs circuits publiés.

2. Principe

Le schéma d'ensemble est donné à la fig. 1, où seul le convertisseur délai-amplitude est représenté en détail.

Les impulsions provenant de deux photomultiplicateurs Radiotechnique 56 AVP sont dirigés par l'intermédiaire de câbles de 197 Ohms vers des limiteuses opérant la mise en forme en amplitude. Les plaques des deux limiteuses sont directement réunies et chargées par un câble court-circuité de longueur L et sa terminaison de 197 Ohms. Ce câble définit la mise en forme en durée. Dans l'un des canaux, une longueur L supplémentaire de câble de 197 Ohms introduit un retard fixe θ égal à la moitié de la durée des impulsions court-circuitées. Deux impulsions parfaitement coïncidentes à la sortie des photomultiplicateurs donneront donc sur les plaques des limiteuses deux impulsions se recouvrant par moitié dans le temps.

Les valeurs du circuit sont: $L = 5$ m soit $\theta = L/0.95\, c = 17.54 \times 10^{-9}$ s et $v_0 = 2$ Volts. En effet, les limiteuses sont des tubes E 180 F fonctionnant avec une tension écran de 100 V et un courant anodique statique de 20 mA.

Le rôle du convertisseur est de séparer du signal de la fig. 2 le "signal de coïncidence", c'est-à-dire la partie comprise entre les niveaux v_0 et v'_0. Son amplitude étant constante, et sa largeur fonction linéaire du retard entre les impulsions des 2 photomultiplicateurs, il suffit d'une intégration par une constante de temps suffisamment grande pour réaliser la conversion délai-amplitude. Les signaux sont alors amplifiés et analysés avec des appareils conventionnels.

Pour les mesures nécessitant une base 2θ assez grande ($\geqslant 10^{-8}$ s), nous adaptons le convertisseur en câble d'impédance plus élevée (1000 Ohms).

[1]) G. C. Neilsson et D. B. James, Rev. Scient. Instr. **26** (1955) 1018.

[2]) G. Jones et J. B. Warren, Journ. Scient. Instr. **33** (1956) 429.

[3]) E. Remy et K. Winter, Journ. Phys. Rad. **18** (1957) 112 A.

[4]) A. W. Sunyar, Bull. Amer. Phys. Soc. Série II, V2 (1957) 37; Peaceful uses of Atomic Energy (Genève, 1958).

[5]) R. L. Chase et W. A. Higinbotham, Rev. Scient. Instr. **28** (1957) 448.

[6]) J. Samuelli et A. Sarazin, Journ. Phys. Rad. **19** (1958) 109 A.

[7]) C. Cottiniet E. Gatti, Il Nuovo Cimento **4** (1956) 1550.

[8]) R. E. Green et R. E. Bell, Nucl. Instr. **3** (1958) 127.

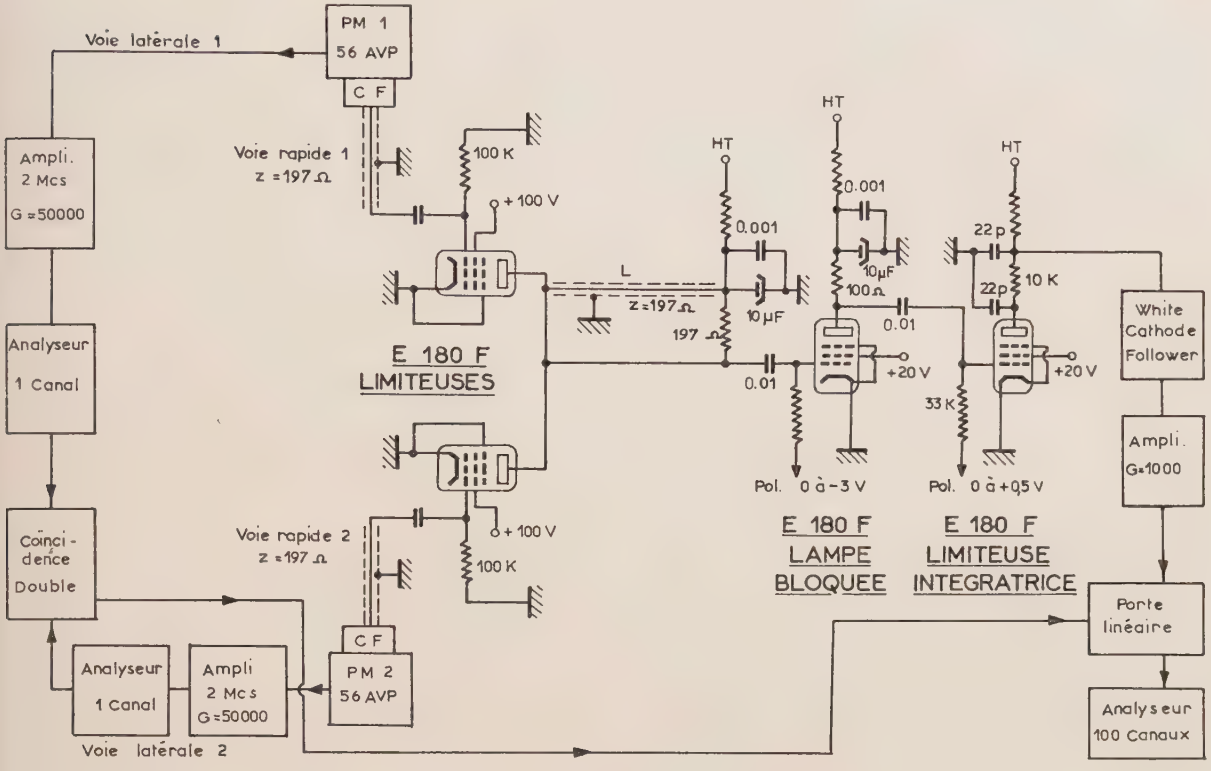

Fig. 1. Convertisseur temps-amplitude.

3. Description

La partie la plus délicate dans un convertisseur de temps est la discrimination entre les impulsions isolées et les coïncidences.

La solution la plus simple consiste à utiliser un discriminateur à diode semi-conductrice[2,3,4]), qui a l'avantage de fonctionner avec des signaux relativement petits. Ce circuit, qui est pratiquement parfait pour un détecteur de coïncidences rapides conventionnel a cependant des inconvénients qui se font gravement sentir dans un analyseur de temps: l'instabilité de la caractéristique de conduction du cristal, le déplacement du point de fonctionnement suivant la valeur du courant moyen dans certains montages, et une petite transmission inévitable des signaux isolés. On observe toujours des déplacements ou distorsions de la caractéristique délai-amplitude du convertisseur.

Les circuits utilisant des tubes multigrilles pour cette discrimination[1,5,7]) possèdent une stabilité intrinsèque meilleurs. Une légère trans-

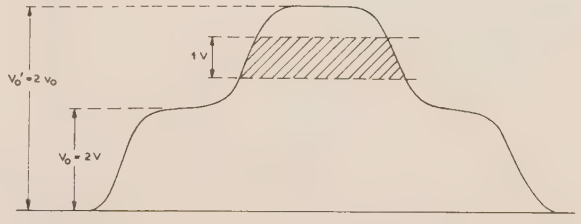

Fig. 2. Impulsions en coïncidence a l'entrée du convertisseur et tranche intégrée

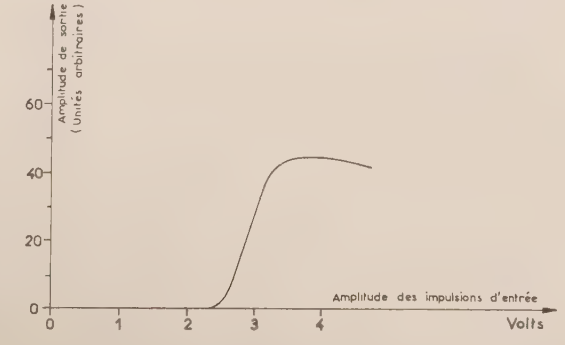

Fig. 3
Réponse de l'ensemble lampe bloquée-limiteuse intégratrice.
Vg_1 Lampe bloquée = — 2.23 V,
Vg_1 Limiteuse intégratrice = + 0.25 V.

mission capacitive subsiste cependant, pour la seconde grille de commande dans le cas de la 6 B N 6.

Notre convertisseur comprend deux penthodes E 180 F. Les deux tubes travaillent avec des points de fonctionnement soigneusement choisis. Tous les deux ont une tension de grille-écran de 20 V seulement; pour $V_{g1} = 0$ Volt, le courant plaque est pratiquement nul; il atteint 8 mA pour $V_{g1} = 1$ V; le courant grille est négligeable, il ne commence à s'établir qu'a partir de $V_{g1} = +0.5$ Volts.

Le premier tube faisant la discrimination est une lampe bloquée au repos, la grille étant polarisée à $V_{g2} < -2$ Volts. Pour les impulsions de coïncidences il fonctionne en amplificateur à seuil rapide. La discrimination est excellente, le niveau des impulsions isolées est pratiquement nul même après amplification ultérieure. La faible charge de plaque ($R = 100$ Ohms) permet de conserver une grande rapidité; nous obtenons alors sur l'anode des impulsions négatives d'amplitude égale à 1.2 Volts pour des impulsions d'entrée dépassant d'environ 1.8 Volts le seuil de discrimination; la durée de ces impulsions est égale à la durée de recouvrement des deux impulsions en coïncidence.

Ces impulsions sont ensuite appliquées au deuxième tube, opérant en limiteuse avec $V_g = 0.25$ Volts. Cette seconde limiteuse garantit une amplitude bien constante, même si l'amplitude de sortie des premières limiteuses varie légèrement par suite d'un comptage élevé sur les photomultiplicateurs.

L'intégration de l'impulsion de coïncidence est effectuée grâce à la grande constante de temps de la charge de plaque de cette seconde lampe.

Le fonctionnement de l'ensemble lampe-bloquée-limiteuse intégratrice est illustré par la fig. 3 qui représente la hauteur des impulsions de sortie en fonction de la hauteur des impulsions d'entrée. Celles-ci proviennent d'un générateur à relai à mercure donnant des impulsions rectangulaires de durée constante et de temps de montée plus court que celui de la lampe bloquée.

La courbe montre qu'on découpe pratiquement une tranche de 1 Volt dans les impulsions d'entrée. En impulsions réelles les temps de montée sont plus longs que celui de la lampe bloquée. La tranche découpée dans l'impulsion de coincidence doit être placée dans la partie centrale de cette impulsion où la montée est la plus rapide. Ainsi une légère variation d'amplitude de l'une ou l'autre des impulsions qui se superposent, donnera une variation minimum à la sortie du convertisseur.

4. Calibrage et Résolution Intrinsèque

La figure 4 montre la courbe amplitude-délai pour une certaine amplification des impulsions

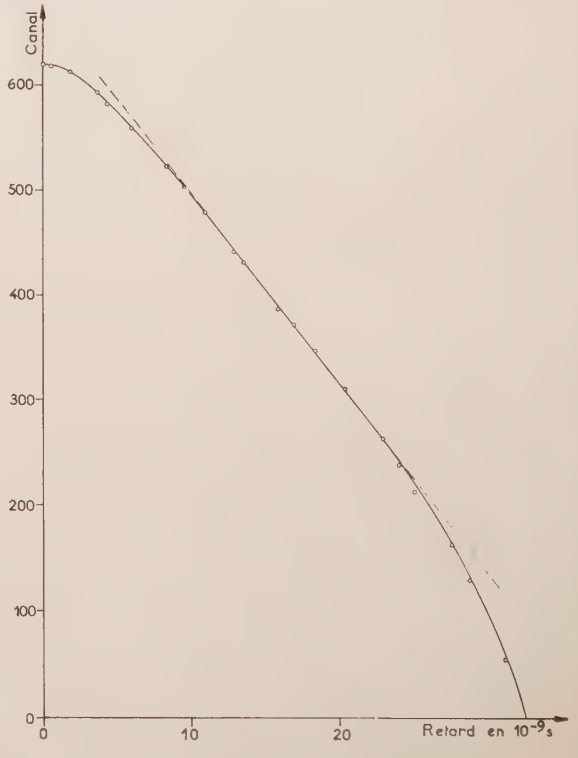

Fig. 4. Courbe amplitude-délai.
Largeur de canal: 5.45×10^{-11} s dans la zône linéaire.

sortant du convertisseur. Elle indique le déplacement de la courbe de résolution intrinsèque en fonction du retard introduit dans l'une des voies.

Les parties courbes correspondent aux montées et aux descentes des impulsions qui se superposent. La pente de la partie rectiligne

dépend de l'amplification. On peut donc réduire ou dilater l'axe des temps pour l'adapter à la sensibilité de la mesure à effectuer. Un amplificateur à seuil à l'entrée de l'analyseur multicanaux élimine la partie courbe aux faibles amplitudes.

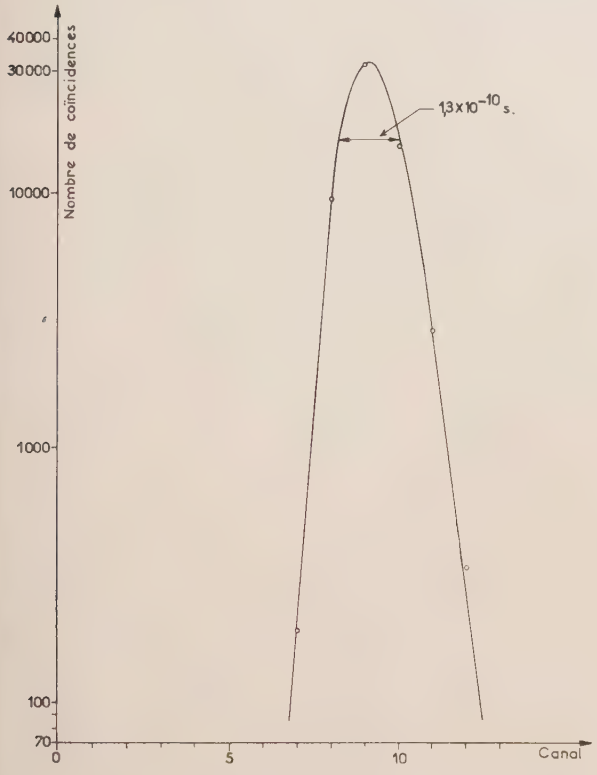

Fig. 5. Courbe de résolution intrinsèque.
Largeur de canal: 7.55×10^{-11} s.

La résolution de l'électronique (fig. 5), sans photomultiplicateurs, a été mesurée avec les impulsions du générateur à relai à mercure. Elle est égale à 1.3×10^{-10} s et correspond à celles des circuits les plus rapides publiés.

5. Résolution avec Photomultiplicateur

Nous avons utilisé des photomultiplicateurs 56 AVP de la Radiotechnique, sur lesquels étaient montés des scintillateurs plastiques NE 102 de 15 mm de diamètre et de 25 mm de hauteur, dont la vie moyenne de désexcitation est égale à 4×10^{-9} sec; le règlage du potentiel de l'électrode de focalisation permettait de n'utiliser que la partie correspondante de la photo-cathode.

La courbe de résolution de la figure 6 a été obtenue en sélectionnant dans les canaux latéraux une énergie de 900 keV définie à 5% près; la source utilisée était une source de Co^{60}.

Fig. 6. Courbe de resolution prompte en Co^{60}.
Largeur de canal: 1.04×10^{-10} s.

D'autre part, R étant le nombre total de photoélectrons produits dans la scintillation, nous avons ajusté la haute tension des photomultiplicateurs de telle sorte que les limiteuses du circuit de coïncidences rapides soient amenées au cut-off par $0.15\,R$ photoélectrons environ. Cette valeur est estimée à 25% près. Dans ces conditions la résolution est $2\tau_0 = 4.16 \times 10^{-10}$ s. L'erreur due au calibrage est de l'ordre de 5%.

La courbe de résolution a une forme sensiblement gaussienne; la gaussienne ayant même largeur à mi-hauteur est indiquée en pointillé et s'écarte assez peu des points expérimentaux;

la pente déterminée en un point situé à 2 décades au-dessous du maximum donne $t_{\frac{1}{2}} \approx 4.5 \times 10^{-11}$ sec, soit approximativement $t_{\frac{1}{2}} = 0.11 \times 2\tau_0$. La valeur trouvée pour $2\tau_0$ est du même ordre que celle publiée par R. E. Bell *et al.*[9]). Elle semble d'autre part, en accord avec la théorie

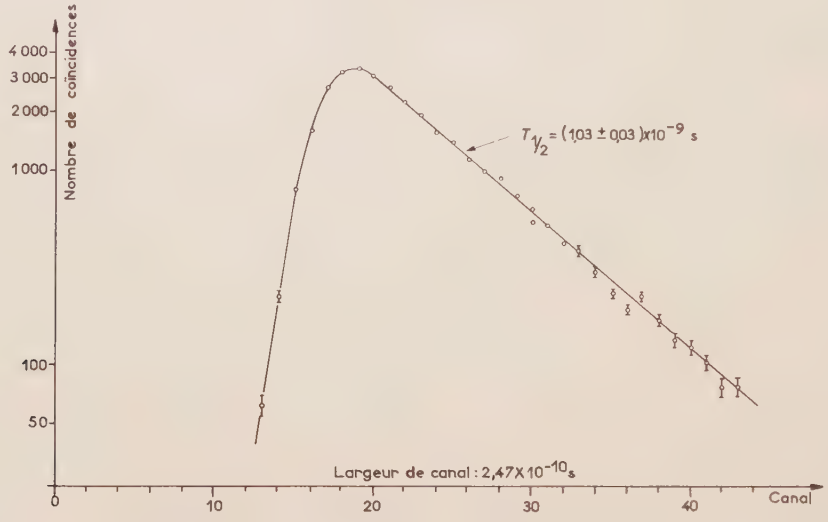

Fig. 7. Coïncidences retardées entre les rayonnements β et les rayonnements γ de haute énergie du W^{182}.

initialement développée par S. Colombo *et al.*[10]) et récemment complétée par E. Gatti et V. Svelto[11]). Notre cas correspond à la méthode B décrite par ces auteurs; en supposant $\tau = 4 \times 10^{-9}$ sec, $\varepsilon_{ph} = 5 \times 10^{-10}$ sec, $\lambda/\tau = 0.25$, $C/R = 0.15$, $R = 450$ on obtient $2\tau_0 \approx 4.3 \times 10^{-10}$ sec.

6. Essais de Fonctionnement

Comme essai final du circuit nous avons repris la mesure de la vie moyenne du niveau excité à 1290 keV du W^{182} qui avait été mesurée par

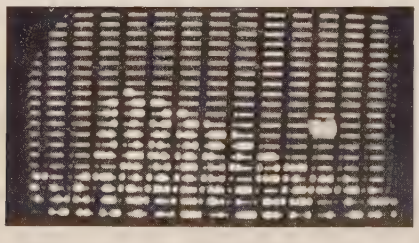

Fig. 8. W^{182}: Résultat d'une mesure. Chaque colonne représente le nombre de coïncidences stockées dans un canal. Les retards β augmentent vers la droite; en raison du codage binaire la décroissance exponentielle est sensiblement linéaire sur l'écran du tube à rayons cathodiques. Le fond continu, visible à gauche et à droite, correspond aux coïncidences fortuites.

Sunyar[12]). L'un des compteurs ne détectait que les rayonnements γ, un absorbant convenable arrêtant les rayonnements β. Nous utilisions des scintillateurs plastiques NE 102. Les figures 7 et 8 représentent la répartition dans le temps des coïncidences entre les rayonnements β et les rayonnements γ de haute énergie. Nous trouvons $t_{\frac{1}{2}} = 1.03 \times 10^{-9}$ sec. L'erreur statistique calculée selon la méthode de Peierls[13]) est inférieure à 1%, et l'erreur de calibrage estimée à environ 2%. Le résultat peut donc être exprimé par $t_{\frac{1}{2}} = (1.03 \pm 0.03) \times 10^{-9}$ sec. Cette mesure constitue une preuve de la linéarité de notre convertisseur.

La stabilité de l'ensemble s'est révélée excellente; nous n'avons pas constaté de variations appréciables sur des périodes de fonctionnement de l'ordre de plusieurs jours.

7. Améliorations à Apporter au Circuit

7.1. SELECTION D'ENERGIE

Les courbes de résolution qui correspondent à différentes hauteurs d'impulsion apparaissent

[9]) R. E. Bell et M. H. Jørgensen, Nuclear Physics **12** (1959) 413.

[10]) S. Colombo, E. Gatti et M. Pignanelli, Il Nuovo Cimento **5** (1957) 1739.

[11]) E. Gatti et S. Svelto, Nucl. Instr. **4** (1959) 189.

[12]) A. W. Sunyar, Phys. Rev. **93** (1954) 1122.

[13]) R. Peierls, Proc. Roy Soc. A **149** (1935) 467.

à des endroits différents sur l'échelle des temps; la courbe de résolution résultante s'élargit donc sensiblement, lorsque la sélection d'énergie effectuée dans les canaux latéraux est trop large. Or il est souvent nécessaire que cette sélection ne soit pas trop restrictive. Un circuit compensateur des hauteurs d'impulsions qui permettra d'utiliser des bandes d'énergies suffisamment larges est en voie de réalisation.

7.2. CIRCUIT ANTI-EMPILEMENT

Lorsque le taux de comptage est trop élevé, les courbes de résolution présentent une remontée du côté des amplitudes décroissantes. Bell a attiré notre attention sur le fait que cette imperfection est due surtout à des superpositions dans les canaux latéraux. Il se peut en effet que des impulsions coïncidentes, bien mises en forme dans le circuit rapide et qui devraient normalement être rejetées en coïncidence triple, en raison des sélections d'énergies latérales, soient néanmoins admises; ceci se produit lorsque deux impulsions se suivant de trop près dans la même voie latérale se superposent de telle sorte que l'impulsion résultante atteigne une amplitude suffisante pour tomber dans la bande d'énergie sélectionnée.

Un circuit anti-empilement est donc indispensable pour chaque photomultiplicateur. Dans les essais décrits plus haut, nous n'avions pas un tel circuit et nous avons fortement réduit le taux de comptage de façon à minimiser cet effet.

Remerciements

Les idées que le Dr. R. E. Bell a bien voulu nous communiquer à l'occasion de sa visite à notre Institut nous ont été extrêmement profitables. Nous l'en remercions très vivement.

NUCLEAR INSTRUMENTS AND METHODS 7 (1960) 56–62; NORTH-HOLLAND PUBLISHING CO.

A TOTAL ABSORPTION GAMMA RAY SPECTROMETER COMBINING SODIUM IODIDE AND PLASTIC SCINTILLATORS†

WILLIAM H. ELLETT and GORDON L. BROWNELL

Physics Research Laboratory, Massachusetts General Hospital, Boston, Massachusetts

Received 10 November 1959

An 18″ × 18″ plastic well scintillator is used to monitor the escape radiation from a 5″ D NaI well crystal. Coincident events in both scintillators are rejected by means of an anticoincidence circuit. The detectors are mounted in a 2 ton lead and mercury shield so they can be used for the radioassay of low activity samples. Design of electronic equipment used with the plastic scintillators is considered and data presented on the effectiveness of the anticoincidence mantle in improving the performance of the NaI crystal by (a) reducing the Compton spectrum (b) increasing its efficiency as a sum spectrometer and (c) reducing its background spectra. Expressions are derived for the efficiency of the plastic mantle in detecting escape radiation from the NaI crystal and compared to experimental data.

1. Introduction

Large sodium iodide well crystals are efficient detectors for small amounts of gamma-emitting isotopes because of their 4π geometry. The total absorption peak (ε_p) of large well crystals is high and relatively energy independent since at high energies total absorption by multiple Compton events tend to compensate for the decreased number of primary photoelectric interactions. This increase in the total absorption peak greatly reduces the number of pulses falling within the Compton spectra. Furthermore, the sum peaks produced by cascade gamma rays are recorded in large well crystals[1]).

Ideally, a large well crystal would function as a total absorption spectrometer, i.e. produce peaks corresponding to the total γ-ray energy emitted in a nuclear transition. Actually, the largest well crystals can only approach this ideal. The 9¼″ × 9″ NaI well crystal at Oak Ridge National Laboratory has a photopeak efficiency ranging from 90% at 0.5 MeV to 55% at 2.5 MeV[2]). At present this is the largest crystal commercially available. The optimum size of large well crystals depends on several factors. Since gamma ray absorption is exponential, a point of dimishing returns is reached depending on the range of gamma ray energies under consideration. Disadvantages of large crystal size are high cost, increased background, and decreased resolution. P. R. Bell of ORNL has shown that many of the performance characteristics of the largest well crystals could be achieved by surrounding a 4¾″ × 5″ NaI crystal with a liquid scintillator anticoincidence mantle[2,3]). The AC mantle detects escape radiation from the NaI crystal and inhibits the recording of pulses corresponding to less than full energy. The total absorption peak efficiency of such a device is, of course, less than that of a 9¼″ × 9″ crystal. However, the anticoincidence device has a higher peak to total area ratio (R) and somewhat better resolution. In addition the anticoincidence mantle reduces the background of the device. The commercial availability of large plastic scintillators for use as anticoincidence mantles has made the fabrication of such devices relatively convenient and inexpensive[4]).

† Supported by the U.S. Public Health Service Grant No. CRT 5030.

[1]) P. Shapiro and R. W. Higgs, Rev. Sci. Instr. **28** (1957) 939.

[2]) R. C. Davis *et al.*, I.R.E. Transactions on Nuclear Science NS-3 **4** (1956) 82.

[3]) P. R. Bell, Science **120** (1954) 625.

[4]) K. I. Roulston and S. I. H. Naqui, Rev. Sci. Instr. **27** (1956) 830.

2. Apparatus

The sum spectrometer constructed at this laboratory utilizes a 5″ D × 5½″ NaI crystal† with a ¾″ × 3⅜″ well. This crystal is mounted coaxially within an 18″ × 18″ plastic scintillator††, fig. 1. The well in the plastic cylinder is

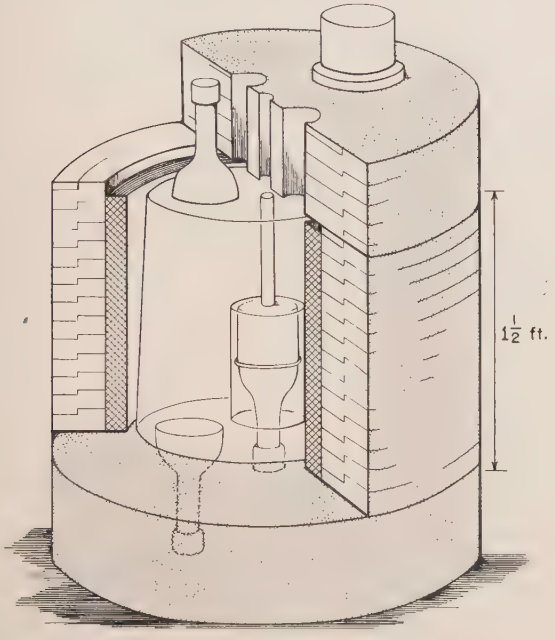

Fig. 1. The gamma-ray spectrometer, showing the coaxial arrangement of the 5″D × 5½″ sodium iodide well crystal and the 18″ × 18″ plastic anticoincidence mantle.

5⅝″ in diameter and 12″ deep. A 1″ hole through the plastic scintillator allows samples to be placed inside the NaI crystal. The complete assembly is shielded on the sides with three inches of lead and one inch of mercury. The top and bottom of the shield are eight inches of cast iron. Quarter inch lead plates within the shield absorb the soft component of the built-up radiation originating in the iron.

The NaI crystal is directly coupled to a 5″ photomultiplier tube with which it is integrally canned in 0.04 inch aluminum. Pulses from the photomultiplier tube are amplified and fed to a 256 channel magnetic core analyzer†††. The plastic scintillator is packed within a ¼″ layer of magnesium oxide. Four 5″ photomultiplier tubes collect light from the plastic. The pulses from the four photomultiplier tubes are summed in either of two modes depending on the activity of the sample being measured. In the analysis of fairly active samples (greater than 5 mμ curie) most of the events recorded in the anticoincidence circuit are caused by escape radiation from the NaI. In this case the signals from the four photomultipliers viewing the plastic scintillator are summed, amplified, and fed into the AC gate of the analyzer through a discriminator which is set to reject unsummed noise pulses. In the analysis of low activity samples, most of the events detected by the plastic are due to background radiation. In this case the signals are summed in pairs and placed in coincidence. A block diagram of information flow for this mode of operation is shown in fig. 2. The coincidence requirement eliminates all counts due to tube noise and results in somewhat more stable operation. However, since both sets of photomultipliers must detect the scintillation, some low energy gamma rays escaping from the NaI are not counted[5]).

A major electronic design problem in using the anticoincidence mantle is the wide range of pulse amplitudes produced in the photomultiplier tubes viewing the plastic scintillator. Pulses produced by escape radiation from the

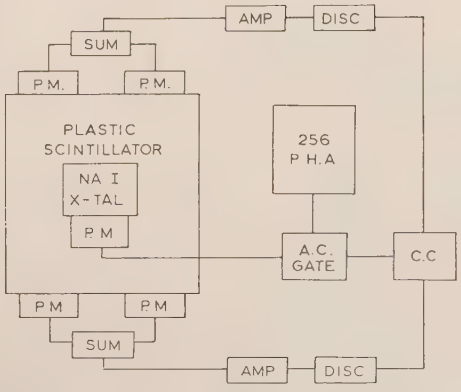

Fig. 2. Information flow using the anticoincidence mantle with pairs of photo multiplier tubes in coincidence. A light tight shield encloses the NaI crystal and its photomultiplier tube.

† Levinthal Electronics Company.
†† Nuclear Enterprises of Canada.
††† R.C.L., Inc. Model 20611.

[5]) C. C. Smith, H. H. Seliger and J. Steyn, J. Res., N.B.S. **57** (1956) 251.

NaI crystal range in size from 1 to 50 millivolts. Superimposed on these signals are frequent multivolt pulses produced by cosmic rays. The required dynamic range of the associated amplifier is over 1000 to 1. After attempting to modify ORNL A-1 amplifiers to handle this range of pulses, the amplifier sections of these this circuit and the main amplifier[7]). When pairs of phototubes are operated in coincidence, tube V_4 in the adding circuit is removed to allow V_{3A} and V_{3B} to function as cathode followers. The overall gain of the preamplifier and main amplifier is 10^5, permitting the operation of the photomultiplier tubes at relatively low voltages.

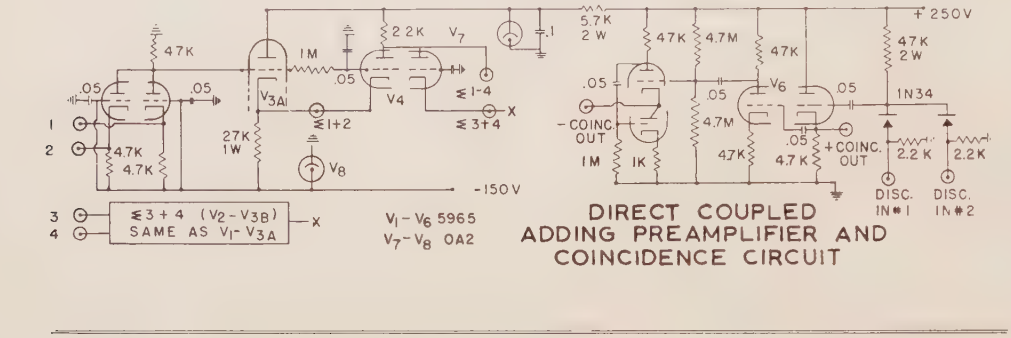

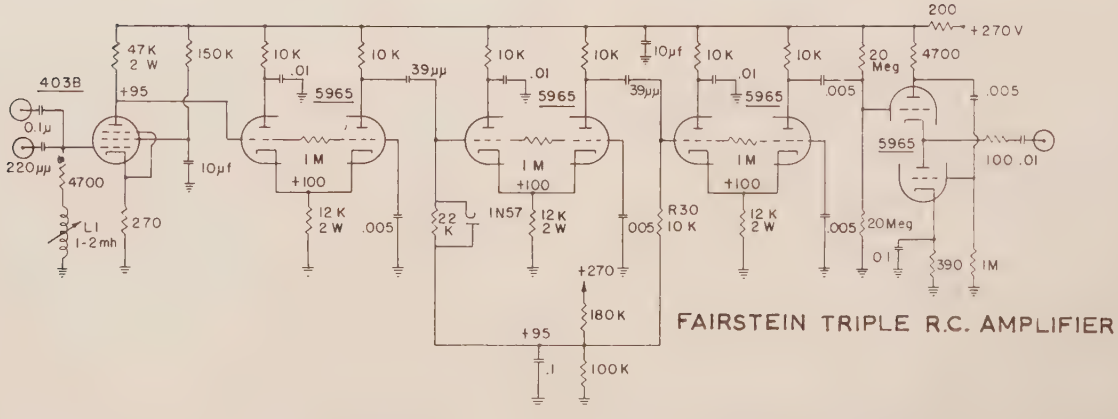

Fig. 3. Circuit diagrams for the adding preamplifier and the Farstein Triple R.C. Amplifier. The 0.1 μF input to the Triple R.C. Amplifier is used with the adding preamplifier, initial clipping being performed at the anode of the photomultiplier tube.

instruments were replaced by the Triple RC Amplifier developed by Edward Fairstein of ORNL[6]). This amplifier has exceptionally fast recovery from large (up to 10 volt) overload pulses. Their use makes it possible to detect 10 millivolt pulses 5 μ sec after receiving a cosmic ray pulse. Positive pulses from the discriminator section of these amplifiers operate a diode and circuit for coincidence operation.

A compatible adding preamplifier was designed to provide sum pulses from two or four phototubes. Fig. 3 shows a schematic diagram of This reduces afterpulsing which is particularly severe after high energy cosmic rays have been detected in the plastic scintillator. The effects of afterpulsing are further reduced by using a low cathode to first dynode voltage in the phototubes and operating the tubes in coincidence.

[6]) E. Fairstein, Double Differentiation in Radiation Detection Amplifiers Using RC Networks-A Nonblocking Counter Amplifier, ORNL Instrumentation and Controls Division Report No. ORNL-2067 (Jan. 31, 1956) Tech. Serv. AEC, Oak Ridge, Tenn.

[7]) Pulse Amplifier Circuit CAPE – 29 – 17, Instrument and Controls Division, Oak Ridge National Laboratory.

3. Efficiency of the AC mantle in Detecting Escape Radiation from the NaI Crystal

Spectra of Zn^{65} taken with and without use of the anticoincidence circuit are shown in fig. 4.

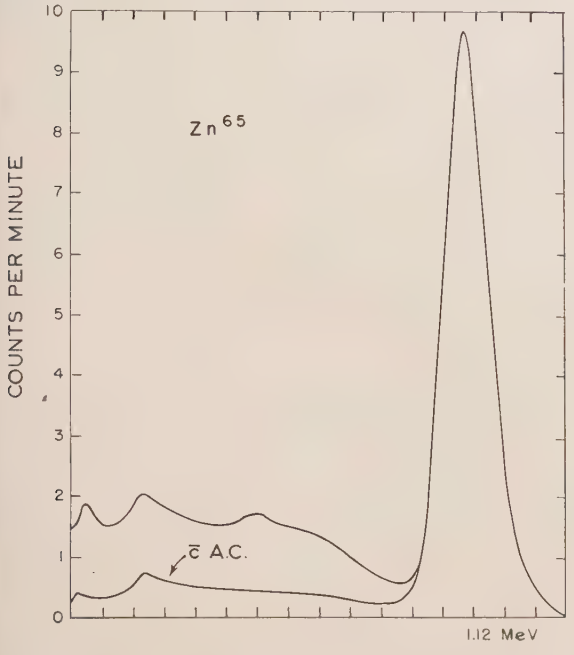

Fig. 4. Spectra of Zn^{65} taken with and without the anticoincidence mantle in operation. Two thirds of the escape Compton gamma rays are detected in the plastic scintillator.

For such a single energy gamma emitter the number of pulses recorded in the Compton distribution, N_c, is proportional to the difference between the total efficiency, ε_t, and peak efficiency, ε_p, of the NaI crystal[8]).

$$N_c = N_0 (\varepsilon_t - \varepsilon_p)$$

where N_0 is the source strength. The effectiveness of the anticoincidence mantle in reducing the Compton distribution depends on two parameters; the cross section of the plastic to the escape quanta from the NaI crystal and the ability of the associated electronics to detect small energy losses in the plastic. The number of escape gamma rays detected by the mantle is ΔN_c;

$$\Delta N_c = N_c \eta_c (E_{min})$$

where $\eta_c(E_{min})$, the detection efficiency of the plastic for an escape Compton gamma, is a function of E_{min}, the minimum energy transfer required to trigger the AC gate. In general, low energy escape radiation requires a small value of E_{min}. However, this factor is not critical with a large well crystal because the NaI serves as a high Z filter for low energy Compton gamma rays and the resultant escape spectrum is practically free of gamma rays below 200 keV †. By integrating the differential Compton cross section for different values of the minimum energy transfer, Roulston and Naqui have calculated the cross sections of plastic for monoenergetic gamma rays[9]). From this data, we have calculated η_c, the detection efficiency of the plastic mantle, as a function of E_{min} for the Compton escape spectrum of Cs^{137}. This theoretical efficiency varies from a high of 81% if all interactions are detected (0 discriminator setting) to 70% if only energy transfers greater than 50 keV serve to trigger an anticoincidence pulse. The measured change in area of the Compton distribution with anticoincidence, $\Delta N_c/N_c$, using the sum of 4 phototubes is 71%. For gamma emitters of higher energy than Cs^{137} the escape spectrum contains relatively more high energy gamma rays and the dependence on

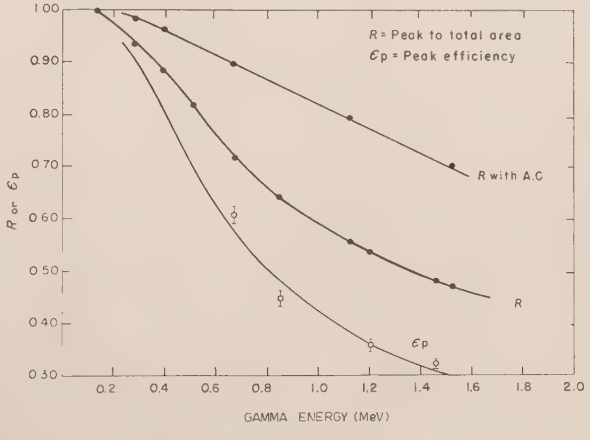

Fig. 5. R, the peak to total area ratio, for single energy gamma emitters with and without anticoincidence and ε_p, the total absorption peak efficiency of the NaI crystal, as a function of initial gamma-ray energy.

† This effect also minimizes the loss of gamma rays in the aluminum and magnesium oxide surrounding the NaI crystal.

[8]) See ref. [1]).

[9]) K. I. Roulston and S. I. H. Naqui, Nucleonics 15 (Oct. 1957) 86.

discriminator setting is correspondingly less. For less energetic gamma emitters the peak to total area ratio is so high without the anticoincidence that relatively little improvement in

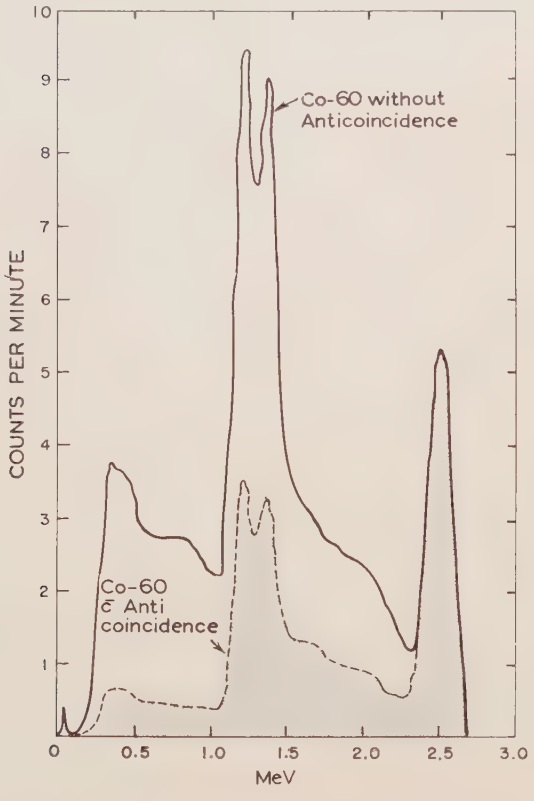

Fig. 6. Spectra of cascade gamma rays produced by Co^{60}. The ratio of sum peak to total area is increased by a factor of 3.3 with anticoincidence.

spectra is produced by its use. The peak to total area ratio (R) for a number of single energy gamma emitters was measured with and without the anticoincidence mantle in operation. These results are shown in fig. 5, where R is plotted as a function of initial gamma ray energy. It is seen that use of the anticoincidence mantle materially improves the peak to total area ratio for high energy gamma emitters.

Spectra of cascade gamma produced by cobalt-60 are shown in fig. 6. The sum peak results from the complete absorption of both gamma rays and its area is not changed by the anticoincidence mantle. However, partial absorption of either the 1.18 MeV or 1.33 MeV gamma rays does produce useful escape radiation and the sum peak to total area ratio is increased by a factor of 3.3 when the anticoincidence mantle is used. The change in area of the 1.18 MeV with anticoincidence reflects the efficiency of the plastic mantle in detecting 1.33 MeV gamma rays†. The measured efficiency for 1.33 MeV gamma rays is 60%. The calculated efficiency based on first collision interactions and 96% geometry is 61%. Evidently most of the high energy gamma rays which interact in the plastic produce pulses large enough to be measured.

The peak efficiency of the NaI crystal was determined by taking the product of the theoretical detection efficiency and experimental peak to total area ratio, ($\varepsilon_p = R\varepsilon_t$), at a number of energies[10,11]). Detection efficiencies were calculated using Grodstein's data on NaI absorption coefficients[12]). To reduce the effects of backscatter into the crystal, measurements of the peak to total area ratio were performed with the crystal suspended in the center of a large steel room. A graph of the peak efficiency as a function of energy is included in fig. 5. Check values taken with gamma-emitting radioactive standards†† are indicated on the graph. The flags on the experimental points represent the standard error of the source calibrations. Because of less favorable geometry the photopeak efficiency of a well crystal decreases as the sample height increases. For Cs^{137} the peak efficiency decreases 10% when the sample height is changed from $\frac{1}{2}''$ to $2''$. When the well is completely filled the peak efficiency is reduced to 78% of its maximum value. The resolution of the NaI crystal also varies to some extent with source position in the well. A point source of Cs^{137} ($E_\gamma = 0.662$ keV) at the bottom of the well gives 12.4% resolution and 11% resolution if positioned $1''$ higher.

† See Appendix 1.

†† Radioactive Solution Standards, Nuclear Chicago Corporation.

[10]) See ref. [1]).

[11]) N. H. Lazar, R. C. Davis and P. R. Bell, I.R.E. Transactions on Nuclear Science, NS-3 **4** (1956) 136.

[12]) G. W. Grodstein, NBS 583 (Ap. 30, 1957).

4. Efficiency of the AC Mantle in Reducing the Background Counting Rate of the NaI Crystal

The effect of the anticoincidence mantle on the background of the NaI crystal is quite marked. In general the integral background counting rate is reduced by a factor of 2, table 1. at 1.46 and 2.6 MeV are due to K^{40} and Tl^{208} (ThC″) in the photomultiplier tube†. Most of the background radiation above 3 MeV is eliminated by the anticoincidence mantle indicating an almost complete removal of primary cosmic ray effects. The lower background

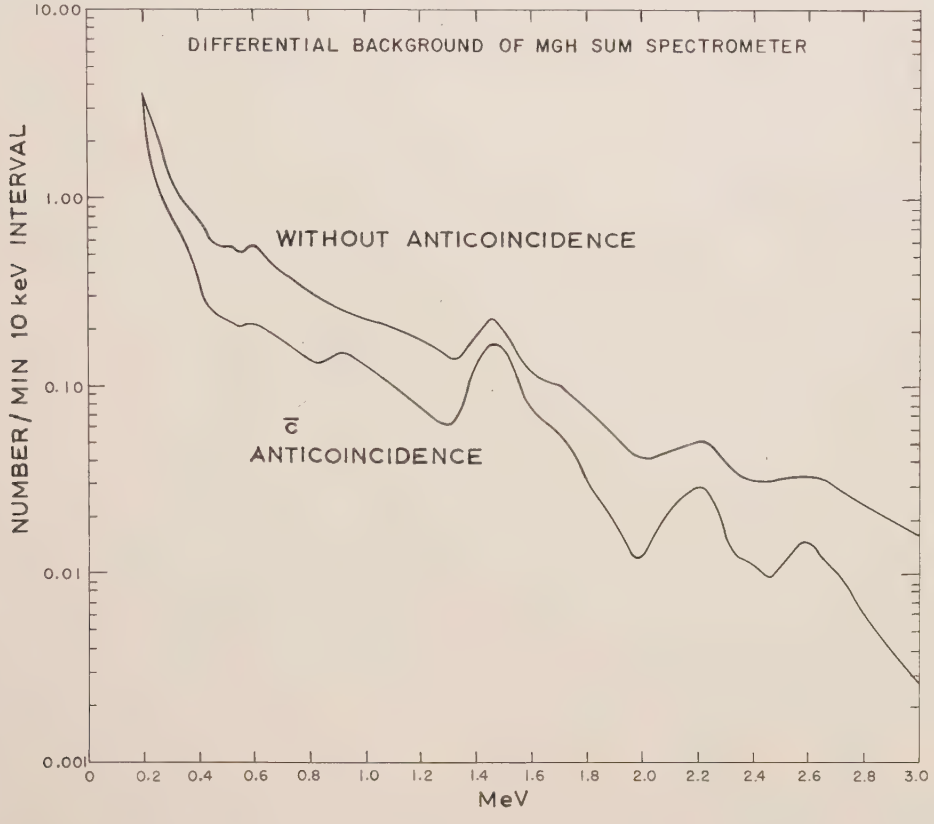

Fig. 7. Differential background spectra of the NaI well crystal with and without anticoincidence.

Table 1

Baseline energy (MeV)	Integral background to 3.1 MeV (C.P.M.)	
	without AC	with AC
0.2	760	400
0.4	440	200
0.6	320	150
1.0	175	90
1.6	61	23

Integral background counting rate of the NaI crystal with and without the anticoincidence mantle in operation.

The differential spectrum with and without the anticoincidence circuit is shown in fig. 7. Peaks counting rate in the AC mode is the result of a reduced Compton spectra in the large crystal and the detection by both scintillators of radioactivity and build-up radiation originating in the shield.

Background spectra, and those of low activity samples, consist of small peaks super imposed on a continuous distribution of gamma ray energies.

† The peak at 2.2 MeV was not present before the plastic scintillator was placed around the NaI detector. The 2.2 MeV gamma rays probably originate from slow neutron capture in the plastic scintillator which serves as an excellent moderator for fast neutrons produced by the interactions of cosmic rays in the heavy shielding. We have been unable to demonstrate the presence of any radium or thorium in the plastic scintillator.

Since the number of primary gamma rays recorded in a total absorption peak is not affected by the AC mantle, the ratio of spectra taken with and without anticoincidence is an aid in locating small peaks hidden in the continuous distribution. Fig. 8, the ratio of the differential background counting rates with and without anticoincidence, shows a clear peak at 0.350 MeV which is not visible on either of the spectra shown in fig. 7. Equally prominent are other total absorption peaks. The background between these peaks is reduced to less than half of its former value. When used with the AC mantle, the NaI crystal is an efficient instrument for the radioassay of low activity samples. As little as 8 $\mu\mu$ curie of Cs^{137} can be measured with a standard deviation of 5% in 50 min. Peaks produced by such small amounts of activity are easily identifiable without subtracting the background spectra.

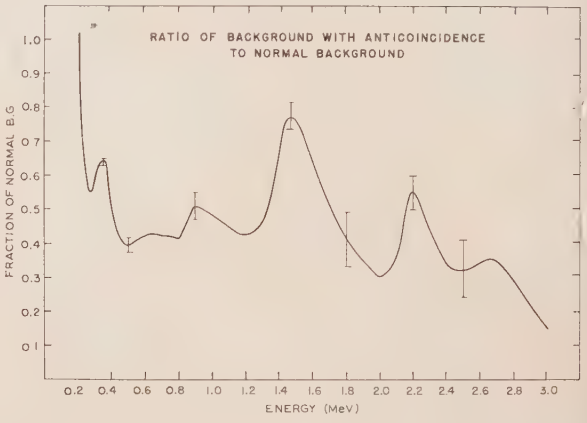

Fig. 8. The ratio of background counting rates with and without anticoincidence. Flags correspond to the standard error in a single energy interval (12 keV).

Appendix 1

CALCULATION OF AC MANTLE EFFICIENCY FOR CASCADE SPECTRA

If a cascade spectra is characterized by two gamma rays (γ_1 and γ_2) in coincidence seven possible combinations produce useful escape radiation; Compton-Compton interactions of gamma rays 1 and 2 respectively (C_1, C_2), peak-Compton interactions (P_1, C_2 and P_2, C_1), Compton-singles (C_1, O_2 and C_2, O_1) and peak-singles (P_1, O_2 and P_2, O_1). The number of Compton singles produced by γ_1 interacting in the NaI crystal $N_{(C_1,O_2)}$ is proportional to the product of the probability of γ_1 producing a Compton and the probability of γ_2 escaping from the NaI crystal without interacting.

$$N_{(C_1,\,O_2)} = N_0\,(\varepsilon_{\tau_1} - \varepsilon_{P_1})\,(1 - \varepsilon_{\tau_2})\ .$$

The number of these Comptons detected by the AC mantle, is

$$\Delta N_{(C_1,\,O_2)} = N_{(C_1,\,O_2)}\,[\eta_{P_2} + \eta_{C_1} - \eta_{P_2}\eta_{C_1}]$$

where η_{P_2} is the detection efficiency of the plastic mantle for γ_2, and η_{C_1} is the detection efficiency of the plastic mantle for the Compton escape radiation from γ_1. Similarly

$$\Delta N_{(C_1,\,P_2)} = N_0\varepsilon_{P_2}\,(\varepsilon_{\tau_1} - \varepsilon_{P_1})\,\eta_{C_1}$$

$$\Delta N_{(C_1,\,C_2)} = N_0\,[(\varepsilon_{\tau_1} - \varepsilon_{P_1})\,(\varepsilon_{\tau_2} - \varepsilon_{P_2})] \cdot [\eta_{C_1} + \eta_{C_2} - \eta_{C_1}\eta_{C_2}]\ .$$

The change in the number of peak singles recorded with anticoincidence provides a direct method of measuring the efficiency of the plastic well for monoenergetic escape radiation.

$$N_{(P_1,\,O_2)} = N_0\,[\varepsilon_{P_1}\,(1 - \varepsilon_{\tau_2})]$$

$$\Delta N_{(P_1,\,O_2)} = N_{(P_1,\,O_2)}\eta_{P_2}$$

$$\eta_{P_2} = \frac{\Delta N_{(P_1,\,O_2)}}{N_{(P_1,\,O_2)}}\ .$$

NUCLEAR INSTRUMENTS AND METHODS 7 (1960) 63–66; NORTH-HOLLAND PUBLISHING CO.

DETECTION OF NEUTRON AND PHOTON INDUCED FISSION BY ZnS(Ag) MIXED WITH URANIUM AND THORIUM COMPOUNDS

NICOLAI MITROFANOV and J. J. VAN LOEF

Laboratorio de Física Nuclear de la Universidad de Chile, Santiago de Chile

Received 23 November 1959

A description is given of a scintillator consisting of ZnS(Ag) mixed with uranium and thorium compounds. The absolute counting efficiency for fast neutron fission is $(3.2 \pm 0.6) \times 10^{-3}\%$ in the case of an uranium, and $(5.4 \pm 1.0) \times 10^{-3}\%$ in the case of a thorium compound mixture. The efficiency is within the experimental error independent of the neutron energy between 2 and 3.6 MeV. The scintillator is shown to be useful for photofission studies due to its very low sensitivity for γ rays.

1. Introduction

During the last few years various types of scintillators have been introduced for neutron counting[1]). In most cases the neutron interacts with the detector through proton recoil or through reactions of the type (n,p) or (n,α). While comparing the neutron counting properties of various ZnS(Ag) phosphor mixtures, Koontz *et al.* also studied neutron fission in ZnS(Ag) phosphors mixed with uranium and thorium compounds[2]). These authors estimated the counting efficiency for neutron fission in an uranium acetate—ZnS(Ag) mixture with neutrons emerging from a heteroenergetic neutron source. The purpose of this investigation was the determination of the counting efficiency of uranyl nitrate—ZnS(Ag) and thorium oxide—ZnS(Ag mixtures respectively for monoenergetic neutrons in the range between 2 and 3.6 MeV. As the sensitivity to gamma rays was expected to be very low, the applicability of these scintillators to photofission was studied.

2. Experiments and Results

ZnS(Ag) powder (Dupont 1101) was mixed with uranyl nitrate and thorium oxide respectively in different atomic ratio and thickness varying up to 200 mg/cm^2. The ZnS(Ag) phosphor mixtures with an aluminium reflector of 3 cm in diameter were mounted on top of a DuMont 6291 photomultiplier tube. The counting was performed with a conventional single-channel spectrometer. The gain of the linear amplifier was chosen so that the background due to alpha activity of uranium was less than 15 volt.

The University of Chile 800-keV Cockcroft-Walton accelerator provided neutrons through the D(d,n)He^3 reaction. An average current of 150 microamperes of magnetically-analysed deuterons of 600 keV bombarding energy was striking a self-regenerating target[3]). A long counter was at 1 meter from the neutron target at 90° with respect to the deuteron beam to monitor the neutrons.

Integral pulse-height spectra were obtained with the scintillators placed 2 cm from the target in the zero degree position. The distributions of alpha and neutron pulses for two mixtures each with a different atomic ratio of uranyl nitrate and ZnS(Ag) are shown in fig. 1. The neutron pulse-height distributions were taken for the same number of counts in the monitor. From a systematic study it resulted

[1]) H. H. Barschall, Handbuch der Physik, vol. **45** (Springer Verlag, Berlin, 1958).

[2]) Koontz, Keepin and Ashley, Rev. Sci. Instr. **26** (1955) 352.

[3]) J. Rapaport and J. J. van Loef, Phys. Rev. **114** (1959) 565.

that the maximum neutron counting rate could be obtained with a 1:6 uranyl nitrate—ZnS(Ag) mixture of about 200 mg/cm² thickness in agreement with the findings of Koontz *et al.*[2]).

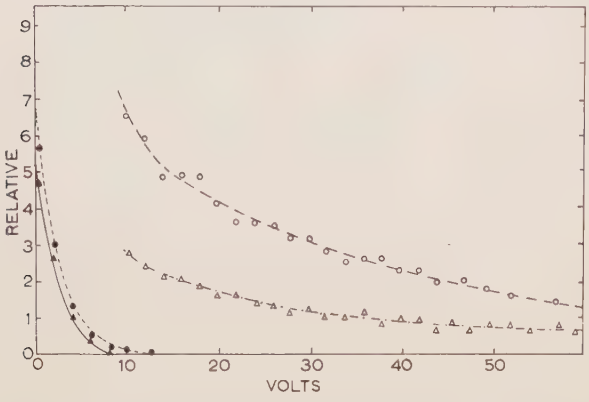

Fig. 1. Integral pulse-height distributions of alpha and neutron pulses at a standard gain for two mixtures each with an atomic ratio of uranyl nitrate–ZnS(Ag) as indicated between brackets: ▲ alpha background (1:20), ● alpha background (1:6), △ neutron pulses (1:20), ○ neutron pulses (1:6).

In order to define a counting efficiency for neutron induced fission in the scintillator all pulses other than fission pulses had to be biased out. Apart from the alpha background arising from the natural activity of uranium, pulses also originated from (n,p) and (n,α) reactions in ZnS[3,4]). These pulses obtained when 200 mg/cm² ZnS(Ag) powder was radiated in the same neutron flux were somwhat bigger in size than the alpha pulses in the uranyl nitrate-ZnS(Ag) (see Fig. 2). As the transparency of ZnS is better than that of the mixture, the pulses due to neutron reactions in ZnS should be smaller in the uranyl nitrate-ZnS(Ag). In the efficiency experiments a bias value was used corresponding to the maximum measured pulse height in ZnS.

The efficiency was determined by comparing the counting rate in the scintillator with that obtained in a Lamphere type of fission ionization chamber[5]) containing a thin foil of natural uranium of known weight. The detectors were located simultaneously at 90° with respect to the deuteron beam at distances such that both counters subtended the same solid angle with respect to the neutron target. As a consequence the neutron flux on each of the two counters was the same. In order to check the excentricity of the deuteron beam on the target, counting rates were also taken with the positions of the detectors reversed. The ratio of counting rates, averaged over these results was 10:1 in favour of the scintillator. The neutron flux was measured by observing the fission disintegration rate in the uranium and using the known fission cross section for natural uranium. The counting rate divided by the flux on the scintillator yielded an efficiency of $(3.2 \pm 0.6) \times 10^{-3}\%$.

The energy dependence of the efficiency for neutrons between 2 and 3.6 MeV was obtained through the angular distribution of the (d,d) neutrons at 600 keV deuteron energy. The scintillator was located at 17 cm from the target at angles of 0°, 45°, 90° and 145°. At each angle the counting rate in the detector was determined for a certain number of monitor counts. The background in each position was obtained by placing a copper bar between counter and target so that the neutron transmission through the bar was less than ten percent. The results of the angular distribution measurement corrected for finite angular resolution is given

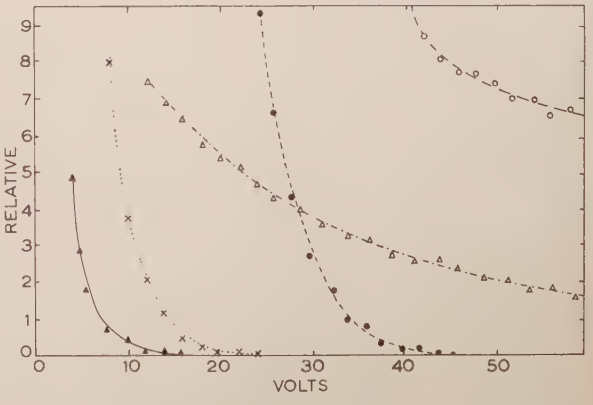

Fig. 2. Integral pulse-height distributions of alpha and neutron pulses at a standard gain for ZnS(Ag) and for ZnS(Ag) mixed with uranyl nitrate and thorium oxide: ▲ alpha background in U–ZnS (1:6). △ neutron pulses in U–ZnS (1:6), × neutron pulses in ZnS, ● alpha background in Th–ZnS (1:3) and ○ neutron pulses in Th–ZnS (1:3).

[4]) G. R. Keepin, Rev. Sci. Instr. **25** (1954) 30.

[5]) A. W. Lamphere and R. E. Greene, Phys. Rev. **100** (1955) 763.

Table 1

Angular distribution of D(d,n)He^3

Deuteron energy	$\theta_{Lab.}$ from neutron source	Relative angular distribution (measured)[a]	Neutron energy (MeV)[b]	Expected angular distribution[c]	Crystal
600 keV	0°	1.00	3.55 ± 0.10	1.00	ZnS(Ag) + $UO_2(NO_3)_2$ (6:1)
	45°	0.53 ± 0.06	3.30 ± 0.15	0.44	
	90°	0.26 ± 0.03	2.58 ± 0.19	0.25	
	135°	0.40 ± 0.04	2.05 ± 0.10	0.38	

[a] The error is the statistical error.
[b] The neutron energy spread at the detector due to target thickness and angular spread.
[c] The angular distribution to be measured by a detector of constant efficiency.

in table 1. For comparison the expected angular distribution[6]) is given in the last column. From the close agreement between these data it is concluded that the efficiency is within the experimental error independent of neutron energy in the range between 2 and 3.6 MeV.

The pulse height distribution of 200 mg/cm² of 1:3 thorium oxide-ZnS(Ag) mixture shown in fig. 2 is obtained with the same gain and the same neutron flux as that used in the previous experiments. More alpha background pulses as well as more neutron induced fission pulses were counted in spite of the lower fission cross section of Th^{232}. This may be due to a better transparency and a higher thorium content of the thorium oxide-ZnS(Ag) mixture. The efficiency of this scintillator was determined by comparing its counting rate, excluding the alpha background pulses, with that in the uranyl nitrate-ZnS(Ag) detector. This resulted in an efficiency of $(5.4 \pm 1.0) \times 10^{-3}$% for 3.5 MeV neutrons.

The low sensitivity of these scintillators to gamma rays[2]) make them suitable to apply for photofission studies. Photofission pulses were detected in the presence of 14 and 17 MeV gamma rays proceeding from the $Li^7(p,\gamma)Be^8$ reaction at 500 keV proton energy. The gamma-ray yield, monitored by a NaI(Tl) scintillation spectrometer, was found to be about 2×10^6 γ/sec. The bias of the uranyl nitrate-ZnS(Ag) detector was chosen so that the counting efficiency for Co^{60} gamma rays was by a factor of 10^5 less than the efficiency for neutron induced fission. At this bias no alpha background pulses were counted. As the interaction probability for 14 MeV gamma rays is by an order of magnitude less than for 1 MeV gamma rays, it was concluded that only fission pulses were recorded. A representative counting rate in the scintillator was 10 counts per minute, which is higher than the counting rate in the fission chamber.

3. Discussion

The counting efficiency for the uranyl nitrate-ZnS(Ag) detector is higher by a factor of three than the value obtained from the work of Koontz *et al.*[2]). However, the results of their experiments are difficult to evaluate quantitatively because the energy distribution of the neutrons falling on the detector is not known. An energy independence of the efficiency between 2 and 5.5 MeV neutron energy is to be expected since the fission cross section of U^{238} in this range is constant within a few percent[7]). Below 2 MeV the efficiency should diminish rapidly with decreasing energy, provided that no slow neutrons are present.

The low counting efficiency of these scintil-

[6]) N. Jarmie and J. D. Seagrave, Charged Particle Cross Sections, Los Alamos Scientific Laboratory, Report LA-2014 (1956).

[7]) W. D. Allen and R. L. Henkel, "Progress in Nuclear Energy" vol. 2 (Pergamon Press, London, 1958).

lators is principally due to the poor optical properties of the uranium and thorium compounds. Furthermore, no binding agent was used between the particles of ZnS and the fissionable material. As a consequence light pulses produced within the zinc sulfide will be internally reflected and thus not be able to escape. This effect may be avoided by using a suitable medium between the particles.

Acknowledgments

We like to thank Messrs González and Rapaport for helping in taking data and Mr. Stuardo for preparing the lithium target.

NUCLEAR INSTRUMENTS AND METHODS 7 (1960) 67–72; NORTH-HOLLAND PUBLISHING CO.

HIGH RESOLUTION NEUTRON SPECTROSCOPY

H. W. NEWSON and R. M. WILLIAMSON

Duke University, Durham, N. C.

Received 9 August 1959

The current state of high resolution spectroscopy with a Van de Graaff accelerator is reviewed. For neutrons in the keV region resolutions of about 3 per cent at 10 keV and 0.7 per cent at 100 keV have been attained. The resolution for 2 MeV protons is about 1.5×10^{-4}; very large ion currents are feasible at this resolution.

1. Introduction

The Duke University 4-MeV, Type DH, Van de Graaff accelerator has been used for both neutron and charged-particle nuclear spectroscopy since 1951. We wish to describe the most recent equipment developed with the help of E. G. Bilpuch and P. F. Nichols for measuring neutron total cross sections in the region 1- to 200-keV neutron energy with very high resolution[1]). We will describe a device called the Homogenizer[2]) which supplies a fluctuating voltage to the target which cancels the energy fluctuation of the Van de Graaff ion beam. We will also comment briefly on laboratory problems associated with Van de Graaff work.

2. Neutron Cross Sections

Fig. 1 shows the central vertical cross section of the target chamber and neutron collimator used for total cross section work. The proton beam, which is moving horizontally from left to right, bombards a thin metallic lithium target which is internally evaporated onto a 1 mil tantalum backing. A conical opening in polythene accepts only neutrons which are coming off the lithium target at an angle of 160° with the incident proton beam. The spread of the acceptance angle may be varied from $\frac{1}{2}°$ to 2° by sliding the inner polythene cone. Before entering the collimator, neutrons leave the chamber through a 5 mil silver window. Left and right banks of BF_3 counters are arranged at the exit opening of the collimator and are shielded from each other. The polythene and BF_3 counters are surrounded by several feet of water.

One half of the collimator is used to monitor neutrons, while the other half counts neutrons which have been attenuated by the sample which is being studied. A half-ring shaped sample interrups the neutron beam outside of the target chamber and just in front of the collimator. A second run is then taken with the second half of the sample in place and the first half removed in order to average out any assymetries.

At present the major limitation on neutron-energy spread is the lithium target thickness, which has never been observed to be less than 1 keV thick for 2-MeV protons, no matter how little lithium is evaporated. The amount of lithium is judged by the neutron yield. We assume that the lithium collects in islands 1 keV thick. Other physicists working with thin films have observed this effect. In addition we believe that very thin lithium oxidizes almost immediately in spite of the fact that a liquid air-cooled, activated charcoal trap is mounted adjacent to the target. (See fig. 1.) This trap does an excellent job of preventing carbon build-up on the target; we are able to bombard a target with 4 to 8 microamperes for 1 to 2 days with less than $\frac{1}{2}$ keV carbon build-up

[1]) Nichols, Bilpuch and Newson, Annals of Physics (to be published in October 1959).

[2]) Parks, Newson and Williamson, Rev. Sci. Instr. 29 (1958) 834.

and oxidation effects. The effective energy spread of the incident beam is 260 eV and it is combined with about a 300 eV target Doppler spread. The Homogenizer allows us to have high proton currents with this resolution.

The neutrons which leave the lithium target in the forward direction and are back-scattered

Fig. 2 shows the observed neutron-energy spreads as a function of neutron energy; (160° Van de Graaff, 1958) fig. 2 also shows the resolution which would be poissble if targets can be made which are as thin as the 300 eV Doppler spread (160° Van de Graaff limit). It also shows the neutron-energy spreads observed by various

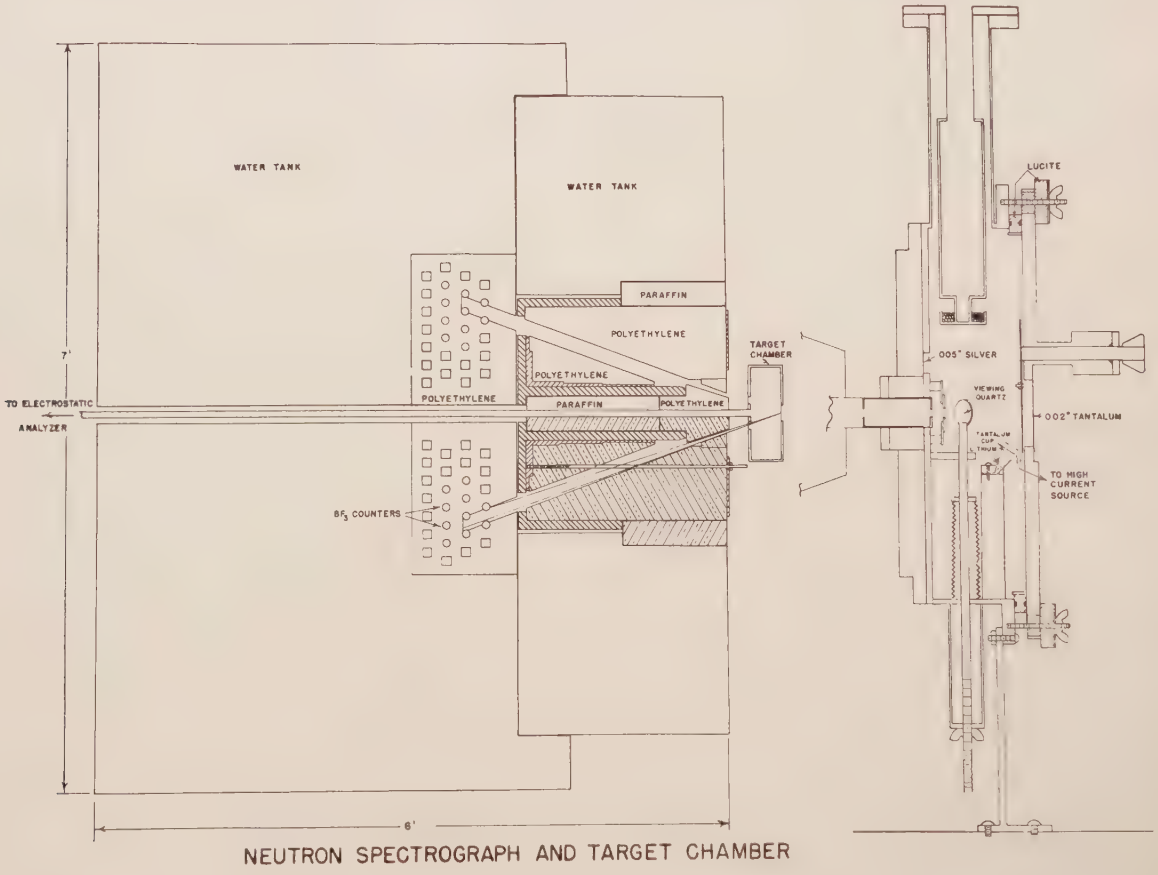

Fig. 1

by the 1 mil tantalum comprise the major source of background. This component can be directly measured at proton energies between the forward and backward neutron thresholds. Above the backward threshold we have measured resonances of known spin which are wide enough to be fully resolved and assigned a neutron background which gives the best fit with the calculated cross section. The background is 4%, 2% and 5% at 20 keV, 40 to 100 keV and 200 keV neutron energies, respectively.

neutron chopper groups and the ORNL Van de Graaff-time-of-flight group.

Figs. 3 and 4 show some recent total cross section data on Fe and Ba. Fig. 3 (Fe) shows that the peak yield of a narrow resonance at 30 keV is almost equal to the calculated peak yield. The lower data was taken in our laboratory with a 122° collimator[3]). Fig. 4 (Ba) shows a number of narrow, weak resonances which were unresolved by our earlier equipment. The major factors in the improvement of the data

[3]) J. H. Gibbons, Phys. Rev. **102** (1956) 1574.

were the small neutron angle spread, the improved neutron monitoring, the careful study of neutron background, and the Homogenizer.

3. Homogenizer

The Homogenizer was developed primarily to do neutron cross section work. However, it will also be a great help in studying the narrow resonances and small cross sections characteristic of charged particle cross sections in medium weight nuclei.

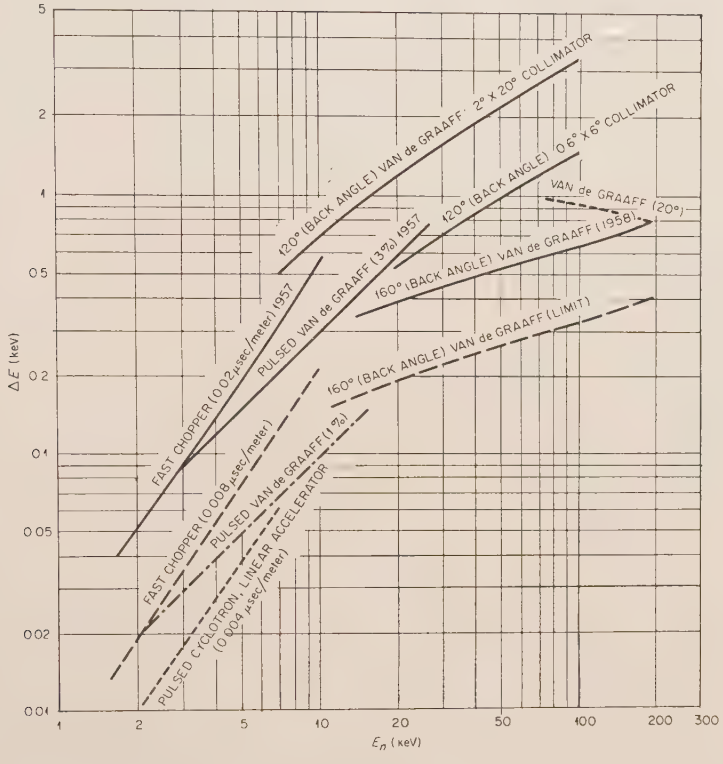

Fig. 2

Fig. 5 shows a block diagram of the Homogenizer. The ion beam from the Van de Graaff accelerator is separated into an atomic and molecular beam at 25° and 17° respectively. The symbols have the following meanings: ◯-slits which provide the control signal for the Van de Graaff and form the object slits for the cylindrical electrostatic analyzer; B-beam limiting slits; G-electron suppressors; I-analyzer image slits; T-slit signal attenuator; ICF-input cathode follower; A-difference amplifier; D-driver tube; V-voltage divider; OCF-output cathode follower. The target voltage can vary from approximately 1000 to 6000 V while the outer analyzer plate can vary from about 12 to 60 V.

Fig. 5 shows the behavior of the Homogenizer when hydrogen beams are being used. The separated molecular hydrogen beam is deflected by the large negative voltage on the inner plate of the electrostatic analyzer. If the beam energy is too high, as shown by the dashed curve, the amplified image slit signal simultaneously applies a positive voltage to the outer analyzer plate and to the unlimated proton beam target at 25°. The ratio between the voltage needed to center the beam at the image slits and the beam energy is a known constant (about 1/111), which depends only on analyzer geometry. Thus, the ratio of the proper target correction voltage and the voltage needed to keep the beam centered at the image slits may be accurately fixed by a resistor divider. The voltage fluctuations of the atomic and molecular hydrogen beams

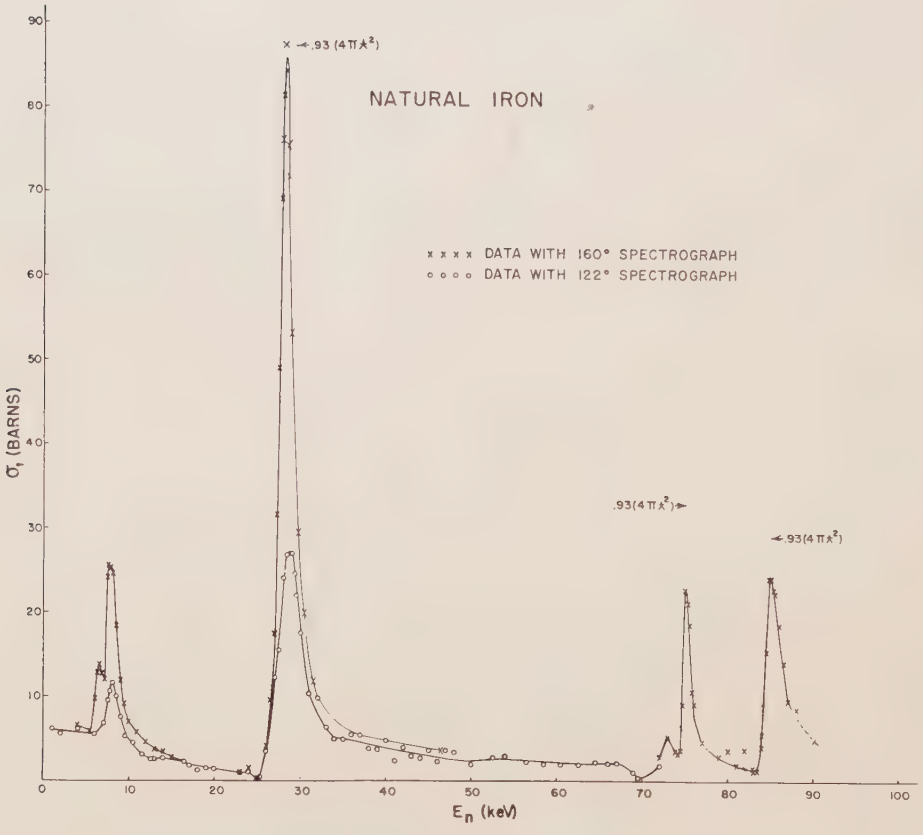
NATURAL IRON
x x x x DATA WITH 160° SPECTROGRAPH
o o o o DATA WITH 122° SPECTROGRAPH
.93 (4πλ²)
.93(4πλ²)
.93(4πλ²)
σt (BARNS)
En (keV)

Fig. 3

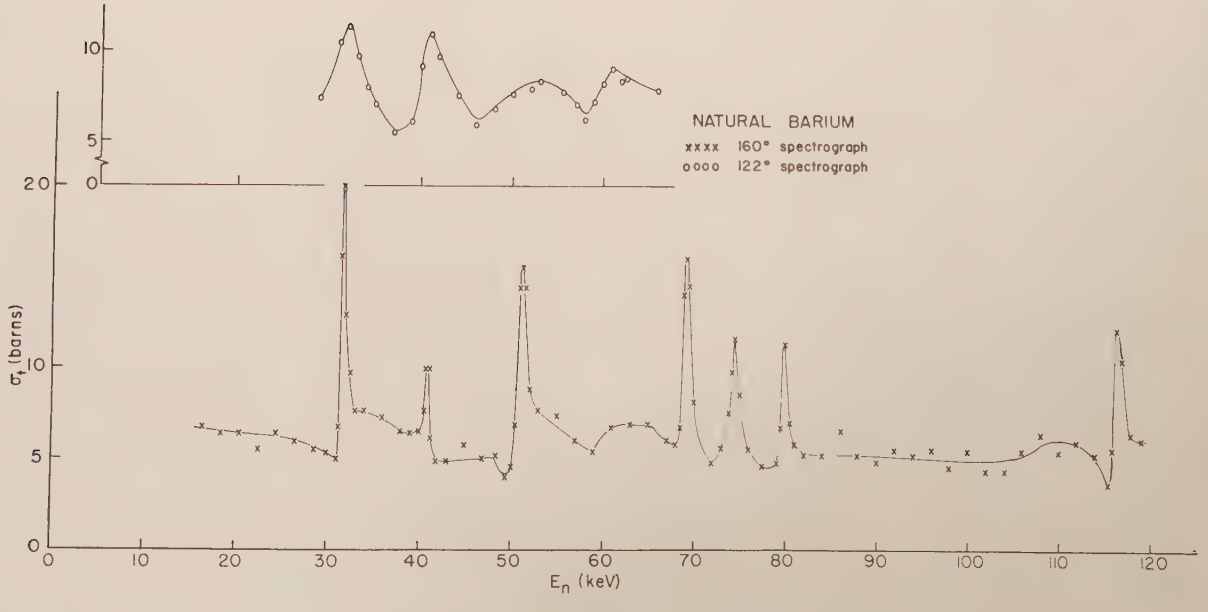
NATURAL BARIUM
xxxx 160° spectrograph
oooo 122° spectrograph
σt (barns)
En (keV)

Fig. 4

are, of course, the same. This use of the analyzer as part of a "null" device means that it is not important that the slit signal amplifier be extremely stable. It is only necessary that the circuit gain be high enough so that the required analyzer plate and target voltages are produced when the beam is off-center at the image slits by an amount which is small compared to the slit separation. Thus, most of the molecular beam gets through the image slits.

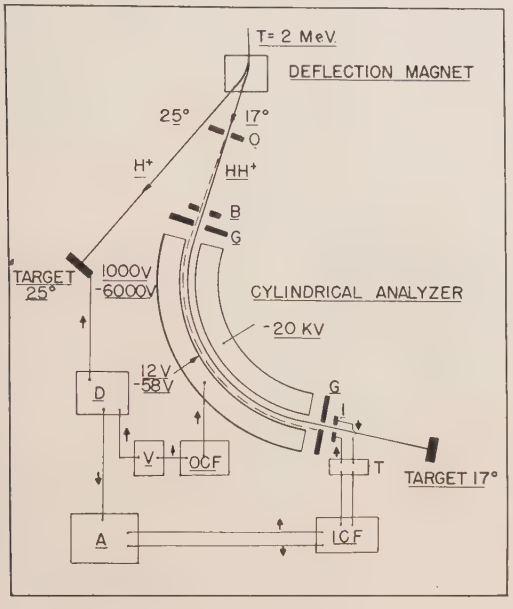

Fig. 5

We would like to point out that this use of the analyzer as part of a "null" device is much superior to the simple use of an amplified signal from the image slits as a correction voltage. In this case, the accuracy of the correction voltage depends on the electronic-circuit gain-stability, and the circuit must be able to ignore changes of beam intensity.

One may also put the proton beam, or any other ion beam, through the analyzer and apply the target correction voltage to the 17° target which follows the analyzer. In this instance, the beam would be limited at the analyzer object slits but only slightly at the image slits.

In principle the Homogenizer could be used on any type of accelerated beam without modifying the accelerator. The cylindrical electrostatic analyzer may be replaced by a magnetic analyzer. Only short electrostatic deflection plates would be needed to supply the correction field.

Fig. 6 shows the 1.76 MeV $C^{13}(p,\gamma)$ resonance. A semithick natural carbon target was bombarded at the 25° port. The heavy line is the calculated fit assuming Γ (natural width) = 150 eV, (Doppler width) 260 eV, and an incident beam Gaussian energy spread $R = 300$ eV at (1/e) of the maximum in the number of beam particles vs. energy distribution. The half height is then 260 eV.

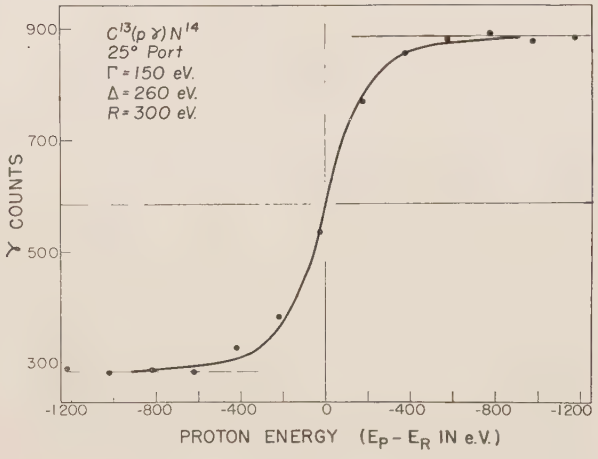

Fig. 6

4. General Comments

The ion beam from our accelerator may be deflected 25° left, 17° left, 0°, 17° right and 25° right. This gives us two separate target areas, and equipment may be set up and adjusted in one area while a group is working at the other. However, the areas are not shielded from each other and this advantage is not realized when the neutron experiments are under way. We have concrete block shielding walls between the deflection magnet and the target areas. It would be better to have two or more target rooms which are completely separate from the machine and deflection magnet and from each other.

We have found that alpha particles as well as deutrons produce a neutron background which is not healthy in the neighborhood of the magnet chamber. We have used needle valves for the control of all our different ion source gasses with

reasonable success. However, one must monitor neutrons very carfully and continuously in order to make sure that He or D_2 are properly turned off. This is a very important safety consideration.

When a new belt is installed in the Van de Graaff, quite a large negative charging current may result from belt-pulley friction when the spray voltage is turned down. If the ion source is on, a very large X-ray flux occurs at the base of the machine. One must be careful to always leave a little positive spray voltage on the belt charging needles, and one must also have an X-ray warning system.

Ion source repair is the major source of down time of a single ended Van de Graaff. We have found it very helpful to have a pressure tank for leak chasing spare ion sources. Another critical item in Van de Graaffs is pulley bearing life. This decreases rapidly with belt tension and some means of indicating belt tension would be most useful.

NUCLEAR INSTRUMENTS AND METHODS 7 (1960) 73–75; NORTH-HOLLAND PUBLISHING CO.

RECOIL TECHNIQUE IN CYCLOTRON BOMBARDMENTS USING POWDER TARGETS

G. ANDERSSON, G. RUDSTAM† and T. STENSTRÖM

The Gustaf Werner Institute for Nuclear Chemistry, University of Uppsala, Sweden

Received 14 November 1959

A new bombardment technique based on the catching of recoils in targets of mixed powders facilitates the carrier-free separation of cyclotron-produced nuclides. The method is applicable even to isotopes of the target element. In preliminary experiments useful yields were about 10% of those obtainable from a pure target.

1. Introduction

The present work was initiated by the problem of preparing β-spectrometer sources of highly neutron deficient nuclides in the rare earth region. Using a synchrocyclotron it is possible to obtain products of (p, xn) reactions in good yields even at fairly high x values, but the general decrease in half-life with increasing x creates serious difficulties in the chemical separation of the product element Z from other reaction products and, in particular, from the target element Z—1. Rapid ion exchange methods, which have been developed in recent years[1]), suffer from the limitation that the columns can be loaded with only small amounts of material, a few tenths of a milligram[2]), if good separation is desired. The usual target technique in a synchrocyclotron, on the other hand, requires at least 100 mg of, for instance, a rare earth oxide in order to ensure maximum yield in the bombardment.

If only less than 1% of the obtainable activity can be chemically processed, nuclear spectroscopic work will in many cases become impossible for intensity reasons. Thus it was most desirable to find a way of removing the bulk of target material prior to the ion exchange procedure. In the following we shall discuss briefly the potentialities of a special recoil technique in this respect and present some preliminary experiments.

It may be pointed out at once that the use of this method is not restricted to any special type of spallation reaction. In particular it should be of value in producing carrier-free isotopes of the target element itself after (p, pxn) reactions.

2. General Speculations

Assume that the element to be bombarded is in the form of a powder, fine-grained enough for all product nuclei of a certain kind to leave their mother grains as a result of the momentum imparted to them in the reaction. If the target powder is intimately mixed in the grain ratio 1:1 with another substance, a recoil catcher, of the same granulation and the same stopping power for the recoils, half of the activity of interest will be found in the catcher. This has to be so chosen, that it can be rapidly separated from the target powder after the irradiation, conveniently by discriminating dissolution. In this way, the total target volume being fixed, 25% of the yield from a pure target is obtained carrier-free in the catcher phase and may be subjected to rapid ion exchange chemistry.

A higher stopping power of the catcher material obviously would result in the collection of a larger fraction of the recoils in the catcher phase. This effect might be utilized to increase the efficiency of the method further by raising

† Present address: SC Division, Genève 23, CERN.

[1]) S. G. Thompson, B. G. Harvey, G. R. Choppin, and G. T. Seaborg, J. Am. Chem. Soc. **76** (1954) 6229.

[2]) P. Gregers Hansen and R. K. Sheline, Nucl. Instr. **2** (1958) 39.

the volume ratio between target and catcher. Simple calculations show that one could obtain more than 50% useful yield in the extreme case that the recoil range in the target is ten times that in the catcher.

3. Range Considerations

In the above discussion it has been tacitly assumed that the ranges of nuclei ejected in spallation reactions are long enough for a practical application of the technique and that the range straggling is negligible. These matters of fundamental importance have to be looked into a little further.

There are only few range determinations for spallation products published. Fung and Perlman[3]) studied recoil losses of Na^{24} from aluminium foils bombarded with 60–340 MeV protons. Their results indicate ranges of the order of 0.3 mg/cm^2, or 1 μ, for the Na^{24} atoms at intermediate bombarding energy. In a similar investigation Volkova and Denisov[4]) determined the ranges of Na^{24} atoms produced in aluminium, silicon, or phosphorus by 660 MeV protons to lie between 0.1 and 0.2 mg/cm^2. A number of heavy recoils from (α, xn) reactions in bismuth were studied by Donovan[5]). The average range in VYNS is about 0.05 mg/cm^2 for bombardment with 40 MeV α-particles. Donovan also demonstrated that the range distribution is very wide.

The theory of penetration of energetic atomic particles through matter has been treated by N. Bohr[6]), who showed that, depending on the velocity of the particles, two different mechanisms come into play in their stopping. Electronic collisions are important above the "Bohr velocity" v_0 ($= 2.2 \times 10^8$ cm/s), while nuclear collisions dominate below v_0. A Monte Carlo calculation of the momentum imparted to the residual nucleus by the nucleon cascade in spallation reactions[7]) indicates recoil energies usually lower than 1 MeV for products of interest here, that is, velocities $< v_0$. Applying the proper range formula[8,9]) to a number of target-catcher combinations (cf. chapter 4), we find the order of magnitude of the ranges to be 0.1 μ for recoil energies between a few hundred keV and 1 MeV, in agreement with the tendencies revealed in the experiments quoted above. It is concluded that the requirement imposed on the grain size may be met by colloidal particles.

The Monte Carlo calculations[7]) further point to a considerable initial energy spread of the recoils. In addition there is a range straggling originating from the slowing-down process, which can be calculated from theory. The formula given in ref.[9]) leads to standard deviations of about 40% for initially monoenergetic particles in the actual cases. Thus one has to expect a very wide distribution of ranges for a given product nucleus. This violates the crude assumption underlying the discussion in chapter 2 and tends to decrease the maximum yield obtainable. The possibilities of approaching ideal conditions, however, should be better the more fine-grained the powders.

4. Experimental Procedures

To check the above ideas a few experiments have been carried out, using the synchrocyclotrons at the Werner Institute, Uppsala, and at CERN, Geneva, for the bombardments. The main problem has been concerned with the preparation of sufficiently fine-grained powder mixtures. Three different target-catcher combinations were tried.

1. KBr TARGET + Cu CATCHER

a. From commercially available powders a grain size of 95–100 μ was selected by sifting.

b. Copper was precipitated from a copper sulphate solution by the addition of zinc and mixed with carefully ground, commercial potassium bromide powder. This gave a more suitable target mixture, although of varying and unknown granularity.

[3]) S. C. Fung and I. Perlman, Phys. Rev. **87** (1952) 623.
[4]) L. V. Volkova and F. P. Denisov, JETP **8** (1959) 372.
[5]) P. F. Donovan, University of California Lawrence Radiation Laboratory Report UCRL – 8347 (1958).
[6]) N. Bohr, Mat. Fys. Medd. Dan. Vid. Selsk. **18**, Nr. 8 (1948).
[7]) G. Rudstam, to be published.
[8]) K. O. Nielsen, Proc. 1955 Harwell Isotope Conf., Ch. 9.
[9]) J. Lindhard and M. Scharff, quoted by R. B. Leachman and H. Atterling, Arkiv Fysik **13** (1957) 101.

In both cases the separation of catcher from target after the irradiation was done by dissolving the potassium bromide in water. The further treatment in order to study the distribution of bromine isotopes between the two phases followed standard radiochemical practice.

2. La_2O_3 TARGET + Cu CATCHER

The procedures were corresponding to 1b, except that dilute acid was used to dissolve the lanthanum oxide.

3. La_2O_3 TARGET + Au CATCHER

A solution of gold and lanthanum in dilute hydrochloric acid was reduced by the addition of hydrazine during stirring, forming gold in colloidal solution. Ammonia was added to precipitate the lanthanum hydroxide, and the precipitate was centrifuged, washed, dried, and finally ignited at 800° C, leaving a brown powder consisting of lanthanum oxide intimately mixed with elemental gold.

After the irradiation, the lanthanum oxide was dissolved out of the mixture with dilute hydrochloric acid. The gold catcher left behind was dissolved in aqua regia and the gold removed by a few extractions with ethyl acetate, leaving a carrier-free solution of spallation products in the water phase.

It may be remarked that this procedure should be applicable to all the rare earth elements.

5. Results

The main results are summarized in the following table.

It is clearly seen that with the grain diameter about 100 μ (1a) most of the products of Br^{79} (p, p2n), Br^{79} (p, p3n), Br^{81} (p, p4n), and Br^{81} (p, p5n) reactions remain in the mother grains. A considerably better result is obtained when the more fine-grained mixture 1b is used. Here the reproducibility of the method is demonstrated, as well as in the last lines of the table. Cerium isotopes from lanthanum is an example of (p, xn) reactions. The La-Au cases show a definite difference in recoil range between Cd^{115}, formed by La^{139} (p, 10p15n), and Ba^{131}, formed by La^{139} (p, 2p7n). This is in accordance with the accepted semi-theoretical picture of the spallation process.

6. Conclusions

Already these preliminary experiments indicate the practical usefulness of the method. No doubt still better results could be obtained with suitable grain sizes and optimal proportions of target and catcher. The work will be carried on along these lines.

We would like to point out, finally, that if the experimental conditions can be satisfactorily controlled, this recoil technique opens up interesting possibilities for the study of ranges of spallation products.

We are indebted to Prof. The Svedberg for valuable discussions on colloid preparation. The cooperation of the cyclotron crews at the Werner Institute and at CERN is gratefully acknowledged.

Target mixture (% by weight)			Bombarding energy (MeV)	Nuclides studied	Distribution of the nuclides	
target	catcher	prep.			target	catcher
24% KBr	76% Cu	1a	170	Br^{76}, Br^{77}	99.5%	0.5%
24% KBr	76% Cu	1b	170	Br^{76}, Br^{77}	88 % 86 %	12 % 14 %
28% La_2O	72% Cu	2	170	Ce^{134}, Ce^{135}, Ce^{137}	88 %	12 %
57% La_2O_3	43% Au	3	590	Cd^{115}	80 %	20 %
57% La_2O_3	43% Au	3	590	Ba^{131}	92.3% 92.0%	7.7% 8.0%

NUCLEAR INSTRUMENTS AND METHODS 7 (1960) 76–88; NORTH-HOLLAND PUBLISHING CO.

COMBINATION OF MAGNETIC ANALYZERS IN NUCLEAR REACTION EXPERIMENTS

BO SJÖGREN

Nobel Institute of Physics, Stockholm 50, Sweden

Received 30 November 1959

Different ways to increase the counting rate in measurements with magnetic analyzing systems are investigated. It is assumed that a good energy resolution is desirable and that the energy spread of the beam from the accelerator is fairly large (cyclotron). The effect of combining the analyzers suitably, as well as the influence of the type and the setting of the target are discussed. Two types of systems are considered, namely analyzers with coincident and with perpendicular bending planes. In both of these cases the energy spread caused by the finite opening angle of the second analyzer is treated, being of importance for reactions with light nuclei. It is found that it should be possible to use a quite large target spot and thick target layer if the measurement is arranged in the proper way. The following circumstances are then important: the dimensions of the system and type of reaction, the bending direction and field gradient of the second analyzer, the target orientation and density and the detector position. The calculations are illustrated by some numerical examples†.

1. Introduction

When nuclear reactions are studied with magnetic analyzers (one for the beam and one for the reaction fragments), it is often desirable to increase the counting rate as much as possible. In the case of angular distributions, for instance, much running time is saved if a high counting rate can be achieved. Furthermore, in coincidence and even double-scattering experiments, in which individual particle groups are to be selected by magnetic analysis, this question would be of special significance. An example of such experiments is the measurement of p–γ-correlations in (d,p)-reactions[1]).

The transmission of a magnetic analyzer is generally small and therefore the intensity at the detector is limited. This means that the number of bombarding particles as well as target nuclei that can take part in the reaction should be as large as possible. However, the number of particles is restricted by the intensity, the energy spread and the spatial extent of the beam from the accelerator. It may also be restricted by the destructive effect of the beam on the target. When the accelerator is a cyclotron the former effect should be most important. This case will be assumed here.

To increase the number of bombarding particles, the size of the target spot can be increased. Then the energy spread of the particles also becomes larger. It is, however, significant in this connection that, if the slits of the system are suitably arranged, the energy generally depends upon at which point the particles hit the target. The number of target nuclei that can participate in the reaction is influenced also, apart from the target spot size, by the target thickness. This latter should be as large as possible, but as a consequence the charged particles get an increased energy spread due to absorption in the target material. Also in this case, the energy depends on where the reaction occurs.

If one wants to make a measurement with good energy resolution, it might thus at first seem to be impossible to use anything but a very small beam spot and a very thin target layer. However, one should be able to achieve the

† Most of the calculations were made in conjunction with the design of the equipment described in ref. [7]).

[1]) G. R. Satchler, Comptes Rendus du Congrès International de Physique Nucléaire, Paris Juillet 1958, and references given there. See also R. Huby, M. Y. Refai and G. R. Satchler, Nuclear Physics 9 (1958) 94.

same resolution with an appreciably large spot and thick target. The reason is that the energy of the incoming as well as of the outgoing particles depends on the reaction point, as was just mentioned. If one wants to increase the counting rate in this way, it is necessary to pay some attention to how the analyzers and the target should be arranged. It is the purpose of the present paper to discuss suitable arrangements for various types of systems of magnetic analyzers.

Quite recently this subject has been treated by B. L. Cohen in a paper[2]) dealing with a system of analyzers having coincident bending planes. Nevertheless, this case will also be treated in the following. The present work was essentially completed when Cohen's paper appeared and it has, apart from some amendments not been revised since then. For this reason, several of the ideas already given in [2]) are found here. However, the two treatments are not identical. It has also been noticed by Bach *et al.*[3]) that, for their system of two horizontal analyzers, quite large target widths can be used for (d,p)-reactions of moderately positive Q-values as the dispersions of their magnets nearly cancel out.

It is assumed throughout the present paper that the analyzers have double-focusing, nonuniform fields[4]). Many of the results, however, are applicable also to analyzers with homogeneous fields. Such analyzers can be double-focusing by the effect of the fringing field[5]). A nonuniform field is characterized (in first-order theory) by its sector angle and the field paramater n ($n < 1$). This parameter is defined by the expressions for the axial and radial field components,

$$B_z = B_0\left(1 - n\frac{r - r_0}{r_0}\right)$$

and

$$B_r = -B_0 n\frac{z}{r_0}$$

respectively, where r_0 is the mean radius and r and z are the cylindrical coordinates. If $n = \frac{1}{2}$ the focusing is stigmatic i.e. radial and axial images coincide. For other n-values the focusing is astigmatic[4]) ($n = 0$ means homogeneous field).

It should be noticed that only first-order effects will be considered in this paper (e.g. sharp field boundaries).

To begin with, the influence of the target thickness will be neglected. Firstly, a system consisting of two horizontal analyzers, which have coincident bending planes is treated. Such a system is described in [3]). Secondly, the case of perpendicular bending planes is considered. A system of this type is under construction at the Amsterdam synchrocyclotron (24 MeV deuterons)[6]) and another has just been put into operation at the small cyclotron of the Nobel Institute (7 MeV deuterons)[7]). In this case the second analyzer is first assumed to be exactly double-focusing and after that, more generally, the second analyzer is assumed to have astigmatic focusing. In both cases the influence of the solid angle of the second analyzer is considered.

The effects of the target thickness will be discussed in the last parts of the paper. It is considered in two steps: first, when the target thickness can be neglected in comparison with the target spot width (i.e. high target density), and after that when the thickness is comparable with this width (low target density).

It is understood that the accelerator is a cyclotron. However, several of the considerations are valid also for other accelerators.

2. Analyzers having Coincident Bending Planes

We consider a system of two magnetic analyzers with coincident medial planes (see fig. 1). The particle beam hits the slit in front of the first analyzer (denoted by 1 in the figure)

[2]) B. L. Cohen, Rev. Sci. Instr. **30** (1959) 415.

[3]) D. R. Bach, W. J. Childs, R. W. Hockney, P. V. C. Hough and W. C. Parkinson, Rev. Sci. Instr. **27** (1956) 516.

[4]) D. L. Judd, Rev. Sci. Instr. **21** (1950) 213;
E. S. Rosenblum, Rev. Sci. Instr. **21** (1950) 586;
D. L. Judd and S. A. Bludman, Nuclear Instruments **1** (1957) 46.

[5]) W. G. Cross, Rev. Sci. Instr. **22** (1951) 717;
See also Experimental Nuclear Physics, editor E. Segrè (Wiley and Sons, Inc., New York 1952).

[6]) L. Koerts and R. Hoekstra, private communication.

[7]) B. Sjögren, to be published in Nuclear Instruments.

and part of it passes this slit and is analyzed. The slit serves as an object for 1. At the image there is a second slit and the target is placed close behind it.

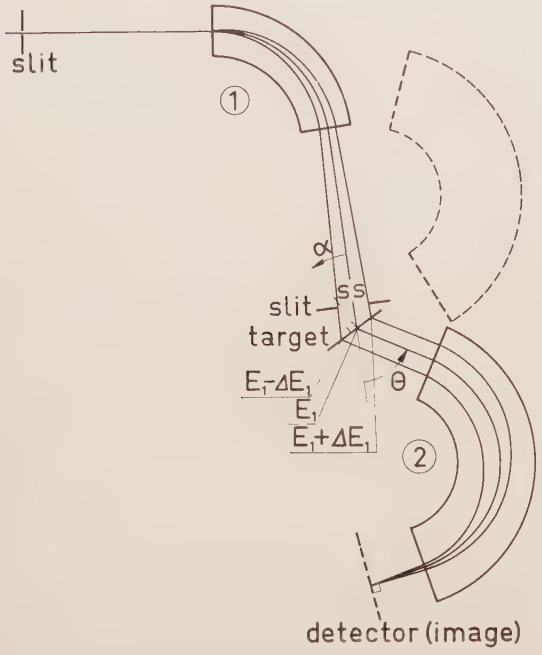

Fig. 1. Two analyzers with coincident bending planes. The broken line indicates the suitable bending direction of analyzer 2 when the incoming and the outgoing particles traverse the same side of the target. The target position in this case is not shown.

It is assumed that the first slit is narrow, as is necessary for good resolution. This means that, if one wants to have a beam with well defined energy on the target, it is necessary to use also a narrow second slit (if the magnification of 1 is not much greater than unity). However, if one uses a wide second slit in this arrangement, the beam hitting the target will have an energy varying from one edge to the other as is indicated in fig. 1. Throughout this paper the width of the object slit of the first analyzer will be neglected and the distance of the target from the radial image slit will be considered as small.

2.1. INFLUENCE OF THE TARGET SPOT WIDTH

The total energy variation of the particles hitting the target is denoted by $2\Delta E_1$ (fig. 1). According to the following definition of the dispersion of an analyzer, ΔE_1 can be expressed in the characteristic parameters of 1:

$$D \equiv 2\frac{\delta y/r_0}{\delta E/E}. \tag{1}$$

δy is the perpendicular distance from the optic axis corresponding to an energy deviation δE. We find

$$\Delta E_1 = \frac{2s}{D_1 r_1} E_1 . \tag{2}$$

The slit width is $2s$ and index 1 refers to the first analyzer. The width of the target spot is $2s/\cos\alpha$, where α is the angle between the incoming beam and the normal to the target plane. By definition α is positive in fig. 1.

We now consider a reaction taking place in the middle of the target spot where the energy of the outgoing particle is E_2 when the incoming particle has energy E_1. E_2 is a function of θ, the measuring angle. The energy difference ΔE_1 causes a difference in E_2 which is

$$\Delta E_2 = \frac{\partial E_2}{\partial E_1}\Delta E_1 . \tag{3}$$

The target spot has a width $2s\cos(\theta-\alpha)/\cos\alpha$ perpendicular to the optic axis of the second analyzer. If the energy of the particles from the whole spot were constant, one would have a width perpendicular to the axis at the image given by $M_{r_2} 2s\cos(\theta-\alpha)/\cos\alpha$. M_{r_2} is the radial magnification (positive when the image is inverted). In the present case, the particle energy is not constant but varies from $E_2 - \Delta E_2$ at one edge of the target spot to $E_2 + \Delta E_2$ at the other. If the second analyzer (its parameters have index 2), is turned as in fig. 1, and if the image width is called $2\Delta y_2$ we find by application of the expressions (1), (2) and (3)

$$\Delta y_2 = \left[\frac{D_2 r_2}{D_1 r_1}\frac{\partial E_2}{\partial E_1}\frac{E_1}{E_2} - M_{r_2}\frac{\cos(\theta-\alpha)}{\cos\alpha}\right] s . \tag{4}$$

Δy_2 vanishes, i.e., according to this first-order calculation, the resolution is independent of the target spot width, if the following condition (the first equality) is fulfilled:

$$\frac{\cos(\theta-\alpha)}{\cos\alpha} = \frac{D_2 r_2}{D_1 r_1 M_{r_2}}\frac{\partial E_2}{\partial E_1}\frac{E_1}{E_2} \equiv K\frac{\partial E_2}{\partial E_1}\frac{E_1}{E_2} \equiv F' . \tag{5}$$

If F is defined by

$$\frac{\cos(\theta - \alpha)}{\cos \alpha} \equiv F \qquad (6)$$

the condition is thus $F = F'$. This can be achieved by choosing a suitable α for a certain θ.

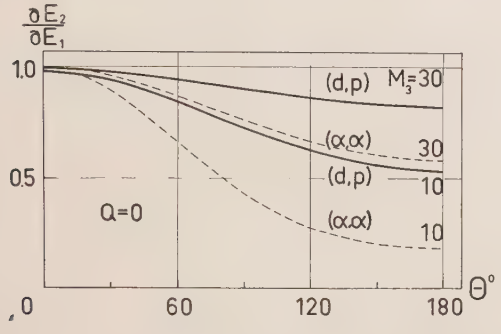

Fig. 2
$\partial E_2/\partial E_1$ as a function of θ for (d,p)- and (α,α)-processes with two different values of the residual nucleus. $Q = 0$

The parameter K and the function F' are also defined by (5). These notations will be used in the following.

If the condition (5) is not fulfilled, (4) corresponds to an equivalent energy variation

$$(\Delta E_2)_{\text{eq.}} = \frac{2M_{r_2}S}{D_2 r_2} \left| F' - F \right| E_2 \qquad (7)$$

or

$$(\Delta E_2)_{\text{eq.}} = \left| 1 - \frac{F}{F'} \right| \frac{\partial E_2}{\partial E_1} \Delta E_1 \,. \qquad (8)\dagger$$

In the expression for F', the factor $\partial E_2/\partial E_1$ depends on θ, the Q-value (divided by E_1), the masses of the target nuclei and the type of reaction[8]). However, its deviation from unity is important only for light target nuclei. In fig. 2, $\partial E_2/\partial E_1$ is plotted as a function of θ for different values of the final nucleus for (d,p)- and $(\alpha,\alpha,)$-processes ($Q = 0$). If the influence of $\partial E_2/\partial E_1$ can be neglected, F' is simply proportional to E_1/E_2. In fig. 3, F' is shown as a function of E_1/E_2 with the proportionality constant K as a parameter. This constant depends only on the geometry of the system. If $\partial E_2/\partial E_1$ deviates appreciably from unity, the F-value obtained from fig. 3 must be corrected with respect to this.

† Cf. equation (12) in Cohen's work.

When F is known, the proper value of α (for $F = F'$) is determined by (6). In fig. 4 a number of curves show α as a function of θ for different F-values. It is thus easy to get the best target-setting in any special case by using these curves. First, F is obtained from fig. 3—it is corrected if necessary—and then fig. 4 gives the corresponding α.

We have hitherto considered an arrangement in which the two analyzers "see" opposite sides of the target. This may be possible for reaction angles up to somewhat more than 90°, but for larger angles the target must be turned so that the analyzers are on the same side of it. Then, however, the second analyzer must also be turned to make possible a compensation for the target width. This case is indicated in fig. 1 by broken lines. It is equivalent to putting a minus

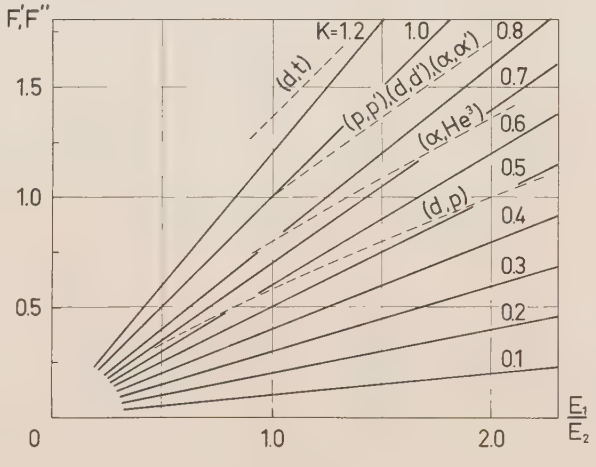

Fig. 3

$$F' = K \frac{\partial E_2}{\partial E_1} \frac{E_1}{E_2}$$

according to (5) and

$$F'' = \frac{\varepsilon_2}{\varepsilon_1 \dfrac{\partial E_2}{\partial E_1}}$$

according to (24) as functions of E_1/E_2 for different values of K.

$$\frac{\partial E_2}{\partial E_1} = 1 \,. \qquad K = \frac{D_2 r_2}{D_1 r_1 M_{r_2}} \,.$$

The stopping powers ε_1 and ε_2 are for Al ($E_1 = 11$ MeV protons, 22 MeV deuterons and 44 MeV α-particles) [9]).

[8]) A. B. Brown, C. W. Snyder, W. A. Fowler and C. C. Lauritsen, Phys. Rev. **82** (1951) 159.

[9]) M. Rich and R. Madey, University of California, Rad. Lab. Report, UCRL-2301, March 1954.

sign in front of F' in (5). For this reason curves for negative F-values have also been plotted in fig. 4. A simplification is achieved here if the following definition is made: D_2 (and K) is positive when the second analyzer has the same bending direction as the first one and negative when this direction is opposite. Then (5) is the relevant condition for all reaction angles and α is obtained directly from fig. 4.

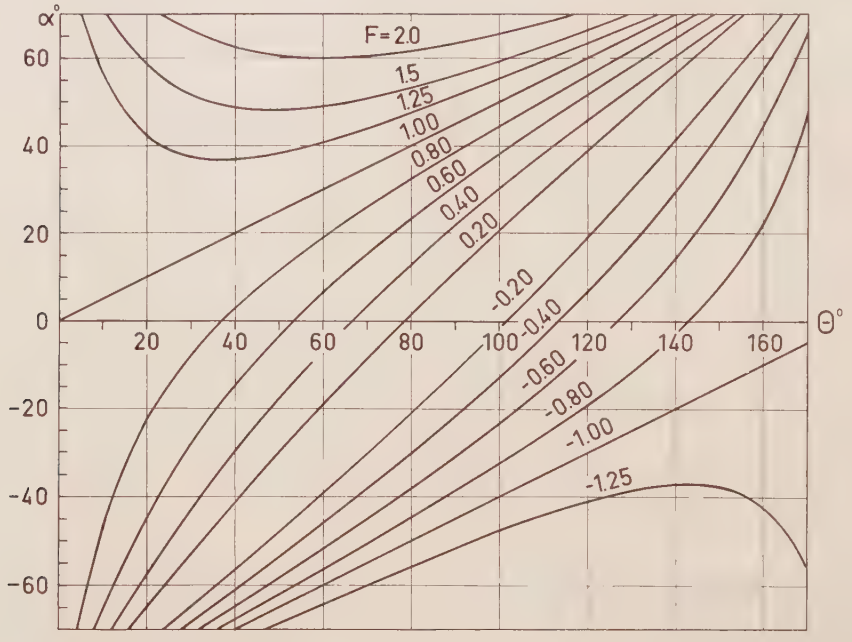

Fig. 4. α as a function of θ obtained from $[\cos(\theta - \alpha)]/\cos\alpha = F$ for different F-values.

2.2. INFLUENCE OF THE OPENING ANGLE OF THE SECOND ANALYZER

Due to the finite value of the opening angle in the radial direction of analyzer 2 (fig. 1), the particles coming from a point on the target have an energy spread determined by $\partial E_2/\partial\theta$. The energy deviation from the mean value E_2 (corresponding to θ) for particles emitted in the direction $\theta + \Delta\theta$ is $(\partial E_2/\partial\theta)\,\Delta\theta$ if $\Delta\theta$ is small. For the position of analyzer 2 given by the full-drawn line in fig. 1 this means that the particles are focused at a point which is nearer to the magnet than the "ordinary" image point (corresponding to constant particle energy). For the position indicated by broken lines in the figure, the focusing point is further away from the magnet. This change of distance is found to be independent of $\Delta\theta$.

In fig. 5, which schematically shows the particle orbits in the second analyzer, the change in the position of the image point is denoted by Δl_r. A first-order calculation gives:

$$\Delta l_r = -\frac{D r_0 \dfrac{M_r}{2E_2}\dfrac{\partial E_2}{\partial\theta}}{1 - \dfrac{M_r}{2E_2\sqrt{1-n}}\dfrac{\partial E_2}{\partial\theta}\sin\phi_0\,\sqrt{1-n}}. \quad (9)$$

(index 2 is dropped from the parameters in this section, r_0 is the mean radius). This expression is valid when $l_r > \Delta l_r$. Δl_r depends on θ. It is a maximum for $\theta = 90°$ and decreases to zero for $\theta = 0°$. (It is approximately proportional to $\sin\theta$ due to the factor $\partial E_2/\partial\theta$ [6].)

Δl_r is of appreciable size only for fairly light nuclei.

The best resolution when measuring in a certain angle is thus obtained by putting the detector a distance $l_r - \Delta l_r$ from the analyzer (fig. 5). Δl_r is determined from (9). It is seen ($\partial E_2/\partial\theta$ negative) that this expression is positive

if the second analyzer has the same bending direction as the first one and negative if the directions are opposite. If the sign of D_2 is chosen as above, (9) is valid for all angles.

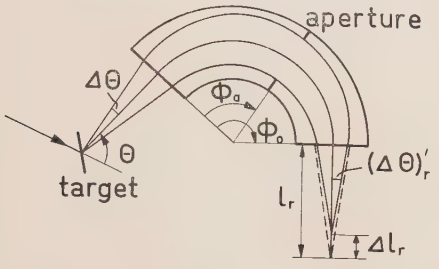

Fig. 5. Change of radial image due to $\partial E_2/\partial\theta$. The bending plane of the analyzer coincides with the reaction plane.

A numerical example may show the order of magnitude of Δl_r. The dimensions $D = 4$, $M_r = 1$, $\phi_0 = 180°$, $E_1/E_2 = 1$, $\theta = 90°$ and mass of residual nucleus = 20, give for a (d,p)-reaction $\Delta l_r = 0.25\, r_0$. If $r_0 = 50$ cm and $2\Delta\theta = 4°$, this means a width of about 0.9 cm at the "ordinary" image (see (12)). For an (α,α')-reaction with $E_1/E_2 = 1.5$ and $\theta = 90°$, we get $\Delta l_r = 0.66\, r_0$ and a width of about 2.9 cm. These widths correspond to $\Delta E_2/E_2 =$ 0.9 and 2.9% respectively according to (1).

The magnification and the other characteristic parameters describing the image formation in the radial direction of analyzer 2 are also influenced by the angular dependence of the particle energy. (The corresponding parameters for the axial focusing, on the other hand, are not influenced, cf. 3.) Thus it is necessary to use corrected values for these quantities. A calculation results in the following expressions (where the primes indicate the corrected values)†:

$$M'_r = M_r - \frac{\Delta l_r}{r_0}\sqrt{1-n}\,\sin\phi_0\,\sqrt{1-n} \qquad (10)$$

$$D' = \frac{1 + M'_r}{1-n} \qquad (11)$$

$$(\Delta\theta_r)' = (\Delta\theta_r)\left[1 - \frac{M_r}{2E_2\sqrt{1-n}}\frac{\partial E_2}{\partial\theta}\sin\phi_0\,\sqrt{1-n}\right] \qquad (12)\text{††}$$

where

$$\Delta\theta_r = \frac{\Delta\theta}{M_r}$$

Finally, the question arises of how the condition (5) for the best target orientation with respect to the energy spread of the incident beam is influenced by $\partial E_2/\partial\theta$. It is found that (5) is still valid if D_2/M_{r_2} is replaced by D'_2/M'_{r_2} obtained from (10) and (11).

In the example above, this means that the fraction D_2/M_{r_2} is increased by approximately 8 and 30% respectively for the two reactions.

3. Analyzers having Perpendicular Bending Planes

We now consider a system in which the two analyzers bend the particles in planes perpendicular to each other. At the target this means that the radial direction of the first analyzer

† The corrected value of the solid angle depends on how the particle orbits are confined in the field. In the case considered by Judd[4]) it is assumed that the available cross-sectional area, called Ar_0^2, is independent of the variable central angle ϕ (cf. fig. 5). Then, if $r_0 = 1$, the solid angle from a point on the optic axis is

$$\frac{\Omega'}{A} = \left[\left\{l_0^4 + \frac{l_0^2+1}{n(1-n)} + \frac{nl_0^2+1}{n(1-n)}(c^2 + 2cl_0\sqrt{1-n})\right\}^{\frac{1}{2}} - c\left\{\frac{nl_0^2+1}{n(1-n)}\right\}^{\frac{1}{2}}\right]^{-1}$$

where l_0 = object distance and

$$c = -\frac{1}{2E_2\sqrt{1-n}}\frac{\partial E_2}{\partial\theta}.$$

If, instead, the opening is defined by an aperture slit as in fig. 5 (but with Judd's assumption for the z-deflection), Ω' depends on this aperture. For the specific case when ϕ_a is assumed to be

$$\frac{\pi}{2\sqrt{1-n}}$$

(Ar_0^2 = available cross-sectional area at ϕ_a)

$$\frac{\Omega'}{A} = \left\{\frac{n(1-n)}{nl_0^2+1}\right\}^{\frac{1}{2}}(1-c)^{-1}$$

from a point on the optic axis.

It may sometimes be necessary to correct the solid angle with respect to $\partial E_2/\partial\theta$ when measuring angular distributions as well as absolute cross-sections.

†† This is for the point on the optic axis. For other target points a term $(y_1/r_0)\sqrt{1-n}\,\sin\phi_0\,\sqrt{1-n}$ (cf. (18)) should be added to the right hand side (y_1 is the perpendicular distance from the optic axis).

corresponds to the axial direction of the other. Fig. 6 schematically shows this case. In order to make the figure clearer, analyzer 2 has been folded out so that the central beam has become a straight line.

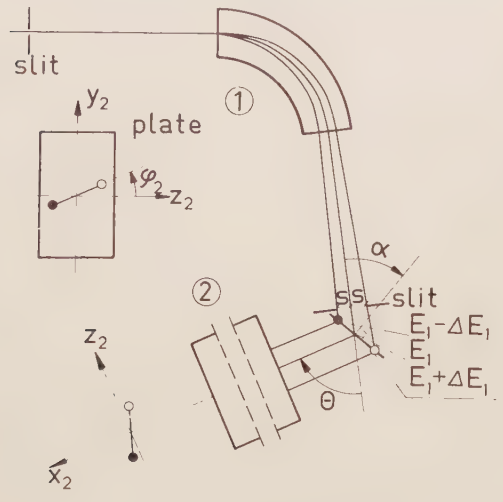

Fig. 6. Two analyzers with perpendicular bending planes.

3.1. STIGMATIC FOCUSING

We assume $n_2 = \frac{1}{2}$ (index 2 for analyzer 2) and for the moment we neglect all influence of $\partial E_2/\partial\theta$. When this stigmatic case has been treated it is easy to discuss the more general one.

In fig. 6 the target points have been marked by a full and an open circle, where the incoming particles have energies $E_1 - \Delta E_1$ and $E_1 + \Delta E_1$ respectively (with the same assumptions as before). The corresponding image points are indicated by the same signs. The target point with energy E_1 is assumed to have its image in the origin of the $x_2y_2z_2$-system (see fig. 6, x_2 is the central beam direction, y_2 is directed out from the paper). These three marked target points lie in the horizontal plane (i.e. the plane of the paper). Their images, however, do not lie in this plane but in another inclined at an angle. The reason is that the particles emerging from the three points have different energies and therefore they are focused at points having different y_2's. In fig. 6 the points are also shown in the y_2,z_2-plane.

A quantitative expression for the tilting angle φ_2 is deduced from (1), (2) and (3) and an argument similar to that leading to (4). We obtain for the displacements y_2 and z_2:

$$y_2 = \frac{D_2 r_2}{D_1 r_1} \frac{\partial E_2}{\partial E_1} \frac{E_1}{E_2} s \tag{13}$$

$$z_2 = M_{z_2} \frac{\cos(\theta - \alpha)}{\cos\alpha} s\,. \tag{14}$$

M_{z_2} is the magnification in the axial direction. Thus the angle φ_2 is obtained from

$$\tan\varphi_2 = \frac{D_2 r_2}{D_1 r_1 M_{z_2}} \frac{\partial E_2}{\partial E_1} \frac{E_1}{E_2} \frac{\cos\alpha}{\cos(\theta - \alpha)}\,, \tag{15}$$

or by use of the definitions of F' and F in (5) and (6)

$$\tan\varphi_2 = \frac{F'}{F} \tag{16}$$

as $M_{z_2} = M_{r_2}$ for $n_2 = \frac{1}{2}$. F' is obtained from fig. 3 and F may be chosen arbitrarily within certain limits (see fig. 4).

If a photographic plate is put in the y_2,z_2-plane, the particles from the same height on the target should fall on a line with a tilting angle φ_2. In practice a photographic plate must be inclined in order that the tracks be readable. Then it is necessary to correct φ_2 with respect to this to obtain the tilting angle on the plate. If, for instance, the length direction of the plate is along the y_2-axis and the angle between the plate and the x_2-axis is β, the tilting angle φ is determined by $\tan\varphi = \tan\varphi_2 \cdot \sin\beta$.

Thus, as far as the assumptions for the calculation are valid, a line broadening caused by the energy spread of the bombarding beam may be eliminated by reading the tracks in strips (or putting the detector slit) at a suitable tilting angle. A contribution to the line broadening is, of course, given by the target spot height, so that it is necessary to have this height small if good resolution is desired.

As an illustration, φ_2 is calculated for the system in [7] ($E_1 = 7$ MeV deuterons, 14 MeV α-particles). In this case $K = 0.60$ (see (5)). $\partial E_2/\partial E_1$ is put equal to unity. The factor F is properly chosen with respect to the absorption

in the target material. It is assumed that the incoming and outgoing particles traverse opposite sides of the target (i.e. $\theta_{max} \approx 90°$ and θ_{min} is not too small, see fig. 4). Then the factor, obtained from (24) (see fig. 3), is F''. Thus, $\tan\varphi_2 = F'/F''$. φ_2 is shown for (d,p)-, (d,d')- and (α,α')-reactions as a function of E_1/E_2 in fig. 7.

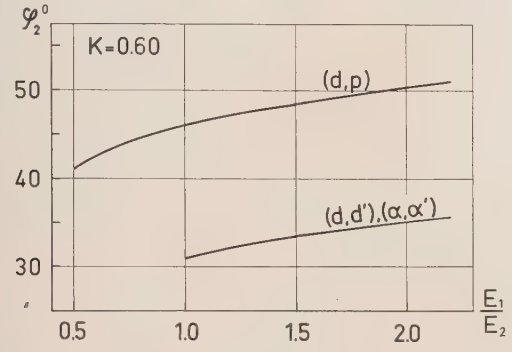

Fig. 7. φ_2 obtained from $\tan\varphi_2 = F'/F''$ as a function of E_1/E_2 for (d,p)-, (d,d')-, and (α,α')-reactions. $n_2 = 0.50$. F' and F'' have been obtained from fig. 3.

3.2. INFLUENCE OF THE OPENING ANGLE OF THE SECOND ANALYZER

In the present case of two perpendicular analyzers it is also important, when using a wide target spot, to know the variation of the reaction angle θ. It is possible to reduce appreciably the line broadening caused by the energy spread $(\partial E_2/\partial\theta)\,\Delta\theta$, if the system is arranged in a suitable manner.

A deviation from the mean value of the reaction angle arises from two causes. Firstly, considering a very small target spot, we have the finite opening angle in the axial direction. As the analyzer is double-focusing, this angle is comparatively large. Secondly, when one uses a wide target spot the angle may vary for different points within the area. This variation depends on where the aperture slit of the second analyzer is placed.

The energy spread caused by the finite opening angle can be compensated by using an analyzer with a convenient astigmatic focusing (n_2 somewhat larger than $\frac{1}{2}$). This method has been suggested by Mileikowsky[10]). By reading the detector plates in strips with the proper tilting angle (depending on $\partial E_2/\partial\theta$), it is possible to attain an increase of the resolution[11]). In Mileikowsky's treatment it is assumed that the target spot is very small. The influence of the target width will here be discussed in the following section dealing with the astigmatic case.

We now consider the z-component of the particle orbits[4]) in the second analyzer. Fig. 8 indicates schematically some ion paths projected in the plane defined by the z-direction and the outfolded optic axis. The image is described by the coordinate system x_2, y_2, z_2, and the indices r and z mean radial and axial focus respectively. y_2 is directed out from the paper. r_2 is the mean radius, l_0 the object distance, ϕ_0 the sector angle defining the region of field, and ϕ_a the position of the aperture (cf. fig. 5 for the radial case). One object point (at a distance z_1 from the optic axis) and its image are indicated by solid circles. The opening angle from this point is given by $\Delta\theta_1$ and $\Delta\theta_2$ and the angle from the object point on the optic axis by $\Delta\theta_0$ (see fig. 8).

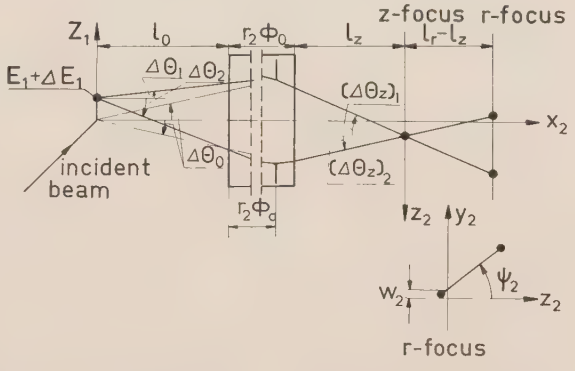

Fig. 8. Particle paths in an astigmatic second analyzer.

For $\Delta\theta_1$ and $\Delta\theta_2$ the following expressions are obtained (first index corresponds to upper sign):

$$\Delta\theta_{1,2} = \frac{a \mp z_1 \cos\phi_a \sqrt{n_2}}{l_0 \cos\phi_a \sqrt{n_2} + \dfrac{r_2}{\sqrt{n_2}} \sin\phi_a \sqrt{n_2}} \,. \qquad (17)\dagger$$

† For Judd's case (no aperture slit) with $r_2 = 1$:

$$\Delta\theta_{1,2} = \left[a\left\{1 - \frac{z_1^2}{a^2\,(1 + n_2 l_0^2)}\right\}^{\frac{1}{2}} \mp \right.$$

$$\left. \mp\, l_0 z_1 \left(\frac{n_2}{1 + n_2 l_0^2}\right)^{\frac{1}{2}}\right] \left(\frac{n_2}{1 + n_2 l_0^2}\right)^{\frac{1}{2}} .$$

[10]) C. Mileikowsky, Ark. f. Fys. **7**, No. 5 (1953) 57.

[11]) L. Bianchi, E. Cotton et C. Mileikowsky, Nuclear Instruments **3** (1958) 69.

The aperture width is $2a$ (symmetric with respect to the x_2,y_2-plane). $\Delta\theta_0$ is obtained for $z_1 = 0$. It is seen from (17) that $\Delta\theta_1 = \Delta\theta_2 = \Delta\theta_0$ if $\phi_a\sqrt{n_2} = \frac{1}{2}\pi$ (i.e. $\phi_a = 127°$ for $n = \frac{1}{2}$). For this aperture setting the angles are thus independent of z_1. If the optimal value of ϕ_a is larger than ϕ_0 it is not possible to achieve this cancellation, but in most cases the z_1-term is quite small. It also follows from (17) that the mean reaction angle is constant across the target spot if $\phi_a\sqrt{n_2} = \frac{1}{2}\pi$. The variation of the mean reaction angle should in most practical cases be very small (for suitable ϕ_a).

The angles corresponding to $\Delta\theta_{1,2}$ at the image are:

$$(\Delta\theta_z)_{1,2} = \pm\frac{z_1\sqrt{n_2}}{r_2}\sin\phi_0\sqrt{n_2} + \frac{\Delta\theta_{1,2}}{M_{z_2}}. \quad (18)$$

3.3. ASTIGMATIC FOCUSING

The energies of the particles emerging from the solid point in fig. 8 in the directions $\Delta\theta_{1,2}$ deviate from the energy of particles following the optic axis by the amounts $(\Delta E_2)_{1,2}$.

$$(\Delta E_2)_{1,2} = \frac{\partial E_2}{\partial E_1}\frac{2E_1}{D_1r_1}\frac{\cos\alpha}{\cos(\theta-\alpha)}z_1 \mp \frac{\partial E_2}{\partial\theta}\Delta\theta_{1,2}$$

(see (2), (3)). At the axial focus the particles in these two directions have the same z_2-value, $z_2 = M_{z_2}z_1$. At the radial focus, however, they hit points which have the coordinates

$$(y_r)_{1,2} = \frac{D_2r_2}{2E_2}(\Delta E_2)_{1,2} \quad (19)$$

and

$$(z_r)_{1,2} = M_{z_2}z_1 \pm (l_r - l_z)\cdot(\Delta\theta_z)_{1,2} \quad (20)$$

as $(\Delta\theta_z)_{1,2}$ are small angles.

It is seen by inserting the expressions for $(\Delta E_2)_{1,2}$ and $(\Delta\theta_z)_{1,2}$ into (19) and (20), that all the particles from the solid point are focused on a straight line at the radial focus. The angular coefficient of this line is

$$\tan\psi_2 = -\frac{D_2r_2M_{z_2}\dfrac{\partial E_2}{\partial\theta}}{2E_2(l_r - l_z)}. \quad (21)\dagger$$

The intersection on the y_2-axis is

$$w_2 = z_1\frac{D_2r_2}{2E_2}\left[\frac{\partial E_2}{\partial E_1}\frac{2E_1}{D_1r_1}\frac{\cos\alpha}{\cos(\theta-\alpha)} + \right.$$

$$\left. + \frac{\partial E_2}{\partial\theta}\left\{\frac{M_{z^2}}{l_r - l_z} + \frac{M_{z_2}\sqrt{n_2}}{r_2}\sin\phi_0\sqrt{n_2}\right\}\right]. \quad (22)$$

The particles from the points on the wide target are thus focused on straight, parallel lines which together give rise to a band. The width of this band (i.e. the resolution) in the y_2 direction is obtained from (22) (see fig. 8). To get a good resolution, the coefficient of z_1 should be small if the object is wide. The detector plates should be read in strips being tilted at the angle ψ_2.

$\partial E_2/\partial\theta$ is negative and therefore the two terms in the square bracket in (22) have opposite signs. This is true when the analyzers are combined as is shown in fig. 6 (the second analyzer on the left side of the beam). In the alternative case the terms have the same sign††. It is desirable that the expression in the bracket be as small as possible i.e. that the terms nearly cancel out. To achieve this, three parameters may be varied (except for r_1 and r_2), D_1, α and n_2. It is clear that the astigmatism $l_r - l_z$ depends on n_2 [4]). E.g. for a 180° analyzer with n_2 near 0.5 and about equal object and image distances $l_r - l_z \approx 5\,(2n_2 - 1)\,r_2$.

D_1 may be changed by changing the pole gap of the first analyzer, but this influences the geometry of the system. The possibility to vary D_1 in this way is probably fairly small. As to α, it influences the energy spread caused by absorption in the target material, and therefore in many cases it should be chosen by considering this effect (see next part). However, it should often be possible to use some "compromise"-value of α, so that the bracket in (22) is appreciably reduced.

It would be interesting to see to what extent w_2 (22) can be minimized by varying n_2 in practice. To illustrate this, some numerical

† The tilting angle ψ_2 is thus independent of z_1, i.e. the position of the point in the target spot from where the particles emerge. Note the misprint in eq. (12) of ref. [10]). The factor M_z should be in the numerator. Further, (21) and (22) are thus independent of $\Delta\theta$, and $\Delta\theta_2$.

†† When the incoming and the outgoing particles pass the same side of the target, $\tan\varphi_2$ referred to the system chosen in fig. 6 is negative. $\tan\psi_2$ is still positive. To get opposite signs of the two terms in the bracket of (22) in this case analyzer 2 cannot be placed on that side of the incident beam which is indicated in fig. 6. It must be turned to the other side. (22) is also valid for this setting if one takes into account the signs of α and θ (assumed to be positive in fig. 6) when determining F, (6).

examples of ψ_2 and w_2 for (d,p)- and (α,α')-reactions (mass of final nucleus = 25) are calculated from (21) and (22). The examples can be applicable to the equipment in ref. [7])†. The parameters have the following numerical values: $r_1 = 80$ cm, $D_1 = 3.5$, $r_2 = 40$ cm, $D_2 = 4.0$. $E_1 = 7$ MeV deuterons. The energy derivatives are obtained from [8]) and it is assumed that M_{z_2} and $M_{r_2} \approx 1$. $F = F''$ (see (24) and fig. 3). The following results are obtained (in the last column is shown the value of w_2 if the second analyzer is placed on the wrong side of the beam):

	$\frac{E_1}{E_2}$	$\theta°$	n_2	$\psi_2°$	w_2/z_1 from (22)	w_2/z_1, if 2 is on the wrong side
d,p	0.6	90	0.53	29	0.1	1.4
			0.56	16	0.4	1.1
		30	0.53	16	0.5	1.2
			0.56	8	0.7	1.1
	1.0	90	0.53	36	0.0	1.7
			0.56	20	0.4	1.3
		30	0.53	21	0.5	1.4
			0.56	11	0.7	1.2
	1.4	90	0.53	41	0.0	1.9
			0.56	23	0.4	1.5
		30	0.53	24	0.5	1.6
			0.56	13	0.7	1.3
α,α'	1.2	90	0.60	31	— 0.4	1.3
			0.64	23	— 0.2	1.1
		30	0.60	19	0.1	1.1
			0.64	14	0.2	1.0

It is seen in the last two columns that for (d,p)-reactions a fairly small value of n_2 is desirable. For (α,α'), on the other hand, a large value (more than 0.60) is favourable.

4. Influence of the Target Thickness

It is not always necessary that the particles coming out from a target have an energy spread which is of the same order of magnitude as the maximum particle absorption in the target layer. If, for example, the incident particles and the outgoing particles pass through opposite sides of the target, the spread should be much less for some reactions. This is due to the fact that for this geometry, a large absorption of some incident particle corresponds more or less to a small absorption of the induced particle (fig. 9). Actually, the angle between the incident beam and the target can in this case be chosen so that the spread does not, within reasonable limits, depend on the target thickness. Furthermore, it is not necessary that the absorptions before and after the reaction cancel out, if only the energy difference of the outgoing particle is correlated to a suitable geometrical displacement. This might occur when the target is very thick (and consequently of low density). Then it should be possible that the energy difference and the corresponding displacement counterbalance each other.

† At present $n_2 = 0.50$.

4.1. TARGET OF HIGH DENSITY

Fig. 9 shows schematically a reaction which takes place at a depth τ in a target with thickness t. The density of the material is high so that the thickness is small compared to the beam spot. The displacement, depending on τ, of the outgoing particle paths is thus negligible. α and other quantities are defined as before.

The stopping powers of the target material are denoted by ε_1 and ε_2 (incoming and outgoing particles respectively) i.e.

$$-\left(\frac{\partial E}{\partial x}\right)_1 \equiv \varepsilon_1 \qquad \text{and} \qquad -\left(\frac{\partial E}{\partial x}\right)_2 \equiv \varepsilon_2 .$$

It is clearly seen from fig. 9 that the induced particles have the following energy decrease due to the target thickness (see (3)):

$$-\Delta E_2 = \tau\left[\frac{\partial E_2}{\partial E_1}\frac{\varepsilon_1}{\cos\alpha} - \frac{\varepsilon_2}{\cos(\theta-\alpha)}\right] + t\frac{\varepsilon_2}{\cos(\theta-\alpha)} . \tag{23}$$

If the coefficient of τ is zero, the decrease is constant, which means that the energy spread is independent of the target thickness. The condition for the bracket to disappear is

$$\frac{\cos(\theta-\alpha)}{\cos\alpha} = \frac{\varepsilon_2}{\varepsilon_1\dfrac{\partial E_2}{\partial E_1}} \equiv F'' . \tag{24}$$

This condition can be fulfilled by choosing a suitable α, which is obtained from fig. 4 if the function F'' has been determined.

F'', defined by (24), depends on the type of reaction, the target material, E_1 and E_2. It is indicated in fig. 3 as a function of E_1/E_2 for (p,p')-, (d,p)-, (d,d')-, (d,t)-, (α,He^3)-, and (α,α')-ractions. When plotting these curves, it has been assumed that the energy of the incident particle is 11 MeV (protons), 22 MeV (deuterons) or 44 MeV (α-particles). For other values of E_1 the curves are very little changed. This is a reason why it is convenient to use E_1/E_2 as variable of the functions in fig. 3.

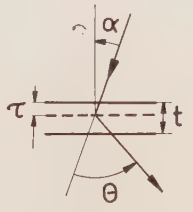

Fig. 9. Target of high density.

Thus, F'' can be obtained from fig. 3 for a certain reaction. Using fig. 4, the corresponding target direction, α, can be determined. For this α the energy spread caused by the absorption of the particles in the target material cancels out to the first order approximation. In the case of two horizontal analyzers, the energy spread depending on the target spot width can also be eliminated by use of a suitable α as was found previously (see (5)). It follows from fig. 3 that these two α's have about the same value (i.e. F' is very near to F'') if the parameter

$$K = \frac{D_2 r_2}{D_1 r_1 M_{r_2}}$$

is suitably chosen. The proper K-value depends on the type of reaction. It would also be necessary to change the parameter when E_1/E_2 varies (to keep F' and F'' almost equal). However, this change is small as is seen in the figure, so that it should scarcely be necessary in practice. Even if the conditions (5) and (24) are not quite fulfilled, a considerable reduction of the energy variation of the outgoing particles is attained. Thus for two analyzers in the same plane the variation is (see (23))

$$\Delta E_2 = t \frac{\varepsilon_1 \dfrac{\partial E_2}{\partial E_1}}{\cos \alpha} \left| 1 - \frac{F''}{F} \right| . \qquad (25)\dagger$$

For (d,p)-reactions, for instance, if the parameter is about 0.6 and E_1/E_2 varies from 0.5 to 2.0, an energy spread of the incident particles of 100 keV and target thickness of the same size results according to this calculation in a width of the particle group at the detector corresponding to less than about 30 keV (see (7) and (25)).

A cancellation of the influence of the target thickness is not possible when incident and outgoing particles traverse the same side of the target (see, however, next section).

4.2. TARGET OF LOW DENSITY (ANALYZERS WITH COINCIDENT BENDING PLANES)

We consider the more general case, i.e. reactions in a geometrically thick target as illustrated in fig. 10. The angles α and θ are positive in the figure. The analyzers are assumed to be combined as in fig. 1.

The particles formed in the plane $\tau = 0$ are focused in the same point at the detector if condition (5) is satisfied. When passing the target material, the energy of the particles decreases by a constant amount.

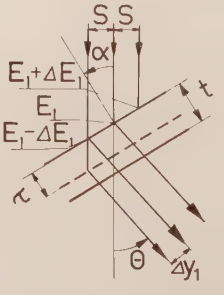

Fig. 10. Target of low density.

If we compare the energy of particles coming from a point at $\tau = 0$ with those coming from the corresponding point in some plane τ (fig. 10) we obtain the following difference:

$$\Delta E_2 = \tau \left[\frac{\varepsilon_1 \dfrac{\partial E_2}{\partial E_1}}{\cos \alpha} - \frac{\varepsilon_2}{\cos (\theta - \alpha)} \right] . \qquad (26)$$

† Cf. equation (B5) in the work by Brown *et al.* [8]) and (5) in that by Cohen [2]).

This corresponds to a displacement Δy_1 perpendicular to the optic axis of the second analyzer.

$$\Delta y_1 = \tau \frac{\sin\theta}{\cos\alpha}. \tag{27}$$

The displacement at the detector is then

$$\Delta y_2 = \tau \left[M_{r_2} \frac{\sin\theta}{\cos\alpha} + \frac{D_2 r_2}{2E_2} \left(\frac{\varepsilon_2}{\cos(\theta - \alpha)} - \frac{\varepsilon_1 \frac{\partial E_2}{\partial E_1}}{\cos\alpha} \right) \right]. \tag{28}$$

This is equal to zero if the following condition is fulfilled:

$$\frac{\cos\alpha}{\cos(\theta - \alpha)} = \frac{\varepsilon_1 \frac{\partial E_2}{\partial E_1}}{\varepsilon_2} - \frac{2E_2 M_{r_2}}{D_2 r_2} \frac{\sin\theta}{\varepsilon_2}. \tag{29}$$

We thus have two conditions, (5) and (29), which should be satisfied simultaneously. If this is true the two sources of energy spread are both compensated. The corresponding α is obtained from fig. 4. We have a possibility to vary the right-hand side of (29) by varying the second term. This term contains ε_2 as a factor and ε_2 may be varied. The second term is comparable to the first one only when ε_2 is small. (It must be expressed in energy per unit length e.g. MeV/cm.)

If (5) and (29) are to be satisfied for the same α, we have the equation

$$\frac{2M_{r_2}}{D_2 r_2} \frac{E_2}{\varepsilon_2} \sin\theta = \frac{1}{F''} - \frac{1}{F'} \tag{30}$$

from which the suitable ε_2 can be determined. F' and F'' can be obtained from fig. 3. This ε_2, obtained from (30), is thus dependent upon the reaction angle θ.

It should be pointed out here that the expressions (29) and (30) are also valid for negative θ's (i.e. analyzer 2 is on the other side of the beam in fig. 1). According to the definition, α is positive in fig. 1. Further, it must be remembered that when the incident and outgoing particles traverse the same side of the target the second analyzer must be turned, or else condition (5) cannot be fulfilled. This corresponds to a negative value of D_2 in (29) and (30). Then F' is also negative and from (28) a negative θ is obtained.

4.3. MULTIFOIL TARGET

A possible arrangement which should permit a variation of ε_2 in (30) is shown in fig. 11. This target consists of several parallel foils of equal thickness t, separated from each other by a distance d. t must be much less than d. The stopping power of this target is thus t/d times the stopping power of the foil material.

If the stopping power of the foil material is ε'_2, then

$$\varepsilon_2 = \frac{t}{d} \varepsilon'_2$$

and the left-hand side of equation (30) is

$$\frac{2M_{r_2}}{D_2 r_2} \frac{E_2}{\varepsilon'_2} \frac{d}{t} \sin\theta.$$

Thus d can be obtained from (30). In order to get some idea of the magnitude of the distance d obtained in this way we consider two reactions, (d,p) and (p,α) (stopping powers are for Al^9)). The thickness t is chosen so that the energy spread (estimated by (25)) of the emerging particles caused by absorption in the target material is no more than roughly 20 keV.

(1) (d,p)-reactions. If $D_2 = -4$, $M_{r_2} = 1$, $r_2 = 50$ cm, $E_1 = E_2 = 7$ MeV, $|\theta| \gtrapprox 90°$ and $t = 0.1$ mg/cm^2, then $d \sin\theta = -2.2$ mm for $K = -0.60$ (see (5) and fig. 3) and -1.8 mm for $K = -0.90$. Thus θ is negative. For D_2 positive, the reaction angles approximately in the region 20–90°, $K = 0.60$ and $t = 3$ mg/cm^2, we find $d \sin\theta = 1.1$ mm, (for $K = 0.90$ and $t = 0.4$ mg/cm^2 $d \sin\theta = 1.6$ mm).

If $D_2 = -4$, $M_{r_2} = 1$, $r_2 = 100$ cm, $E_1 = E_2 = 22$ MeV (the energy of the big cyclotron at the Nobel Institute), $|\theta| \gtrapprox 90°$, $K = -0.60$, and $t = 0.3$ mg/cm^2, $d \sin\theta = -1.7$ mm. For the forward angles (D_2 positive) with $t = 10$ mg/cm^2 we find $d \sin\theta = 1.0$ mm.

(2) (p,α)-reactions. Suppose $D_2 = 4$, $M_{r_2} = 1$, $r_2 = 100$ cm, $E_1 = E_2 = 11$ MeV, $K = 0.90$, $t = 0.03$ mg/cm^2, and $|\theta| \lessapprox 60°$. Then $d \sin\theta = -2.1$ mm. For larger angles and D_2 negative, $d \sin\theta = -2.4$ mm.

When a larger energy spread is allowed, t as well as the distances are increased. In practice a small number of foils should be reasonable.

In (p,α)-, (d,α)-, (α,p)-reactions, for example, it is not possible, as in a (d,p)-reaction, to choose the target angle α (from 24) so that the energy spread caused by absorption in the target material of a single foil is compensated. However, there should be a possibility of increasing the strength of the target without influencing the resolution for such reactions by using a multifoil arrangement. The resolution should be comparable with that obtained with one foil of the same thickness.

Fig. 11. Multifoil target.

4.4. TARGET OF LOW DENSITY (ANALYZERS WITH PERPENDICULAR BENDING PLANES)

When the analyzers are combined as in fig. 6 it might also be possible to achieve some compensation of the energy spread caused by absorption in the target. The argument is the same as in the preceding two sections. The condition for compensation is

$$\frac{2E_1}{D_1 r_1}\frac{\sin\theta}{\varepsilon_1} = F'' - F\,. \qquad (31)$$

The signs of θ and α (positive in (31)) are defined as in sections 3.1 and 3.3 (see fig. 6). For several parallel foils $\varepsilon_1 = (t/d)\,\varepsilon'_1$ with the notations as before, and therefore $d \sin\theta$ is obtained from (31). The energy spread has approximately the same order of magnitude as for a single foil (25). In the stigmatic case θ can be positive as well as negative, but in the astigmatic case a negative θ is not suitable (see 3.3).

5. Concluding Remarks

(1) As has been shown, it is possible to compensate the energy spread caused by a finite value of $\partial E_2/\partial\theta$ when the analyzers have coincident bending planes as well as when these planes are perpendicular to each other. In the former case the detector should be movable along the optic axis. If a wide target spot is used in the latter case, it is important that the second magnet be on the proper side of the beam. The influence of the energy spread depending on the opening angle is greatest for light nuclei, (but also for rather heavy nuclei when very high resolution is necessary). A compensation permits a large opening angle to be used (double-focusing fields).

(2) A system of analyzers having coincident bending planes has an important advantage. The width of the target spot in the axial direction can be large, (as also in the radial direction, 2.1). For the other type of system treated here, there is not a corresponding possibility. However, the first mentioned type of system requires a large experimental room, which may be a serious draw-back. In this respect the other type is more favourable as it gives a more compact equipment.

(3) One should be aware of the limitations of the calculations discussed here. The assumptions are not entirely valid in practice (note e.g. the influence of not quite plane target foils and all second-order effects which are difficult to estimate). Furthermore, only reasonable settings can, of course, be chosen (cf. fig. 4). However, it should often be possible to increase the counting rate appreciably by compensating different sources of the energy spread as has been discussed here (see also [2]). When designing new analyzing systems (fixing dimensions and degree of flexibility) calculations of the present type may be a valuable guide.

6. Acknowledgements

My thanks are due to Dr. K. G. Malmfors for valuable discussions and to Karin Oelsner B.Sc. who has corrected the English.

NUCLEAR INSTRUMENTS AND METHODS 7 (1960) 89–98; NORTH-HOLLAND PUBLISHING CO.

AN ELECTRON ACCELERATOR IN PRESSURIZED TANK FOR 3 mA AT 1.5 MV DIRECT VOLTAGE

G. HENNEBERKE

Scientific Equipment Division of N.V. Philips' Gloeilampenfabrieken, Eindhoven, The Netherlands

Received 14 December 1959

A 14-stage accelerating tube is supplied by a 7-stage Cockcroft-Walton generator with selenium rectifying units. The potential distribution across the accelerating tube is ensured by a parallel resistor. Special care has been devoted to the electron-optical part and this makes it possible to control a 3 mA electron beam with a current of 110 μA through the parallel resistor at a generator load of 3.2 mA. Focussing and intensity of the beam are independent of the high tension. X-ray intensities of 300 r/min at a distance of one metre from the target are readily attainable.

1. Introduction

Electrons are accelerated up to very high voltages and beam intensities of a few milliamperes in order to obtain a high-intensity radiation source. If the accelerated electrons fall upon a target of a material of high nuclear charge (tungsten, gold, etc.), the result is X-radiation and this is formed at an efficiency proportional to the energy of the electrons. With high-velocity electrons the depth of X-ray penetration within the irradiated materials increases, whilst absorption in the target is reduced and the angular distribution becomes more favourable. If the accelerated electrons leave the accelerator via a thin metal foil, they form a radiation source with an efficiency of about 75%, but with a lower penetration depth in the material irradiated than the corresponding X-rays. This paper describes a cascade generator that can be used for both types of radiation and is already being applied for X-radiation. Adjustable sources of radiation are now applied in a number of totally different fields. As regards electron accelerators, it is in medicine that most experience was gained with X-rays, for diagnostics as well as therapeutics. The deep penetration achieved by the radiation from the machine in question leads to dose distributions within the human body which are physically far preferable for therapeutic treatment to what can be obtained with the customary 200 or 400 kV X-radiation[1]).

The high beam intensity is here of primary importance. Direct irradiation with electrons of 1.5 MV is only feasible for surface treatment as their penetration into the human tissue is only about 5 mm[2]).

Both direct and indirect irradiation are likely to become very important for sterilizing foodstuffs and medicine in the future. Sterile conditions must as a rule prevail during the whole process of drug manufacture, because many organic compounds cannot stand high-temperature sterilization. Many laboratories are now looking for a method of non-sterile and far cheaper manufacture followed by a final sterilization by radiation.

In chemical technology there is a large number of possible applications of high-energy X-rays and electrons, such as "vulcanizing" rubber without sulphur and heat under atmospheric pressure, manufacturing special plastics having better electrical and mechanical properties and longer life thanks to the absence of residual catalyzer, and improving the adherence of bonding agents. In polymerising techniques the application of radiation has the substantial advantage that it can be dosed far more

[1]) D. W. Fry, Phil. Tech. Rev. **14** (1952/53) 1.
[2]) W. J. Oosterkamp, de Ingenieur **14** (1952) 061.

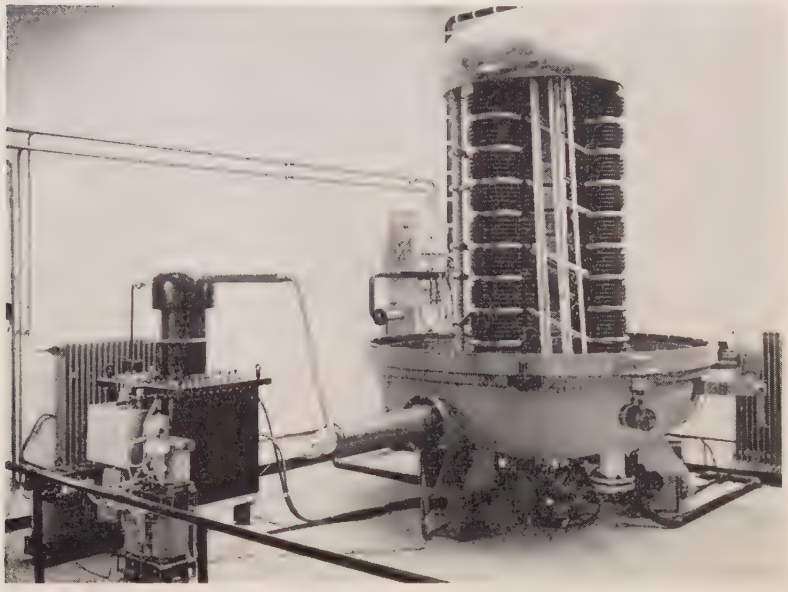

Photo 1. H.T. transformer, lead-in insulator and opened pressure tank. Two of the three columns made up of capacitor and selenium units are visible. On top is visible the top electrode and the inlet duct of the gas-drying installation. Between the two columns are visible part of the accelerating tube, the parallel resistor, the control rods for the control units in the top electrode, an induction coil and three damping resistors. To the right of the bottom of the tank is the drive for the locking ring with cam.

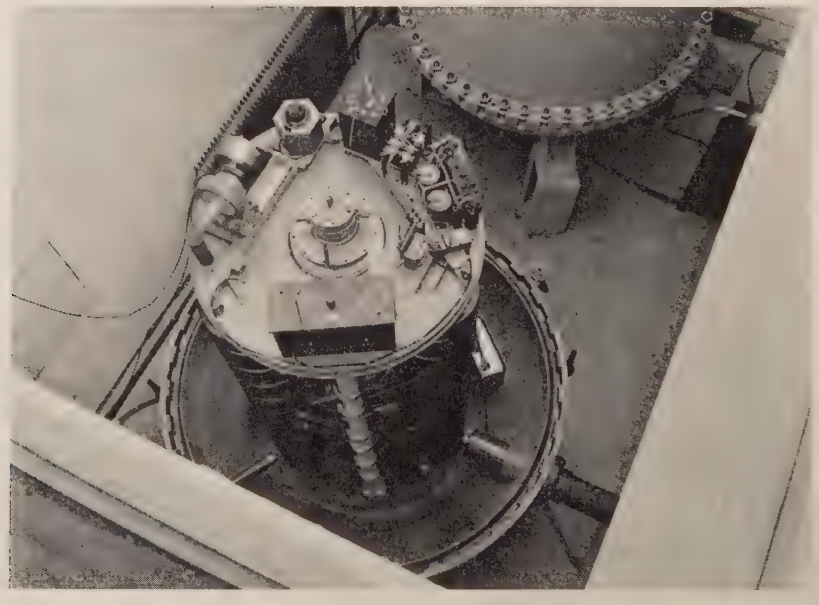

Photo 2. Top view of opened tank with top electrode removed. In the centre of the base plate of the top electrode is visible the electron gun and the upper porcelain container of the accelerating tube. The tank in the background does not belong to the tank base in the foreground.

uniformly than a catalyzer, so that the incorporated parameters can be determined more accurately.

In radiography high-energy X-rays are being increasingly used for quickly gathering information on casting strains, welding faults and other mechanical properties.

These are only a few of the numerous application possibilities, and in every instance high beam intensity obviously results in a proportional time-saving.

2. General Description of the Machine

A high-tension generator covered by a mushroom-shaped top electrode (photo 1) is housed inside a cylindrical steel tank with a diameter of 2.30 m and a height of 4 m. This top electrode, being under high tension, incorporates an electron gun (photo 2) that can be operated from earth potential by means of rotatable nylon rods. The top electrode also contains the supply equipment of the electron gun and the appertaining post-acceleration equipment (see accelerating tube). The energy required by these supply devices is provided by an electric motor on the bottom of the tank via a driving belt. The electron gun is placed on top of a porcelain accelerating tube located between the elements of the generator and between tankbottom and top electrode. This design corresponds to that of a similar ion accelerator[3]) developed in Philips Research Laboratories.

[3]) A. C. van Dorsten and J. H. Spaa, Nuclear Instruments **1** (1957) 259.

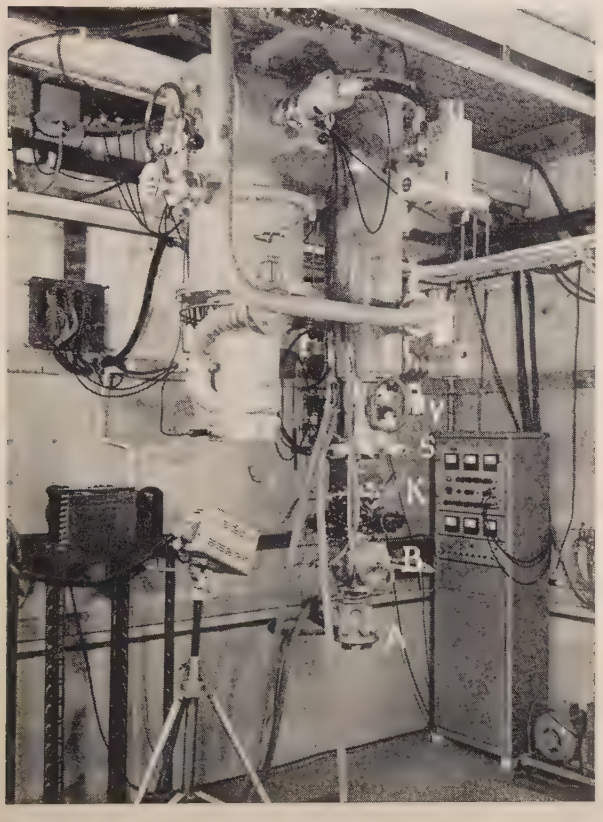

Photo 3. Steel extension of the accelerating tube with high-vacuum oil diffusion pump, vacuum-measuring equipment and target assembly. Visible in the foreground is a television camera for observing the behaviour of irradiated materials. The control panel of the high-vacuum equipment is visible in the background. For the meaning of the letters, see Photo 5.

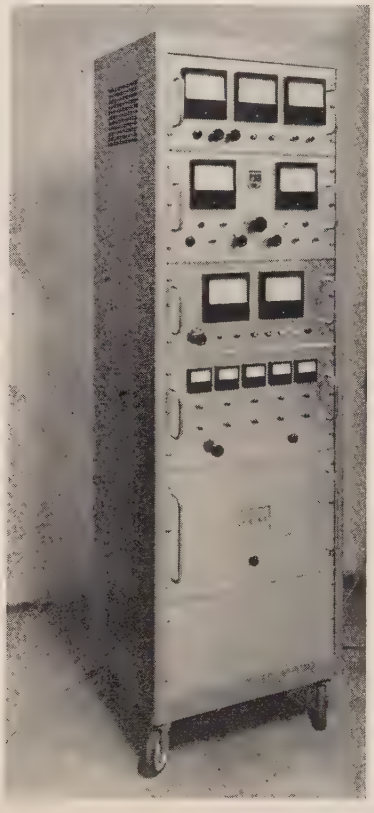

Photo 4. Control panel of electron accelerator. The high tension is controlled on the top panel, the second panel measures the high tension with the aid of a generating voltmeter fitted in the upper part of the tank. The third panel measures the vacuum and the beam current. The fourth panel controls and measures the beam-regulating unit in the top electrode.

The evacuated accelerating tube changes at the bottom of the tank into a metal tube communicating through the floor with the target room. Here the vacuum pumps, the vacuum-measuring equipment and the target assembly are fitted to the tube (photo 3).

The tank, when operated, is filled with nitrogen under 10 atm. In comparison with ordinary air, this means that the arcking lengths are increased about tenfold, so that a far more compact construction can be applied than would be possible under atmospheric pressure. Apart from the tank, the machine consists of a supply transformer (photo 1) and appertaining 500 c/s converter, a nitrogen container with compressor-installation, a nitrogen drying-installation, a vacuum-control panel (photo 3) and a general control panel (photo 4) placed in a separate control room. Between the radiation room and the tank room on the one side and the control room on the other side there is a concrete shielding limiting the radiation level in the control room and outside the building below the tolerance dose rate of 5 mr/h.

Special attention was paid to the locking device between the lower and upper parts of the tank. These were formerly bolted together (photo 2, top) but locking is now effected by means of a ring provided with cams (photo 1 and photo 2, below).

3. The High-Tension Generator

The Cockcroft and Walton or cascade circuit applied here has been exhaustively described[4–10]).

The circuit is in effect a number of rectifier stages connected in series. Each stage consists of two capacitors and two rectifying valves, admitting the current only in the direction towards the high-tension electrode. The former "kenotrons" have been replaced by selenium rectifiers arranged in series[3,11,12,13]).

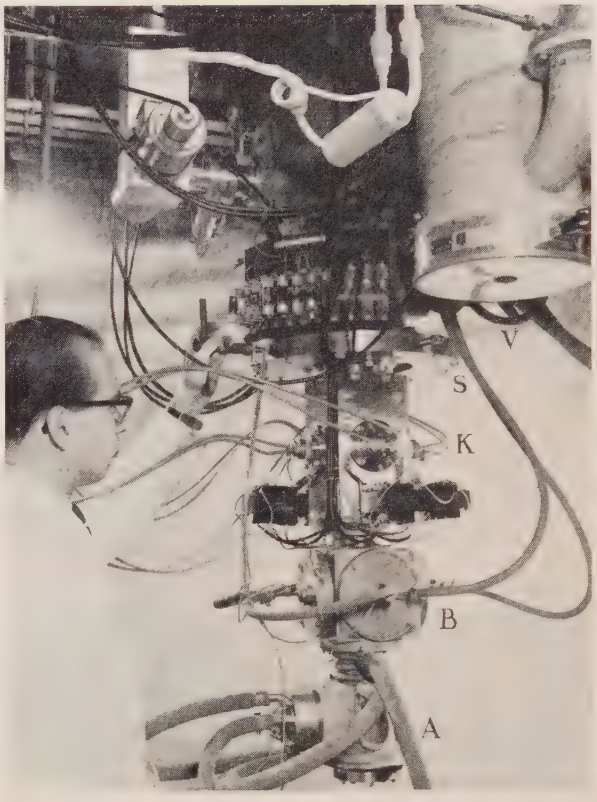

Photo 5. Target assembly. Visible from bottom to top: A. Target chamber with water-cooling ducts; B. Beam-measuring block; K. Spot-wobbler; S. Sliding part; V. High-vacuum valve.

Fig. 1 shows the basic lay-out of a 2-stage generator for negative potential.

Fig. 2 shows the voltages after switching-on at the points marked in fig. 1 in the idealized case without generator load. The circuit is built up of three columns, each consisting of a series-stacking of capacitor-valve-capacitor, etc.

$$(C_{A_1}, V'_1, C_{D_2})\ (V_1, C_{A_2}, V_2)\ (C_{D_1}, V_2)\ .$$

Owing to the load, the high tension in an n-stage generator becomes less than $2n \times$ the peak voltage of the input transformer as would appear from fig. 2.

The load also causes a ripple on the direct voltages. With the adopted compact construction,

[4]) S. Gradstein Phil. Tech. Rev. **1** (1936) 6.
[5]) A. Kuntke, Phil. Tech. Rev. **2** (1937) 161.
[6]) A. Bouwers, Elektrische Höchstspannungen.
[7]) E. Everhart and P. Lorrain, Rev. Scient. Instr. **24** (1953) 221.
[8]) W. Heilpern, Helv. Ph. Acta **28** (1955) 485.
[9]) P. Lorrain *et al.*, Can. J. Phys. **35** (1957) 299.
[10]) H. Stamm, Wissenschaft. Zschr. der Hochschule für Elektrotechnik **2**, Heft 1 (1956) 33.
[11]) W. Ch. v. Geel, Phil. Tech. Rev. **4** (1939) 104.
[12]) D. M. Duinker, Phil. Tech. Rev. **5** (1940) 200.
[13]) J. J. A. Ploos van Amstel, Phil. Tech. Rev. **9** (1947) 267.

some parasitic capacitance of the rectifiers is inevitable, and this, together with the stray capacitance between the direct voltage and alternating voltage capacitors gives rise to a voltage drop and a voltage ripple.

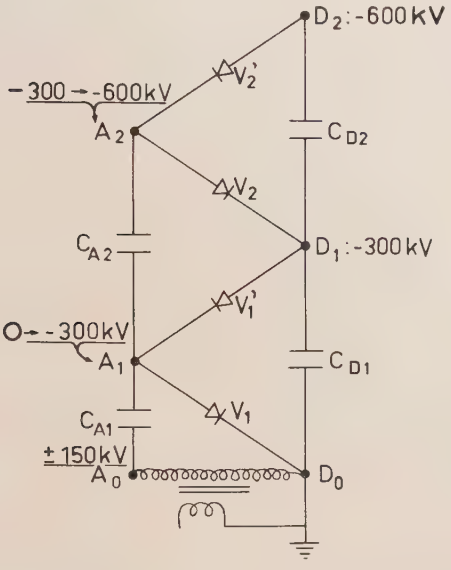

Fig. 1. Simplified diagram of a two-stage cascade generator. C_A: alternating-voltage capacitors. C_D: direct-voltage capacitors. V: selenium rectifiers. The voltages indicated at points A and D are the rated voltages belonging to an alternating voltage of 150 kV in point A_0 relative to D_0.

In the present construction the junctions between the columns may be used to incorporate series self-inductances, but this is only done in the alternating-voltage column. The junctions of the direct-voltage column have been utilized for incorporating damping resistors[14]), the circuit being that shown in fig. 3. Photo 1 shows an inductor and three damping resistors fitted between two columns composed of insulators of uniform appearance accommodating in turn capacitors and selenium rectifiers. In this way a 7-stage accelerator loaded with 3.2 mA can produce a high tension of 1500 kV from a transformer peak voltage of 150 kV. For reducing the ripple, a frequency of 500 c/s was chosen.

4. The Electron Gun (fig. 4)

Electrons are emitted by a coiled tungsten filament G. At full output of the high-tension generator this filament is at a 1500 kV potential. For a clear understanding and in calculations it is advisable to distinguish the electrodes controlling the beam as to their velocity potential ϕ,

[14]) N. F. Verster, H. P. J. Brekoo and J. Jansen, Internal Report.

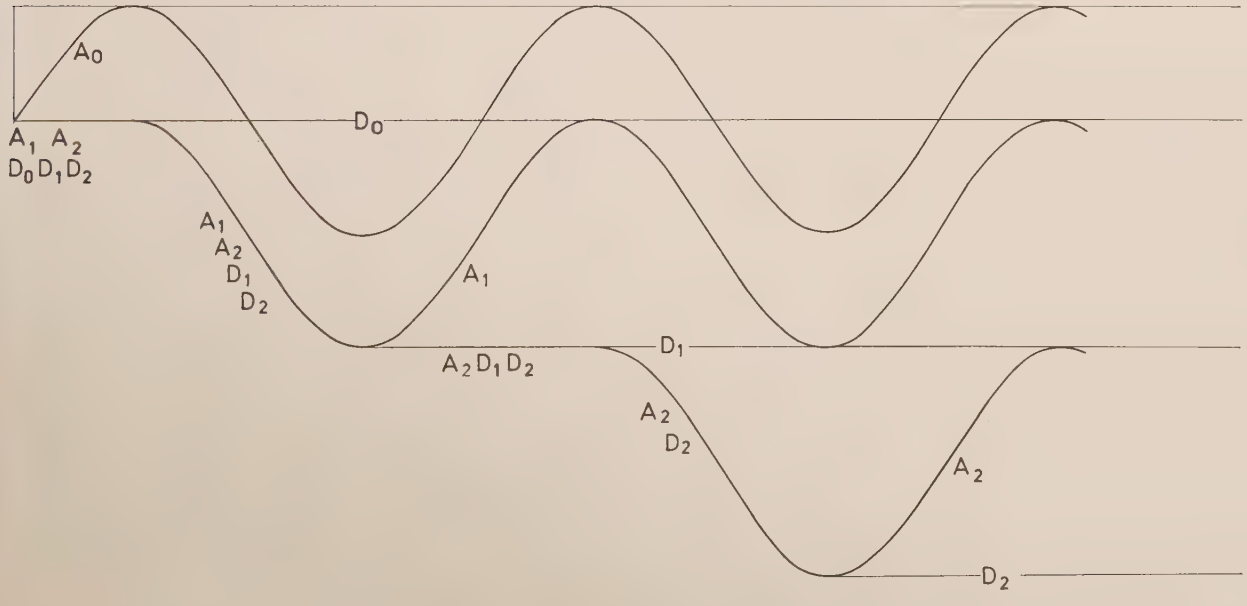

Fig. 2. Voltage variation in the points indicated in fig. 1 in the idealized case and without generator load. C_{A1} is charged up to the peak voltage of the transformer. The voltage across the other capacitors is double the amount of the peak voltage.

which is measured relative to the potential corresponding to zero-velocity electrons. The

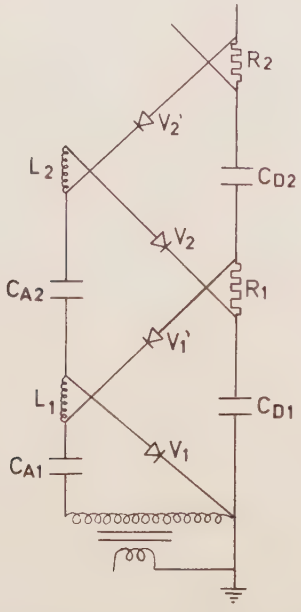

Fig. 3. Simplified diagram of a two-stage cascade generator with self-inductances L for compensating the stray capacitances and parasitic capacitances of the rectifiers. R are damping resistors for protecting the rectifiers in the event of current impulses.

latter, therefore, is the filament potential, ϕ being 0 and V being — 1500 kV. The electrons liberated from the filament are made to converge on the entry aperture 0 of the accelerating tube by the Wehnelt cylinder W. Between the Wehnelt cylinder and the entry aperture there is a high-vacuum valve K by which the accelerating tube can be closed, so that the vacuum within the tube can be maintained when the filament has to be replaced. The entry aperture of the tube has a velocity potential ϕ_A that can be controlled between 0 and 5 kV, so that this aperture also functions as extraction anode.

Among the quantities that can be regulated on the control desk (photo 4, 4th panel from top) are the following:

1. the voltage across the filament, and hence the emission of the filament.
2. the Wehnelt-cylinder voltage;
3. the extraction voltage;
4. the focussing voltage (see accelerating tube.)

All these voltages and the appertaining currents can be read from a television screen. This has been effected as follows: The bottom plate of the top electrode has an opening on which the meters in the top electrode have been fitted face-downward. The lower part of the tank has an opening through which the dials can be illuminated from the outside and watched by a TV camera.

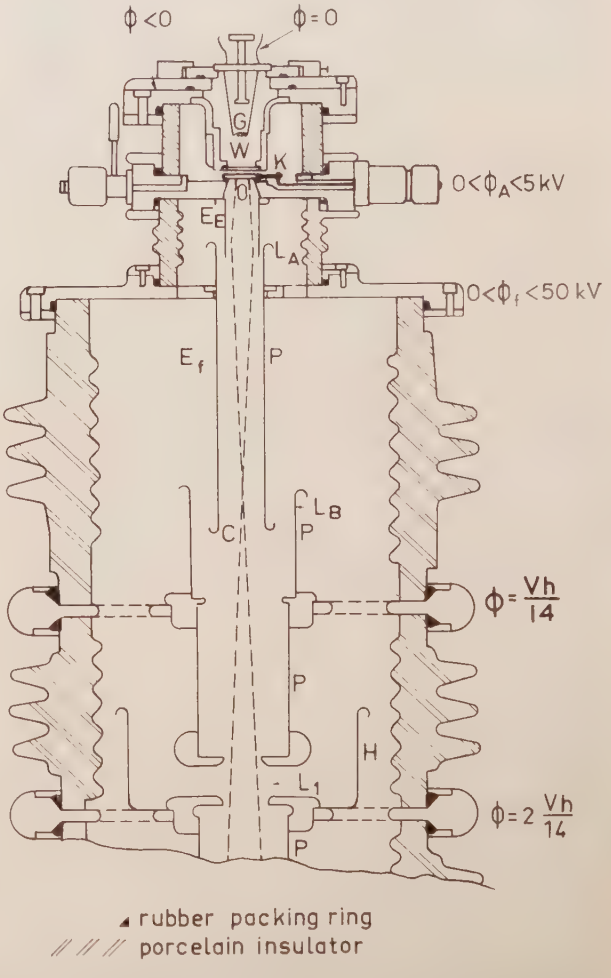

Fig. 4. Electron gun and upper section of the accelerating tube. G = tungsten filament, $\phi = 0$. W = Wehnelt electrode, $\phi < 0$ adjustable. K = high-vacuum valve by means of which the housing of the electron gun can be separated from the accelerating tube. O = entry aperture of the tube. E_E = extraction electrode. L_A = focussing lens. E_f = focussing electrode. L_B = transition lens. L_1 = upper tube lens. H = protecting cover. P = cylindrical tubing.

5. The Accelerating Tube

In high-tension vacuum engineering it is possible to retain a voltage V/K across a length

L/K ($K > 1$), whilst at the same V and L it is impossible to maintain a voltage V across length L without arcking.

It is therefore recommended to have a stepwise potential distribution along the tube, which is in fact an inherent feature of the cascade generator (points D_0, D_1, etc. in fig. 1). This would result in voltage intervals along the tube of more than 200 kV, which is still excessively high in vacuum for the dimensions employed. That is why the tube has been designed in fourteen stages with somewhat more than 100 kV for each stage. Concentrating the field strength within the tube by means of electrostatic lenses has the advantage of sharp focussing, which easily outweighs the drawback of the greater field strength as long as large currents (above 1 mA) are involved. Such a concentration of field strength is readily realized by means of a conductive length of tubing (P, fig. 4), which furthermore protects the porcelain against stray particles. At the location of the lens this protection is provided by a screening hood H. The subdivision of the cascade-stage voltage is effected with a parallel resistor of $10^{10}\ \Omega$.

The strength of an electrostatic lens is given by the product of a geometric factor and a function of the voltage ratio. Therefore all lens strengths within the tube and hence the path of the beam remain constant when the high tension is varied. It is accordingly possible in principle to design a tube with an H.T.-independent constant focus, which could not, however, be varied. It would also mean that all voltages in and after the electron gun had to be varied proportionally with the high tension, which is hardly feasible. However, when separately controlled voltages are introduced with the aim of determining the optimum shape of the beam experimentally or varying the focus, then the transition zone between controlled electrode and electrode with H.T.-proportional voltage will form a lens the strength of which varies with the high tension. This results in a variation in beam path and focus due to a variation in high tension alone.

[15]) N. F. Verster, Internal Report.
[16]) J. C. Francken, Phil. Tech. Rev. **21** (1959) 11.

As far as we know, the situation in existing accelerators was that after variation of the high tension also a control voltage had to vary. In the machine in question the image of the electron-gun filament is formed in the transition lens (L_B in fig. 4). The result is a so-called cross-over, by which the effect of the transition lens, apart from higher-order effects, is eliminated[15]). A second condition is that the dimensions of the tube should be such that the image of the cross-over is projected on the target; a third condition is that the entry and exit angle of the cross-over are adapted to the tube dimensions. If these conditions are fulfilled, it is found possible to maintain a constant current and a constant focus when the high tension is varied between 500 and 1500 kV without the necessity of adjusting any other control element.

Let us now examine the path of the electrons after crossing the entry aperture of the tube (fig. 4).

After passing a field-free region ($0 < \phi_A < 5$ kV adjustable) they are influenced by a focussing lens L_A. The strength of this lens is determined by the ratio between ϕ_A and ϕ_f; $0 < \phi_f < 50$ kV adjustable. By controlling ϕ_f and ϕ_A it is possible to concentrate the beam into a cross-over in transition lens L_B. This cross-over is projected by the lenses L_1–L_{13} on the target.

Calculations concerning such a complex arrangement of lenses are made most systematically with the aid of matrices. If we neglect space charge effects and lens errors (e.g. spherical aberrations) there is a linear relationship between

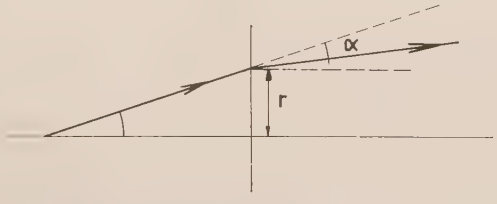

Fig. 5. Working of simple lens $\alpha :: r$.

entry and exit beam; this can be determined from measurements of the axis potential on a rotation-symmetrical resistance network corresponding with the lens-configuration[16]).

An ordinary lens deflects an incident ray by an angle which is the product of incidence height r and strength S of the lens: $\alpha = rS = r/f$, f being the focal length (fig. 5). The relation between entry and exit beam accordingly becomes (fig. 6)

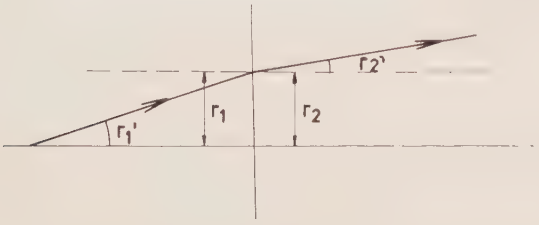

Fig. 6. Relation between incident ray r_1 and emergent ray r_2 for a simple lens.

$$r_2 = 1r_1 + 0r'_1 \qquad (1)$$

$$r'_2 = -\frac{1}{f} r_1 + r'_1 \qquad (2)$$

r'_1 and r'_2 being the deflection angles of entry and exit beam. If we represent the entry and exit beams by the two-dimensional vectors $\mathbf{r}_1$ and $\mathbf{r}_2$, then we may put (1) and (2) in abbreviated form as $\mathbf{r}_2 = M_L \mathbf{r}_1$, in which M_L is the lens matrix:

$$M_L = \begin{vmatrix} 1 & 0 \\ -\frac{1}{f} & 1 \end{vmatrix}$$

the determinant of which has the value

$$1 \times 1 - \frac{1}{f} \times 0 = 1 .$$

For a field-free space of length l, the equations (fig. 7) are

$$r_4 = 1r_3 + lr'_3$$

$$r'_4 = 0r_3 + 1r'_3$$

and the matrix becomes

$$M_0 = \begin{vmatrix} 1 & l \\ 0 & 1 \end{vmatrix} ;$$

the determinant likewise being unity. Introducing l as unit length changes the calculation into multiplication of a number of matrices of the type

$$\begin{vmatrix} 1 & pl \\ 0 & 1 \end{vmatrix}, \quad \begin{vmatrix} 1 & 1 \\ 0 & 1 \end{vmatrix} \quad \text{and} \quad \begin{vmatrix} 1 & 0 \\ -\frac{1}{f} & 1 \end{vmatrix},$$

This has the advantage of being systematic and of the fact that all matrices to be multiplied

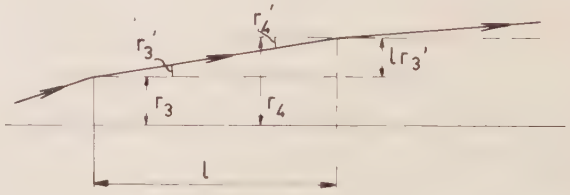

Fig. 7. Relation between incident ray r_3 and emergent ray r_4 in a field-free space.

retain unity as the determinant, which provides an easy check for calculation errors.

The above calculation is not valid for the upper part of the tube, where the lenses are most powerful and the electron velocity lowest. Here the whole potential variation has to be measured, and the space-charge divergence due to the repulsive force between the electrons has to be included in the differential equation describing the trajectory of the electrons. The total trajectory must then be computed with the aid of the differential equation in several small steps. All calculations may be greatly facilitated by using the transformation $R = r\phi^{\frac{1}{2}}$.

6. The Vacuum System (photo 3)

The vacuum in electron gun, accelerating tube and target assembly is effected by an oil-diffusion pump with a capacity of 1000 litres per sec. at a pressure of 10^{-5} mm Hg. Pre-vacuum pumping is done with a rotary oil pump attaining a pressure between 5 and 2×10^{-3} mm Hg during operation. Between diffusion pump and tube are an oil vapour condensor (baffle) cooled with freon to $-30°$ C and a high-vacuum valve. The reliable sealing of all fourteen tube elements and the electron gun is effected with the aid of rubber ○ rings. It is interesting to know that if the pressure in the tank is raised from 0 to 10 atm excess pressure, the vacuum is slightly improved. During operation a pressure of 3×10^{-6} mm Hg, measured at the bottom of the tube, is attained. The high vacuum can be continuously checked with the aid of Penning-type cold-cathode ionisation

gauges that can be fitted in various positions. These connection spots are provided with liquid-air traps by means of which organic vapours can be condensed. The high-vacuum equipment and the appertaining refrigeration systems are operated via a separate control box (photo 3).

7. The Target Assembly (photos 3 and 5)

The accelerating tube is closed also at the lower part by a high-vacuum valve V, so that the vacuum within the tube can be maintained when the target has to be exchanged.

The target is a tungsten plate with forced water-cooling. This cooling requires special provisions as direct cooling of the tungsten is not feasible because of steam development and the risk of impairing the vacuum-sealing. The tungsten must be incorporated in a copper block and the latter is cooled. To reduce absorption of the X-radiation set up in the tungsten as far as possible, the target has been so designed that the tungsten plate is at an angle of 45° to the electron beam, whilst the cooling is effected from the side (fig. 8). The data on diameter and

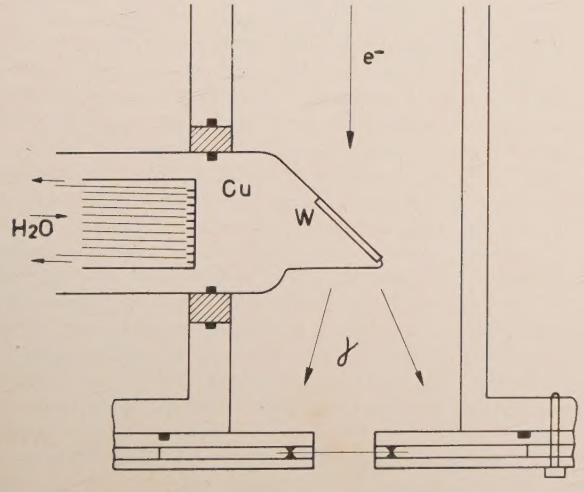

Fig. 8. Electron target with housing. The tungsten plate W is contained in a copper block with forced water-cooling. After removal of the target the electrons can emerge out of the vacuum via a very thin window.

centring of the electron beam are provided by a beam-measuring block B consisting of a four-sector diaphragm (fig. 9) fitted above the target. The four sectors are insulated from each other and from the other equipment. The absolute value of the incident currents is a

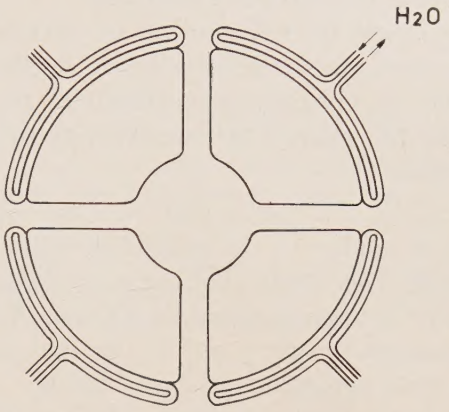

Fig. 9. Beam-measuring diaphragms, consisting of 4 water-cooled sectors, insulated from each other and from earth.

measure of the focussing of the beam and the ratio of the current intensities a measure of the centring. Centring can be regulated with the aid of a sliding part S, fitted directly under the aforesaid high-vacuum valve. With this sliding part the entire target assembly may be displaced a few mm in any horizontal direction. One condition for designing a sliding part of this kind is that the mechanical pressure is taken up outside the vacuum. This condition has to be met to prevent seizure of the sliding surfaces.

When the electron beam of 1.5 MV and 3 mA is focussed on a diameter of 5 mm, the tungsten is loaded with 225 W/mm², which is 3 × the permissible maximum. Defocussing the beam on triple the area by means of ϕ_f is possible, but has the drawback of broadening the beam in the accelerating tube to the same extent. That is why it was preferred to effect defocussing outside the accelerating tube. To do this, a spot-wobbler was fitted below the sliding part. It contains four electrostatic deflection plates, one pair of which is fed by 50 c/s and the other pair by 500 c/s. The 500 c/s voltage is tapped from the 500 c/s generator supplying the H.T. transformer (see H.T.-transformer). This generator is fed by 50 c/s. Owing to the slip in this generator, the 500 and 50 c/s frequencies applied to the

spot-wobbler are not related to each other by a simple integral ratio, so that no Lissajous figure is obtained, but the beam is uniformly distributed about the enlarged target area.

The angle of deflection of an electron in a transversal electric field as set up by the spot-wobbler is inversely proportional to the mass and to the square of the velocity of the electron, and hence:

$$\alpha \propto \frac{1}{\frac{1}{2}mv^2}$$

Here m applies to the relativistic mass of the electron. This means that the $\frac{1}{2}mv^2$-value of an electron having traversed 1.5 MV is not 1.5 MeV, because relativistic $\frac{1}{2}mv^2$ is the first term of the series expansion of E_k = kinetic energy.

From the Einstein relation it follows that:

$$\frac{\frac{1}{2}mv^2}{E_k} = \frac{E_k + 2E_0}{2E_k + 2E_0}.$$

E_0 is the rest energy of the electron (0.511 MeV). It is thus apparent that $\frac{1}{2}mv^2/E_k$ lies somewhere between 1 and 0.5; for $E_k = 1.5$ MeV, $\frac{1}{2}mv^2 \approx 0.95$ MeV.

From $m/m_0 = (E_k + E_0)/E_0$ it follows that $m/m_0 = 4$ at $E_k = 1.5$ MeV. The beam at the target is given a diameter of 15 mm with the aid of the spot-wobbler. At 1400 kV and 2.5 mA an X-ray dose rate of 250 r/min was measured at a distance of 1 metre from the target.

Acknowledgement

The accelerator described in this paper was developed for and supplied to the Diamond Research Laboratory, Johannesburg, South Africa, which we thank for permitting this publication.

NUCLEAR INSTRUMENTS AND METHODS 7 (1960) 99–100; NORTH-HOLLAND PUBLISHING CO.

BOOK REVIEWS

Nuclear Electronics. Part I of Proceedings of the international symposium on nuclear electronics organized by the French society of Radioelectriciens in Paris, September 1958. International atomic energy agency, Kärntner Ring, Wien I, Austria.

The book contains 450 pages covering 50 communications presented during five sessions on different subjects. Session I, on Scintillation Radiation Detectors reveals that much work has been done in improving the properties of photomultipliers, especially their time-resolution capability. Although European designs are now available which are in line with or even better than American standard types in this respect, a paper by G. A. Morton, R.C.A. describes interesting development tubes having a special electrode structure. Time resolution is $\approx 10^{-11}$ sec. Photocathodes with higher quantum efficiency are also being developed (trialkali cathodes). Interesting is also the transmission type multiplier (designed by Sternglass reported by Wiegand in a later session). This promises very good time resolution and may also give image amplification.

The properties of scintillators is dealt with in four papers. The fact that scintillator decay time is dependent on the kind of ionizing particle can be used for counting one kind of radiation in the presence of background of another, as discussed by Owen.

From Session II, Radiation Detectors using ionizing methods and gamma-ray spectrometers may be mentioned a summary on ionizing detectors by Fachini, papers about gas scintillators and about the utilization of semiconductors as proportional detectors for ionizing radiation (Bomal *et al.*)

Session III is devoted to Fast pulse techniques. Wiegand discusses fast electronics in high-energy physics. Other valuable contributions are several papers on fast coincidence circuits, scalers, and related techniques. An interesting attack on the coincidence circuit problem is described by Morton and Matheson, who use a special coincidence tube for work in the range of 10^{-10} sec or less. Orman gives some data on fast oscilloscopes especially of the pulse-sampling type now becoming popular. Two papers discuss ways of building time analyzers with ultrashort time-resolution capability. The dead time of pulse-height analyzers used in pulsed-accelerator work is decreased to a few microseconds with the help of electrostatic storage as discussed by Pieper. A simple millimicrosecond pulse and light pulse generator using a Rosenblum counter is described by Fleury.

Session IV deals with Classical pulse electronics. After introductory remarks by Gatti on recent advances in this field several papers consider different constructions of pulse-height and time analyzing equipment. A modification of the common magnetic-memory type kicksorter is described by MacMahon who appreciably shortens the dead time by using coarse and fine steps in the analog-to-digital conversion procedure.

Session V is devoted to Measurements on and Control of Reactors. It contains valuable information for the reactor engineer. Not only are specific electronic problems such as detector electronics, ratemeters, etc. considered, but also the physical behavior of the reactors of importance for developing the control systems.

The organizers of this Conference should by thanked for their initiative to collect in this form the conference information on this rapidly developing field.

P. A. TOVE

HERBERT GOLDSTEIN: *Fundamental Aspects of Reactor Shielding*, Addison-Wesley Publishing Company, Inc., Reading, Mass., USA, 1959. 416 pages. Price: US $ 9.50.

It is a common notion that the science of reactor shielding, although of great practical importance, lacks intrinsically interesting features. The name of Herbert Goldstein in connection with a book on reactor shielding indicates that this is a misconception. Goldstein has, in his "classical" textbook of classical mechanics, already demonstrated his ability of conveying to his readers some of his own deep understanding for fundamental physical principles. It is therefore with great anticipation that the reader opens the present volume, and he will not be disappointed. Even a person uninitiated in this particular field soon realizes that there exist a vast number of shielding problems well worth a theoretical treatment, which will in turn throw light upon the basic physical processes involved.

However, reactor shielding is and remains mainly the concern of the power plant designer, who wants reliable figures in the most straight-forward way. Consequently the book also takes on the character of a handbook, with ample information about experimental methods and facilities and, last but not least, a great number of tables and diagrams. The extensive bibliographies contribute to the impression that the author has taken into account practically all the information available on the subject. It is most likely that Goldstein has once more produced a classic in scientific literature.

E. K. SOKOLOWSKI

Directory of Nuclear Reactors. Vol. II: *Research, Test and Experimental Reactors.* International Atomic Energy Agency, Vienna, 1959. Price: U.S. $ 3.50; U.K. 21/– Stg; A.S. 73.50.

The International Atomic Energy Agency has now published the second volume of the Directory of Nuclear Reactors. In this volume which succeeds the part on power reactors, are treated research, test and experimental reactors, currently in operation or under construction. Because of the vast number of reactors under this heading,

only about half of the existing facilities have been included. However, a further volume is being prepared, comprising reactors, the data of which were not available in time for the present publication. It is to be hoped that the USSR, which is not represented in the present volume, will contribute data to the forthcoming part.

The reactors included in volume II are divided into the following categories: light-water-moderated pool-type, light-water-moderated tank-type, liquid-homogeneous, solid-homogeneous, heavy-water-moderated, graphite-moderated and organic-moderated. Unfortunately, fast critical assemblies have been omitted.

All that was said in recommendation of the first volume of the series is valid for the second one. The presentation of the data is clear and consistent and in most instances elucidated by drawings of fuel elements and reactor sections. Capital and operating costs are given whereever possible. An extensive bibliography accompanies each presentation. It is beyond doubt that a great need is filled by this work.

E. K. SOKOLOWSKI